AD_____

GRANT NO: DAMD17-95-1-5027

TITLE: Cholinesterase Structure: Identification of Residues and Domains Affecting Organophosphate Inhibition and Catalysis

PRINCIPAL INVESTIGATOR(S): Palmer W. Taylor, Ph.D.

CONTRACTING ORGANIZATION: University of California, San Diego
La Jolla, California 92093-0934

REPORT DATE: April 1996

TYPE OF REPORT: Annual

PREPARED FOR: U.S. Army Medical Research and Materiel Command
Fort Detrick, Frederick, Maryland 21702-5012

DISCLAIMER NOTICE

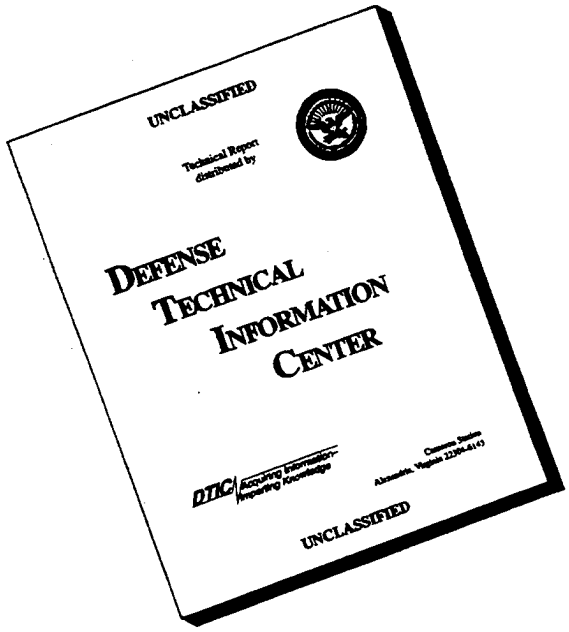

THIS DOCUMENT IS BEST QUALITY AVAILABLE. THE COPY FURNISHED TO DTIC CONTAINED A SIGNIFICANT NUMBER OF PAGES WHICH DO NOT REPRODUCE LEGIBLY.

REPORT DOCUMENTATION PAGE

Form Approved
OMB No. 0704-0188

1. AGENCY USE ONLY *(Leave blank)*	2. REPORT DATE	3. REPORT TYPE AND DATES COVERED
	April 1996	Annual (6 Mar 95 - 5 Mar 96)

4. TITLE AND SUBTITLE
Cholinesterase Structure: Identification of Residues and Domains Affecting Organophosphate Inhibition and Catalysis

5. FUNDING NUMBERS
DAMD17-95-1-5027

6. AUTHOR(S)
Palmer W. Taylor, Ph.D.

7. PERFORMING ORGANIZATION NAME(S) AND ADDRESS(ES)
University of California, San Diego
La Jolla, California 92093-0934

8. PERFORMING ORGANIZATION REPORT NUMBER

9. SPONSORING / MONITORING AGENCY NAME(S) AND ADDRESS(ES)
U.S. Army Medical Research and Materiel Command
Fort Detrick
Frederick, Maryland 21702-5012

10. SPONSORING / MONITORING AGENCY REPORT NUMBER

11. SUPPLEMENTARY NOTES

12a. DISTRIBUTION / AVAILABILITY STATEMENT
Approved for public release; distribution unlimited

12b. DISTRIBUTION CODE

13. ABSTRACT *(Maximum 200 words)*

In the initial year of the grant, we have made excellent progress in several arenas:

1) A crystal structure of a mouse acetylcholinesterase-fasciculin 2 complex has been solved.

2) Studies with enantiomeric organophosphates have yielded vital information on their binding orientation in the ground and transition states.

3) Studies in oxime reactivation of inhibited cholinesterase have uncovered the basis for enhanced reactivity of HI-6 compared to 2-PAM.

4) The interactions of fasciculin 2 with acetylcholinesterase have been studied by kinetic and site-specific mutagenesis methods.

14. SUBJECT TERMS
acetylcholinesterase, organophosphates, enantiomers, reactivators, fasciculin, x-ray crystal structure, site-specific mutagenesis

15. NUMBER OF PAGES
122

16. PRICE CODE

17. SECURITY CLASSIFICATION OF REPORT	18. SECURITY CLASSIFICATION OF THIS PAGE	19. SECURITY CLASSIFICATION OF ABSTRACT	20. LIMITATION OF ABSTRACT
Unclassified	Unclassified	Unclassified	Unlimited

GENERAL INSTRUCTIONS FOR COMPLETING SF 298

The Report Documentation Page (RDP) is used in announcing and cataloging reports. It is important that this information be consistent with the rest of the report, particularly the cover and title page. Instructions for filling in each block of the form follow. It is important to ***stay within the lines*** to meet ***optical scanning requirements***.

Block 1. Agency Use Only *(Leave blank)*.

Block 2. Report Date. Full publication date including day, month, and year, if available (e.g. 1 Jan 88). Must cite at least the year.

Block 3. Type of Report and Dates Covered. State whether report is interim, final, etc. If applicable, enter inclusive report dates (e.g. 10 Jun 87 - 30 Jun 88).

Block 4. Title and Subtitle. A title is taken from the part of the report that provides the most meaningful and complete information. When a report is prepared in more than one volume, repeat the primary title, add volume number, and include subtitle for the specific volume. On classified documents enter the title classification in parentheses.

Block 5. Funding Numbers. To include contract and grant numbers; may include program element number(s), project number(s), task number(s), and work unit number(s). Use the following labels:

C	- Contract	**PR**	- Project
G	- Grant	**TA**	- Task
PE	- Program Element	**WU**	- Work Unit Accession No.

Block 6. Author(s). Name(s) of person(s) responsible for writing the report, performing the research, or credited with the content of the report. If editor or compiler, this should follow the name(s).

Block 7. Performing Organization Name(s) and Address(es). Self-explanatory.

Block 8. Performing Organization Report Number. Enter the unique alphanumeric report number(s) assigned by the organization performing the report.

Block 9. Sponsoring/Monitoring Agency Name(s) and Address(es). Self-explanatory.

Block 10. Sponsoring/Monitoring Agency Report Number. *(If known)*

Block 11. Supplementary Notes. Enter information not included elsewhere such as: Prepared in cooperation with...; Trans. of...; To be published in.... When a report is revised, include a statement whether the new report supersedes or supplements the older report.

Block 12a. Distribution/Availability Statement. Denotes public availability or limitations. Cite any availability to the public. Enter additional limitations or special markings in all capitals (e.g. NOFORN, REL, ITAR).

- **DOD** - See DoDD 5230.24, "Distribution Statements on Technical Documents."
- **DOE** - See authorities.
- **NASA** - See Handbook NHB 2200.2.
- **NTIS** - Leave blank.

Block 12b. Distribution Code.

- **DOD** - Leave blank.
- **DOE** - Enter DOE distribution categories from the Standard Distribution for Unclassified Scientific and Technical Reports.
- **NASA** - Leave blank.
- **NTIS** - Leave blank.

Block 13. Abstract. Include a brief *(Maximum 200 words)* factual summary of the most significant information contained in the report.

Block 14. Subject Terms. Keywords or phrases identifying major subjects in the report.

Block 15. Number of Pages. Enter the total number of pages.

Block 16. Price Code. Enter appropriate price code *(NTIS only)*.

Blocks 17. - 19. Security Classifications. Self-explanatory. Enter U.S. Security Classification in accordance with U.S. Security Regulations (i.e., UNCLASSIFIED). If form contains classified information, stamp classification on the top and bottom of the page.

Block 20. Limitation of Abstract. This block must be completed to assign a limitation to the abstract. Enter either UL (unlimited) or SAR (same as report). An entry in this block is necessary if the abstract is to be limited. If blank, the abstract is assumed to be unlimited.

*U.S.GPO:1993-0-358-779

FOREWORD

Opinions, interpretations, conclusions and recommendations are those of the author and are not necessarily endorsed by the US Army.

____ Where copyrighted material is quoted, permission has been obtained to use such material.

____ Where material from documents designated for limited distribution is quoted, permission has been obtained to use the material.

____ Citations of commercial organizations and trade names in this report do not constitute an official Department of Army endorsement or approval of the products or services of these organizations.

____ In conducting research using animals, the investigator(s) adhered to the "Guide for the Care and Use of Laboratory Animals," prepared by the Committee on Care and Use of Laboratory Animals of the Institute of Laboratory Resources, National Research Council (NIH Publication No. 86-23, Revised 1985).

____ For the protection of human subjects, the investigator(s) adhered to policies of applicable Federal Law 45 CFR 46.

__✓__ In conducting research utilizing recombinant DNA technology, the investigator(s) adhered to current guidelines promulgated by the National Institutes of Health.

__✓__ In the conduct of research utilizing recombinant DNA, the investigator(s) adhered to the NIH Guidelines for Research Involving Recombinant DNA Molecules.

__✓__ In the conduct of research involving hazardous organisms, the investigator(s) adhered to the CDC-NIH Guide for Biosafety in Microbiological and Biomedical Laboratories.

PI - Signature 4/1/96 Date

TABLE OF CONTENTS:

(5) INTRODUCTION:

This project has been directed towards examining ligand interactions, particularly organophosphates and other potent inhibitors, with acetylcholinesterase, by kinetic, physicochemical and recombinant DNA methods. The studies are directed to analyzing mechanisms of inhibition by organophosphates, their spontaneous hydrolysis, reactivation by oximes and the sites of interaction of reversible inhibitors.

Through these studies we not only hope to understand mechanisms of catalysis, inhibition and reactivation, but also develop means for making cholinesterase itself a useful antidote.

(6) BODY:

Our studies, to date, have employed site-specific mutagenesis, kinetic analysis, X-ray crystallography, fluorescence spectroscopy and ligand design. Below are described the projects in which we have made substantive inroads.

A. Crystallographic Analysis of the Mouse Acetylcholinesterase Fasciculin Complex

i. Production of Mammalian Acetylcholinesterase by Recombinant DNA Methods

Several groups, including our own, have been expressing recombinant cholinesterases for mutagenesis studies and a few groups have developed expression systems based on permanent transfectants and clonal selection of cells. For suitable crystallographic studies, we found it was necessary to achieve very high expression levels over short intervals so that the media is quickly subjected to purification without freezing. Typically purifications involve 70-100 mg batches of enzyme and this can be produced in a few days. The procedure involves growing cells in serum-free medium, harvesting and affinity chromatography (Marchot et al., 1996).

ii. Crystallization of an Acetylcholinesterase-Fasciculin Complex

After many trials with free enzyme without great success, we found that addition of fasciculin in a 1.2 molar stoichiometric excess, yielded high quality crystals: The only problem was that the unit crystal was large containing six monomers. Through the help of Drs. Robert Sweet and Joel Sussman at Brookhaven, Drs. Yves Bourne, Pascale Marchot and I were able to obtain diffraction patterns down to 3Å and solve the structure of the complex (Bourne et al., 1995).

The study provided the first crystal structure of a mammalian cholinesterase and enabled one to analyze interactions of a high affinity peptide inhibitor with the enzyme with high resolution at the binding interfaces.

In the description of the results, one picture is worth a thousand words and the coordinates are perhaps worth a million words. Coordinates have been made available to workers in the field and will generally be made available through Brookhaven within the month. The published article (Bourne et al., 1995) describes the three contact points: (1) tip of loop one in fasciculin with a furrow at the rim of the gorge on AChE, (2) insertion of loop two in fasciculin into the gorge mouth, (3) interaction of a proline loop in AChE with two tyrosines in the core of the fasciculin molecule. This approach has suggested several mutants in fasciculin for study, and we are presently engaged in a major study of linkages between interactive residues on fasciculin and AChE. We hope to report on this next year.

B. Studies of Enantiomeric Specificity of Organophosphates

We have felt that enantiomeric organophosphates would provide a novel approach to mutagenesis studies since: (a) the enantiomers are chemically identical in the absence of the disymmetric surface, (b) their absolute stereochemistry is known, and (c) a series of their compounds are available through collaborative studies with Drs. Harvey Berman at SUNY, Buffalo and Charles Thompson at the University of Montana.

Using a series of R- and S-phosphonates: cycloheptyl-2, 2 dimethyl butyl-, and isopropyl-methylphosphonylthiocholines, we showed that the 250-fold preference for the S-isomer can be eliminated by mutation of the acyl pocket phenylalanines (295 and 297). In fact, a three fold preference for the R-isomer is achieved. These specificity differences have been analyzed in relation to organophosphate structure and catalytic parameters for hydrolysis (Hosea, et al., 1995).

Further studies have compared the cyclohexyl, methylphosphonothiocholines with the methyl and ethyl thioates, which have a neutral leaving group. Mutation of Asp74 to the neutral isosteric Asn results in a 100-fold reduction in the rate of reaction by cycloheptyl methylphosphonyl-thiocholine whereas no change in rate is seen for the neutral thioates. The enantiomeric ratio for the thiocholines do not change. This indicates that both the R- and S-isomers have their leaving groups positioned out the gorge. These findings confirm the orientation of the attacking serine facing the plane formed by the other three substituents. In the penta-coordinate, trigonal bipyramidal transition state, the attacking serine and the thio containing leaving groups are in the apical positions. Thus, for both the acyl pocket and the Asp74 mutations, the data are consistent with the proposed orientations of the transition states for the R- and S-enantiomers (Hosea et al., in prepatation). Energy minimization of the bound phosphonates is being analyzed by molecular dynamics. The influence of other residues in the choline site (W86, Y337) are also being analyzed.

C. Studies on Fasciculin Interactions with the Peripheral Site

The crystal structure of the fasciculin-AChE has enabled us to determine residues likely to be involved in the interaction. Accordingly we have

developed a COS cell expression system using a glutamine synthetase-methionine sulfoxime amplification system. We have synthesized a synthetic gene for expression of fasciculin using a erabutoxin leader sequence. Fasciculin has been expressed with the correct sequence and specific activity and we are now producing several fasciculin mutants. T8A, T9A, R11Q, K32G, R27W, M33A and K45D. We have a fasciculin antibody which enables us to examine expression of the inactive or less active isomers.

Other studies with fasciculin are directed to its influence on the ionic strength dependence of substrate entry into the enzyme active center and the ionic strength dependence of fasciculin binding.

D. Studies of Oxime Reactivation of Ethoxymethylphosphonyl-AChE

Our initial studies were done in collaboration with Drs. Yacov Ashani and B.P. Doctor (Ashani et al., 1995). These studies show: (a) differences in reactivity for the two enantiomeric conjugates, (b) the influence of various residues surrounding the active center on the entry of oximes, (c) the basis for the enhanced reaction of HI-6 over 2-PAM. These studies will soon be extended with the enantiomerically resolved organophosphates

(7) CONCLUSIONS:

The studies of the structure of AChE coupled with the detailed analysis of enantiomeric phosphonates and other specific inhibitors have yielded important information on enzyme structure in relation to function. We will continue this line of study, but extend the work to conformation in solution since we feel that the crystal structure does not reflect the catalytically active conformational states of acetylcholinesterase.

(8) REFERENCES:

1. Radić, Z., Quinn, D.M., Vellom, D.C., Camp, S. and Taylor, P. Allosteric Control of Acetylcholinesterase Catalysis by Fasciculin, *J. Biol. Chem.*, 270:20391-20399 (1995).

2. Taylor, P. and Radic', Z. The Cholinesterases: From Genes to Proteins. *Ann. Rev. Pharmacol.* 34:281-320 (1994).

3. Marchot, P., Ravelli, R.B.G., Raves, M.L., Bourne, Y., Vellom, D.C., Kanter, J., Camp, S., Sussman, J.L. and Taylor, P. Soluble Monomeric Acetylcholinesterase from Mouse: Expression, Purification, and Crystallization in Complex with Fasciculin. *Protein Science*, April 1996, in press.

4. Hosea, N.A., Berman, H.A. and Taylor, P. Specificity and Orientation of Trigonal Carboxyl Esters and Tetrahedral Alkylphosphonyl Esters in Cholinesterases, *Biochemistry* 34:11528-11536 (1995).

5. Ashani, Y., Radić, Z., Tsigelny, I., Vellom, D.C., Pickering, N.A., Quinn, D.M., Doctor, B.P. and Taylor, P. Amino Acid Controlling Reactivation of a Chiral Organophosphonyl Conjugate of Acetylcholinesterase by Mono- and Bisquaternary Oximes. *J. Biol. Chem.*, 270:6370-6380 (1995).

6. Bourne, Y., Taylor, P. and Marchot, P. Acetylcholinesterase Inhibition by Fasciculin: Crystal Structure of the Complex. *Cell* 83:502-512 (1995).

7. Tsigelny, I., Van den Born, H.K.L., Radić, Z., Marchot, P. and Taylor, P. Theoretical Analysis of the Structure of the Peptide Fasciculin and its Docking to Acetylcholinesterase. *Protein Science*, 4:703-715 (1995).

8. Taylor, P., Radić, Z., Hosea, N.A., Camp, S., Marchot, P. and Berman, H.A. Structural Bases for the Specificity of Cholinesterase Catalysis and Inhibition. In: *Toxicology Letters*. 82/83, 453-458 (1995).

9. Taylor, P., Radic', Z., Kreienkamp, H-J., Maeda, R., Luo, Z., Fuentes, M.E., Vellom, D. and Pickering, N. Gene Expression and Ligand Specificity of Acetylcholinesterase and the Nicotinic Receptor: A Tale of Distinction at Two Cholinergic Sites, Biochemical Journal (Transactions). 22:740-745 (1994).

(9) APPENDIX:

Copies of the above articles are enclosed.

THE JOURNAL OF BIOLOGICAL CHEMISTRY
Vol. 270, No. 35, Issue of September 1, pp. 20391–20399, 1995
Printed in U.S.A.

Allosteric Control of Acetylcholinesterase Catalysis by Fasciculin*

(Received for publication, March 31, 1995, and in revised form, May 3, 1995)

Zoran Radić‡, Daniel M. Quinn§, Daniel C. Vellom¶, Shelley Camp, and Palmer Taylor

From the Department of Pharmacology, University of California San Diego, La Jolla, California 92093-0636

The interaction of fasciculin 2 was examined with wild-type and several mutant forms of acetylcholinesterase (AChE) where Trp^{86}, which lies at the base of the active center gorge, is replaced by Tyr, Phe, and Ala. The fasciculin family of peptides from snake venom bind to a peripheral site near the rim of the gorge, but at a position which still allows substrates and other inhibitors to enter the gorge. The interaction of a series of charged and uncharged carboxyl esters, alkyl phosphoryl esters, and substituted trifluoroacetophenones were analyzed with the wild-type and mutant AChEs in the presence and absence of fasciculin. We show that Trp^{86} is important for the alignment of carboxyl ester substrates in the AChE active center. The most marked influence of Trp^{86} substitution in inhibiting catalysis is seen for carboxyl esters that show rapid turnover. The extent of inhibition achieved with bound fasciculin is also greatest for efficiently catalyzed, charged substrates. When Ala is substituted for Trp^{86}, fasciculin becomes an allosteric activator instead of an inhibitor for certain substrates. Analysis of the kinetics of acylation by organophosphates and conjugation by trifluoroacetophenones, along with deconstruction of the kinetic constants for carboxyl esters, suggests that AChE inhibition by fasciculin arises from reductions of both the commitment to catalysis and diffusional entry of substrate into the gorge. The former is reflected in the ratio of the rate constant for substrate acylation to that for dissociation of the initial complex. The action of fasciculin appears to be mediated allosterically from its binding site at the rim of the gorge to affect the orientation of the side chain of Trp^{86} which lies at the gorge base.

The fasciculins, 61 amino acid peptides found in venom of snakes of the mamba or *Dendroaspis* family, are potent inhibitors of most acetylcholinesterases (EC 3.1.1.7) (AChEs)[1] (1). Three fasciculins have been identified to date with nearly identical amino acid sequences: fasciculin 1 (FAS1), FAS2, and FAS3. FAS3 binds to rat brain AChE with a dissociation constant one order of magnitude lower than that for FAS1 and FAS2 (2). The sequence and crystal structure of FAS1 (3) show that these toxins fall within a larger family of "three finger" *Elapidae* toxins which include erabutoxin, cardiotoxins, α-bungarotoxin, and α-cobratoxin. These latter toxins, however, do not inhibit AChE, whereas FAS at low concentrations does not block acetylcholine receptor function (4, 5).

Torpedo and most mammalian AChEs are inhibited by FAS at picomolar concentrations, whereas the closely related butyrylcholinesterases (EC 3.1.1.8) (BuChE) require FAS concentrations approaching millimolar for inhibition (5, 6). Three domains in AChE and butyrylcholinesterase appear responsible for their distinct substrate and inhibitor specificities (7–10). Two of them, the acyl pocket and choline-binding site of the active center, should be virtually inaccessible to FAS since they are located at the base of a narrow gorge leading to the active center of the cholinesterases. FAS, however, should access binding sites peripheral to the active center as evidenced by protection of the enzyme from FAS inhibition by micromolar concentrations of propidium and millimolar concentrations of acetylthiocholine (ATCh). This concentration range of ATCh results in substrate inhibition rather than maximal catalytic rates (2, 5). Thus, FAS appears to be specific for a peripheral site on AChE. The high affinity of FAS is primarily a reflection of a slow dissociation rate yielding a half-time of several hours, while the rate of association between FAS and AChE is only one to two orders of magnitude slower than expected for a diffusion-controlled reaction between a peptide and a protein (2, 6).

The mechanism of AChE inhibition by FAS might involve physical occlusion of the entrance to the active center gorge by the peptide, modification of the electrostatic field affecting substrate entry into the gorge, and/or an allosteric influence on the active center affecting the commitment to catalysis of bound substrate. The capacity of the FAS·AChE complex to react with diisopropyl fluorophosphate (2) reveals that the active serine at the base of the gorge remains potentially accessible to reaction with substrates. In this article we analyze the possible mechanisms of inhibition by FAS by measuring kinetic constants for inhibition of wild-type and several mutant cholinesterases. In addition, we examine the capacity of FAS to affect AChE specificity for carboxyl and alkylphosphoryl ester acylation and for conjugation with substituted trifluoroacetophenones.

MATERIALS AND METHODS

Enzymes—Wild-type and mutant mouse AChEs were expressed in HEK-293 cells following transfection of the cells with the encoding cDNA as described previously (7, 8). Cells containing the recombinant plasmids stably integrated into the DNA were used, and AChE was concentrated from the serum-free medium in which the expressing cells were grown.

Fasciculin—Purified and lyophilized FAS2 was kindly provided by Dr. Carlos Cervenansky, Instituto de Investigaciones Biologicas, Montevideo, Uruguay. Concentrations of FAS stock solutions were determined by absorbance (ϵ_{276} = 4900 M^{-1} cm^{-1}) (1).

Inhibitors—*m*-Tertbutyl trifluoroacetophenone (TFK) and *m*-trimethylammonium trifluoroacetophenone (TFK+) were synthesized as described earlier (11, 12). Paraoxon was obtained from Sigma and echothiophate from Ayerst Laboratories Inc. (Philadelphia, PA) (Structure I).

* This work was supported by United States Public Health Service Grant GM18360 (to P. T.). The costs of publication of this article were defrayed in part by the payment of page charges. This article must therefore be hereby marked "*advertisement*" in accordance with 18 U.S.C. Section 1734 solely to indicate this fact.

‡ Visiting Fellow from the Institute for Medical Research and Occupational Health, University of Zagreb, 41000 Zagreb, Croatia.

§ Visiting Professor: Dept. of Chemistry, University of Iowa, Iowa City, IA 52242.

¶ Present address: Dept. of Chemistry, City University of New York, Brooklyn, NY 11210.

[1] The abbreviations used are: AChE, acetylcholinesterase; FAS, fasciculin; ATCh, acetylthiocholine; TFK, *m*-tertbutyl trifluoroacetophenone; TFK+, *m*-trimethylammonium trifluoroacetophenone; PA, phenylacetate; *p*NPA, *p*-nitrophenylacetate.

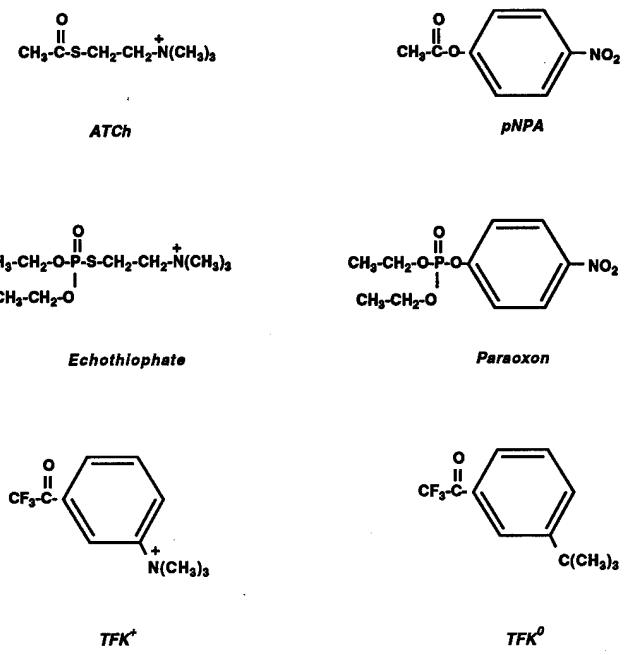

STRUCTURE I.

Enzyme Activity—Hydrolysis of ATCh, phenylacetate (PA), and *p*-nitrophenylacetate (*p*NPA) was measured spectrophotometrically using the method of Ellman *et al.* (13) for ATCh, or measurement of phenol or *p*-nitrophenol release at 270 and 405 nm, respectively. Kinetic constants for hydrolysis of the above substrates by wild-type AChE and butyrylcholinesterase and mutant AChEs were determined using a nonlinear fit of the data to the following equation (modified from Ref. 14):

$$v = \frac{(1 + b\ S/K_{ss})}{(1 + S/K_{ss})} * \frac{V}{(1 + K_m/S)} \qquad \text{(Eq. 1)}$$

where S denotes the substrate concentration, K_m and K_{ss} Michaelis-Menten and substrate inhibition constants, and b the productivity ratio of the ternary S*E*S complex to the *E*S complex (*cf.* 7).

Enzyme Inhibition—Reversible inhibition constants in the picomolar range were determined upon overnight incubation of aliquots of enzymes with increasing concentrations of FAS and fitting the remaining enzyme activities to the following equation:

$$v_{i\beta} = v_i\,[1 + \beta\ F(K_i + v_i/k)] \qquad \text{(Eq. 2)}$$

where v_i is described by (15):

$$v_i = k\{(E\text{-}K_i - F) + [(K_i + F + E)^2\text{-}4FE]^{1/2}\}/2 \qquad \text{(Eq. 3)}$$

and K_i is a reversible inhibition constant for fasciculin, F, and is also equal to k_{-F}/k_F. Equations 1 and 2 were derived from Scheme I:

$$\begin{array}{ccc} & \overset{K_s}{} & \overset{\beta\ k}{} \\ FE + S & \rightleftharpoons & FES \longrightarrow FE + P \\ {\scriptstyle k_{-F}}\downarrow\uparrow{\scriptstyle k_F} & & {\scriptstyle k_{-F}}\downarrow\uparrow{\scriptstyle k_F} \\ F & & F \\ + & & + \\ E & \overset{K_s}{\rightleftharpoons} & ES \longrightarrow E + P \\ + & & + \\ S & & S \\ {\scriptstyle K_{ss}}\downarrow\uparrow & & {\scriptstyle K_{ss}}\downarrow\uparrow \\ & \underset{K_s}{} & \underset{b\ k}{} \\ SE + S & \rightleftharpoons & SES \longrightarrow SE + P \end{array}$$

SCHEME I

with the constraints of F = 0 for Equation 1, and $K_m \ll S \ll K_{ss}$ and F ~ *E* for Equation 2.

Rate constants for FAS and trifluoroacetophenone association and dissociation were determined as described earlier (6). Rate constants for inhibition of the enzymes with paraoxon and echothiophate as well as rate constants of association of trifluoroacetophenones were determined by following the time course of the onset of inhibition using ATCh as substrate and three or more inhibitor concentrations as described earlier (16).

RESULTS

Rate and Equilibrium Constants for Fasciculin Binding to Mutant Acetylcholinesterases—FAS inhibition of wild-type and Trp^{86} substituted AChEs, measured with ATCh and *p*NPA as substrates, is shown in Fig. 1. All of the enzymes were inhibited by FAS except for Trp^{86}Ala, where the presence of FAS actually increased enzyme activity toward *p*NPA. None of the enzymes could be inhibited completely at high FAS concentrations. Residual uninhibited activities were always higher when measured with 1 mM *p*NPA compared to 1 or 10 mM ATCh. A nonlinear fit of experimental data to Equation 2 yielded K_i, the equilibrium dissociation constant for FAS, and β, the fraction of residual activity reflecting partial productivity of the F*E*S complex. These data are tabulated in Table I. Dissociation constants for FAS inhibition, K_i, were indistinguishable when measured with both substrates but were increased up to 10-fold by the various mutations. Residual enzyme activities ranged from below the experimental error of detection (~0.2%) in the case of wild-type AChE to 80 and 160% of the control activity in the Trp^{86}Ala mutant for ATCh and *p*NPA, respectively. Thus, the primary effect of substitutions at Trp^{86} is on the capacity of FAS to influence catalytic parameters once bound to enzyme rather than on FAS binding *per se*.

This behavior contrasts with the marked increases in K_i and lack of effect on β that three substitutions at peripheral site residues, Trp^{286}Arg, Tyr^{72}Asn, Tyr^{124}Gln, have on FAS interactions with AChE. It also distinguished from the virtual lack of effect that substitutions at the acyl pocket and position 337 have on FAS inhibition (6). With these mutants residual activities of the FAS complexes measured with ATCh were equivalent to those for wild-type enzyme. The residues at positions 286, 72, and 124 constitute part of the peripheral site and are located at the entrance of the active center gorge. They are directly accessible to FAS and might be expected to be in direct contact with FAS. Accordingly, their replacement should influence the dissociation constant of FAS. The two aromatic residues Trp^{86} and Tyr^{337} in the choline-binding site are located deep within the active center gorge and seem inaccessible for direct contact by FAS. Therefore, a minimal effect of their replacement by Ala on K_i of the FAS-AChE complex is not surprising. However, while Tyr^{337}Ala was almost totally inhibited by saturating FAS concentrations (>99%), hydrolysis of ATCh by Trp^{86}Ala was only inhibited about 20% at saturating FAS concentrations. Catalytic hydrolysis of *p*NPA was activated in the presence of FAS.

The small increase in K_i arising from substitutions at Trp^{86} is due to the increase in the dissociation rate constant for FAS, k_{-F} (Table II), as previously observed for the Tyr^{124}Gln and Asp^{74}Asn mutants (6). Rates of FAS association are not affected by any of the mutations where the rate constants are sufficiently slow for detection by conventional measurement.

The presence of ATCh in concentrations up to 1 mM did not affect FAS association or dissociation rate constants. FAS therefore binds with the same affinity to free enzyme and enzyme·ATCh complex. Only high ATCh concentrations, sufficient to cause substrate inhibition in wild-type AChE, decrease the rates of FAS association with wild-type and mutant enzymes (6). The decrease may be a consequence of either a modified electric field in AChE or, more likely, competition between occupation of ATCh and FAS at peripheral sites.

The Influence of Trp^{86} Substitutions on Substrate Hydrolysis—The dependences of enzyme activity on ATCh and pNPA concentrations, measured in the absence and presence of sat-

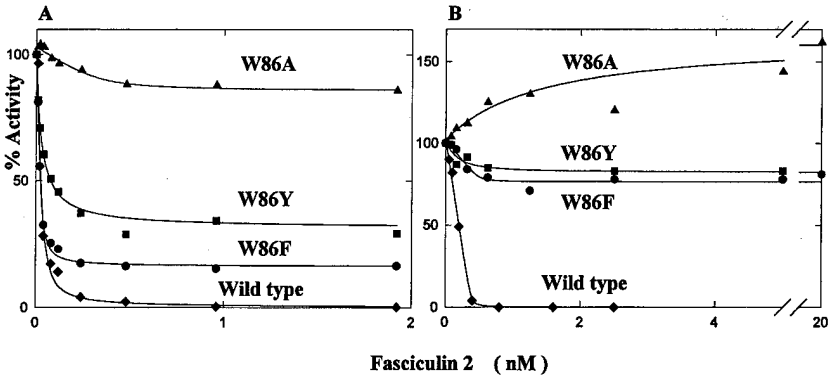

FIG. 1. **Influence of varying FAS concentrations on the activity of wild-type and mutant mouse AChE.** Enzyme activity was measured using ATCh (*A*) and *p*NPA (*B*) as substrates at concentrations denoted in Table I. Theoretical curves were obtained by fitting experimental points to equation (2). Trp at position 86 in the wild-type enzyme was replaced by Phe (*F*), Tyr (*Y*), and Ala (*A*). The recombinant DNA-derived enzymes were incubated overnight (14–16 h) with FAS prior to assay.

TABLE I

Inhibition constants for fasciculin 2 with wild-type and mutant aChEs

Equilibrium dissociation constants, K_i, and fractions of residual activity, β were obtained by nonlinear regression of Equation 2 from the sets of experimental points as illustrated in Fig. 1. Following incubation of the enzyme with FAS alone, measurements of catalysis were conducted at the specified substrate concentrations for ATCh and *p*NPA. Values are means ± standard errors.

Enzyme	Substrate	K_i	β
		pM	
AChE wild-type	1.0 or 10 mM ATCh	4.8 ± 1.8 (6)	0 (≤0.002)
	1.0 mM *p*NPA	3.7 ± 2.4 (2)	0 (≤0.06)
		4.5 ± 2.0 (8)	
W86F	10 mM ATCh	4.1 ± 1.8 (4)	0.13 ± 0.01 (5)
	1.0 mM *p*NPA	8.2 ± 3.8 (3)	0.57 ± 0.10 (3)
		5.8 ± 3.8 (7)	
W86Y	10 mM ATCh	18 ± 8 (4)	0.34 ± 0.02 (3)
	1.0 mM *p*NPA	17 ± 4 (2)	0.72 ± 0.14 (2)
		17 ± 7 (6)	
W86A	30 mM ATCh	33 ± 16 (3)	0.80 ± 0.04 (2)
	1.0 mM *p*NPA	77 ± 33 (2)	1.60 ± 0.2 (4)
		51 ± 32 (5)	

TABLE II

Rate constants for inhibition of AChE by fasciculin 2

Rate constants of association k_F and of dissociation k_{-F} are obtained by nonlinear regression of the equation describing the approach to inhibition at equilibrium (6). The ratio k_{-F}/k_F yields the equilibrium dissociation constant K_i. Experiments were conducted in the presence of the specified ATCh concentrations. Values below the line represent means ± standard errors of all values irrespective of ATCh presence.

Enzyme	ATCh	k_F	k_{-F}	K_i
	mM	10^8 *min*$^{-1}$ *M*$^{-1}$	10^{-3} *min*$^{-1}$	*pM*
AChE wild-type	1.0	1.9 ± 0.3 (4)	3.5 ± 1.5 (2)	18
	0	2.6 ± 0.4 (6)	5.0 ± 1.6 (4)	19
		2.3 ± 0.5 (10)	4.5 ± 1.8 (6)	20
W86F	1.0	2.1 ± 0.2 (3)	10 ± 1 (2)	48
	0	2.8 ± 1.1 (6)	11 ± 5 (4)	39
		2.6 ± 0.9 (9)	11 ± 4 (6)	42
W86Y	1.0	2.0 ± 0.7 (4)	15 ± 10 (2)	65
	0	1.8 ± 0.6 (7)	7 ± 0.7 (3)	41
		1.8 ± 0.6 (11)	10 ± 6 (5)	56
W86A	1.0	1.5 ± 0.8 (7)	52 ± 21 (4)	350
	0	1.4 ± 0.5 (9)	27 ± 9 (8)	180
		1.4 ± 0.6 (16)	34 ± 17 (12)	240

urating FAS are shown in Fig. 2. The relatively high enzyme concentrations (2–8 nM) used in these experiments enabled detection of residual activity in the presence of FAS. Experimental data fitted to Equation 1 yielded the constants reported in Table III; also included are the constants for hydrolysis of a neutral substrate PA, which has a high turnover rate.

Substitutions of Phe, Tyr, or Ala for Trp at position 86 influence catalysis to the largest extent with the most efficient substrate ATCh. Replacements of the indole ring of Trp with other aromatic substituents reduce k_{cat}/K_m by an order of magnitude, whereas deletion of the ring leaving the aliphatic side chain in alanine reduces k_{cat}/K_m by two orders of magnitude.

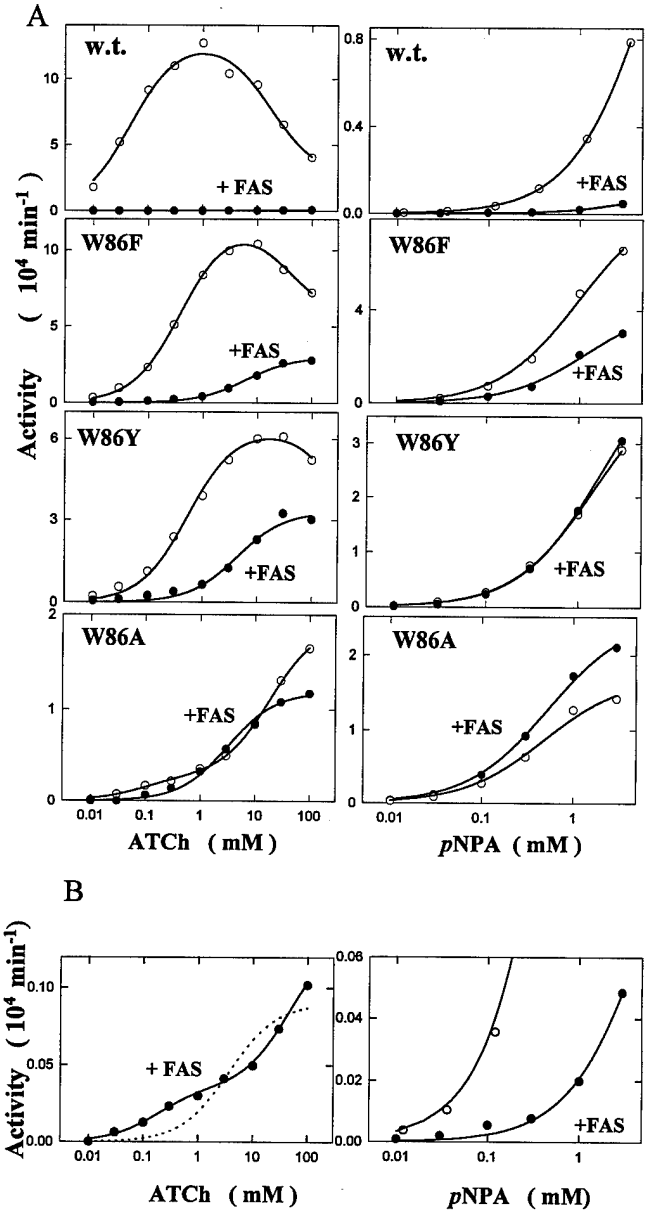

FIG. 2. **Influence of fasciculin on acetylcholinesterase catalysis.** *A*, representative plots of activity *versus* substrate concentration for high (*ATCh*) and low (*pNPA*) turnover substrates in the presence and absence of saturating (40–200 nM) FAS. Curves were obtained by nonlinear regression of Equation 1 to fit the experimental points. Fasciculin was incubated with the enzyme for at least 1 h prior to the activity measurements. *B*, substrate concentration dependence for catalysis of ATCh and *p*NPA by wild-type AChE·FAS complex. Data show enlarged *ordinates* from the *top panels*. The *solid line* was obtained by a nonlinear regression of Equation 1 to fit the experimental points. The *dotted line* shows the best fit to the data assuming Michaelis-Menten kinetics.

The reductions in k_{cat}/K_m are reflected mainly in larger K_m values except for the Trp^{86}Ala mutation where k_{cat} is reduced 50-fold. However, the Trp^{86}Ala enzyme shows substrate activation which will effectively increase catalysis at high substrate concentrations.

In the case of PA, a neutral but relatively high turnover substrate, k_{cat} was decreased only 2–3-fold for the aromatic substituents, and 10-fold for the Ala substitution. Since the K_m values also decrease slightly upon substitution of Phe or Tyr for Trp^{86}, k_{cat}/K_m is virtually unaffected. *p*NPA is a relatively poor substrate whose k_{cat}/K_m for the wild-type enzyme is nearly three orders of magnitude less than that for ATCh. All three substitutions for Trp^{86} led to an increase of k_{cat}/K_m for *p*NPA; this is a cumulative effect of lowering K_m and increasing k_{cat}.

Thus, the mutations reduced k_{cat} in a similar manner for the two substrates of rapid turnover, ATCh and PA, while two neutral substrates, PA and *p*NPA, have their K_m values similarly affected. k_{cat}/K_m was affected the most for ATCh and *p*NPA, while for PA k_{cat} was most affected.

Inhibition of Wild-type and Mutant Enzyme Substrate Hydrolysis by Fasciculin—FAS inhibition is most marked with the wild-type enzyme showing a reduction of activity by three orders of magnitude for the efficient substrates and by about 10-fold for *p*NPA (Table III). Most of the reduction arises from a diminution in k_{cat}. In all of the mutant enzymes, such large reductions in k_{cat} associated with FAS association are not evident. Substitution of Tyr or Phe for Trp results in a smaller reduction of k_{cat}/K_m for the two fast substrates upon FAS binding, and mainly arises from changes in K_m. FAS has little influence on either k_{cat} or K_m for *p*NPA. In the case of the Trp^{86}Ala enzyme, an apparent activation is measured for all three substrates. It is noteworthy that in the presence of FAS the mutant enzymes exhibit relatively similar catalytic parameters.

The Influence of Trp^{86} Substitutions and Fasciculin on Substrate Inhibition—Of the three carboxyl ester substrates only ATCh exhibited substrate inhibition in the range of substrate concentrations used. The upper concentration boundary for detection of catalysis is limited by the high rate of general base hydrolysis for ATCh and by the solubilities for aromatic esters. Introduction of smaller aromatic residues, Phe and Tyr, in place of Trp^{86} increased the substrate inhibition constant, K_{ss}, stepwise to a value 60 times larger than the wild-type constant. By contrast for the Trp^{86}Ala mutant, substrate activation was observed and no substrate inhibition was measurable (Table III). The parameter b, reflecting the efficiency of the hydrolysis of the ternary complex (*cf.* Equation 1), increased from 0.2 in wild-type to 0.4 for Trp^{86}Phe and to 8.2 for Trp^{86}Ala, whereas for the Trp^{86}Tyr mutant, ascertaining whether the mutation affects K_{ss} or b is difficult owing to the lack of pronounced substrate inhibition or activation.

The binding of FAS to the wild-type and mutant enzymes completely abolished substrate inhibition by ATCh. In fact, Fig. 2*B* shows elements of substrate activation (b = 6.8) for hydrolysis of ATCh by the complex of wild-type AChE with bound FAS. This is similar to the activation observed for ATCh hydrolysis by the Trp^{86}Ala mutant in the absence of FAS. Substrate activation should not arise as a result of FAS-ATCh competition since the FAS dissociation rate is inherently slow (*cf.* Table I).

Fasciculin Inhibition of Wild-type and Mutant Enzyme Phosphorylation by Charged and Uncharged Organophosphates—Rate constants for time-dependent inhibition of the enzymes by echothiophate and paraoxon were determined in the absence and presence of saturating concentrations of FAS (Table IV). Reaction rates for enzymes in the absence of FAS followed pseudo-first-order kinetics. However, in the presence of FAS, the time courses of inhibition were frequently biphasic. The fast phase always had the greater amplitude, but the kinetics required rate constants that differ by a factor of two to eight to fit the data. This phenomenon was independent of FAS concentration in the range of 20–120 nM where enzyme concentrations were lower than 0.3 nM. Reaction rates were determined from the initial linear portion of the inhibition curves.

The largest reduction of a second-order phosphorylation constant, approaching three orders of magnitude, was produced by Trp^{86}Ala substitution in reaction with echothiophate (Table IV). With the same mutation, paraoxon inhibition was affected only 3-fold. Substitution of Trp^{86} with Phe decreased the sec-

TABLE III

Catalytic parameters for hydrolysis of carboxyl ester substrates by mutant and wild-type AChEs

Constants were obtained by nonlinear regression analysis of Equation 1 as shown in Fig. 2. Values are means of 3–5 separate measurements. Standard errors were typically less than 30% for the measurements. Units for tabulated constants are: mM for K_m, 10^5 min^{-1} for k_{cat} and min^{-1} M^{-1} for k_{cat}/K_m.

Enzyme	Acetylthiocholine			Phenylacetate			p-Nitrophenylacetate		
	K_m	k_{cat}	k_{cat}/K_m	K_m	k_{cat}	k_{cat}/K_m	K_m	k_{cat}	k_{cat}/K_m
Wild-type	0.047[a]	1.4	3×10^9	1.5	1.9	1.3×10^8	4.6	0.22	5×10^6
+*FAS*	0.20[b]	0.004	2×10^6	2.3	0.009	3.9×10^5	3.9	0.014	4×10^5
W86F	0.32[c]	1.2	4×10^8	0.5	0.98	2.0×10^8	1.7	0.88	5×10^7
+*FAS*	11	0.30	3×10^6	5.1	0.98	1.9×10^7	2.5	0.43	2×10^7
W86Y	0.47[d]	0.64	1×10^8	0.6	0.59	1.0×10^8	1.6	0.43	3×10^7
+*FAS*	5.4	0.33	6×10^6	2.7	0.64	2.4×10^7	2.1	0.49	2×10^7
W86A	0.066[e]	0.028	4×10^7	0.67	0.20	3.0×10^7	0.81	0.17	2×10^7
+*FAS*	2	0.13	7×10^6	0.98	0.57	5.8×10^7	0.51	0.25	5×10^7

[a] K_{ss} = 17 mM, b = 0.2;
[b] K_{ss} = 96 mM, b = 6.8;
[c] K_{ss} = 50 mM, b = 0.4;
[d] K_{ss} > 300 mM, 0 < b < 1;
[e] K_{ss} = 20 mM, b = 8.2. In the presence of FAS K_{ss} and b were only measurable for the wild-type enzyme (see Fig. 2*B*). For all other substrates and enzyme combinations, appreciable substrate inhibition or activation was not detected, hence b approaches 1 or K_{ss} is substantially greater than the highest substrate concentration employed.

TABLE IV

Constants for phosphorylation of enzymes by echothiophate and paraoxon

The second order rate constant for inhibition (k_i), reversible inhibition constant (K_i) and maximal rate of phosphorylation (k_{+2}) were derived as described in Ref. 16.

Enzyme	k_i (10^6 M^{-1} min^{-1})	K_i (μM)	k_{+2} (min^{-1})
		Echothiophate	
AChE wild-type	3.5 ± 1.1 (5)	0.92 ± 0.35	3.0 ± 0.8
+*FAS*	0.37 ± 0.09 (3)	9.5 ± 3.5	3.3 ± 0.3
W86F	0.48 ± 0.05 (4)	10 ± 4	4.8 ± 2.0
+*FAS*	0.11 ± 0.04 (4)	3.2 ± 2	0.34 ± 0.08
W86Y	3.0 ± 1.4 (3)	1.5 ± 1.0	4.5 ± 1.4
+*FAS*	0.23 ± 0.05 (4)	2.1 ± 0.7	0.48 ± 0.04
W86A	0.0044 ± 0.0015 (3)	233 ± 68	1.1 ± 0.3
+*FAS*	0.27 ± 0.07 (3)	17 ± 12	3.7 ± 1.9
		Paraoxon	
AChE wild-type	1.6 ± 0.3 (3)	5.6 ± 2.1	11 ± 3
+*FAS*	2.4 ± 0.8 (3)	1.7 ± 1.1	3.4 ± 1.3
W86F	0.71 ± 0.08 (3)	4.2 ± 0.7	3.2 ± 0.7
+*FAS*	0.50 ± 0.19 (3)	3.6 ± 1.9	1.8 ± 1.2
W86Y	1.2 ± 0.6 (4)	1.4 ± 0.4	2.8 ± 1.7
+*FAS*	0.30 ± 0.09 (3)	4.3 ± 0.4	1.3 ± 0.3
W86A	0.46 ± 0.18 (3)	3.0 ± 0.8	1.8 ± 0.6
+*FAS*	0.17 ± 0.08 (3)	7.3 ± 1.7	1.2 ± 0.3

ond-order inhibition constants for echothiophate and paraoxon 7- and 3-fold, respectively, while the inhibition constant for the $Trp^{86}Tyr$ mutant enzyme was not affected (Table IV). The changes in inhibition parameters were mainly a consequence of an increase in K_i for echothiophate and a decrease in maximal phosphorylation rate for paraoxon.

FAS association had more effect on inhibition by echothiophate with its cationic leaving group than by the neutral congener, paraoxon. The second-order inhibition rate constant for the wild-type enzyme·FAS complex decreased 10-fold for echothiophate as a result of an increase in its K_i; paraoxon's overall inhibition rate constant is largely unchanged, although both K_i and k_{+2} were decreased in a compensatory fashion in the presence of FAS. FAS binding to the $Trp^{86}Phe$ and $Trp^{86}Tyr$ mutants only modestly affects inhibition by paraoxon, whereas echothiophate inhibition is decreased up to 10-fold as a consequence of a slower phosphorylation rate. FAS had a minimal effect on inhibition of the $Trp^{86}Ala$ mutant by paraoxon, but the second-order inhibition constant for echothiophate was increased 100-fold. This mutant enzyme shows both enhanced affinity and reactivity for the cationic organophosphate in the presence of FAS.

Fasciculin Inhibition of Wild-type and Mutant Enzyme Conjugation by Charged and Uncharged Substituted Trifluoroacetophenones—Substitution of aromatic and aliphatic residues for Trp^{86} results in destabilization of the hemiketal conjugates for both the charged and uncharged *m*-trimethylammonium trifluoroacetophenone and *m*-terbutyl trifluoroacetophenone isosteres (Table V). These substrate analogs differ from the carboxyl and phosphoryl esters in that the reaction product is a conjugate formed without the loss of a leaving group. Recent x-ray crystallographic studies of the complex do indeed show bond distances consistent with formation of a hemiketal conjugate (17). While mutations at position 86 are limited to 20-fold or smaller increases in the rates of dissociation of the neutral trifluoroacetophenones conjugate, the rates of dissociation of the charged conjugate are affected by one to two orders of magnitude and rates of formation up to an order of magnitude. This results in up to 1000-fold destabilization of charged conjugate for $Trp^{86}Ala$ mutant and only a 20-fold destabilization of the neutral conjugate.

Second-order inhibition rates for trifluoroacetophenones re-

TABLE V

Constants for acylation of enzymes by m-trimethylammonium trifluoroacetophenone and m-tertbutyl trifluoroacetophenone

Rate constants for formation k_F and decomposition k_{-F} of enzyme conjugates with trifluoroacetophenones were obtained by nonlinear regression of the equation describing an approach to equilibrium of bimolecular association and unimolecular dissociation (6). The association rate constants were corrected for the fraction of ketone in the unhydrated state (12).

Enzyme	k_F (10^9 M^{-1} min^{-1})	k_{-F} (min^{-1})	K_i (pM)
		m-Trimethylammonium trifluoroacetophenone	
AChE w.t.	210 ± 20 (7)	0.0011 ± 0.0003 (3)	0.0053
+*FAS*	22 ± 4 (3)	0.024 ± 0.01 (3)	1.1
W86F	110 ± 30 (5)	0.019 ± 0.006 (3)	0.17
+*FAS*	6.9 ± 2.5 (3)	0.14 ± 0.07 (4)	20
W86Y	110 ± 30 (4)	0.045 ± 0.008 (3)	0.40
+*FAS*	36 ± 22 (3)	0.15 ± 0.08 (3)	4.2
W86A	19 ± 9 (3)	0.15 ± 0.08 (3)	7.7
+*FAS*	24 ± 8 (5)	0.077 ± 0.022 (3)	3.2
		m-Tertbutyl trifluoroacetophenone	
AChE w.t.	3.0 ± 0.4 (4)	0.011 ± 0.001 (3)	3.7
+*FAS*	0.70 ± 0.15 (4)	0.060 ± 0.006 (3)	85
W86F	6.5 ± 0.3 (4)	0.036 ± 0.008 (3)	5.5
+*FAS*	1.8 ± 0.5 (3)	0.16 ± 0.03 (3)	91
W86Y	4.8 ± 1.4 (4)	0.16 ± 0 (3)	33
+*FAS*	0.32 ± 0.09 (3)	0.16 ± 0.04 (3)	510
W86A	2.6 ± 0.8 (4)	0.20 ± 0.04 (3)	78
+*FAS*	3.1 ± 0.8 (4)	0.13 ± 0.05 (3)	43

flect both formation of a reversible complex and subsequent covalent bond formation. Since rates of conjugate formation for both isosteres and all mutants showed a linear dependence on concentration, formation of conjugates was treated as a simple bimolecular association. When correlated for the ratio of non-hydrated to hydrated species (12), the measured second-order reaction rate constants for the non-hydrated ketones fell well in the range of rates for diffusion-limited reactions (10^9-10^{11} M^{-1} min^{-1}). These values are very similar to a rate of association of 4×10^{10} M^{-1} min^{-1} determined for the reversible inhibitor *N*-methylacridinium (18) and exceed k_{cat}/K_m for ATCh. Even though NMR measurements for similar trifluoroacetophenones (19) and the crystal structure of the AChE·TFK$^+$ complex (17) show that trifluoroacetophenones bind to the active serine covalently forming a hemiketal, the rate of the TFK$^+$ reaction appears limited by diffusion in the concentration range where measurements are practical.

Bound FAS affects the reaction rates of trifluoroacetophenones for both the wild-type and mutant enzymes. Rates of conjugate formation with the wild-type and Trp^{86}Phe enzymes decreased in the fasciculin complexes, and rates of conjugate dissociation increased to a greater extent with the charged than with neutral isostere. This results in a 10-fold greater increase in K_i for the charged isostere. Bound FAS also affected the interaction of both trifluoroacetophenones with Trp^{86}Tyr and Trp^{86}Ala. While bound FAS increased K_i for Trp^{86}Tyr 10-fold, the K_i for Trp^{86}Ala mutant decreased about 2-fold. It is interesting that a 1000-fold difference in K_i between charged and uncharged isosteres for wild-type AChE is significantly reduced 5–100-fold when FAS is bound to the mutant or wild-type enzymes.

Bound FAS decreased rates of diffusion of the cationic TFK$^+$ into the enzyme gorge by an order of magnitude. Since bound FAS may restrict diffusion-limited entry into the gorge, the reductions in rate of TFK$^+$ association may reflect the gating influence of the positively charged FAS molecule toward entry of cationic substrates into the gorge. In addition, substitution of aromatic and aliphatic residues at position 86 diminishes the stability of the hemiketal conjugates formed between the substituted trifluoroacetophenones and AChE. These factors are reflected in a larger k_{-F} and a smaller k_F. As the overall k_F diminishes, diffusion is no longer rate-limiting. With the substitutions at position 86 which form the less stable complexes, FAS has a greatly diminished influence on the reaction. FAS affects rates of dissociation of the conjugate presumably by allosterically influencing the site of TFK binding. The overall effect of FAS binding is similar in magnitude to substitution of Ala for Trp^{86}.

DISCUSSION

In this study we have examined the influence of a peptidic peripheral site inhibitor, FAS 2, on the catalytic parameters of AChE. Substantial evidence has accumulated to show that FAS binds at a peripheral site to regulate substrate catalysis (1, 2, 5, 6). We show here by examining mutations in the choline binding subsite at the base of the gorge that FAS, by acting near the rim of the gorge, controls the overall configuration of the substrate-binding site. By comparing charged and uncharged substrates, one approaches the question of whether FAS affects initial entry of substrate into the gorge or the subsequent steps of catalytic turnover of bound substrate. To this end it becomes useful to deconstruct the catalytic parameters, k_{cat} and K_m, where possible, into primary constants. For Scheme II below:

$$E + AB \underset{k_{-1}}{\overset{k_1}{\rightleftharpoons}} E{*}AB \xrightarrow{k_2} EA + B \xrightarrow{k_3} E + A$$

$$K_m = \frac{(k_{-1} + k_2)}{k_1} \cdot \frac{k_3}{(k_2 + k_3)} \qquad k_{cat} = \frac{k_2 \cdot k_3}{k_2 + k_3} \qquad k_{cat}/K_m = \frac{k_1 \cdot k_2}{k + k_2}$$

SCHEME II

we have examined three classes of substrates designated by AB: (*a*) the carboxylic acid esters: ATCh, *p*NPA, and PA. These acetoxy esters differ about 600-fold in catalytic efficiency, k_{cat}/K_m, with the following order ATCh>PA>*p*NPA; (*b*) the symmetric organophosphates which only differ in their leaving groups: the charged, diethoxyphosphoryl thiocholine (echothiophate), and uncharged diethoxyphosphoryl *p*-nitrophenol (paraoxon). These two compounds yield structurally identical

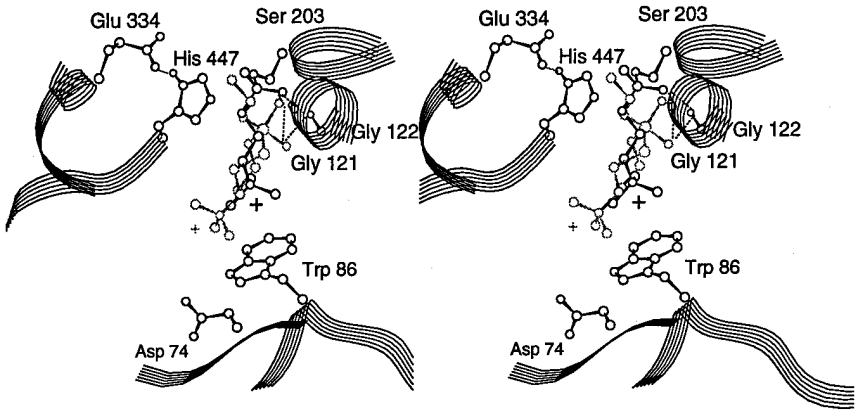

FIG. 3. **Presumed orientation of the transition states for acylation of AChE by ATCh (*black*) and echothiophate (*gray*) obtained by molecular modeling of the acylation transition state for the reaction of the two compounds with AChE.** Molecular dynamics modeling was performed as described in Ref. 28.

covalent conjugates with the active serine. Echothiophate and paraoxon have the same leaving groups as ATCh and *p*NPA, respectively. In contrast to the carboxyl esters, only rates of acylation require consideration in analyzing substrate kinetics. For organophosphates K_m (now defined as K_i) is reduced to $(k_1 + k_2)/k_1$, and k_{cat} is reduced to k_2; (*c*) isosteric trifluoroacetophenones which contain charged and uncharged moieties at the *meta* position. The conjugation reaction here only involves nucleophilic addition by Ser^{200} to form the hemiketal without loss of a leaving group. Consequently K_m reduces to the ratio of k_{-1} and k_1. There is no substrate turnover, and k_{cat} is zero.

Since the AChE·FAS complex remains catalytically active and susceptible to phosphorylation by diisopropyl fluorophosphate (2), or other organophosphates (Table IV), FAS does not serve as a physical barrier to block totally substrate entry into the AChE active center gorge. Rather, binding of FAS to the enzyme appears to affect the chemical acylation step of the catalytic reaction described by k_2. This is indicated by pronounced reductions in k_{cat} and k_{cat}/K_m for the three carboxyl esters, as opposed to modest increases in their K_m values. Values of k_{cat} and k_{cat}/K_m for hydrolysis of ATCh and PA by human AChE in the presence of FAS decrease significantly in D_2O buffers, while in the absence of FAS the isotope effect of D_2O is small (20). These findings indicate that FAS reduces the rate of ATCh and PA acylation described by k_2.

In addition, cationic ligands may find their entry to the active center diminished due to the electrostatic restrictions imposed by bound FAS. Positively charged ATCh, unlike the other two neutral substrates, has a 5-fold greater K_m for the AChE·FAS complex compared to AChE. Also, charged organophosphates and trifluoroacetophenones react with AChE·FAS complex at rates an order of magnitude slower than with AChE. The Trp^{86}Ala enzyme is an exception where FAS accelerates an inherently slow rate of echothiophate inhibition while exerting little influence on the reaction with the neutral organophosphates.

Substitution of Trp^{86} by two other aromatic residues, Phe and Tyr, abolishes the capacity of FAS to reduce acylation rates, whereas introduction of Ala at this position results in bound FAS causing a slight increase of acylation rates for all substrates. Thus, unlike the other residues in the choline binding site (*i.e.* Tyr^{337}) and acyl pocket (*i.e.* Phe^{295}, Phe^{297}) (6), the indole ring of Trp^{86} is linked to the mechanism of FAS inhibition. The aromatic substitutions, however, slightly enhance the increase in K_m induced by FAS for the two most effective substrates ATCh and PA. This suggests that an aromatic residue at position 86 influences k_1 or k_{-1} in the FAS·AChE complex. For catalytic hydrolysis of both ATCh and PA, k_{-1} is likely to be increased by FAS, while we might also expect a reduction of k_1 for the charged substrate ATCh. Catalytic hydrolysis of *p*NPA is far slower (Table III), and it has been suggested, based on solvent isotope effects on acylation rates, that it is rate limited by the chemical acylation step (21, 22).

Introduction of an aliphatic residue at position 86 exerts a large reduction in the catalytic rates for both fast substrates PhAc and ATCh. With the less efficient catalysis, the influence of FAS is diminished so that the FAS complexes of these mutant enzymes have catalytic constants which approach those of wild-type enzyme·FAS complex. The mild acceleration in catalytic rate for the Trp^{86}Ala AChE·FAS complex is likely to be a consequence of an increase in the acylation rate constant k_2, indicating an enhanced capacity to stabilize acylation transition state upon FAS binding. This conclusion is supported by the observation that the binding of FAS increases the affinity of the Trp^{86}Ala mutant for both charged and neutral trifluoroacetophenones, substrate transition state analogs. Hydrolysis of ATCh by the Trp to Ala mutant enzyme is enhanced upon binding of FAS primarily through enhancing k_2, suggesting an improved fit of the ATCh transition state in the active center gorge.

Ordentlich and colleagues (23) previously examined the Trp^{86}Ala mutation on rates of catalytic hydrolysis of ATCh, *p*NPA, and other carboxyl esters. They also observed a dramatic reduction on ATCh hydrolysis with the Trp^{86}Ala mutation and smaller effects on other substrates. They suggested that Trp^{86} is not involved in the stabilization of uncharged substrates. However, the Trp^{86} to Ala mutation accompanies a large volume change which must be accommodated by either collapse of the peptide backbone or entry of several water molecules into the gorge. Analysis of the kinetics through stepwise replacement of Trp by Tyr, Phe, and then Ala suggests that subtle changes in alignment of the associated carboxyl ester are sufficient to dramatically decrease catalysis. Moreover, occupation of the peripheral site by FAS may affect the alignment of the substrate through an allosteric influence mediated between the lip of the gorge and its base. Support for this linkage comes from previous studies of AChE structure involving circular dichroism, fluorescence spectroscopy, and site-specific mutagenesis when propidium is bound to the peripheral site (24–26). Efficient catalysis requires an optimal alignment of substrate, and FAS exhibits its most dramatic effects on inhibition parameters for the fast substrate. When alignment is compromised through residue substitution at position 86, FAS has a far smaller effect on catalysis and can, in some cases, slightly increase k_{cat}/K_m.

Since both Trp^{86} mutations and FAS affect substrate inhibition parameters, the binding of a second substrate molecule at the FAS site may also mediate its effect on catalysis through Trp^{86} (6, 27). Although FAS binding and Trp^{86} substitutions occur at two different locations, they both influence the alignment of residues in the site of ATCh catalysis and prevent the most productive binding orientation of substrate. Substrate

activation of the residual activity in the FAS-AChE complex (Fig. 2*B*), however, may be a consequence of ATCh interaction with still another site on the enzyme.

The effect of Trp^{86} substitutions on acylation by the organophosphates resembles that seen for the carboxylic acid esters. The substrate pairs of ATCh and of echothiophate and *p*-nitrophenyl acetate and paraoxon share identical leaving groups, and their reaction rates show similar sensitivities to Trp^{86} substitution. This underscores the importance of residue 86 in affecting the position of the leaving group. However, FAS is a less effective inhibitor of echothiophate acylation in the wild-type enzyme by at least two orders of magnitude. Compared to ATCh, the thiocholine leaving group in echothiophate is directed slightly farther away from Trp^{86} and closer to the anionic residue of Asp^{74}, due to the tetrahedral geometry around the phosphorus in echothiophate (Fig. 3).[2] The difference in the leaving group orientations in the transition state complexes with FAS-AChE may cause Trp^{86} substitutions to affect acylation rates in markedly different manners since stabilizing forces contributed by Trp^{86} decrease with the sixth power of distance (29). This conclusion is supported by the significantly greater acceleration of echothiophate inhibition in Trp^{86}Ala·FAS complex as compared to the mild acceleration of ATCh hydrolysis.

The geometry of the planar trifluoroacetophenones and the positioning of the carbonyl oxygen toward the oxyanion hole should direct quaternary ammonium or tertbutyl groups to a position equivalent to that of choline in ATCh, in close apposition to Trp^{86} as confirmed by crystal structure of the charged TFK·AChE complex (17). These tetrahedral adducts resemble the acylation transition state analogues of ATCh hydrolysis. That FAS affects k_{cat}/K_m for substrates and K_i for trifluoroacetophenones to similar extents suggests that the major mode of FAS action is to affect stabilization of the transition state for hydrolysis of substrates.

Correlations of the free energy of association of the TFKs with AChE in the absence and presence of FAS with molar refractivities and hydrophobicities of residues at position 86 (Fig. 4) support such a mechanism. In the absence of FAS, the pK_i values for both TFKs increase with both molar refractivity and hydrophobicity constants for the residues at position 86 indicating that this residue is directly involved in stabilization of the TFK·enzyme complex. In the presence of FAS, the contributions to the energy of stabilization of the aromatic residues at position 86 remain unchanged and roughly equivalent to that of Ala. Hence FAS association at a distant location on AChE appears to negate the stabilization energy conferred by the electron-rich indole ring, perhaps by allosterically influencing its alignment.

Recently, it was suggested that products of acetylcholine hydrolysis or perhaps solvent molecules required for catalysis could exchange with bulk solvent through an opening in the AChE gorge wall behind Trp^{86}, termed the "back door" (31, 32). A vectoral movement of substrate and products would pose additional energetic requirements for acylation and deacylation in catalysis. Mutagenesis of residues in the region of the putative back door region has not yielded supportive evidence for this hypothesis (33), nor is there substantive evidence for choline dissociation being a rate limitation. One might assume that diminished FAS inhibition, arising from the smaller side

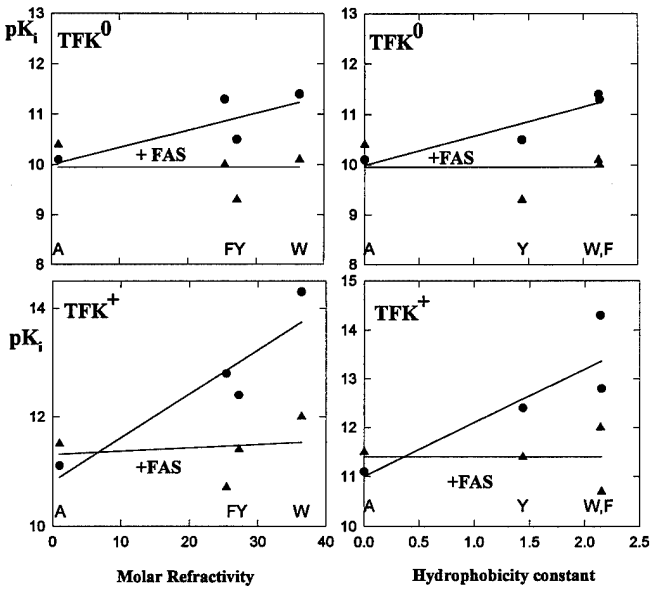

FIG. 4. **Relationship between the inhibition constant of trifluoromethyl acetophenones (*TFK*^{0} and *TFK*$^+$) and the molar refractivity and hydrophobicity of the side chain at residue 86 in the AChE choline subsite.** Molar refractivity and hydrophobicity indexes for amino acid residues were taken from Ref. 30 and analyzed according to Nair *et al.* (29). Measurements were made in the presence and in the absence of 40 nM FAS following incubation with FAS for at least 1 h.

[2] N. Hosea, H. A. Berman, and P. Taylor, manuscript submitted.

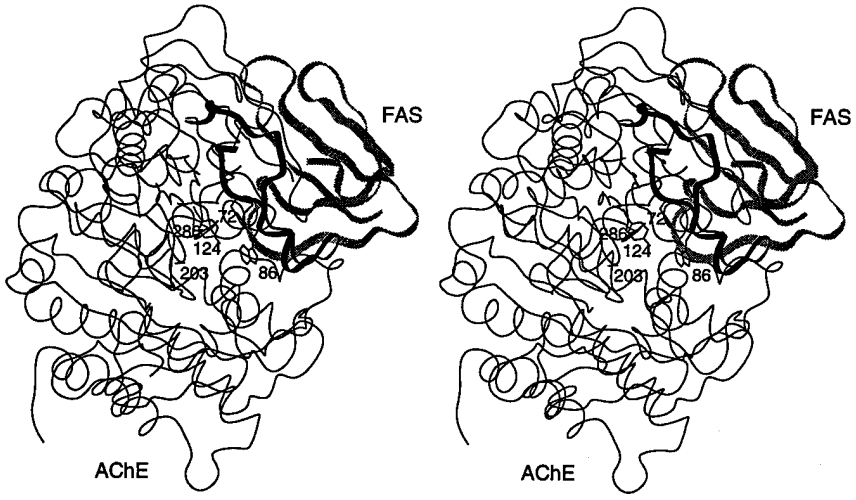

FIG. 5. **Stereo ribbon diagram of a model of the fasciculin·AChE complex (34).** The first disulfide AChE loop (Cys^{69}-Cys^{96}) is represented by a *bold ribbon*. Side chains of Trp^{86}, active Ser^{203}, and peripheral site residues Tyr^{72}, Tyr^{124}, and Trp^{286} are displayed and labeled with their numbers. FAS represented by the *gray ribbon* is sitting atop the disulfide loop, while interacting with peripheral site residues.

chain at position 86, might arise from increasing the opening at the putative back door thereby increasing the rate of exchange of ligands between bulk solvent and the active center gorge. The catalytic constants may, however, point to the opposite conclusion. FAS most effectively blocks acylation of rapidly reacting substrates and the most rapid catalysis is achieved with an indole residue at position 86. Also, rates of dissociation of positive and neutral trifluoroacetophenones increase with small side chains at position 86. The binding of FAS further increases these dissociation rates, whereas one might expect a decrease if it directly or indirectly closed the back door.

While the three-dimensional structure of AChE·FAS complex is still unknown, one may speculate on a possible sequence of events associated with FAS binding and enzyme inhibition. Identification of interacting residues on AChE through site-specific mutagenesis (6), combined with an computational analysis of the interacting forces between FAS and AChE (34), suggests that a likely area of their interaction is the most amino-terminal disulfide loop in AChE encompassing residues 69–96 (Fig. 5). This loop covers the active center gorge as a "lid" with Trp^{86} residing at its tip. Tyr^{72}, one of the aromatic residues that form the peripheral site, is located at the base of the loop, while the adjacent residues Tyr^{124} and Trp^{286}, which also contribute to the peripheral site, reside on the other two AChE loops. Binding of a ligand to the peripheral site could therefore serve to partly close the lid. A conformational change of a homologous loop in a lipase from *Candida rugosa* was shown from the crystal structure to be essential for catalysis (35), wherein an open site is found in the active state. While there are no indications from crystallography of mobility of the homologous loop in AChE (36), flexibility of such a loop may be required for efficient catalysis. Substitutions of two aspartates at positions 92 and 93 in *Torpedo californica* AChE (equivalent to Asp^{94} and Asp^{95} in mouse AChE) with neutral residues at the base of this loop yield inactive enzyme (37) and are expected to break at least two salt bridges.

Hence FAS inhibition may arise from an influence on two steps in the catalytic process. For cationic ligands where catalysis is efficient, FAS may serve to partially gate their entry therein diminishing k_1 in Scheme I. It also exerts an allosteric influence on the alignment of all substrates in the active center gorge. This occurs in the transition state where it apparently affects the configuration of the leaving group in achieving productive acylation. Capping a potentially mobile loop which extends between the lip of the gorge, containing the peripheral site, and its base, where Trp^{86} resides, represents an attractive structural basis for an allosteric linkage. This may serve to decrease the stability of the initial complexes in the active center and/or diminish the commitment to catalysis, represented by k_2/k_{-1} (22).

REFERENCES

1. Karlsson, E., Mbugua, P. M. & Rodriguez-Ithurralde, D. (1984) *J. Physiol. (Paris)* **79,** 232–240
2. Marchot, P., Khelif, A., Ji, Y. H., Mansuelle, P. & Bougis, P. E. (1993) *J. Biol. Chem.* **268,** 12458–12467
3. Le Du, M. H., Marchot, P., Bougis, P. E. & Fontecilla-Camps, J. C. (1992) *J. Biol. Chem.* **267,** 22122–22130
4. Endo, T. & Tamiya, N. (1987) *Pharmacol. & Ther.* **34,** 403–451
5. Karlsson, E., Mbugua, P. M. & Rodriguez-Ithurralde, D. (1985) *Pharmacol. & Ther.* **30,** 259–276
6. Radić, Z., Duran, R., Vellom, D. C., Li, Y., Cervenansky, C. & Taylor, P. (1994) *J. Biol. Chem.* **269,** 11233–11239
7. Radić, Z., Pickering, N., Vellom, D. C., Camp, S. & Taylor, P. (1993) *Biochemistry* **32,** 12074–12084
8. Vellom, D. C., Radić, Z., Li, Y., Pickering, N. A., Camp, S. & Taylor, P. (1993) *Biochemistry* **32,** 12–17
9. Harel, M., Sussman, J. L., Krejci, E., Bon, S., Chanal, P., Massoulié, J. & Silman, I. (1992) *Proc. Natl. Acad. Sci. U. S. A.* **89,** 10827–10831
10. Loewenstein, Y., Gnatt, A., Neville, L. F. & Soreq, H. (1993) *J. Mol. Biol.* **234,** 289–296
11. Nair, H. K. & Quinn, D. M. (1993) *Bioorg. Med. Chem. Lett.* **3,** 2619–2622
12. Nair, H. K., Lee, K. & Quinn, D. M. (1993) *J. Am. Chem. Soc.* **115,** 9939–9941
13. Ellman, G. L., Courtney, K. D., Andres, V., Jr. & Featherstone, R. M. (1961) *Biochem. Pharmacol.* **7,** 88–95
14. Aldridge, W. N. & Reiner, E. (1972) *Enzyme Inhibitors As Substrates* pp. 1–328, North-Holland, Amsterdam
15. Ackermann, W. W. & Potter, V. R. (1949) *Proc. Soc. Exp. Biol. Med.* **72,** 1–9
16. Radić, Z., Gibney, G., Kawamoto, S., MacPhee-Quigley, K., Bongiorno, C. & Taylor, P. (1992) *Biochemistry* **31,** 9760–9767
17. Harel, M., Silman, I. & Sussman, J. L. (1995) in *Enzymes of the Cholinesterase Family* (Quinn, D. M., ed) Plenum, New York, in press
18. Nolte, H.-J., Rosenberry, T. L. & Neumann, E. (1980) *Biochemistry* **19,** 3705–3711
19. Linderman, R. J., Leazer, J., Roe, R. M., Venkatesh, K., Selinsky, B. S. & London, R. E. (1988) *Pest. Biochem. Physiol.* **31,** 187–194
20. Rosenberry, T. L., Eastman, J. & Haas, R. (1995) in *Enzymes of the Cholinesterase Family* (Quinn, D. M., ed) Plenum, New York, in press
21. Rosenberry, T. L. (1975) *Adv. Enzymol. Relat. Areas Mol. Biol.* **43,** 103–218
22. Quinn, D. M. (1987) *Chem. Rev.* **87,** 955–979
23. Ordentlich, A., Barak, D., Kronman, C., Flashner, Y., Leitner, M., Segall, Y., Ariel, N., Cohen, S., Velan, B. & Shafferman, A. (1993) *J. Biol. Chem.* **268,** 17083–17095
24. Epstein, D. J., Berman, H. A. & Taylor, P. (1979) *Biochemistry* **18,** 4749–4754
25. Berman, H. A., Becktel, W. & Taylor, P. (1981) *Biochemistry* **20,** 4803–4810
26. Barak, D., Kronman, C., Ordentlich, A., Ariel, N., Bromberg, A., Marcus, D., Lazar, A., Velan, B. & Shafferman, A. (1994) *J. Biol. Chem.* **269,** 6296–6305
27. Radić, Z., Reiner, E. & Taylor, P. (1991) *Mol. Pharmacol.* **39,** 98–104
28. Ashani, Y., Radić, Z., Tsigelny, I., Vellom, D. C., Pickering, N. A., Quinn, D. M., Doctor, B. P. & Taylor, P. (1995) *J. Biol. Chem.* **270,** 6370–6380
29. Nair, H. K., Seravalli, J., Arbuckle, T. & Quinn, D. M. (1994) *Biochemistry,* **33,** 8566–8576
30. Hansch, C. & Leo, A. (1979) *Substituent Constants for Correlation Analysis in Chemistry and Biology,* pp. 1–339, John Wiley & Sons, New York
31. Axelsen, P. H., Harel, M., Silman, I. & Sussman, J. L. (1994) *Protein Sci.* **3,** 188–197
32. Gilson, M. K., Straatsma, T. P., McCammon, J. A., Ripoll, D. R., Faerman, C. H., Axelsen, P. H., Silman, I. & Sussman, J. L. (1994) *Science* **263,** 1276–1278
33. Shafferman, A. Ordentlich, A., Barak, D., Kronman, C., Ber, R., Bino, T., Ariel, N., Osman, R. & Velan, B. (1994) *EMBO J.* **13,** 3448–3455
34. Van den Born, H. K. L., Radić, Z., Marchot, P., Taylor, P. & Tsigelny, I. (1995) *Protein Sci.* **4,** 703–715
35. Grochulski, P., Li, Y., Schrag, J. D. & Cygler, M. (1994) *Protein Sci.* **3,** 82–91
36. Sussman, J. L., Harel, M., Frolow, F., Oefner, C., Goldman, A., Toker, L. & Silman, I. (1991) *Science* **253,** 872–879
37. Bücht, G., Artursson, E., Haggstrom, B., Radić, Z., Osterman, A. & Hjalmarsson, K. (1994) *Biochem. Biophys. Acta* **1209,** 265–273

Annu. Rev. Pharmacol. Toxicol. 1994. 34:281–320

THE CHOLINESTERASES: FROM GENES TO PROTEINS

Palmer Taylor and Zoran Radić[1]
Department of Pharmacology, University of California, San Diego, La Jolla, California 92093

KEY WORDS: acetylcholinesterase, butyrylcholinesterase, alternative mRNA processing, serine hydrolase, site-specific mutagenesis

INTRODUCTION

Linkages between cholinesterases and the pharmacological sciences extend back to the mid-nineteenth century when the first organophosphate was synthesized (1) and physostigmine was recognized in the western world for possessing pharmacological activity (2). However, not until Sir Henry Dale (3) delineated two components of the cholinergic nervous system was the suggestion made that physostigmine inhibited an enzyme that catalyzed the breakdown of choline esters. Dale's and later Loewi & Navratil's (4) studies established a role for acetylcholine as a labile neurotransmitter. The high turnover number of acetylcholinesterase (AChE), the specificity of its inhibitors, and the selectivity of thiocholine-metal ion interactions provided the bases for sensitive in vitro and in situ assay systems (5–7). Several cholinesterase inhibitors remain of value as medicinal agents and insecticides, but others possess the potential for insidious use as chemical warfare agents (8).

Despite this long history of study, less than a decade has passed since the primary structure of a cholinesterase was determined (9), and only in 1991 was its crystal structure solved (10). Clearly, these recent events have added a new perspective to cholinesterase research wherein all facets of gene expression become amenable to study and structure-function relationships within this family of enzymes can be approached at an atomic level

[1]Visiting Fellow from Institute for Medical Research and Occupational Health, University of Zagreb, Croatia

0362-1642/94/0415-0281$05.00

of resolution. This review deals primarily with the new structural information that has emerged since these developments. Not only has this structural framework added a dimension to the study of catalytic mechanisms and inhibitor specificity, but it has also enabled investigators to extend the interpretations of earlier studies where conclusions were arrived at without benefit of a structural template.

The reader should refer to other reviews for complementary or background information. Classic though somewhat dated reviews detail catalytic mechanisms (11), biochemical and catalytic properties (11, 12), and genetics of the cholinesterases (13, 14). Recently, short overviews (15, 16) and an exhaustive review (17) with a perspective on structure have been written. A recent monograph details several of the ongoing research events in the field (18).

THE CHOLINESTERASE FAMILY OF PROTEINS

The initial sequence of cholinesterase showed no global amino acid homology with any other serine hydrolases despite similarity of functional parameters and a common pentapeptide sequence around the active center serine (9). Rather, sequence identity was evident between cholinesterase and the carboxyl-terminal region of thyroglobulin (9, 19). This discovery provided the first indication that the cholinesterases defined a new family of serine hydrolases and that this gene family possessed an unexpected diversity in that non-hydrolase functions could be subserved by a common structural matrix. Soon after *Torpedo* AChE was cloned, the *Drosophila* cholinesterase gene was located from genetic studies and its sequence determined (20). This was followed by a butyrylcholinesterase (BuChE) sequence determined by amino acid sequencing (21) and by molecular cloning (22, 23). Mammalian AChEs proved more intractable, but in 1990 the mouse, bovine, and human enzyme sequences were completed (24–26). Other cholinesterase sequences, rabbit BuChE (27), rat AChE (28), *Anopheles* cholinesterase (29), and chicken AChE (30) have been reported. Distinct hydrolases from *Dictyostelium* (31, 32), *Drosophila* and other insects (33–36), the fungi *Geotrichum* and *Candida* (37), and mammals show sequence identities. Included in the mammalian group are microsomal carboxyl esterases (38, 39), lysophospholipase (40), and cholesterol esterase (41). Other proteins, while apparently not similar in primary structure, show a common folding pattern termed the α/β hydrolase fold (42). Included in this group are a wheat carboxypeptidase with a serine hydrolase mechanism (43), dienelactone hydrolase (44), and haloalkane dehalogenase (45).

In addition, members of the tactin family, glutactin and neurotactin, are homologous to the cholinesterases, but like thyroglobulin lack hydrolase activity (46, 47). No mammalian homologue of the tactins is yet known,

but in *Drosophila* tactins are believed to function in establishing contacts between heterologous cells during development. In short, a functionally eclectic family of proteins has emerged whose functional capacities extend well beyond simple hydrolase function (Figure 1). Several recent reviews have tabulated sequence identities within this family (42, 48, 49).

Since the initial AChE cloning relied on amino acid sequence to obtain oligonucleotide probes, the disulfide bond profile was established not long after in AChE (50) and BuChE (51). Labeling with radioactive DFP distinguished the catalytic serine, S_{200} (52). The histidine, H_{440}, involved in the catalytic triad was established through mutagenesis (53), but the third component in the triad, a diacidic amino acid, E_{327}, was not defined until the crystal structure was solved (10). All members of the family possess histidine in the 440 reference position, while either glutamate (as in the cholinesterases) or aspartate is found at the position corresponding to E_{327}. Corresponding residues to E_{327} and H_{440} can be found in the hydrolases of this series; however, in some cases, the alignments require liberty in gapping the residues. The three disulfide loops (50, 51) are conserved in several proteins in the family (all cholinesterases and the *Dictyostelium* proteins); others contain the amino-terminal two loops while *Culex* Est B and juvenile hormone esterase contain only the most amino-terminal loop. The third loop present in the cholinesterases, in addition to containing the histidine of the catalytic triad, functions in intersubunit contacts forming a four-helix bundle involved in subunit association (10). An additional cysteine is found very near the carboxyl-terminus that is involved in intersubunit disulfide bonds.

Intersubunit disulfide bonding occurs with identical catalytic subunits to form dimers; typically, noncovalent associations of dimers form homomeric tetramers. Heteromeric oligomers also form between the catalytic subunits and either a lipid-linked subunit or a collagen-containing subunit. These species are shown in Figure 2*A*. In mouse AChE one splicing variant does not contain a carboxyl-terminal cysteine, resulting in a monomeric enzyme species. In some cholinesterases, an eighth cysteine is found as a free sulfhydryl in variable locations. Its role in situ is unknown, but it proved invaluable for obtaining crystals of heavy metal derivatives of *Torpedo* AChE (10).

RELATIONSHIP OF PROTEIN STRUCTURE TO GENE ORGANIZATION

A comparison of protein and gene structures of the cholinesterases from different species provides additional insights into structure-function relationships. Typically, the cholinesterases have been defined as AChEs (EC 3.1.1.7) and BuChEs (EC 3.1.1.8). The latter have broad specificity with

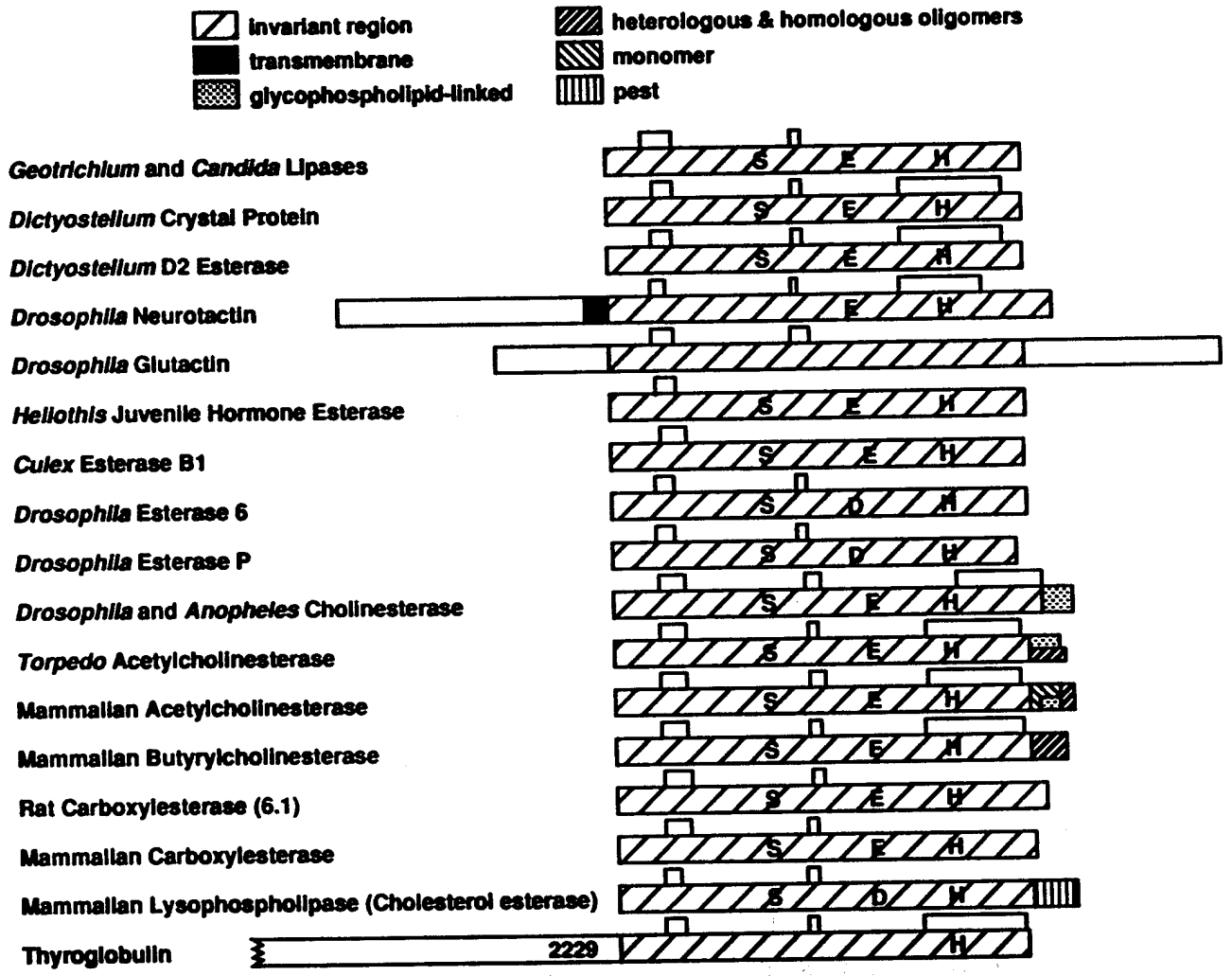

Figure 1 Relationships of some of the proteins with sequence similarities to the cholinesterases. The serines, histidines and glutamates in homologous positions to S_{200}, H_{440}, and E_{327} in *Torpedo* acetylcholinesterase are shown. Intrasubunit-disulfide bonds are shown by the bracketed loops above the sequence (modified from Ref. 16).

respect to the size of the substrate acyl group, while for AChE, a marked reduction in catalysis is seen between propionylcholine and butyrylcholine (54). Over the decades several selective inhibitors for AChE and BuChE have been found (55).

Drosophila appears to harbor only a single cholinesterase gene, which has features of both the AChEs and BuChEs in its encoded protein sequence (20). Similarly, its catalytic specificity is also intermediate between the two enzymes (56). Hence, it seems likely that the acetyl and butyryl subtypes of cholinesterase, which are found in lower vertebrates (57), diverged in the broad time frame between insects and lower vertebrates. Interestingly, genetic and biochemical evidence suggests multiple cholinesterase genes, perhaps three, in *Caenorhabditis elegans* (58, 59). Since the *C. elegans* genes have not been cloned, ancestral relationships in terms of sequences and specificity have yet to be ascertained.

Genomic clones of *Drosophila* cholinesterase (20), *Torpedo* AChE (60), human AChE (61), mouse AChE (61), and human BuChE (62) have been isolated. The *Drosophila* gene contains multiple exons, whereas *Torpedo* and mammalian AChE genes have relatively simple organizations. At present, our knowledge of AChE gene organization is more advanced than for BuChE, and there is as yet no evidence for alternative splicing of the BuChE gene. The open reading frame of human BuChE gene is encoded in over 50 kb of sequence and contains very large introns, whereas the comparable region in the mammalian AChE genes are encoded within 4.5–4.7 kb. The *Torpedo* AChE gene is larger; it requires 25 kb of sequence. However, the exon-intron junctions are identical in the open reading frames for AChE and BuChE, except for an additional intron located between exons 2 and 3 in mammalian AChE (Figure 2*B*).

Alternative mRNA processing is found at the 5′ and 3′ ends of the AChE gene (60, 61, 63–67), but only the splicing at the 3′ end of the open reading frame is responsible for the various molecular species of AChE. This splice occurs at amino acid 535 in the *Torpedo* sequence (68) and at 543 in mouse and human (61). Splicing in *Torpedo* gives rise to two splice alternatives, a hydrophilic peptide of 40 amino acids in length and a hydrophobic peptide of 38 amino acids; the latter appears to be cleaved after cysteine 537 with the concomitant addition of a glycophospholipid. A cDNA clone isolated from *Torpedo marmorata* has raised the possibility of a continuation of exon 4 into the retained intron (64); however, the existence of this mRNA species or the gene product awaits documentation.

In the mouse enzyme two splicing alternatives give rise to a hydrophilic species: either splicing exon 4 to exon 6 yielding a cysteine containing a 40-amino acid peptide or a direct extension into the retained intron yielding a 30-amino acid extension devoid of a cysteine (61). Hence, the latter

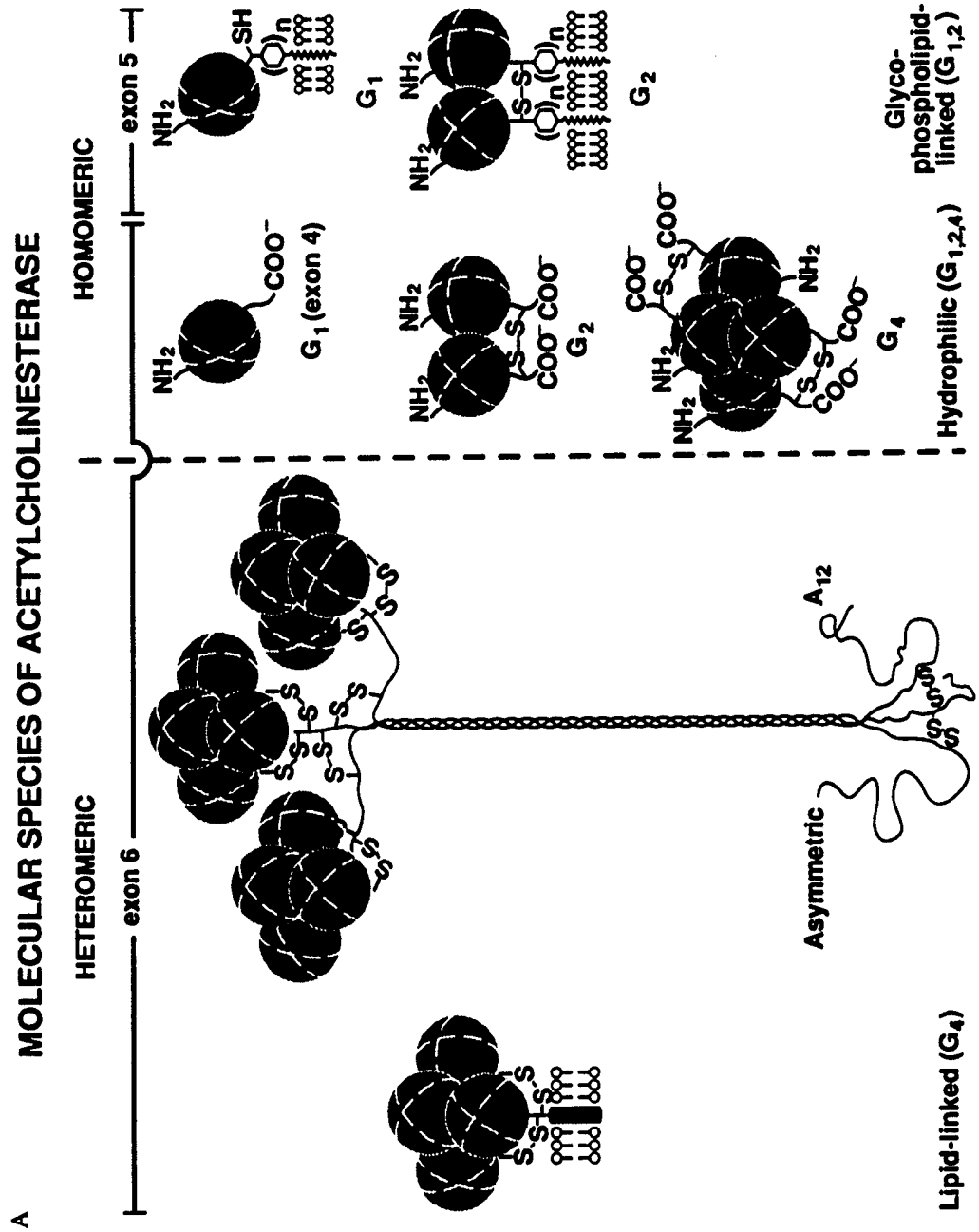
A
MOLECULAR SPECIES OF ACETYLCHOLINESTERASE
HETEROMERIC
HOMOMERIC
exon 6
exon 5
Lipid-linked (G_4)
Asymmetric
A_{12}
G_1 (exon 4)
G_1
G_2
G_2
G_4
Hydrophilic ($G_{1,2,4}$)
Glyco-phospholipid-linked ($G_{1,2}$)

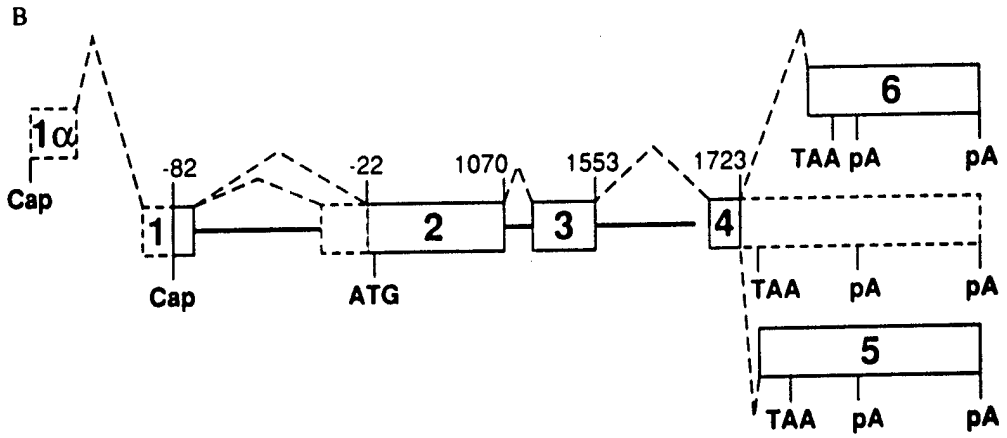

Figure 2 (*A*) Molecular species of acetylcholinesterase. The species are divided into two classes: a heteromeric class consists of catalytic subunits disulfide bonded to either a lipid-linked subunit or a triple helix of collagen-containing subunits. The homomeric class exists as monomers, dimers, and tetramers and can be divided to the hydrophilic or amphiphilic (glycophospholipid-linked) forms. The alternative exons that give rise to the various molecular species are also shown. Nomenclature designating hydrodynamic properties (A = asymmetric and G = globular) and number of catalytic subunits is also shown (17). (*B*) Structure of the genes encoding mammalian acetylcholinesterase and the exon numbering system. Alternative exon splices are shown by the dotted lines. The transcriptional start sites (Cap), translational start site (ATG), translational stop signals (TAA), and polyadenylation signals (pA) are also marked (modified from Ref. 16).

species should only exist as a monomer. The glycophospholipid-linked species in mouse and human are encoded by splicing exon 4 to exon 5 yielding 43- and 42-amino acid peptides, respectively, at their carboxyl-termini. All but 14 of the amino acids are cleaved with the addition of a glycophospholipid (24, 61). mRNA protection and expression studies verify the existence of such species in intact tissue and in transfected cells (66, 67). Hence, AChE contains a constant catalytic core consisting of the first 543 amino acids in mammals or 535 amino acids in *Torpedo*, which are encoded within three exons in mammalian AChE and two exons in *Torpedo* AChE. In mammalian BuChE the open reading frame is encoded in two exons. In this region is found the essential catalytic residues required for activity. The alternatively spliced regions in AChE only encode the remaining few amino acids (from 2 to 40) at the very carboxyl-termini of the respective processed enzymes. This domain governs intersubunit linkages and the cellular dispositions of the enzymes.

Avian AChE shows an interesting variant on this theme since it contains additional coding sequence at the position between exons 2 and 3 in the mammalian enzyme (30). The included sequence gives rise to a 20-kd increase in molecular mass of the enzyme. Variations in this region are responsible for the polymorphism of molecular weight seen in AChE from

quail (69). Alternative splicing giving rise to cholinesterases with distinct carboxyl-termini have yet to be found in the avian AChE or in BuChE from any species.

Although early studies indicated a greater complexity in the cholinesterase genes, mammalian AChE (61), avian AChE (69), and mammalian BuchE (62) are apparently each encoded by single genes. The human AChE gene is localized to 7q22 (70, 71) and human BuChE to 3q26 (71–73). The mouse gene is found at the distal end of chromosome 5, an area of synteny with 7q (74).

THREE-DIMENSIONAL STRUCTURE OF ACETYLCHOLINESTERASE

Crystallographic Analysis

The dimeric, glycophospholipid-linked form of *Torpedo* AChE was treated with phosphatidylinositol-specific phospholipase C to yield a soluble form of the enzyme amenable to crystallization (75). A structure at 2.8Å resolution has been solved and crystals suitable for higher resolution studies are available (10). Three amino acids at the amino- and carboxyl-termini, the noncleaved portion of the glycophospholipid, and a very short exposed loop, residues 485–489, showed sufficient disorder to preclude detection.

The subunits contain a 12-stranded β-sheet surrounded by 14 α-helices. They are ellipsoid in shape (45 × 60 × 65Å) and associate as dimers in a four-helix bundle. A tetramer of *Electrophorus electricus* AChE has also been crystallized (76). A low resolution structure revealed a subunit arrangement of a dimer of dimers.

Identities in Folding Patterns

The structure of *Geotrichum* lipase, an enzyme homologous in sequence, became known at about the same time as that for *Torpedo* AchE (77). These two enzymes show the same folding pattern and also contain the identical positional alignments of the Glu, His, and Ser catalytic triad discussed below. A common folding pattern is seen in the cholinesterase family (10, 49), termed the α/β hydrolase fold (49); it consists of the β_1 through β_8 sheets and the connecting α-helices. Surprisingly, a serine carboxypeptidase from wheat, a dienelactone hydrolase from *Pseudomonas*, and a haloalkane dehalogenase from *Xanthobacter* also show the same folding pattern, despite the absence of sequence identity. Even with the disparities in sequence, the structures of these proteins have converged to position the catalytic triad not only in the same three-dimensional configu-

ration but also at corresponding positions in the turns at the ends of the β-sheets and α-helices.

Modeling of Other Cholinesterase Structures

AChE and BuChE exhibit 51–54% amino acid residue identity and modeling of BuChE on the basis of the AChE structure has been carried out, yielding a virtually identical configuration of the peptide backbone (78). Conservation of the intrasubunit disulfide bond positions and the conservation of the α/β hydrolase fold, despite considerable variations in primary structure, suggest that modeling will provide a useful framework for structural studies of other proteins in the homologous series.

The Active Center and Catalytic Triad

The crystal structure established that a E_{327} H_{440} S_{200} triad with appropriate hydrogen bonding distances and alignment was at the base of a narrow gorge 20Å in depth (10). Such triads, involving a dicarboxylic amino acid withdrawing a proton from a serine through the imidazole of histidine, are characteristic of the other families of serine hydrolases. This arrangement in the cholinesterases and *Geotrichum* lipase differs from other serine hydrolases in two respects: most enzymes in the cholinesterase family use a glutamate instead of the aspartate found in the previously characterized serine hydrolases to supply the negative charge; and the steric arrangement of residues in AChE is the mirror image of the pancreatic serine hydrolases (10). Otherwise, orientation of the side chains and hydrogen bond distances show the side chains of the triads virtually superimposable in three-dimensional space.

The gorge is lined with 14 aromatic residues. Some are deep within the gorge while most others define a large aromatic patch on the wall of the gorge. Just below the rim of the gorge lies D_{72}, at the base of the gorge lies E_{199}, and deeper into the molecule lies D_{443}. Several other anionic residues are located farther from the gorge. E_{199} is the closest anionic side chain to contact distance with trimethylammonio group acetylcholine when bound. A single negative charge at the base of the gorge seems inconsistent with a rate acceleration for binding of cationic ligands ascribable to the presence of 6–9 negative charges (79, 80). However, a global analysis of surface potentials (81) and of the orientation of the molecular dipole intrinsic to AChE with respect to the active center gorge (82) predict substantial charge accelerations for cationic substrates or inhibitors entering the gorge. Various hypotheses have also been proposed regarding the role of aromatic residues in the gorge [aromatic guidance, (10)] that facilitate diffusion of the substrate to the active center. The aromaticity may also preclude the necessity of displacement of slow-exchanging water molecules at the base

of the cleft upon ligand binding and hence it could simply play a passive role. BuChE contains six fewer aromatic residues within its gorge, yet exhibits only a threefold reduction in catalytic efficiency, as measured by k_{cat}/K_m.

Crystallographic analysis of the AChE-decamethonium and AChE-edrophonium complexes (83, 84) and the positioning of the active center serine near the carbonyl carbon of acetylcholine enable one to model the bound substrate and perform experiments on energy minimization docking. Aromatic residues clearly play an important role in stabilization of the complex. The choline moiety appears to be stabilized by W_{84} and F_{330} in AChE whose orbitals lie close to the trimethylammonio surface, as defined by its van der Waal's radii. Also, the van der Waal's surfaces of choline and E_{199} are found within 1–2Å of each other.

Several considerations allow estimation of the free energy contributions stabilizing a bound quaternary group. Studies of neutral substrate interactions with AChE (85, 86), the synthesis of cage-like compounds containing aromatic residues to stabilize quaternary ammonium ligands (87), and the crystal structure of phosphorylcholine-antibody complexes (88) all point to a role for aromatic residues being in close apposition to the quaternary moiety in the stabilization of this diverse set of complexes. However, this argument can be carried too far if longer-range electrostatic forces are ignored. In fact, both electrostatic (Coulombic) and hydrophobic forces are likely to contribute to stabilization of the complex. The approach of partitioning free energy to both the electrostatic and hydrophobic force contributions to a quaternary ligand binding site was made almost a half-century ago by Pauling and colleagues when they compared energetics of binding of phenyltrialkylammonium ions to an antibody raised to quaternary ligands (89).

As we continue around the binding site for acetylcholine (Ach), the active site serine hydroxyl should be positioned close to the carbonyl carbon on Ach. In turn, the carbonyl oxygen should be stabilized through hydrogen bonding to two amide backbone hydrogens at positions 119, 121, and/or 201 (10). A clear delineation of the acyl pocket is provided by the side chains of F_{288} and F_{290} pointing inward toward the binding site. These two residues would be expected to constrain the dimensions of the acyl pocket in AChE (Figure 3).

The Peripheral Anionic Site

J.-P. Changeux proposed an allosteric mechanism of inhibition of AChE nearly 30 years ago. He examined the inhibition of steady state kinetic parameters by various inhibitors and inhibitor combinations (90). A periph-

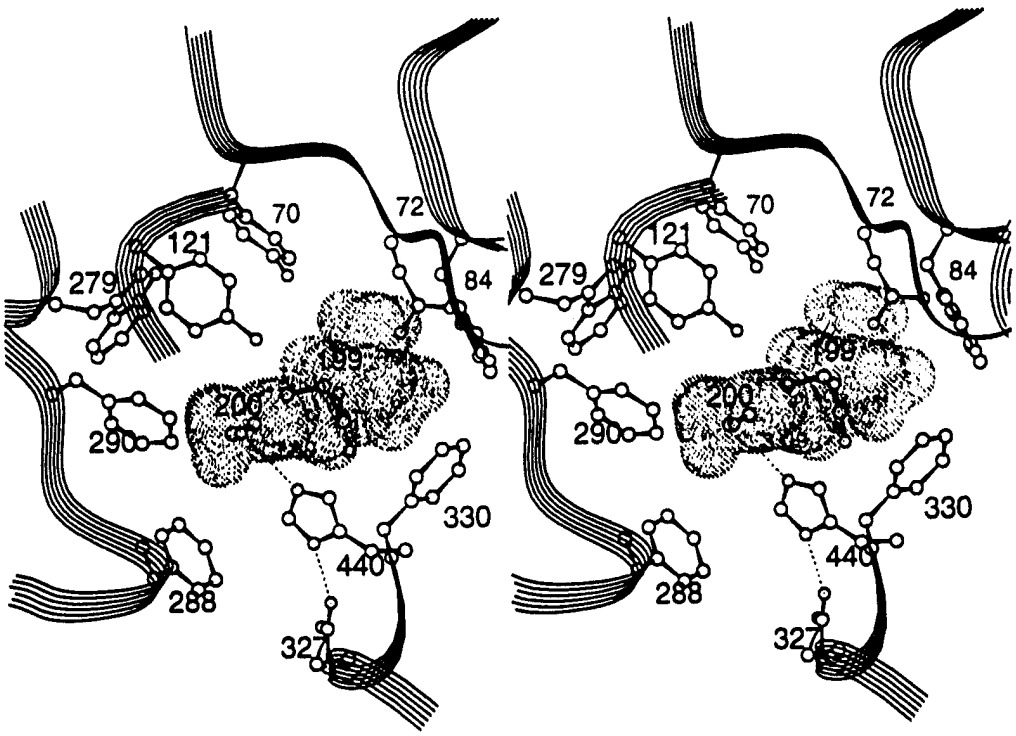

Figure 3 Structure of *Torpedo* acetylcholinesterase showing the positions of critical side chains and bound acetylcholine positioned by energy minimization (131, 132). (*a*) The catalytic triad: S_{200}, H_{440}, E_{327}. (*b*) The choline binding subsite: W_{84}, Y_{330}, E_{199}. (*c*) The acyl pocket: F_{288}, F_{290}. (*d*) The peripheral anionic site: Y_{70}, Y_{121}, W_{279}, D_{72}.

eral site, which likely gives rise to allosteric inhibition, was subsequently identified by direct titrations with the fluorescent inhibitor, propidium (91: see inset for structures). Criteria such as (*a*) the inability of agents that phosphorylate the active center serine to alter propidium binding; (*b*) the capacity of reversible inhibitors such as edrophonium and N-methylacridinium, which bind at the active center, to associate with AChE simultaneously with propidium to form ternary complexes; and (*c*) the mode of propidium inhibition of AChE acylation by substrates all point to a peripheral anionic site for the binding and allosteric actions of this inhibitor (91, 92). Moreover, measurements of fluorescence energy transfer between certain fluorescent alkyl phosphonates and propidium suggest that approximately 20Å separate the excited state dipoles between the alkylphosphate donor and the propidium acceptor of resonance energy transfer (92). Labeling studies using propidium to protect labeling by a photoactive reagent, DDF (93), and direct labeling by azidopropidium (94), have identified two sets of peptides (residues 270–278 and 251–266 in *Torpedo*) that should contribute to the binding surface of the peripheral anionic site. Finally, a terpyridine platinum coor-

dination complex acts in a manner similar to propidium as an inhibitor and labels H_{280} in human AChE (95). The locations of the exposed surface of these residues are near the rim of the active center gorge. Hence, ligand association with the peripheral site may prevent access of substrates to the gorge by physical obstruction to restrict entry to the gorge, by charge repulsion imparted by the association of a cationic ligand, or by an allosteric mechanism in which the active center conformation is altered. In this connection, it is noteworthy that the cationic Pt-terpyridine complex inhibits catalysis of acetylcholine to a greater extent than neutral substrates (95).

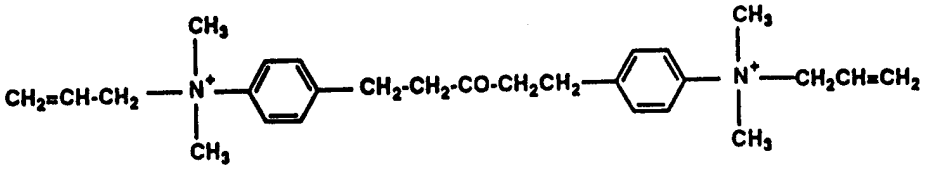

BW284C51

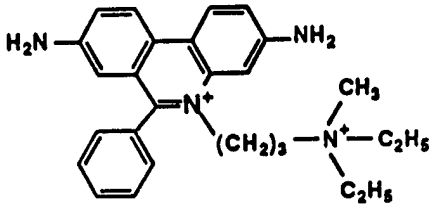

Propidium

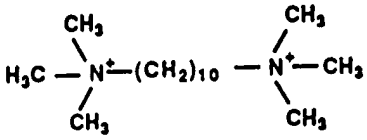

Decamethonium

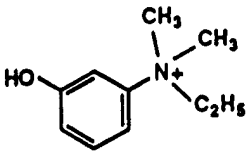

Edrophonium

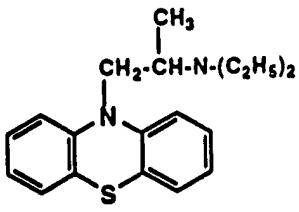

Ethopropazine

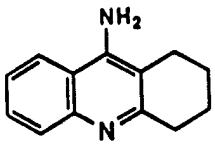

Tetrahydro-9-aminoacridine (Tacrine)

Three related peptide snake toxins of the fasciculin family bind to mammalian and *Torpedo* AChE but not to avian AChE or mammalian BuChE with K_Ds in the picomolar range (96, 97). These peptides of 6500 Da bind to AChE phosphorylated with DFP, but binding is prevented by propidium and certain *bis*-quaternary inhibitors. Hence, fasciculin emerges as a strong candidate for binding to the peripheral site on AChE as well (96, 97).

The function of the peripheral anionic site in catalysis in vivo and its role in synaptic activity remain open issues. It may be involved in forming

an initial complex to facilitate substrate transfer down the gorge (95). Competition between high concentrations of substrate and propidium suggest a role in substrate inhibition (98), and it has been proposed that the site serves as a sensor to maintain constant catalytic rates over a range of ionic strengths (99). Several *bis*- and *tris*-quaternary ligands bind to the peripheral site, and *bis*-quaternary ligands with large interquaternary distances (~14Å or greater) prevent the binding of both active center and peripheral site ligands (91, 92). Steric overlap between the *bis*-quaternary ligand with ligands selective for the peripheral and active sites could be responsible for this mutually exclusive binding.

Molecular Basis of Ligand Specificity at the Active Center

The dimensions of the active center gorge determined from X-ray crystallography (10) and chemical modification studies help to elucidate the specificity and orientation of bound ligands.

Early studies of Wilson & Quan (100) demonstrated the importance of a *meta* hydroxyl group in enhancing the inhibition capacity of phenyl trialkylammonium ligands. The crystal structure of the edophonium-AChE complex shows that the hydroxyl group bisects the hydrogen bond between the imidazole nitrogen in H_{440} and the serine hydroxyl group (S_{200}) and should alter the hydrogen bonding scheme (83). In addition, the aromatic ring of edrophonium is stabilized through π orbital overlap with W_{84} and, perhaps, F_{330}. The role of this site in binding of quaternary ammonium groups was also established by chemical labeling experiments where edrophonium selectively protects DDF labeling of peptides containing W_{84} in *Torpedo* (101) and presumed a peptide in *Electrophorus* AChE homologous to F_{330} (84, 102). Longer-range electrostatic interactions also appear to play a role. E_{199} resides at the base of the gorge and the distance separating the van der Waals radii of its carboxylate oxygen and the quaternary methyl groups is within 1.5Å.

Tricyclic ring-containing inhibitors such as tacrine (tetrahydro-9-aminoacridine, see inset for structures) occupy a location similar to that of edrophonium, although further rotation of the F_{330} side chain to accommodate an aromatic ring in the complex between tacrine and AChE is evident (83, 84). The tricyclic ring system inserts between F_{330} and W_{84}, causing increased stabilization by virtue of the π-orbitals. Early studies provided evidence for a charge-transfer complex between N-methylacridinium and a tryptophan in AChE (103). Moreover, the binding of N-methylacridinium and 3-aminopyridinium-1,10 decane results in near complete quenching of their fluorescence upon binding (104). The role of the indole side chain in W_{84} in acridinium binding seems clear in that it should provide the electron-rich donor ring system for association with the cation-containing

ring acceptor of acridinium. This tryptophan may well account for the changes mentioned above in absorption and fluorescence spectra typical of a charge-transfer complex.

The tricyclic ring system must not completely occlude the nucleophilic serine or the alignment of the other members of the catalytic triad since Barnett & Rosenberry found that the binding of these compounds can actually augment catalysis of neutral substrates such as ethylacetate (105). Accordingly, charge neutralization and the insertion of an aromatic ring system within the cleft enhance the catalytic surface for neutral ester substrates provided the size of the alcohol portion of the ester is kept small. Given the steric constraints of the gorge, the finding becomes even more intriguing and may argue for intrinsic flexibility within the gorge.

The portion of the active center accommodating the acyl portion of the substrate reveals that two phenylalanines, F_{288} and F_{290}, have their side chains directed into the active center and, as such, define the steric constraints of the active center. In BuChE, the conserved phenylalanines are replaced with L and I or V, providing a hydrophobic but less dimensionally constrained acyl pocket. Presumably, the phenylalanine side chains account for the marked fall-off in AChE catalysis in going from propionylcholine to butyrylcholine (54), the specificity of certain organophosphates (i.e. isoOMPA) for butyrylcholinesterase (55) and the marked stereospecificity seen with organophosphate inhibition of AChE when the moieties attached to the phosphorus differ greatly in molecular dimensions (106). Such observations would also predict that the stereoselectivity of organophosphate reactions with BuChE are much lower than with AChE.

Site of Bis-*Quaternary Ligand Association*

The site of *bis*-quaternary ligands possessing large interquaternary distances can be ascertained, in part, from kinetic studies. Early studies by Belleau and colleagues (107, 108) and by Wilson and colleagues (109) demonstrated that *bis*-quaternary and some monoquaternary inhibitors actually enhance the rate of acylation of the enzyme by neutral substrates. This enhancement is indicative of the *bis*-quaternary ligand-enzyme complex maintaining access to the active center serine for acylating agents and perhaps altering conformation of the active center to affect reactivity. In addition, series of *bis*-quaternary ligands were examined for their capacities to bind to the sulfonylated and phosphorylated AChEs (110). Only when the phosphorylating agent or the groups surrounding the ammonio group in the quaternary ion became bulky did modification of the active center serine by phosphorylation or sulfonylation affect the affinity of the *bis*-quaternary ligand (110). In addition, *bis*-quaternary ligands bind in a mutually exclusive manner with ligands selective for the active center (i.e. edrophonium and N-methylacridinium) and the peripheral site

(propidium, gallamine, and d-tubocurarine). The simplest explanation would suggest an overlap of binding surfaces. Since the interquaternary extension between the nitrogens in decamethonium is ~14Å and the two trimethylammonio groups will add another 6Å in length, the potential spanning distance is large. The crystal structure of the AChE-decamethonium complex shows one trimethylammonio group lodged between F_{330} and W_{84}; the other extends out of the active center gorge and is enlodged in the vicinity of W_{279}, Y_{70}, and Y_{121}, which reside near the lip of the gorge (83, 84). The latter residues have also been implicated in binding at the peripheral anionic site (10, 92–94). Studies with spin-labeled *bis*-quaternary ligands show immobilization of both ends of the bound molecule and a separation between the ammonio-linked nitroxides consistent with an extended bound conformation (111). Other *bis*-quaternary fluorophores have further defined the characteristics of the ligand binding site (111a).

A self-consistent picture of the binding loci of the active center, peripheral anionic site, and *bis*-quaternary ligands is emerging. Having identified the major domains in the molecule responsible for specificity, their precise roles in catalysis and in the energetics of inhibitor binding have been analyzed further through mutagenesis and molecular modeling. These studies are detailed in a subsequent section.

CATALYTIC PARAMETERS AND MECHANISMS

The catalytic potential of the cholinesterases is wide ranging with oxyesters, thioesters, selenoesters, amides, anilides, carbamoylesters, and phosphorylesters all being susceptible to catalysis (11, 12, 17, 112). Often the range of substrate catalytic potential goes unrecognized owing to the high rate of acetylcholine turnover ($k_{cat}/K_m = 10^8 M^{-1}\ sec^{-1}$) and the 10^{14} enhancement of enzyme catalyzed over H_2O catalyzed ester hydrolysis for the efficient substrates (113, 114).

A general scheme for catalysis can be represented for an ester or related substrate designated by AcOR:

$$\text{E-OH} + \text{AcOR} \underset{k_{-1}}{\overset{k_1}{\rightleftharpoons}} (\text{E-OH}\cdots\text{AcOR}) \xrightarrow{k_2} \underset{\textit{acylation}}{\text{E-OAc} + \text{ROH}} \xrightarrow[H_2O]{k_3} \underset{\textit{deacylation}}{\text{E-OH} + \text{AcO}^- + \text{H}^+}$$

Scheme I

In the above scheme formation of a reversible complex with an acyl ester

is followed by acylation to form E-OAc represented by the first order rate constant k_2, and then deacylation, represented by the first order rate constant, k_3. The general features of the catalytic cycle of acylation and deacylation have been widely studied in the serine hydrolases. Serine 200 is likely to be rendered more nucleophilic by the catalytic triad. Formation of the acyl enzyme proceeds through formation of a tetrahedral intermediate which relaxes back to the trigonal, acyl enzyme. The imidazole in H_{440} may also assist by accepting the released proton. Deacylation also proceeds through a tetrahedral intermediate by attack of the acyl-enzyme bond from an internal H_2O. The H_2O may be rendered more nucleophilic by a neighboring carboxylate or imidazole residue.

In the above scheme,

$$k_{cat} = \frac{k_2\, k_3}{k_2 + k_3} \qquad \text{(Equation 1)}$$

$$K_m = \frac{k_{-1} + k_2}{k_1} \cdot \frac{k_3}{k_2 + k_3} \qquad \text{(Equation 2)}$$

$$\frac{k_{cat}}{K_m} = \frac{k_1 \cdot k_2}{k_{-1} + k_2} \qquad \text{(Equation 3)}$$

k_{cat} is governed by the energy barriers for acylation and deacylation and is the geometric mean of the two rate constants. K_m equals the equilibrium constant for the initial association only when $k_3 \gg k_2$ and $k_{-1} \gg k_2$. k_{cat}/K_m measures the initial steps leading up to formation of the acyl enzyme. Attempts to trap the acyl intermediate suggest that acylation and deacylation occur at comparable rates at V_{max} (115). This, in turn, indicates that k_2 and k_3 are of comparable magnitude for acetylcholine. For acetylcholine, k_{cat} approaches 10^4 sec^{-1} and $K_m = 5 \times 10^{-5}$ M. Accordingly, $k_{cat}/K_m = 2 \times 10^8$ M^{-1} sec^{-1}, a value approaching the diffusion limitation for k_1 (80, 114, 116).

AChE catalyzed hydrolysis of ACh and its thiol ester analogue acetylthiocholine (ATCh) approaches catalytic perfection (117) and under such conditions we might expect the transition state barriers for diffusion, acylation, and deacylation to be roughly equivalent. Hence, over a large concentration range, diffusion of substrate to the active center denoted by k_1 is essentially rate limiting.

By contrast, neutral esters and other less optimal substrates may require an induced fit to achieve acylation. Under such conditions, k_1 might be divided into two (or more) steps where k_a now reflects the diffusion step and k_b induced fit to optimize substrate orientation (118).

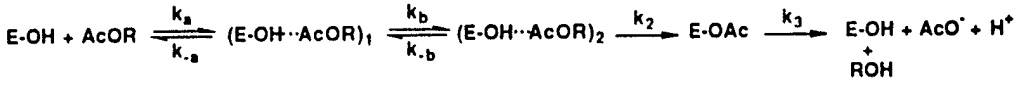

Scheme 2

In this situation:

$$\frac{k_{cat}}{K_m} = \frac{k_a\, k_b\, k_2}{k_2\,(k_{-a} + k_b) + k_{-a}\, k_{-b}} \qquad \text{(Equation 4)}$$

For a common acyl group, deacylation rates should be the same; hence, we may find sets of substrates where the *a* step of diffusion of reactants or the *b* step of isomerization is rate limiting. Rosenberry (118) and Quinn and colleagues (114, 116, 119) have examined the influence of pH and fraction of deuterated substrate (isotope inventories) on catalytic parameters to deconstruct Michaelis-Menten parameters into individual rate constants and ascertain rate-limiting steps. For example, linear proton inventory plots for v/K_m have been observed for various acyl esters, which indicate that a single proton transfer rather than transfer of multiple protons is involved in the rate-limiting step of the reaction (119). Hence, no evidence can be adduced for a charge-relay system or multifunctional proton transfer in the reaction (119). The pH dependences also indicate that the rate-limiting step changes between efficient and poor substrates (118) and between ACh and benzoylcholine (116). Efficient substrates such as ACh are limited by diffusion of substrate, while others may depend either on isomerization steps leading to acylation or the acylation step itself.

In the extreme case for carbamoylating and phosphorylating agents, deacylation or the k_3 step is rate limiting in turnover. Effectively, these agents become hemisubstrates when the observation times become shorter than the deacylation half-lives.

Substrate Inhibition and Activation

Since the comprehensive studies of Augustinsson in the 1940s (54), substrate inhibition has been a hallmark of cholinesterase catalysis. It has been sufficiently characteristic to use it as a means of distinguishing AChEs from BuChEs. The mechanism of substrate inhibition is not well resolved and, in fact, data do not clearly distinguish between influence occurring on the acylation or deacylation step (98, 112, 120). If we consider the overall scheme:

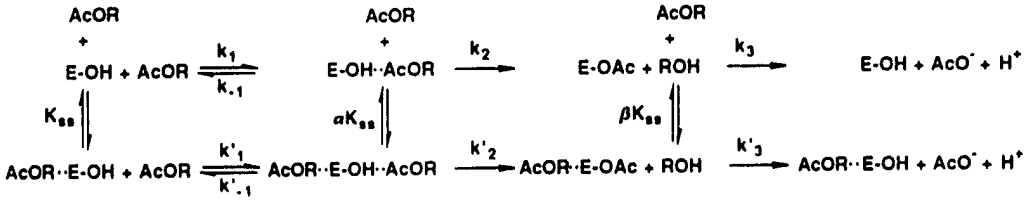

Scheme 3

If excess substrate affects acylation $k_2 \neq k_2'$, while an influence on the deacylation sequence is reflected in $k_3 \neq k_3'$. For substrate inhibition either $k_2' < k_2$ or $k_3' < k_3$. Values of k_2' or $k_3' = 0$ denote excess substrate causing complete inhibition. The BuChEs (121–123) and certain mutations of AChE (123) show substrate activation. If activation and inhibition are occurring through substrate binding to a common site, we might expect both to be dependent on similar sets of residues in the molecule.

SITE-SPECIFIC MUTAGENESIS—CHOLINESTERASE CHIMERAE

Mutagenesis studies in the absence of a three-dimensional structure were largely restricted to residues where sequence conservation, sequence proximity, or a natural mutation suggested a role in function (53, 124–126). The report of a crystal structure added a new dimension as well as a flurry of activity in this arena of investigation.

Expression Systems

Initial studies of mutagenesis were done by mRNA injections into oocytes (125, 127) and transient transfections of cDNA into a receptive cell such as COS (53) or HEK cells (128). mRNA injection of single cells is labor intensive and the limited expression has not permitted a detailed analysis of kinetic and inhibition parameters. Similar limitations apply to transient transfections, particularly in the case of the *Torpedo* enzyme, where efficient protein folding does not occur at 37°C (53, 126) and expression at lower temperatures compromises cell viability. Although the high turnover rates of the cholinesterases facilitate their detection, details of substrate inhibition are only revealed at high substrate concentrations (10–100 mM). At substrate concentrations well above the K_m (~50 μM) general base catalysis of the esters will contribute substantially to basal ester hydrolysis.

Determinations of k_{cat} or k_{cat}/K_m, as measures of turnover and catalytic efficiency, necessitate titrations of stoichiometry of active sites. This entails antibody precipitation to determine total cholinesterase protein, ascertaining

active center concentrations with high-affinity phosphorylating agents or purifying the enzyme to homogeneity. Each approach has particular advantages and limitations.

Stable transfectants of mammalian embryonic cell lines have yielded expression levels about an order of magnitude higher than transient transfection (129, 131). Finally, expression systems in baculovirus-*Spodoptera* (132) and *Escherichia coli* (133) have produced 3 mgs and over 100 mg of enzyme per liter of culture system, respectively. However, the former system presents difficult cloning steps to achieve expression, while in the latter system, generation of active enzyme required denaturation followed by refolding. Only ~3% of the enzyme renatured as an active entity.

Kinetic Parameters for Mutant Enzymes

The ratio k_{cat}/K_m, a second-order rate constant, is typically used as the measure of catalytic efficiency to compare mutant enzymes. This ratio reflects the catalytic through put under nonsaturating conditions while k_{cat} reflects maximal turnover. To describe substrate inhibition, two constants, K_m and K_{ss}, represent the concentration-dependence of catalysis and inhibition by excess substrate. An additional parameter, b, has been incorporated into kinetic schemes (112) to reflect the maximal extent of inhibition or activation by excess substrate with the mutant enzymes (123).

In a scheme where we do not differentiate whether binding of a second substrate molecule affects acylation or deacylation and $K_{ss} = \alpha K_{ss}$,

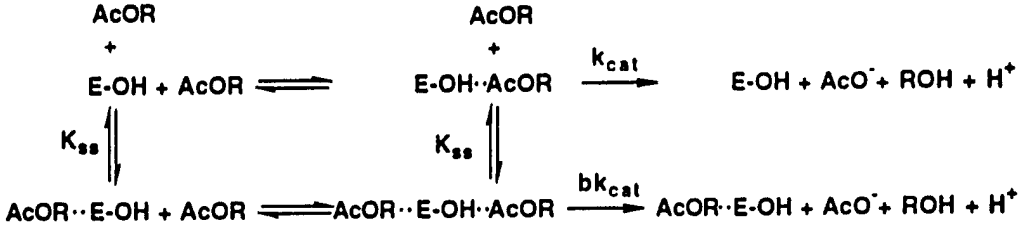

Scheme 4

then

$$v = \frac{1 + b\,[S] / K_{ss}}{1 + [S] / K_{ss}} \cdot \frac{V_{max}}{1 + K_m / [S]} \qquad \text{(Equation 5)}$$

when $b = 0$,

$$v = \frac{V_{max}}{1 + [S] / K_{ss} + K_m / [S] + K_m / K_{ss}} \qquad \text{(Equation 6)}$$

Hence, in this scheme substrate inhibition is described in terms of the dissociation constant for the inhibitory site, K_{ss}, and the relative efficiency of the ternary versus the Michaelis-Menten complex to acylate and deacylate substrate, b. This scheme is also applicable to substrate activation where $b > 1$ rather than $b < 1$. When $b = 1$, Michaelis-Menten kinetics are observed.

Reversible inhibition has been evaluated by IC_{50}'s and by measurement of dissociation constants. IC_{50}'s leave considerable uncertainties regarding inhibition mechanisms and the form of the enzyme to which the inhibitor binds. IC_{50}'s for competitive inhibitors are dependent on the K_m of the substrate relative to the substrate concentration, whereas for noncompetitive inhibitors they are independent of this ratio. Since K_m's may also be affected by mutations in the enzyme, a change in IC_{50} in the extreme case could reflect a change in K_m and not in K_I for the inhibitor. By contrast, K_I is independent of K_m. A second advantage of ascertaining the inhibition mechanism is that the influence of mutation can be compared for the same species of enzyme in the kinetic scheme. For convenience, the free species without bound substrate (i.e. E-OH) is often used; dissociation of its complex is reflected in the competitive inhibition constant.

In the case of inhibitors that carbamoylate or phosphorylate the active site serine, IC_{50}'s become parameters of limited applicability to mechanistic considerations or correlating data obtained under different conditions. Data for these inhibitors should be described in terms of a time-dependent parameter and a constant describing the concentration dependence of inhibition.

Summary of Mutation Analyses[2]

Table 1 summarizes the reported cholinesterase mutants by dividing them into several structural domains: (*a*) catalytic triad; (*b*) active center-acyl pocket; (*c*) active center-choline binding subsite; (*d*) peripheral-site(s)—rim of the gorge; (*e*) carboxyl-terminus; (*f*) glycosylation; (*g*) cholinesterase chimeras. The essential observations are detailed below:

CATALYTIC TRIAD Mutagenesis has confirmed the role for the E_{327} H_{440} S_{200} linkage in catalysis (53, 129, 134, 135). Although mutation of several other conserved diacidic amino acids results in inactive enzyme (129, 136), these residues are likely to be critical for folding into a correct tertiary conformation rather than directly involved in the acylation and deacylation steps (136). In fact, recent evidence suggests that a conformation of chicken

[2]Residue identification refers to the species under study. The parentheses refer to the *Torpedo* sequence, which serves as an alignment reference for other enzymes.

Table 1 Cholinesterase Mutations[a]

Enzyme and Residues[b]	*Torpedo* Equivalent	Catalytic, Inhibitor Specificity and Structural Change	Reference
Catalytic Triad			
TA S_{200}A,C	200	A is inactive; C may be inactive or possess 0.1% of wild-type activity	53
HA S_{203}A,C	200		129
HB S_{204}C,T,D,Q,H	200		135
TA H_{440}Q	440	Inactive; AChE with the other conserved histidine mutated is active, H_{425}	53
HA H_{447}A	440		129
TA E_{327}Q,D	327	Inactive	134
HA E_{334}D,Q,A	327	Inactive	129
Active Center-Acyl Pocket			
MA F_{295}L	288	↓ ATCh k_{cat}/K_m, ↑ BTCh k_{cat}/K_m; ↑ isoOMPA inhibition rate	131
HA F_{295}L,A	288	Similar to above	138
HB L_{286}K,Q,R,D	288	↑ K_m, change in inhibitor specificity	135
MA R_{296}S	289	Little change in activity	131
MA F_{297}I	290	↓ ATCh k_{cat}/K_m; ↓ BTCh k_{cat}/K_m; ↑ isoOMPA inhibition rate; K_{ss} ↑, b ↑	131
MA F_{295}Y	288	Little change in substrate specificity	123
MA F_{297}Y	290	↑ K_{ss}	123
DC F_{368}Y,S	290	Increased organophosphate resistance	139
HA F_{297}V,A	290	↓ ATCh k_{cat}/K_m; ↑ BTCh k_{cat}/K_m, ↑ isoOMPA inhibition	138
MA V_{300}G	293	Little change in activity	131
MA F_{295}L, F_{297}I	288, 290	↓ ATCh k_{cat}/K_m; ↑ BTCh k_{cat}/K_m; ↑ isoOMPA inhibition rate	131
HA F_{295}L, F_{297}V	288, 290	↓ ATCh k_{cat}/K_m; ↑ BTCh k_{cat}/K_m; ↑ isoOMPA inhibition	138
TA F_{288}L, F_{290}I	288, 290	↓ ATCh→ ↑ BTCh catalysis; ↑ isoOMPA inhibition	78
MA F_{295}L, F_{296}S, F_{297}I	288, 289, 290	↓ ATCh k_{cat}/K_m	131

Table 1 (*Continued*)

Enzyme and Residues[b]	*Torpedo* Equivalent	Catalytic, Inhibitor Specificity and Structural Change	Reference
Active Center—Choline Binding Site			
HA $Y_{337}A$	330	↓ substrate inhibition	130
MA $Y_{337}A,F$	330	Change in inhibitor specificity (esp. A)	123
TA $E_{199}Q,D$	199	↓ k_{cat}/K_m ↓ substrate inhibition (esp. D), change in inhibitor specificity, diminished aging rate	132, 53, 166
HA $E_{202}Q,D,A$	199	↓ k_{cat}/K_m ↓ substrate inhibition, change in inhibitor specificity	130
HA $W_{86}A$	84	↓ k_{cat}/K_m ATCh, ↓ propidium affinity, ↓ edrophonium affinity	130, 138
HB $Y_{440}D$	442	↑ K_m; change in inhibitor specificity	135
Gorge Entry (Peripheral Anionic Site)			
HA D_{74} E,N,G,K	72	↓ *Bis*quaternary, propidium, and dibucaine inhibition; ↓ Substrate inhibition	129, 130
MA $D_{74}N$	72	↑ K_m ↑ K_{ss}	123
HB $D_{70}G$[c]	72	Succinylcholine and dibucaine inhibition	125, 140
DC $Y_{109}D,G,K$	72	G ↑ preference BTCh K lower substrate affinity	142
TA $W_{279}A$	279	↓ Propidium and *bis*quaternary inhibition	78
HA $W_{286}A$	279	↓ Propidium and *bis*quaternary inhibition	130
MA $W_{286}R$	279	↓ Propidium and *bis*quaternary inhibition	123
MA $W_{286}A$	279	↓ Propidium and *bis*quaternary inhibition	123
MA $Y_{72}N$	70	↓ Propidium and *bis*quaternary inhibition	123
MA $Y_{124}Q$	121	↓ Propidium and *bis*quaternary inhibition	123
MA $Y_{72}N$; $Y_{124}Q$	70, 121	↓ Propidium and *bis*quaternary inhibition	123
MA $Y_{72}N$; $W_{286}R$	70, 272	↓ Propidium and *bis*quaternary inhibition	123
MA $Y_{124}Q$; $W_{286}R$	121, 279	↓ Propidium and *bis*quaternary inhibition	123
MA $Y_{72}N$; $Y_{124}Q$; W_{286}, R,A	70, 121, 279	↓ Propidium and *bis*quaternary inhibition	123
MA $Y_{72}N$; $Y_{124}Q$; $W_{286}R,A$; $D_{74}N$	see above	↓ Propidium and *bis*quaternary inhibition	123

Other Catalytic and Structural Functions			
HB $E_{441}G,E_{443}G$	443, 445	Decreased BTCh catalysis and dibucaine inhibition	140
HA $Y_{114}A$	116	Restores function to D_{70} mutants	140
HB $F_{561}Y$	563	Restores function to D_{70} mutants	140
HB $S_{425}P^c$	427	Associated with D_{70} resistance	125, 140
HB $G_{390}V^c$	392	↓ Succinylcholine, dibucaine and tacrine inhibition	163
HA $H_{322}N^c$	315	YT blood group antigen	161
HA $P_{561}R^c$	541	Allelic variation in glycophospholipid signal sequence	161
HA $F_{338}A$	331	Associates with F_{295}	138, 130
MA $F_{338}G$	331	Associates with F_{295}; ↑ K_{ss}	123
HA Y_{341}	334	↓ Substrate inhibition	138
DC $F_{115}S^c$	78	Increased organophosphate resistance	164
DC $I_{199}V^c$	129	Increased organophosphate resistance	164
DC $G_{303}A^c$	227	Increased organophosphate resistance	164
Intersubunit Association			
TA C_{537}, truncation	537	Secreted	126, 165
HA $C_{580}A$	572	Secreted monomer	128
DC C_{615}, truncation	537	Secreted	145, 146, 151
Glycosylation			
HA $N_{265}Q$	258	Diminished secretion	150
HA $N_{350}Q$	343	Diminished secretion	150
HA $N_{464}Q$	457	Diminished secretion	150
HA $N_{265}Q,N_{350}Q$	258, 393	Greater diminution of secretion	150
HA $N_{256}Q,N_{464}Q$	258, 457	Greater diminution of secretion	150
HA $N_{350}Q,N_{464}Q$	343, 457	Greater diminution of secretion	150
HA $N_{765}Q,N_{350}Q,N_{464}Q$	258, 343, 457	Greater diminution of secretion	150

Table 1 (*Continued*)

Enzyme and Residues[b]	*Torpedo* Equivalent	Catalytic, Inhibitor Specificity and Structural Change	Reference
Chimerae			
TA Exon 4 deletion, exon 3–5 linkage		Glycophospholipid-linked inactive enzyme	126
HB Linkage of mutant and non-mutant enzymes	various	Augments or diminishes influence of the mutant	125, 140
MA Substituted N-terminal and/or C-terminal sequences with BuChE sequence	$B_{1-174}A_{175-575}$ $B_{1-174}A_{175-487}$- $B_{488-575}$	B_{1-174} confers BW specificity of BuChE	131
HB Substituted AChE sequence for BuChE	$B_{1-57}A_{58-133}$- $B_{134-575}$	Imparts partial AChE character	141

[a] MA = Mouse acetylcholinesterase; HA = human acetylcholinesterase; TA = *Torpedo* acetylcholinesterase; HB = human butyrylcholinesterase, DC = *Drosophila* cholinesterase

[b] Other residues, $D_{397}N$ in *Torpedo*, $D_{175}N$, $D_{404}N$ in human have been reported to produce inactive enzyme. $E_{92}Q,L$ results in inactive enzyme in *Torpedo*. Little or no change in activity was reported for $E_{84}Q$, $D_{95}N$, $D_{131}N$, $D_{333}N$, $D_{349}N$ in human and $D_{93}N$ in *Torpedo* (18)

[c] Natural mutations

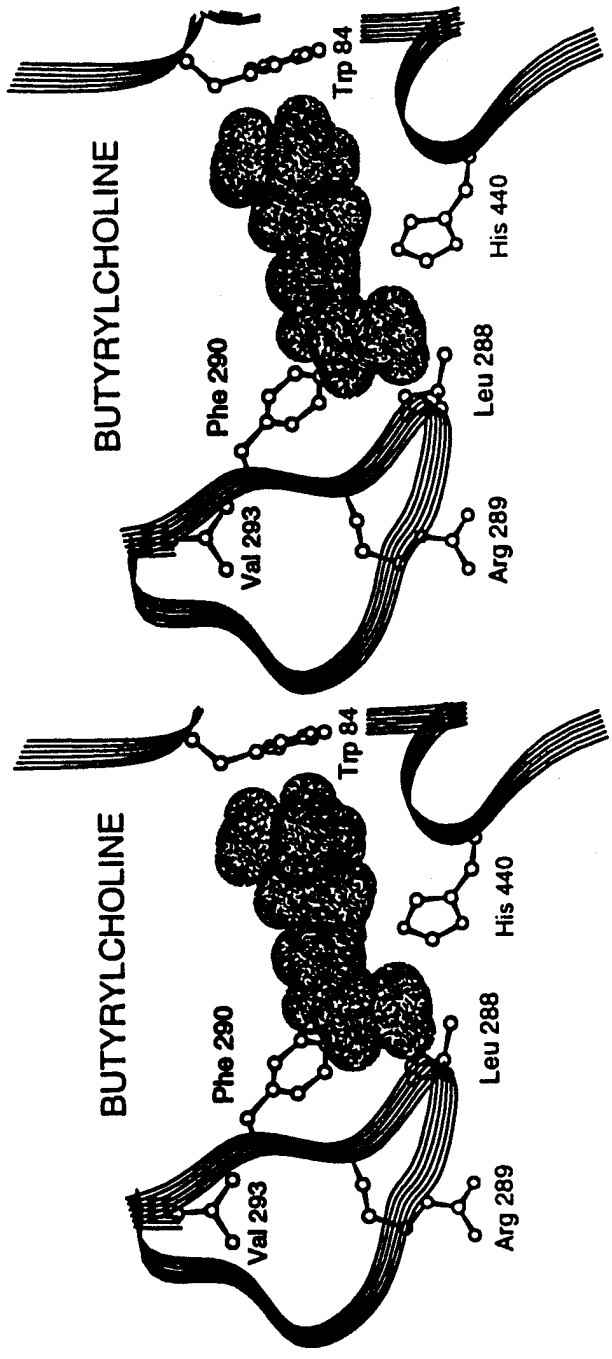

Figure 4 Structure of bound butyrylcholine within the substrate binding site of the F_{288} Mutant of Acetylcholinesterase. Energy minimization was done with the Biosym Insight II program (131).

AChE is produced that is DFP reactive, but catalytically inactive towards Ach (137). Whether the catalytically inactive mutants achieve a tertiary conformation approaching the active enzyme or are simply degraded as a nascent peptide chain is unknown. Some mutations of the active center (i.e. $S_{(200)}C$) show low activity (53, 135), and it will be of interest to achieve high expression to analyze them for catalytic properties.

The functional existence of a catalytic triad does not prove the existence of a charge-relay system or rate-limiting proton transfer (119). Rather the optimal alignments of these residues may be critical for confering a proton-withdrawing, inductive effect on the serine and/or a sink capacity for released protons.

ACTIVE CENTER ACYL POCKET Based on the residue differences between AChE and BuChE, the residues outlining the acyl pocket have been substituted in mammalian AChE to produce multiple mutant enzymes (Figure 4). Substitution of $F_{295(288)}$ and $F_{297(290)}$ in AChE to the corresponding residues found in BuChE has increased BuChE character as measured by an increased ratio of butyrylthiocholine (BTCh) to acetylthiocholine (ATCh) catalyzed hydrolysis, changes in the substrate activation and inhibition profiles, and increased susceptibility to inhibition by the BuChE-specific inhibitor, isoOMPA (131, 138). The $F_{295(288)}L$, $F_{297(290)}I$ double mutant (78, 131, 138) and the $F_{295(288)}L$, $R_{296(289)}S$, $F_{297(290)}I$ triple mutant (131) showed similar BuChE character, but were far less active. A detailed analysis of the individual F_{295} and F_{297} mutants uncovered several interesting properties of the acyl pocket. First, the $F_{295}L$ mutant of mouse AChE, while slightly less efficient towards ATCh hydrolysis, hydrolyzed BTCh with a k_{cat}/K_m greater than that found for native BuChE (131). Similar behavior was seen for the human $F_{295}L$ and $F_{295}A$ mutations (138). The $F_{297}I$ mutation is notable in its increased K_m for both ATCh and BTCh and for the elimination of substrate inhibition. In fact, the concentration dependence of BuChE catalyzed hydrolysis of BTCh and ATCh is best described in terms of substrate activation (123, 131) and the F_{297} mutation alone is sufficient to reverse the substrate inhibition in AChE and achieve a large measure of the activation seen with BuChE (123). $F_{338(331)}$, which comes in close proximity to F_{295} through ring stacking, also has a marked influence on diminishing substrate inhibition (123).

Drosophila cholinesterase has a single phenylalanine in its acyl pocket; a natural mutation to Y produces a enzyme conferring insecticide resistance to several bulky organophosphates (139).

ACTIVE CENTER-CHOLINE BINDING SUBSITE Four side chains appear to be of particular importance in stabilizing the quaternary moiety of choline. The

crystal structure shows the trimethylammonio-methylene group of decamethonium or the dimethylethylammonio group of edrophonium appears to make a three-point contact with the indole ring of $W_{(84)}$ (84). $F_{(330)}$ and $Y_{(442)}$ are also in close apposition, and some movement of the side chain $F_{(330)}$ towards the aromatic ring of edrophonium is also evident in this complex. The van der Waal's outer shell of the carboxylate of $E_{(199)}$ comes within 1.5Å of that of the trimethylammonio group.

Replacement of $W_{86(84)}$ by A results in a marked reduction in ATCh catalysis and diminished binding of edrophonium (130). A follow-up study shows that the loss of activity is selective for the quaternary substrate since the isosteric, 2,2 dimethylbutyl acetate ester shows little diminution of activity (138). This finding illustrates the importance of the quaternary ammonium-indole interaction in the stabilization of complexes of substrate and inhibitors. However, a large difference in molecular volume is also inherent to this substitution. $W_{(84)}$ is conserved in all the cholinesterases.

The second aromatic residue in this domain is not conserved; the AChEs contain an F or Y at position 337(330) and BuChE has A at 332(330). Several inhibitors selective for BuChE or AChE depend on this difference. The $Y_{337}A$ mutation results in an 10- to 20-fold reduction in edrophonium affinity but little or no reduction in decamethonium affinity (123, 130, 138). By contrast, the affinities of the acridines and particularly certain phenothiazines are increased by this mutation (123). This behavior appears to depend on the phenothiazine side chain and was most marked with ethopropazine where a 2700-fold decrease in K_I was evident. This decrease was virtually identical to its difference in K_I between AChE and BuChE (123). Huperzine shows a decreased affinity with the $Y_{337}A$ substitution (A Saxena, N Qian, IM Kovach, AP Kozikowski, D Vellom, et al, submitted). Taken together, the data indicate that the aromatic group at 337(330) contributes to stabilization of the complexes (i.e. ring stacking and quaternary aromatic interactions in the case of edrophonium and stabilization of the caged structure in the case of huperzine). However, addition of the tricyclic ring system and, in particular, certain substitutions on the exocyclic chain create steric hindrance with the aromatic ring in $F_{(330)}$ or $Y_{(330)}$ This is reflected in lower affinities of inhibitors of larger volume for AChE than for either BuChE or the $Y_{337(330)}A$, AChE mutant (123). The 337(330) residue change has minimal influence on ATCh catalysis. Shafferman and colleagues have shown that the Y_{337} to A mutation diminishes substrate inhibition in human AChE (130) and suggest a direct linkage to the peripheral site. However, upon mutation of Y_{337} to A in mouse AChE substrate inhibition is still evident when examined over a wider range of substrate concentrations (123), which indicates that a substrate inhibition mechanism involving the 337 residue is not universal.

Furthermore, $Y_{(442)}$ also contributes to the choline binding site surface. In BuChE, with $F_{328(330)}$ changed to A, the role of $Y_{440(442)}$ may be more influential. Altered catalytic parameters are found with the $Y_{440}A$ mutation in BuChE (135).

Mutagenesis experiments also revealed that the charge on $E_{(199)}$ stabilizes binding in this region. Edrophonium affinity is markedly reduced (132, 130) and k_{cat}/K_m for ATCh is lowered by a factor of 50 with the $E_{199}Q$ mutation (132). Hence, the energy of stabilization of edrophonium can be partitioned between both the electrostatic and π-electron bonding forces. Similar analyses are possible for other inhibitors, substrates, and transition state mimics. The $E_{199}D$ mutation has less influence on k_{cat}/K_m but markedly affects substrate inhibition (130, 132).

THE PERIPHERAL ANIONIC SITE: GATING AT THE RIM OF THE GORGE Mutagenesis studies reveal that three residues, $W_{286(279)}$, $Y_{72(70)}$ and $Y_{124(121)}$ are critical for dictating specificity of BW284c51, decamethonium, and propidium (123) (Figure 5). These residues are also essential for binding of the peptide, fasciculin (Z Radić, R Duran, DC Vellom, Y Li, C Cervenansky & P Taylor, submitted). Decamethonium and BW284c51 likely span between the choline binding subsite and a portion of the peripheral anionic site whereas propidium and fasciculin are peripheral site selective ligands. In the case of BW284c51 a partitioning of free energy shows essentially linear free energy relationships for summing the contributions of the three residues

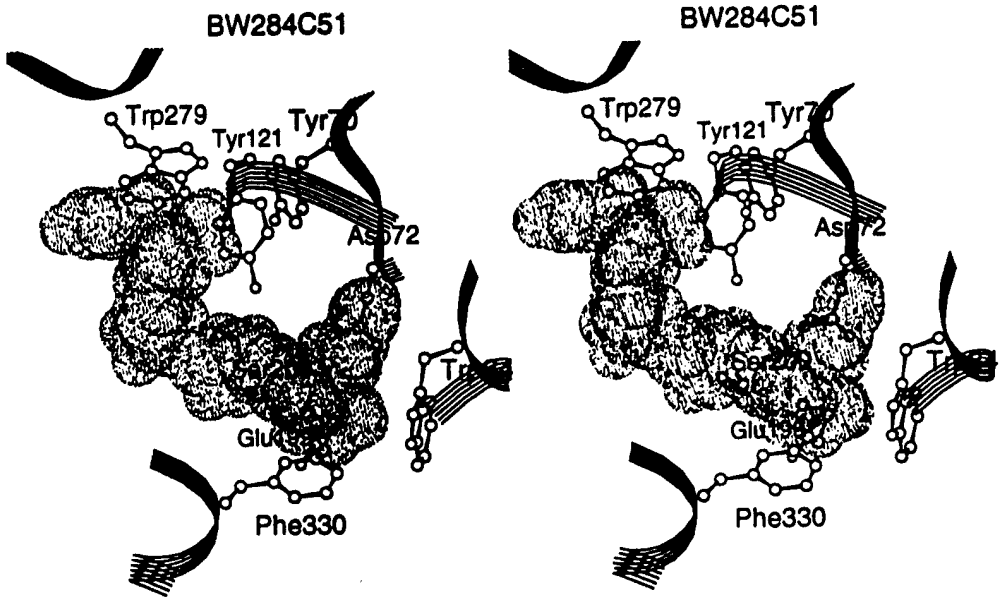

Figure 5 Positions of critical amino acid side chains for an energy minimized complex between BW284c51 and acetylcholinesterase (123).

to stabilization of the complex (123). W_{286} appears to be the most important residue for BW284c51, although each ligand shows slightly different partitioning of free energy. The involvement of only a small number of residues in stabilizing specific complexes is buttressed by the observation that a $BuChE_{1-174}$ $AChE_{175-575}$ chimera behaves like the $Y_{72}N,Y_{124}Q$ mutation and the $Y_{72}N,Y_{124}Q,W_{286}R$ mutation behaves similarly to mouse BuChE for inhibition by BW284c51. This is not the case for decamethonium and propidium, which suggests different binding loci for the latter ligands on the two respective cholinesterases (123).

$D_{74(72)}$ also affects the binding of these ligands (123, 125, 140) and it too is positioned rather close to the rim of the gorge. The site near the rim of the gorge defined by W_{286}, Y_{72}, Y_{124}, D_{74} has several features in common with the W_{86}, F_{337}, Y_{342}, E_{202} site found at the base of the gorge. Since *bis*-quaternary ligands span between the two sites, a similar complement of residues may thus be stabilizing each end of the *bis*-quaternary ligand.

$D_{74(72)}$ is conserved in BuChE as D_{70}. In fact, mutation of this residue to G is responsible for succinylcholine-induced paralysis in man (13, 14, 124, 125); an increased K_m and resistance to dibucaine inhibition and succinylcholine catalysis can be demonstrated in the mutant enzyme (140). Curiously, other mutations that concommitantly appear with the $D_{70}G$, H_{114}, Y_{561} and P_{425} restore some of the catalytic efficiency of the $D_{70}G$ mutation (140). Studies involving a BuChE template and replacement of residues with those found in AChE (135) and BuChE-AChE chimerae (141) have yielded results complementary to those obtained with the AChE template. In *Drosophila*, Y_{109} corresponds to D_{70} and mutations here influence inhibitor specificity (142).

Occupation of the peripheral site affects the conformation of the active center and the configuration of bound ligands at the active center (143, 144). Mutagenesis studies should further delineate the residues involved in this allosteric linkage (123, 138).

The three domains outlined above appear primarily responsible for the reported selectivity of AChE and BuChE for substrates and inhibitors. Specificity for acyl chain length and the propensity for substrate activation or inhibition are governed largely by the two phenylalanines, $F_{295(288)}$ and $F_{297(290)}$, whose side chains outline the acyl pocket. This region also governs the reactivity of isoOMPA for the enzyme; steric hindrance precludes isoOMPA from rapidly reacting with AChE. The BuChE selectivity of ethopropazine arises from its ability to be accommodated in the choline binding subsite. The diethylamino-2-propyl side chain exhibits interference with $F_{337(330)}$ in AChE whereas $A_{332(330)}$ in BuChE enables the fit (123). Finally, the site near the rim of the gorge dictates specificity of the *bis*-quaternary inhibitors and peptides that cannot fit at the base of the gorge; BW284c51, propidium, and fasciculin are the prime examples.

CARBOXYL-TERMINUS Several mutations of this region have emerged from a knowledge of the sequence and alternatively spliced forms. Gibney et al (126) documented the cassette characteristics of the individual exons. By splicing the invariant exons encoding the *Torpedo* enzyme to the exon encoding the glycophospholipid signal (exon 5) through loop-out mutagenesis, the glycophospholipid-linked form of AChE was synthesized in transfected COS cells. By dropping an intermediate exon, a truncated, but inactive, enzyme carrying the glycophospholipid-linkage was formed. By deleting the terminal exons (5 and 6), the expressed enzyme was secreted into the medium and lacked the glycophospholipid attachment. A natural splice variant in the mouse enzyme yields AChE with the same properties with virtually all of the enzyme appearing in the media (66, 67). Hence, the exon encoding the glycophospholipid linkage signal is both necessary and sufficient for generating the signal sequence for processing and addition of the glycophospholipid. Removal of the cysteine from exon 6 (128) or formation of a truncated hydrophilic form of the enzyme results in secretion of a monomeric enzyme (126). Similar dependencies of membrane attachments have been documented in *Drosophila* cholinesterase (145, 146).

An important development in the study of the assembly process has been the cloning of the gene that encodes the collagen-containing tail species in the *Torpedo* enzyme (147). Although there appear to be multiple tail subunits, coexpression of the cDNA encoding the catalytic subunit and that encoding the tail unit gave rise to the expected asymmetric species for both *Torpedo* and rat catalytic subunit cDNAs (28, 147). Moreover, truncation of the tail subunit cDNA showed that the amino-terminal portion of the tail molecule contains the sulfhydryl necessary for the intersubunit disulfide linkage (148).

Transfection of the cDNAs encoding the hydrophilic (exon 6) and glycophospholipid-linked (exon 5) forms of AChE generates the expected multiplicity of species seen in vivo (149). Hence, assembly to the various oligomeric species of AChE and processing occur with the transfected cDNAs. Transfection of mouse and human genomic constructs into various cell lines shows tissue selective splicing of mRNA to achieve a diversity of gene products (D Vellom, S Camp, and P Taylor, submitted).

GLYCOSYLATION Human AChE contains three N-linked glycosylation recognition sequences at N_{265}, N_{350}, and N_{464}. Deletion of the recognition sequences singly and in combination diminishes biosynthesis and secretion of the enzyme. The influence appears progressive since an enzyme deficient in all three signals shows the least expression, followed by the mutation with two of the three signals deleted (150). Glycosylation increases the thermal stability of the enzyme, but did not affect the catalytic parameters. Initial studies with the *Drosophila* enzyme also indicate that active enzyme can be synthesized in the absence of glycosylation (146, 151).

CHOLINESTERASE CHIMERAE Construction of cholinesterase chimerae has been useful in analyzing gene structure in relation to function and in identifying domains of the molecule responsible for particular functional characteristics. The initial approach deleted exon 5 and demonstrated secretion of the *Torpedo* enzyme (126); variants of this construct are discussed above. Attachment of the carboxyl-terminal signal sequence contained in exon 5 to upstream exons or to sequence encoding the amino-terminal portion of the collagen-containing tail unit yielded glycophospholipid-attached enzymes (126, 149). A second approach entailed forming BuChE chimerae between wild-type and naturally occurring mutants (125) and enabled examination of the influence of secondary mutations on the $D_{70}G$ mutation (125). Hence, portions of carboxyl-terminal domain of the molecule can modulate the consequences of an amino-terminal modification. Formation of active chimerae between AChE and BuChE have led to assigning domains responsible for inhibitor specificity, for delimiting the selection of residues in site-specific mutagenesis (131, 141). Comparisons of specificity between site-specific mutants and chimerae can often rule out an influence of several residues on inhibitor specificity.

Relationship of Ligand Binding Sites on Acetylcholinesterase to Those on Other Acetylcholine-Binding Proteins

Examination of the high resolution structure of AChE in relation to its functional characteristics and specificity of ligand binding sites may provide insights into the structure of other Ach binding proteins. We have already alluded to the similarities in both the proximal aromatic clusters and the more distant negative charges residing at the choline binding subsite and at the peripheral anionic site in AChE. Further parallels can be drawn with the aromatic clusters in the phosphorylcholine binding antibody and in chemically synthesized host ligands that bind quaternary ligands (87, 88, 152). Chemical labeling studies also show proximity of tyrosines and tryptophan in the vicinity of the ligand binding site on the acetylcholine receptor (153–155). Moreover, tacrine, a ligand that inhibits AChE by binding at the choline subsite (83, 123) also shows a propensity to inhibit K^+-channels. Mutagenesis studies are beginning to define the nature of a quaternary ammonium binding site within the K^+ channel, and a tyrosine substitution for threonine enhances tetraethylammonium inhibition of K^+ conductance (156). However, apart from using proximal aromatic residues and longer range electrostatic forces to stabilize the quaternary ligands and perhaps a more global organization of charges to form a macromolecular dipole to direct the binding of the ligand, there may be few specific parallels between the recognition sites on acetylcholine binding proteins.

In the case of the nicotinic acetylcholine receptor, the ligand binding site appears not to be in the central ion cavity or "gorge"; rather, agonists bind

at distinct sites at the periphery of the receptor (157). Entry of Ach to its two binding sites on the receptor appears to be normal to the axis defined by the ion permeability channel through the membrane. Finally, Ach binding sites are formed at subunit interfaces on the nicotinic receptor rather than being central to one of the subunits.

The muscarinic receptor presents an even different situation since the binding site must be constructed from within the seven membrane-spanning regions (158), a constraint not found for a globular protein or an extracellular domain of a membrane-associated protein.

Ach binds with relatively low affinity to an activatible state of the nicotinic receptor ($K_D \approx 10^{-4}$M), but short-term exposure results in desensitization and concomitant formation of a high-affinity state for Ach, $K_D = 5 \times 10^{-8}$M (153, 159, 160). This low dissociation constant may be contrasted with an AChE K_m of 0.5–1.0 $\times$ 10^{-4}M. Deconstruction of the AChE K_m would indicate that Ach dissociation constant (k_{-1}/k_1 in Scheme 1) is actually larger than K_m. Each state of the nicotinic receptor is designed to recognize the parent ligand whose acetoxy group is planar or trigonal, while in the case of AChE, the site is designed to force the formation of a transition state that is best approximated by a tetrahedral conformation around the carbonyl-containing carbon. The dissociation constant of the enzyme for this transition state, K_{TS}, can be estimated from $K_{TS} = K_m \cdot k_u/k_c$, where k_c/k_u (the ratio of catalyzed and uncatalyzed ester hydrolysis) is the catalytic enhancement provided by the enzyme. The product of K_m ($\sim 10^{-4}$ M) and k_u/k_c ($\sim 10^{-13}$) (113) yields a value of $\sim 10^{-17}$M and reflects a uniquely high affinity for the labile transition state of the substrate. Hence, receptors and AChE are designed to recognize and catalytically force or accommodate distinct conformations of acetylcholine. Accordingly, these unique binding characteristics are likely to be reflected in major differences in molecular and spatial characteristics of their respective binding sites.

Literature Cited

1. Clermont P. 1854. Note sur la préparation de quelques éthers. *CR Acad. Sci. Paris* 39:338–41
2. Argyll-Robinson D. 1863. The calibar bean as a new agent in ophthalmic practice. *Edinburgh Med. J.* 8:815–20
3. Dale HH. 1914. The action of certain esters of choline and their relation to muscarine. *J. Pharmacol. Exp. Ther.* 6:147–90
4. Loewi O, Navratil E. 1926. Über humorale Übertragbarkeit der Herznervenwirkung. XI. Über der Mechanismus der Vaguswirkung von Physostigmin und Ergotamin. *Pfluegers Arch.* 214:689–96
5. Ellman GL, Courtney KD, Andres V

Jr, Featherstone RM. 1961. A new and rapid colorimetric determination of acetylcholinesterase activity. *Biochem. Pharmacol.* 7:88–95
6. Koelle GB, Friedenwald JS. 1949. A histochemical method for localizing cholinesterase activity. *Proc. Soc. Exp. Biol. Med.* 70:617–22
7. Karnovsky MS, Roots L. 1964. A direct coloring thiocholine method for cholinesterase. *J. Histochem. Cytochem.* 12:219–32
8. Taylor P. 1990. Anticholinesterase agents. In *The Pharmacological Basis of Therapeutics*, ed. AG Gilman, LS Goodman, TW Rall, F Murad, AS Nies, P Taylor, pp. 131–49. New York: Pergamon. 8th ed.
9. Schumacher M, Camp S, Maulet Y, Newton M, MacPhee-Quigley K, et al. 1986. Primary structure of *Torpedo californica* acetylcholinesterase deduced from cDNA sequences. *Nature* 319:407–9
10. Sussman JL, Harel M, Frolow F, Oefner C, Goldman A, et al. 1991. Atomic structure of acetylcholinesterase from *Torpedo californica:* a prototypic acetylcholine-binding protein. *Science* 253:872–79
11. Quinn DM. 1987. Acetylcholinesterase: enzyme structure, reaction dynamics, and virtual transition states. *Chem. Rev.* 87:955–79
12. Rosenberry TL. 1975. Acetylcholinesterase. *Adv. Enzymol. Relat. Areas Mol. Biol.* 43:103–218
13. Whittaker M. 1986. Cholinesterases. In *Monographs in Human Genetics*, ed. RS Sparkes, 11:125. Basel: Karger
14. Soreq H, Zakut H. 1990. Cholinesterase genes: multileveled regulation. In *Monographs in Human Genetics*, ed. RS Sparkes, 13:1–102. Basel: Karger
15. Sussman JL, Silman I. 1992. Acetylcholinesterase: structure and use as a model for specific cation protein interactions. *Curr. Opin. Struct. Biol.* 2:721–29
16. Taylor P. 1991. The cholinesterases. *J. Biol. Chem.* 266:4025–28
17. Massoulié J, Pezzementi L, Bon S, Krejci E, Vallette FM. 1993. Molecular and cellular biology of the cholinesterases. *Prog. Neurobiol.* 41: 31–91
18. Shafferman A, Velan B, eds. 1992. *Multidisciplinary Approaches to Cholinesterase Functions*. New York: Plenum. 293 pp.
19. Swillens S, Ludgate M, Mercken L, Dumont JE, Vassart G. 1986. Analysis of sequence and structure homologies between thyroglobulin and acetylcholinesterase: possible functional and clinical significance. *Biochem. Biophys. Res. Commun.* 137:142–48
20. Hall LMC, Spierer P. 1986. The *Ace* locus of *Drosophila melanogaster:* structural gene for acetylcholinesterase with an unusual 5′ leader. *EMBO J.* 5:2949–54
21. Lockridge O, Bartels CF, Vaughan TA, Wong CK, Norton SE, Johnson LL. 1987. Complete amino acid sequence of human serum cholinesterase. *J. Biol. Chem.* 262:549–57
22. Prody CA, Zevin-Sonkin D, Gnatt A, Goldberg O, Soreq H. 1987. Isolation and characterization of full-length cDNA clones coding for cholinesterase from fetal human tissues. *Proc. Natl. Acad. Sci. USA* 84:3555–59
23. McTiernan C, Adkins S, Chatonnet A, Vaughan TA, Bartels CF, et al. 1987. Brain cDNA clone for human cholinesterase. *Proc. Natl. Acad. Sci. USA* 84:6682–86
24. Rachinsky TL, Camp S, Li Y, Ekström TJ, Newton M, Taylor P. 1990. Molecular cloning of mouse acetylcholinesterase: tissue distribution of alternatively spliced mRNA species. *Neuron* 5:317–27
25. Doctor BP, Chapman TC, Christner CE, Deal CD, De La Hoz DM, et al. 1990. Complete amino acid sequence of fetal bovine serum acetylcholinesterase and its comparison in various regions with other cholinesterases. *FEBS Lett.* 266:123–27
26. Soreq H, Ben-Aziz R, Prody CA, Seidman S, Gnatt A, et al. 1990. Molecular cloning and construction of the coding region for human acetylcholinesterase reveals a G+C-rich attenuating structure. *Proc. Natl. Acad. Sci. USA* 87:9688–92
27. Chatonnet A, Lorca T, Barakat A, Aron E, Jbilo O. 1991. Structure of rabbit butyrylcholinesterase gene deduced from genomic clones and from a cDNA with introns. *Cell Mol. Neurobiol.* 11:119–30
28. Legay C, Bon S, Vernier P, Coussen F, Massoulié J. 1993. Cloning and expression of a rat acetylcholinesterase subunit: generation of multiple molecular forms and complementarity with a *Torpedo* collagenic subunit. *J. Neurochem.* 60:337–46
29. Hall LMC, Malcolm CA. 1991. The acetylcholinesterase gene of *Anopheles stephensi*. *Cell. Mol. Neurobiol.* 11: 131–41
30. Maulet Y, Ballivet M. 1991. Two

different genes encoding cholinesterases in chicken. See Ref. 162, p. 186
31. Rubino S, Mann SKO, Hori RT, Pinko C, Firtel RA. 1989. Molecular analysis of a developmentally regulated gene required for *Dictyostelium* aggregation. *Dev. Biol.* 131:27–36
32. Bomblies L, Biegelmann E, Döring V, Gerisch G, Krafft-Czepa H, et al. 1990. Membrane-enclosed crystals in *Dictyostelium discoideum* cells, consisting of developmentally regulated proteins with sequence similarities to known esterases. *J. Cell Biol.* 110:669–79
33. Oakeshott JG, Collet C, Phillis RW, Nielsen KM, Russell RJ, et al. 1987. Molecular cloning and characterization of esterase-6, a serine hydrolase of *Drosophila*. *Proc. Natl. Acad. Sci. USA* 84:3359–63
34. Collet C, Nielsen KM, Russell RJ, Karl M, Oakeshott JG, Richmond RC. 1990. Molecular analysis of duplicated esterase genes in *Drosophila melanogaster*. *Mol. Biol. Evol.* 7:9–28
35. Mouches C, Pauplin Y, Agarwal M, Lemieux L, Herzog M, et al. 1990. Characterization of amplification core and esterase B1 gene responsible for insecticide resistance in *Culex*. *Proc. Natl. Acad. Sci. USA* 87:2574–78
36. Hanzlik TN, Abdel-Aal YAI, Harshman LG, Hammock BD. 1989. Isolation and sequencing of cDNA clones coding for juvenile hormone esterase from *Heliothis virescens*. Evidence for a catalytic mechanism for the serine carboxylesterases different from that of the serine proteases. *J. Biol. Chem.* 264:12419–25
37. Shimada Y, Sugihara A, Tominaga Y, Izumi T, Tsunasawa S. 1989. cDNA molecular cloning of *Geotrichum candidum* lipase. *J. Biochem.* 106:383–88
38. Long RM, Satoh H, Martin BM, Kimura S, Gonzalez FJ, Pohl LR. 1988. Rat liver carboxylesterase: cDNA cloning, sequencing, and evidence for a multigene family. *Biochem. Biophys. Res. Commun.* 156:866–73
39. Korza G, Ozols J. 1988. Complete covalent structure 60-kDa esterase isolated from 2,3,7,8-tetrachlorodibenzo-p-dioxin-induced rabbit liver microsomes. *J. Biol. Chem.* 263:3486–95
40. Han JH, Stratowa C, Rutter WJ. 1987. Isolation of full-length putative rat lysophospholipase cDNA using improved methods for mRNA isolation and cDNA cloning. *Biochemistry* 26: 1617–25
41. Kyger EM, Wiegand RC, Lange LG. 1989. Cloning of the bovine pancreatic cholesterol esterase/lysophospholipase. *Biochem. Biophys. Res. Commun.* 164: 1302–9
42. Ollis DL, Cheah E, Cygler M, Dijkstra B, Frolow F, et al. 1992. The α/β hydrolase fold. *Prot. Eng.* 5:197–211
43. Cooper A, Russey H. 1989. Characterization of the yeast KEX1 gene product: a carboxypeptidase involved in processing secreted precursor proteins. *Mol. Cell. Biol.* 9:2706–14
44. Franken SM, Rozeboom HJ, Kalk KH, Dijkstra BW. 1991. Crystal structure of haloalkane dehalogenase: an enzyme to detoxify halogenated alkanes. *EMBO J.* 10:1297–302
45. Pathak D, Ngai KL, Ollis D. 1988. X-ray crystallographic structure of dienelactone hydrolase at 2.8 Å. *J. Mol. Biol.* 204:435–45
46. Olson PF, Fessler LI, Nelson RE, Campbell AG, Fessler JH. 1990. Glutactin, a novel *Drosophila* basement membrane related glycoprotein with sequence similarity to serine esterases. *EMBO J.* 9:3593–601
47. De la Escalera S, Backamp E-O, Moya F, Piovant M, Jimenez F. 1990. Characterization and gene cloning of neurotactin, a *Drosophila* transmembrane protein related to cholinesterases. *EMBO J.* 9:3593–601
48. Gentry MK, Doctor BP. 1991. Alignment of amino acid sequences of acetylcholinesterases and butyrylcholinesterases. See Ref. 162, pp. 394–98
49. Cygler M, Schrag J, Sussman JL, Harel M, Silman I, et al. 1993. Relationship between sequence conservation and three-dimensional structure in a large family of esterases, lipases, and related proteins. *Protein Sci.* 2: 366–82
50. MacPhee-Quigley K, Vedvick TS, Taylor P, Taylor SS. 1986. Profile of disulfide bonds in acetylcholinesterase. *J. Biol. Chem.* 261:13565–70
51. Lockridge O, Adkins S, La Du BN. 1987. Location of disulfide bonds within the sequence of human serum cholinesterase. *J. Biol. Chem.* 262: 12945–52
52. MacPhee-Quigley K, Taylor P, Taylor SS. 1985. Primary structures of the catalytic subunits from two molecular forms of acetylcholinesterase: a comparison of NH2-terminal and active center sequences. *J. Biol. Chem.* 260: 12185–89
53. Gibney G, Camp S, Dionne M, MacPhee-Quigley K, Taylor P. 1990. Mu-

tagenesis of essential functional residues in acetylcholinesterase. *Proc. Natl. Acad. Sci. USA* 87:7546–50
54. Augustinsson KB. 1948. Cholinesterases: a study in comparative enzymology. *Acta Physiol. Scand.* 15 (Suppl. 52:1–182
55. Silver A. 1974. *The Biology of Cholinesterases*. Amsterdam: North-Holland
56. Gnagey AL, Forte M, Rosenberry TL. 1987. Isolation and characterization of acetylcholinesterase from *Drosophila*. *J. Biol. Chem.* 262:1140–45
57. Toutant J-P, Massoulié J, Bon S. 1985. Polymorphism of pseudocholinesterase in *Torpedo marmorata* tissues: comparative study of the catalytic and molecular properties of this enzyme with acetylcholinesterase. *J. Neurochem.* 44:580–92
58. Johnson CD, Rand JB, Herman RK, Stern BD, Russell RL. 1988. The acetylcholinesterase genes of *C. elegans:* identification of a third gene (ace-3) and mosaic mapping of a synthetic lethal phenotype. *Neuron* 1:165–73
59. Arpagaus M, Richier P, L'Hermitte Y, Le Roy F, Bergé J, et al. 1992. Nematode acetylcholinesterases: several genes and molecular forms of their products. See Ref. 18, pp. 65–74
60. Maulet Y, Camp S, Gibney G, Rachinsky TL, Ekström TJ, Taylor P. 1990. A single gene encodes glycophospholipid-anchored and asymmetric acetylcholinesterase forms: alternative coding exons contain inverted repeat sequences. *Neuron* 4:289–301
61. Li Y, Camp S, Rachinsky TL, Getman DK, Taylor P. 1991. Gene structure of mammalian acetylcholinesterase: alternative exons dictate tissue-specific expression. *J. Biol. Chem.* 266:23083–90
62. Arpagaus M, Kott M, Vatsis KP, Bartels CF, La Du BN, Lockridge O. 1990. Structure of the gene for human butyrylcholinesterase. Evidence for a single copy. *Biochemistry* 29:124–31
63. Sikorav JL, Krejci E, Massoulié J. 1987. cDNA sequences of *Torpedo marmorata* acetylcholinesterase: primary structure of the precursor of a catalytic subunit; existence of multiple 5'-untranslated regions. *EMBO J.* 6: 1865–73
64. Sikorav JL, Duval N, Anselmet A, Bon S, Krejci E, et al. 1988. Complex alternative splicing of acetylcholinesterase transcript in *Torpedo* electric organ; primary structure of the precursor of the glycolipid-anchored dimeric form. *EMBO J.* 7:2983–93
65. Schumacher M, Maulet Y, Camp S, Taylor P. 1988. Multiple messenger RNA species give rise to the structural diversity in acetylcholinesterase. *J. Biol. Chem.* 263:18979–87
66. Li Y, Camp S, Taylor P. 1993. Tissue-specific expression and alternative mRNA processing of the mammalian acetylcholinesterase gene. *J. Biol. Chem.* 268:5790–97
67. Li Y, Camp S, Rachinsky TL, Bongiorno C, Taylor P. 1993. Promoter elements and transcriptional control of the mouse acetylcholinesterase gene. *J. Biol. Chem.* 268:3563–72
68. Gibney G, MacPhee-Quigley K, Thompson B, Vedvick T, Low MG, et al. 1988. Divergence in primary structure between molecular forms of acetylcholinesterase. *J. Biol. Chem.* 263:1140–45
69. Rotundo RL, Gomez AM, Fernandez-Valle C, Randall WR. 1988. Allelic variants of acetylcholinesterase forms in avian nerves and muscle and encoded by a single gene. *Proc. Natl. Acad. Sci. USA* 52:7121–25
70. Getman DK, Eubanks J, Evans G, Taylor P. 1992. Assignment of the human acetylcholinesterase gene to chromosome 7q22. *Am. J. Hum. Genet.* 50:170–77
71. Ehrlich G, Viegas-Pequignot E, Ginzberg D, Sindel L, Soreq H, Zakut H. 1992. Mapping the human acetylcholinesterase gene to chromosome 7q22 by fluorescent in situ hybridization coupled with selective PCR amplification from a somatic hybrid cell panel and chromosome-sorted DNA libraries. *Genomics* 13:1192–97
72. Gaughan G, Park H, Priddle J, Craig I, Craig S. 1991. Refinement of the localization of human butyrylcholinesterase to chromosome 3q26.1-q26.2 using a PCR-derived probe. *Genomics* 11:455–58
73. Allderdice PW, Gardner HAR, Galutira D, Lockridge O, La Du BN, McAlpine PJ. 1991. The cloned butyrylcholinesterase (*BCHE*) gene maps to a single chromosome site, 3q26. *Genomics* 11:452–54
74. Rachinsky TL, Crenshaw EB III, Taylor P. 1992. Assignment of the gene for acetylcholinesterase to distal mouse-chromosome 5. *Genomics* 14:511–14
75. Sussman JL, Harel M, Frolow F, Varon L, Toker L, et al. 1988. Purification and crystallization of a dimeric form of acetylcholinesterase from *Torpedo*

californica subsequent to solubilization with phosphatidylinositol-specific phospholipase. *J. Mol. Biol.* 203:821–23
76. Schrag JD, Schmid MF, Morgan DG, Phillips GN, Wah C, Tang L. 1988. Crystallization and preliminary X-ray diffraction analysis of 11S acetylcholinesterase. *J. Biol. Chem.* 263: 9795–801
77. Schrag JD, Li Y, Wu S, Cygler M. 1991. Ser-His-Glu triad forms the catalytic site of the lipase from *Geotrichum candidum*. *Nature* 351: 761–64
78. Harel M, Sussman JL, Krejci E, Bon S, Chanal P, et al. 1992. Conversion of acetylcholinesterase to butyrylcholinesterase, modeling and mutagenesis. *Proc. Natl. Acad. Sci. USA* 89: 10827–31
79. Rosenberry TL, Neumann E. 1977. Interaction of ligands with acetylcholinesterase. Use of temperature-jump relaxation kinetics in the binding of specific fluorescent ligands. *Biochemistry* 16:3870–78
80. Nolte HJ, Rosenberry TL, Neumann E. 1980. Effective charge on acetylcholinesterase active sites determined from the ionic strength dependence of association rate constants with cationic ligands. *Biochemistry* 19:3705–11
81. Tan RC, Truong TN, McCammon JA, Sussman JL. 1993. Acetylcholinesterase: electrostatic steering increases the rate of ligand binding. *Biochemistry* 32:401–3
82. Ripoll DR, Faerman CH, Axelsen PH, Silman I, Sussman JL. 1993. An electrostatic mechanism for substrate guidance down the aromatic gorge of acetylcholinesterase. *Proc. Natl. Acad. Sci. USA* 90:5128–32
83. Sussman JL, Harel M, Silman I. 1992. Three dimensional structure of acetylcholinesterase. See Ref. 18, pp. 95–108
84. Harel M, Schalk I, Ehret-Sabatier L, Bouet F, Goeldner M, et al. 1993. Quaternary ligand binding site of acetylcholinesterase as revealed by X-ray crystallography and photoaffinity labelling. *Proc. Natl. Acad. Sci. USA*. 90:9031–35
85. Hasan FB, Cohen SG, Cohen JB. 1980. Hydrolysis by acetylcholinesterase. Apparent molal volumes and trimethyl and methyl subsites. *J. Biol. Chem.* 255:3898–904
86. Cohen SG, Salih E, Solomon M, Howard S, Chishti SB, Cohen JB. 1989. Reactions of 1-bromo-2-[^{14}C]pinacolone with acetylcholinesterase from *Torpedo nobiliana*. Effects of 5-trimethylammonio-2-pentanone and diisopropyl fluorophosphate. *Biochem. Biophys. Acta* 997:167–75
87. Dougherty DA, Stauffer DA. 1990. Acetylcholine binding by a synthetic receptor: implication for biological recognition. *Science* 250:1558–60
88. Segal DM, Padlan EA, Cohen GH, Rudikoff S, Potter M, Davies DR. 1974. The three-dimensional structure of phosphorylcholine—binding mouse immunoglobulin Fab and the nature of the antigen binding site. *Proc. Natl. Acad. Sci. USA* 71:4295–302
89. Pressman D, Grossberg AL, Pence LH, Pauling L. 1946. The reaction of antiserum homologous to the p-azo phenyltrimethylammonium group. *J. Am. Chem. Soc.* 68:250–55
90. Changeux J-P. 1966. Responses of acetylcholinesterase from *Torpedo marmorata* to salts and curarizing drugs. *Mol. Pharmacol.* 2:369–92
91. Taylor P, Lappi S. 1975. Interaction of fluorescence probes with acetylcholinesterase. The site and specificity of propidium binding. *Biochemistry* 14: 1989–97
92. Berman HA, Yguerabide J, Taylor P. 1980. Fluorescence energy transfer on acetylcholinesterase: spatial relationship between peripheral site and active center. *Biochemistry* 19:2226–35
93. Weise C, Kreienkamp HJ, Raba R, Pedak A, Aaviksaar A, Hucho F. 1990. Anionic subsites of the acetylcholinesterase from *Torpedo californica:* affinity labelling with the cationic reagent *N,N*-dimethyl-2-phenyl-aziridinium. *EMBO J.* 9:3885–88
94. Amitai G, Taylor P. 1991. Characterization of peripheral anionic site peptides of AChE by photoaffinity labeling with monoazidopropidium (MAP). See Ref. 162, p. 285
95. Haas R, Adams EW, Rosenberry MA, Rosenberry TL. 1992. Substrate-selective inhibition and peripheral site labeling of acetylcholinesterase by platinum(terpyridine)chloride. See Ref. 18, pp. 131–40
96. Marchot P, Khelif A, Ji YH, Mansuelle P, Bougis PE. 1993. Binding of ^{125}I-fasciculin to rat brain acetylcholinesterase. The complex still binds diisopropyl fluorophosphate. *J. Biol. Chem.* 268:12458–67
97. Cervenansky C, Dajas F, Harvey AL, Karlsson E. 1991. The fasciculins. In *Snake Toxins*, ed. AC Harvey, pp. 303–21. New York: Pergamon
98. Radić Z, Reiner E, Taylor P. 1991.

Role of the peripheral anionic site on acetylcholinesterase: inhibition by substrates and coumarin derivatives. *Mol. Pharmacol.* 39:98–104

99. Berman HA, Nowak MW. 1992. Influence of ion composition of the medium on acetylcholinesterase conformation. See Ref. 18, pp. 149–56
100. Wilson IB, Quan C. 1958. Acetylcholinesterase studies on molecular complementariness. *Arch. Biochem. Biophys.* 73:131–38
101. Kreienkamp HJ, Weise C, Raba R, Aaviksaar A, Hucho F. 1991. Anionic subsites of the catalytic center of acetylcholinesterase from *Torpedo* and from cobra venom. *Proc. Natl. Acad. Sci. USA* 88:6117–21
102. Schalk I, Ehret-Sabatier L, Bouet F, Goeldner M, Hirth C. 1992. Structural analysis of acetylcholinesterase ammonium binding sites. See Ref. 18, pp. 117–20
103. Shinitzky M, Dudai Y, Silman I. 1973. Spectral evidence for the presence of tryptophan in the binding site of acetylcholinesterase. *FEBS Lett.* 30: 125–28
104. Mooser G, Sigman DS. 1974. Ligand binding properties of acetylcholinesterase determined with fluorescent probes. *Biochemistry* 13:2299–307
105. Barnett P, Rosenberry TL. 1977. Catalysis by acetylcholinesterase: acceleration of the hydrolysis of neutral acetic acid esters by certain aromatic cations. *J. Biol. Chem.* 252:7200–6
106. Berman HA, Leonard K. 1989. Chiral reactions of acetylcholinesterase probed with enantiomeric methylphosphonothioates. Noncovalent determinants of enzyme chirality. *J. Biol. Chem.* 264:3942–50
107. Belleau B, DiTullio V. 1970. Kinetic effects of alkyl quaternary ammonium salts on the methanesulfonylation of the acetylcholinesterase catalytic center. Significance of substituent volumes and binding enthalpies. *J. Am. Chem. Soc.* 92:6320–25
108. Belleau B, DiTullio V, Tsai Y-H. 1970. Kinetic effects of leptocurares and pachycurares on the methanesulfonylation of acetylcholinesterase. A correlation with pharmacodynamic properties. *Mol. Pharmacol.* 6:41–45
109. Wilson IB. 1967. Conformation changes in acetylcholinesterase. *Ann. NY Acad. Sci.* 144:664–79
110. Taylor P, Jacobs NM. 1974. Interaction between bisquaternary ammonium ligands and acetylcholinesterase: complex formation studied by fluorescence quenching. *Mol. Pharmacol.* 10:93–107
111. Wee VT, Sinha BK, Taylor P, Chignell CF. 1976. Interaction of spin-labeled bisquaternary ammonium ligands with acetylcholinesterase. *Mol. Pharmacol.* 12:667–77
112. Aldridge WN, Reiner E. 1972. *Enzyme Inhibitors as Substrates*, Amsterdam: Elsevier. 328 pp.
112a. Himel CM, Taylor JL, Pape C, Millar DB, Christopher J, Kurlansik L. 1979. Acridine araphanes: a new class of probe materials for biological receptors. *Science* 205:1277–79
113. Bazclyansky M, Robey E, Kirsch JF. 1986. Fractional diffusion limited component of reactions catalyzed by acetylcholinesterase. *Biochemistry* 25: 125–32
114. Quinn DM, Pryor AN, Selwood T, Lee BH, Acheson SA, Barlow PN. 1991. The chemical mechanism of acetylcholinesterase reactions. Biological catalysis at the speed limit. See Ref. 162, pp. 252–57
115. Froede HC, Wilson IB. 1984. Direct determination of acetyl-enzyme intermediate in the acetylcholinesterase catalysis of acetylcholine and acetylthiocholine. *J. Biol. Chem.* 259:11010–13
116. Quinn DM, Selwood T, Pryor AN, Lee BH, Leu L-S, et al. 1992. Cryptic catalysis and cholinesterase function. See Ref. 18, pp. 141–48
117. Albery WJ, Knowles JR. 1976. Evolution of enzyme function and the development of catalytic efficiency. *Biochemistry* 15:5631–40
118. Rosenberry TL. 1975. Catalysis by acetylcholinesterase: Evidence that the rate-limiting step for acylation with certain substrates precedes general acid-base catalysis. *Proc. Natl. Acad. Sci. USA* 72:3834–38
119. Pryor AN, Selwood T, Leu L-S, Andracki MA, Lee BH, et al. 1992. Simple general acid-base catalysis of physiological acetylcholinesterase reactions. *J. Am. Chem. Soc.* 114:3896–900
120. Krupka RM, Laidler KJ. 1961. Molecular mechanisms for hydrolytic enzyme action II. Inhibition of acetylcholinesterase by excess substrate. *J. Am. Chem. Soc.* 83:1448–54
121. Augustinsson KB, Bartfai T, Mannervik B. 1974. A steady state model for butyrylcholinesterase from horse plasma. *Biochem. J.* 141:825–34
122. Cauet G, Friboulet A, Thomas D. 1987. Horse serum butyrylcho-

linesterase kinetics: a molecular mechanism based on inhibition studies with dansylaminoethyl trimethylammonium. *Biochem. Cell. Biol.* 65:529–35
123. Radic Z, Pickering N, Vellom DC, Camp S, Taylor P. 1993. Three distinct domains in the cholinesterase molecule confer selectivity for acetylcholinesterase and butyrylcholinesterase inhibitors. *Biochemistry*. 32:12074–84
124. La Du BN, Bartels CF, Nogueira CP, Arpagaus M, Lockridge O. 1991. Proposed nomenclature for human butyrylcholinesterase genetic variants identified by DNA sequencing. *Cell. Mol. Neurobiol.* 11:79–90
125. Neville LF, Gnatt A, Padan R, Seidman S, Soreq H. 1990. Anionic site interactions in human butyrylcholinesterase disrupted by two single point mutations. *J. Biol. Chem.* 265: 20735–38
126. Gibney G, Taylor P. 1990. Biosynthesis of *Torpedo* acetylcholinesterase in mammalian cells. Functional expression and mutagenesis of the glycophospholipid-anchored form. *J. Biol. Chem.* 265:12576–83
127. Soreq H, Seidman S. 1992. *Xenopus* oocyte microinjection: from gene to protein. *Methods Enzymol.* 207:225–65
128. Velan B, Grosfeld H, Kronman C, Leitner M, Gozes Y. 1991. The effect of elimination of intersubunit disulfide bonds on the activity, assembly, and secretion of recombinant human acetylcholinesterase: expression of acetylcholinesterase CYS-580-Ala mutant. *J. Biol. Chem.* 266: 23977–84
129. Shafferman A, Kronman C, Flashner Y, Leitner M, Grosfeld H, et al. 1992. Mutagenesis of human acetylcholinesterase; identification of residues involved in catalytic activity and in polypeptide folding. *J. Biol. Chem.* 267:17640–48
130. Shafferman A, Velan B, Ordentlich A, Kronman C, Grosfeld H, et al. 1992. Substrate inhibition of acetylcholinesterase: residues involved in signal transduction from the surface to the catalytic center. *EMBO J.* 11: 3561–68
131. Vellom DC, Radic Z, Li Y, Pickering NA, Camp S, Taylor P. 1993. Amino acid residues controlling acetylcholinesterase and butyrylcholinesterase specificity. *Biochemistry* 32:12–17
132. Radic Z, Gibney G, Kawamoto S, MacPhee-Quigley K, Bongiorno C, Taylor P. 1992. Expression of recombinant acetylcholinesterase in a *Baculovirus* system: kinetic properties of glutamate 199 mutants. *Biochemistry* 31:9760–67
133. Fischer M, Ittah A, Liefer I, Gorecki M. 1993. Expression and recognition of biologically active human acetylcholinesterase from *E. coli*. *Cell Mol. Neurobiol.* 13:25–38
134. Duval N, Bon S, Silman I, Sussman JL, Massoulié J. 1992. Site-directed mutagenesis of active site-related residues in *Torpedo* acetylcholinesterase. Presence of a glutamic acid in the catalytic triad. *FEBS Lett.* 309:421–23
135. Gnatt A, Lowenstein Y, Yaron A, Schwarz M, Soreq H. 1993. Site-directed mutagenesis of active site residues reveals plasticity of human butyrylcholinesterase in substrate and inhibitor interactions. *J. Neurochem.* In press
136. Krejci E, Duval N, Chatonnet A, Vincens P, Massoulié J. 1991. Cholinesterase-like domains in enzymes and structural proteins: functional and evolutionary relationships and identification of a catalytically essential aspartic acid. *Proc. Natl. Acad. Sci. USA* 88:6647–51
137. Chatel JM, Grassi J, Frobert Y, Massoulié J, Vallette FM. 1993. Existence of an inactive pool of acetylcholinesterase in chicken brain. *Proc. Natl. Acad. Sci. USA* 90:2476–80
138. Ordentlich A, Barak D, Kronman C, Flashner Y, Leitner M, et al. 1993. Dissection of the human acetylcholinesterase active center—Determinants of substrate specificity. *J. Biol. Chem.* 268:17083–95
139. Fournier D, Bride J-M, Hoffmann F, Karch F. 1992. Acetylcholinesterase: two types of modifications confer resistance to insecticide. *J. Biol. Chem.* 267:14270–74
140. Neville LF, Gnatt A, Loewenstein Y, Seidman S, Ehrlich G, Soreq H. 1992. Intramolecular relationships in cholinesterases revealed by oocyte expression of site-directed and natural variants of human BCHE. *EMBO J.* 11:1641–49
141. Lowenstein Y, Gnatt A, Neville LF, Soreq H. 1993. A chimeric human cholinesterase: identification of interaction sites responsible for recognition of acetyl-, butyrylcholinesterase specific ligands. *J. Mol. Biol.* 234:289–96
142. Mutero A, Pravalorio M, Simeon V, Fournier D. 1992. Catalytic properties

of cholinesterases: importance of tyrosine 109 in *Drosophila* protein. *NeuroReport* 3:39–42

143. Epstein DJ, Berman HA, Taylor P. 1979. Ligand-induced conformational changes in acetylcholinesterase investigated with fluorescent phosphonates. *Biochemistry* 18:4749–54
144. Berman HA, Becktel W, Taylor P. 1981. Spectroscopic studies on acetylcholinesterase: influence of peripheral-site occupation on active-center conformation. *Biochemistry* 20: 4803–10
145. Fournier D, Mutero A, Rungger D. 1992. *Drosophila* acetylcholinesterase: expression of a functional precursor in *Xenopus* oocytes. *Eur. J. Biochem.* 203:513–19
146. Fournier D, Mutero A, Pravalorio M, Bride J-M. 1992. *Drosophila* acetylcholinesterase: analysis of structure and sensitivity to insecticides by in vitro mutagenesis and expression. See Ref. 18, pp. 75–82
147. Krejci E, Coussen F, Duval N, Chatel JM, Legay C, et al. 1991. Primary structure of a collagenic tail subunit of *Torpedo* acetycholinesterase: co-expression with catalytic subunit induces the production of collagen-tailed forms in transfected cells. *EMBO J.* 10:1285–93
148. Duval N, Krejci E, Grassi J, Coussen F, Massoulié J, Bon S. 1992. Molecular architecture of acetylcholinesterase collagen-tailed forms: construction of a glycolipid-tailed tetramer. *EMBO J.* 9:3255–61
149. Duval N, Massoulié J, Bon S. 1992. H and T subunits of acetylcholinesterase from *Torpedo*, expressed in COS cells, generate all types of globular forms. *J. Cell Biol.* 118:641–53
150. Velan B, Kronman C, Ordentlich A, Flashner Y, Leitner M, et al. 1993. N-glycosylation of human acetylcholinesterase effects enzyme stability and secretion efficiency but not enzymatic activity. *Biochem. J.* In press
151. Mutero A, Fournier D. 1992. Post-translational modifications of *Drosophila* acetylcholinesterase. In vitro mutagenesis and expression in *Xenopus* oocytes. *J. Biol. Chem.* 267: 1695–700
152. McCury A, Jimenez L, Stauffer DA, Dougherty DA. 1992. Biomimetic catalysis of S_N2 reactions through cation-π interactions. The role of polarizability in catalysis. *J. Am. Chem. Soc.* 114:10314–21
153. Changeux J-P, Galzi J-L, Devillers-Thiery A, Bertrand D. 1992. The functional architecture of the acetylcholine nicotinic receptor explored by affinity labelling and site-directed mutagenesis. *Q. Rev. Biophys.* 25:395–432
154. Abramson SN, Li Y, Culver P, Taylor P. 1989. An analog of lophotoxin reacts covalently with Tyr^{190} in the α-subunit of the nicotinic acetylcholine receptor. *J. Biol. Chem.* 264:12666–72
155. Cohen JB, Sharp SD, Liu WS. 1991. Structure of the agonist-binding site of the nicotinic acetylcholine receptor: [^{3}H]acetylcholine mustard identifies residues in the cation-binding subsite. *J. Biol. Chem.* 266:23354–64
156. Heginbotham L, MacKinnon R. 1992. The aromatic binding site for tetraethylammonium ion on potassium channels. *Neuron* 8:483–91
157. Unwin NJM. 1993. Nicotinic acetylcholine receptor at 9 Å resolution. *J. Mol. Biol.* 229:1101–24
158. Hulme EC, Kurtenbach E, Curtis CA. 1991. Muscarinic acetylcholine receptors: structure and function. *Biochem. Soc. Trans.* 19:133–38
159. Taylor P, Johnson DA, Brown RD. 1983. The linkage between ligand occupation and response of the nicotinic acetylcholine receptor. In *Advances in Membranes and Transport*, ed. A Kleinzeller, BR Martin, pp. 407–43. New York: Academic
160. Sine SM, Claudio T, Sigworth FJ. 1990. Activation of *Torpedo* acetylcholine receptors in mouse fibroblasts: Single channel current kinetics reveal distinct agonist binding affinities. *J. Gen. Physiol.* 153:305–12
161. Bartels CF, Zelinski T, Lockridge O. 1993. Mutation at codon 322 in the human acetylcholinesterase (ACHE) gene accounts for YT blood group polymorphism. *Am. J. Hum. Genet.* 52:928–36
162. Massoulié J, Bacou F, Barnard E, Chatonnet A, Doctor BP, Quinn DM, eds. 1991. *Cholinesterases: Structure, Function, Mechansism, Genetics and Cell Biology*. Washington, DC: Am. Chem. Soc. 414 pp.
163. Mason P, Adkins S, Gouet P, Lockridge O. 1993. Recombinant human butyrylcholinesterase G39OV, the fluoride-2 variant expressed in Chinese hamster ovary cells, is a low affinity variant. *J. Biol. Chem.* 268:14329–41
164. Fournier D, Mutero A, Pravalorio M,

Bride JM. 1993. *Drosophila* acetylcholinesterase: mechanism of resistance to organophosphates. *Chem. Biol. Interact.* 87:233–38

165. Kerem A, Kronman C, Bar-Nun S, Shafferman A, Velan B. 1993. Interrelations between assembly and secretion of recombinant human acetylcholinesterase. *J. Biol. Chem.* 268: 180–84
166. Saxena A, Doctor BP, Maxwell DM, Lenz DE. Radicac Z, Taylor P. 1993. The role of glutamate 199 in the aging of cholinesterase. *Biochem. Biophys. Res. Commun.* In Press

PRS 95-364

Protein Science (1996), 5:000–000. Cambridge University Press. Printed in the USA.

Soluble monomeric acetylcholinesterase from mouse: Expression, purification, and crystallization in complex with fasciculin

PASCALE MARCHOT,[1,6] RAIMOND B.G. RAVELLI,[2] MIA L. RAVES,[3,5] YVES BOURNE,[4,7] DANIEL C. VELLOM,[1,8] JOAN KANTER,[1] SHELLEY CAMP,[1] JOEL L. SUSSMAN,[3,5] AND PALMER TAYLOR[1]

[1] Department of Pharmacology, University of California at San Diego, La Jolla, California 92093-0636
[2] Department of Crystal and Structural Chemistry, Bijvoet Center for Molecular Research, 3584 Utrecht, The Netherlands
[3] Biology Department, Brookhaven National Laboratory, Upton, Long Island, New York 11973
[4] Department of Molecular Biology, The Scripps Research Institute, La Jolla, California 92037
[5] Department of Structural Biology, Weizmann Institute of Science, Rehovot 76100, Israel

(RECEIVED October 25, 1995; ACCEPTED January 12, 1996)

Abstract

A soluble, monomeric form of acetylcholinesterase (mAChE), truncated at its carboxyl-terminal end, was generated from a cDNA encoding the glycophospholipid-linked form of the mouse enzyme by insertion of an early stop codon at position 549. Insertion of the cDNA behind a cytomegalovirus promoter and selection by aminoglycoside resistance in transfected HEK cells yielded clones secreting large quantities of mAChE into the medium. The enzyme sediments as a soluble monomer at 4.8 S. High levels of expression coupled with a one-step purification by affinity chromatography have allowed us to undertake a crystallographic study of the fasciculin–mAChE complex. Complexes of two distinct fasciculins, Fas1-mAChE and Fas2-mAChE, were formed prior to the crystallization and were characterized thoroughly. Single hexagonal crystals, up to 0.6 mm × 0.5 mm × 0.5 mm, grew spontaneously from ammonium sulfate solutions buffered in the pH 7.0 range. They were found by electrophoretic migration to consist entirely of the complex and diffracted to 2.8 Å resolution. Analysis of initial X-ray data collected on Fas2-mAChE crystals identified the space group as $P6_122$ or $P6_522$ with unit cell dimensions $a = b = 75.5$ Å, $c = 556$ Å, giving a V_m value of 3.1 Å^3/Da (or 60% of solvent), consistent with a single molecule of Fas2-AChE complex (72 kDa) per asymmetric unit. The complex Fas1-mAChE crystallizes in the same space group with identical cell dimensions.

Keywords: acetylcholinesterase; crystallization; fasciculin; peptide–macromolecule complex; snake toxin

Reprint requests to: Palmer Taylor, Department of Pharmacology, University of California at San Diego, La Jolla, California 92093-0636.
[6] Permanent address: Laboratoire de Biochimie, CNRS, Unité de Recherche Associée 1455, Institut Fédératif de Recherche Jean Roche, Université d'Aix-Marseille II, Faculté de Médecine Secteur Nord, 13916 Marseille cedex 20, France.
[7] Permanent address: Laboratoire de Cristallisation et Cristallographie des Macromolécules Biologiques, CNRS, Institut Fédératif de Recherche Concertée-1, 31 Ch. Joseph Aiguier, 13402 Marseille cedex 20, France.
[8] Present address: Department of Biochemistry, Brooklyn College of the City University of New York, Brooklyn, New York 11210-2889.

Abbreviations: AChE, acetylcholinesterase; $(NH_4)_2SO_4$, ammonium sulfate; BSA, bovine serum albumin; CMV, cytomegalovirus; DTNB, dithiobis-2-nitrobenzoic acid; FPLC, fast performance liquid chromatography; HEK, human embryonic kidney; ImMal, imidazole malate; PEG, polyethyleneglycol; PNGaseF, peptide:*N*-glycanase F; Mes, 2-(*N*-morpholino)ethane sulfonic acid; NaAc, sodium acetate.

Acetylcholinesterase's only well-documented action is the termination of receptor activation by the neurotransmitter, acetylcholine, at synaptic junctions through ester hydrolysis (cf. Massoulié et al., 1993; Taylor & Radić, 1994). Inhibition of acetylcholinesterase gives rise to a panoply of symptoms. In skeletal muscle, fasciculations are observed initially, followed by flaccid paralysis.

Fasciculins are the only known peptide inhibitors of AChE, with dissociation constants as low as 1–10 pM. These 7-kDa peptides, which are found in mamba snake venoms (cf. Cerveñansky et al., 1991), form three loops emerging from a dense core containing the disulfide bridges. They belong to the structural family of three-fingered peptidic toxins from Elapidae venoms, which include the nicotinic receptor-blocking α-neurotoxins (Changeux et al., 1970; Endo & Tamiya, 1991), the muscarinic receptor pep-

Editor: This change is made to correspond with the first line of the abstract

tide agonists (Adem et al., 1988; Segalas et al., 1995), and the cardiotoxins that interact with cell membranes (Bougis et al., 1981; Dufton & Hider, 1991). Despite a common structural motif, the toxins in this family are directed to diverse targets, yet their modes of action are highly selective. Several lines of evidence show that the fasciculins bind to a peripheral site of AChE, a region distinct from the catalytic center and located at the rim of the active site gorge. This site shares a common region with the binding site of some peripheral-site cationic inhibitors and with the site at which the substrate, when present in large excess, binds. In addition, fasciculins appear not to totally occlude access of small molecules to the catalytic site (Marchot et al., 1993; Radić et al., 1995). Rather, they influence AChE catalysis in an allosteric fashion, although a partial gating influence may also restrict the rate of entry into the gorge for substrates whose catalysis is rate-limited or near-limited by diffusion (Eastman et al., 1995; Radić et al., 1995; van den Born et al., 1995).

The X-ray structure of a dimeric AChE from *Torpedo californica* has been solved at 2.8 Å resolution (Sussman et al., 1991). Since then, substantial information regarding the fasciculin binding site on mouse AChE has been obtained by site-directed mutagenesis (Radić et al., 1994, 1995). The X-ray structures of fasciculins, Fas1 and Fas2, have been solved at 1.9 Å and 2.0 Å resolution, respectively (Le Du et al., 1992, 1995). Analysis of the structures, however, allowed one only to hypothesize on the nature of the fasciculin determinants responsible for binding to AChE.

The predominant monomeric and dimeric forms of native AChE contain a hydrophobic domain at their carboxyl-terminus, either as an attached glycophospholipid or an amphipathic sequence (Massoulié et al., 1993), both being likely to limit the propensity for crystallization. In the dimeric *Torpedo* AChE, the diglyceride on the glycophospholipid, which serves as the hydrophobic anchor in the membrane, was enzymatically cleaved prior to crystallization (Sussman et al., 1988).

We have generated a soluble, monomeric AChE from mouse (mAChE), representative of a catalytic subunit (~65 kDa), from a cDNA lacking the coding sequence for the extreme carboxyl terminus. High levels of expression in HEK cells, coupled with a one-step purification by affinity chromatography on an inhibitor-conjugated resin, have allowed us to undertake an X-ray crystallographic study of the fasciculin–AChE complex.

Results and discussion

Insertion of a stop codon in place of the Cys 549 codon of mouse AChE (Rachinsky et al., 1990; Li et al., 1991, 1993) maintains the catalytic core of the molecule, but truncates 37 amino acids from the nascent peptide. This eliminates the signal for attachment of the hydrophobic glycophospholipid to the carboxy-terminal residue (Gly 557) of the processed native enzyme (Fig. 1). Thus, the recombinant DNA-derived enzyme is nine residues shorter than the processed amphiphilic enzyme and, importantly, lacks a hydrophobic glycophospholipid or amphipathic helix at its carboxyl-terminus found on other forms of AChE. HEK cells in which the mutated cDNA was stably integrated were grown in the presence of serum, then allowed to express mAChE in a serum-free medium. Typically, 0.2–0.5 mg of mAChE was secreted over a 3-day period in a 10-cm dish covered with 10 mL of medium, and secretion at a high level could

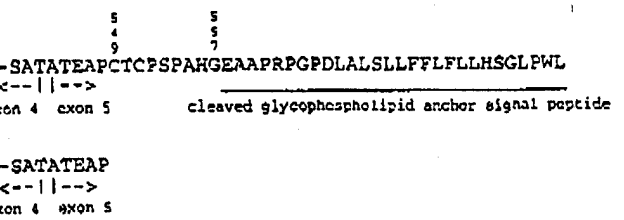

Fig. 1. Carboxyl-terminal sequences of native and truncated mouse AChE. The signal for attachment of the hydrophobic glycophospholipid to Gly 557 in the processed native enzyme (top sequence) has been eliminated by insertion of a stop codon in place of the Cys 549 codon. The resulting enzyme, mAChE, is monomeric and devoid of a carboxyl-terminal hydrophobic segment (bottom sequence). Sequence Ser-Ala-Thr is encoded by the end of exon 4; sequence Ala-Thr-Glu is encoded by the beginning of exon 5 (Li et al., 1993). Mouse AChE residue numbering is used.

be maintained for up to one month. Sedimentation of mAChE from the collected medium on sucrose gradients in the presence of 1% Triton X-100 yielded a single, symmetric peak sedimenting at 4.8 S (Fig. 2), consistent with the recombinant enzyme sedimenting as a monomer. Indeed, dimers of the catalytic subunit containing the glycophospholipid sediment at 6.0 S, whereas cleavage of the phospholipid yields a sedimentation constant of 6.5 S (D.C. Vellom, unpubl. data). Similar behavior has been reported for corresponding forms of *Torpedo* AChE (Duval et al., 1992).

Purification and characterization of mAChE

Similar to the procedure adopted for purification of the 11S form of *T. californica* AChE (Taylor & Jacobs, 1974), affinity chromatography was used to purify milligram quantities of mAChE from the tissue culture medium. Typically, 30–50 mg of enzyme in 2–4 L of medium were subjected to purification by selective retention on an *m*-aminophenyltrimethyl-ammonium-

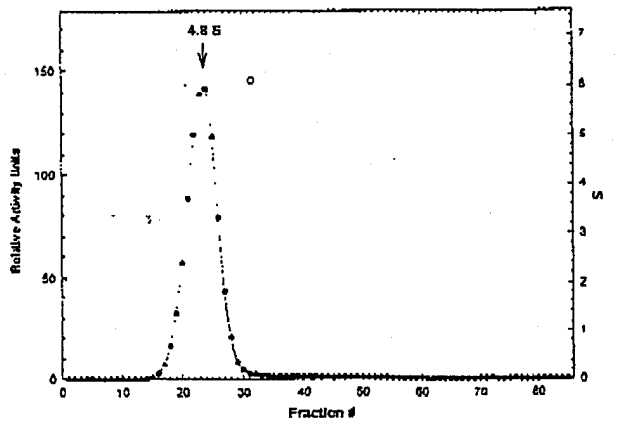

Fig. 2. Hydrodynamic analysis of mAChE-containing harvested culture media. The sample (100 μL), supplemented with sedimentation standards, was centrifuged in a 3–20% sucrose gradient in the presence of Triton X-100, then fractionated as described in the text. Sedimentation positions of two standards, carbonic anhydrase (3.3 S) and alkaline phosphatase (6.1 S), are shown as dotted open circles.

conjugated column and subsequent elution by decamethonium. Owing to the high concentration of decamethonium used, mAChE eluted as a single, sharp peak with only minor tailing representing a few percent of the initial activity loaded on the column. Purification yields ranged from 60% to 95% of the activity initially detected in the medium. The specific activity of purified mAChE, 2,206 units mg^{-1}, corresponds to a k_{cat} of 16.2×10^4 min^{-1}, in good agreement with the value reported previously (Vellom et al., 1993). Routine storage at −20 °C of purified mAChE mixed with glycerol 1:1 (v/v) was not consistent with reliable crystallization. An immediate and dramatic loss of activity was observed upon flash-freezing of the purified enzyme in liquid nitrogen. mAChE, however, could be stored for weeks on ice without loss of activity or alteration of the gel-filtration or SDS-PAGE patterns.

Electrophoretic analysis of the purified mAChE suggests that the enzyme displays slight heterogeneity. Indeed, SDS-PAGE resulted in two diffuse and partially overlapping bands with a ratio of about 1:1 and an average apparent mass of ca. 65 kDa (Figs. 3, 4A), whereas native gel electrophoresis resulted in a diffuse and particularly broad band, larger than expected from a protein with three *N*-glycosylation sites (Fig. 4B). Reducing the volume of the loaded sample or/and increasing the crosslinking of the stacking gel did not change these patterns significantly. Removal of the N-linked carbohydrate side chains from mAChE by digestion with PNGaseF, then subsequent analysis by SDS-PAGE, resulted in sharpening of the two bands, causing them to migrate closer to each other, and lowering their apparent mass to ca. 55 kDa (Fig. 3). The purified mAChE could therefore be composed of two roughly equal populations of monomeric enzyme differing slightly in their carbohydrate composition, ~~but probably not in their amino acid sequences~~. Similar observations have been reported for purified recombinant human AChE (Velan et al., 1992). Independent analysis of the chromatographic fractions from the affinity column showed that the two bands co-elute throughout the elution peak, suggesting identical ~~catalytic~~ properties for the two forms. The two forms were still observed upon SDS-PAGE analysis of the fasciculin–mAChE complexes and of the dissolved crystals (Fig. 4; see below), and therefore are not distinguished by complexation with fasciculin and subsequent crystallization.

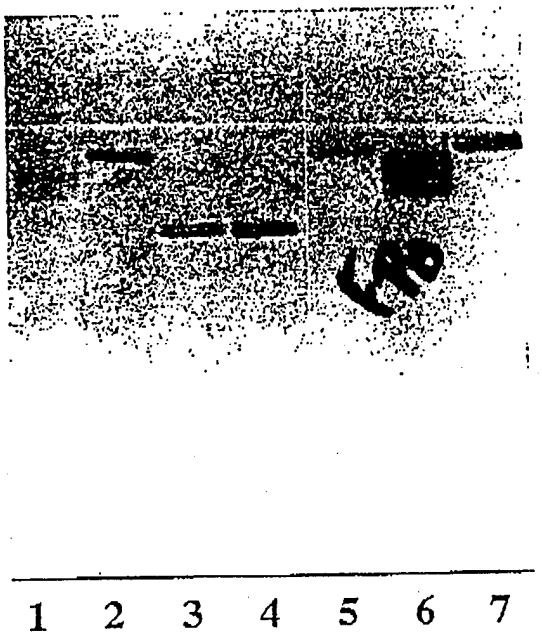

Fig. 3. Electrophoretic analysis of native and deglycosylated mAChE. SDS-PAGE (15% resolving/5% stacking gel, 20 cm × 20 cm) under reducing conditions: lanes 1 and 6, purified mAChE; lanes 2 and 7, BSA (66 kDa); lanes 3 and 4, mAChE deglycosylated with PNGaseF; lane 5, BSA treated with PNGaseF. The thin band at the bottom of the gel corresponds to PNGaseF (36 kDa, lanes 3, 4, and 5).

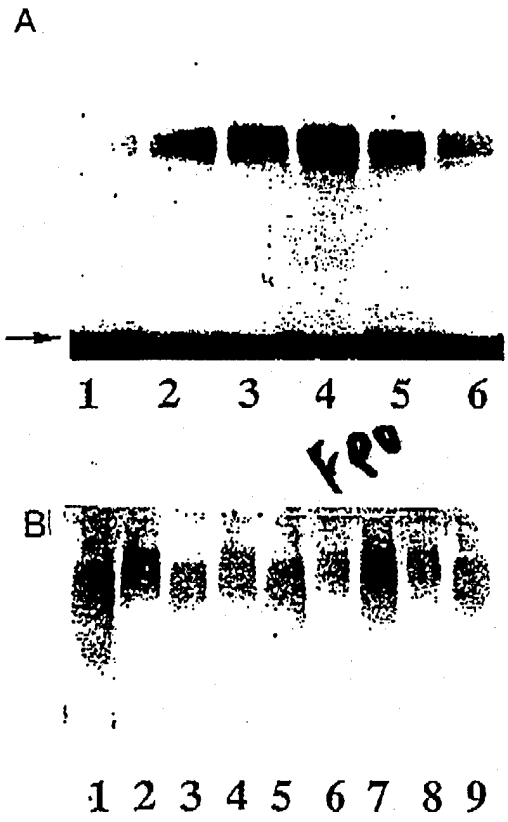

Fig. 4. Electrophoretic analysis of mAChE and fasciculin–mAChE complexes. A: SDS-PAGE (4–20% gradient gel, 8 cm × 8 cm) under reducing conditions: lanes 2, 3, and 4, purified mAChE; lane 1, mAChE complexed to Fas1; lane 5, mAChE complexed to Fas2; lane 6, washed and dissolved Fas2-mAChE hexagonal crystal; mAChE migrates as two diffuse and overlapping bands; arrow at the bottom of the gel indicates the fasciculin band (lanes 1, 5, and 6). B: Native gel electrophoresis (7.5% resolving/5% stacking gel, 8 cm × 8 cm) with migration toward the anode: lanes 1, 3, 5, and 9, purified mAChE; lane 2, mAChE complexed to Fas1; lane 4, mAChE complexed to Fas2; lanes 6, 7, and 8, washed and dissolved triangular, needle-shaped, and hexagonal Fas2-mAChE crystals, grown in $(NH_4)_2SO_4$; the shift toward the cathode in the position of the complexes (lanes 2, 4, 6, 7, and 8) relative to the free mAChE is evident.

Complexation of mAChE with fasciculins and characterization of the complexes

Special care has been taken for complexation of Fas1 and Fas2, respectively, to mAChE and characterization of the complexes

prior to crystallization. The fasciculin–mAChE complexes were preformed at, or close to, the high protein concentrations required for crystallization, i.e., a concentration $\sim 10^8$-fold greater than the K_i of Fas2 for mouse AChE (Radić et al., 1994), together with an 1.2 molar excess of fasciculin. Slightly higher residual activity was observed repeatedly for the Fas2-mAChE complex compared to the Fas1-mAChE complex. Both complexes were analyzed by gel electrophoresis (after removal of the unbound excess fasciculin) and gel filtration chromatography (before and after removal). SDS-PAGE of the complexes was performed with a gradient gel appropriate for the large difference in size of the fasciculin and the mAChE molecules (Fig. 4A). Although fasciculin migrated together with the free dodecylsulfate, it ran as a thin, intense band at the bottom of the gel. The migration pattern of initially complexed mAChE was found to be identical to free mAChE. In order to establish actual complexation of Fas1 or Fas2 to mAChE and not only their simultaneous presence, native gel electrophoresis was performed both on the free and complexed mAChE (Fig. 4B). The bound fasciculin was found to diminish the mobility of mAChE, as expected from the increased Mw or/and basicity of the complex compared to the free enzyme. Identical electrophoretic patterns were observed for the Fas1- and Fas2-mAChE complexes.

Gel filtration chromatography of the free mAChE and the fasciculin–mAChE complexes led to single, symmetric absorbance peaks (data not shown). No difference in the chromatographic mobility of the fasciculin–mAChE complexes with regard to mAChE could be detected, most probably because of the limited resolution for a mass change from ~65 kDa to ~72 kDa. Screening the chromatographic fractions for their AChE activity, however, required 10^3-fold less dilution of the fasciculin–mAChE fractions than the mAChE fractions, consistent with the level of residual activity (in the 0.1% range) recorded upon complexation of mAChE. Screening for fasciculin activity of the fractions eluting from chromatography of the fasciculin–mAChE complexes performed *before* removal of the unbound fasciculin revealed an included free fasciculin peak eluting at a position consistent with its mass. No such fasciculin peak was detected upon equivalent screening of the fractions eluting from chromatography of the fasciculin–mAChE complexes performed *after* removal of the unbound fasciculin, thereby affirming the total removal of the excess fasciculin.

Crystallization of the fasciculin–mAChE complexes

Crystals spontaneously grew within 2–5 days in hanging drops and within a week in sitting drops. Various crystal morphologies were obtained in two major conditions based on the use of PEG or $(NH_4)_2SO_4$ as precipitating agents. Thick needles with hexagonal sections, extending across the droplet and sometimes hollowed at one end, grew similarly from PEG 600, 2000, 4000, or 10000 solutions buffered with 0.1 M NaAc or ImMal at pHs between 6.5 and 7.5. In contrast, three different crystal forms were obtained from 1.25 M to 1.45 M $(NH_4)_2SO_4$, buffered to pH 6.5 to 7.5 with ammonia. Short and large needles with hexagonal sections, thick triangles, stars, and crowns, all made of stacked thin triangular platelets, as well as symmetric hexagons with slightly variable geometry, were generally found in the same drop, although with varying distribution depending on the precise $(NH_4)_2SO_4$ concentration or pH (Fig. 5A,B). Growth of hexagonal needles as perpendicular axes from the triangles or

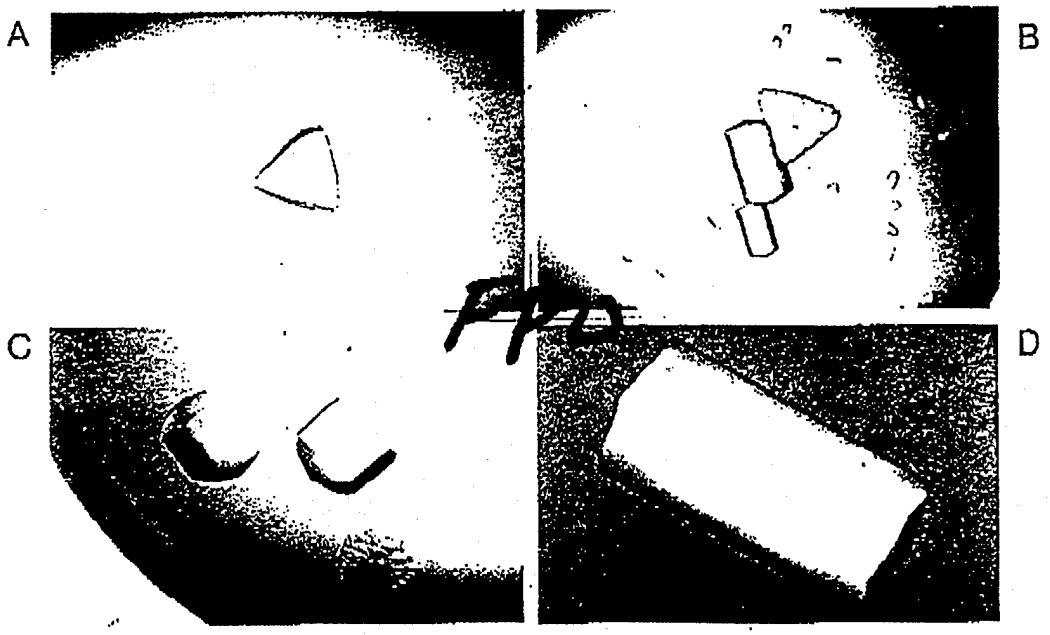

Fig. 5. Photographs of fasciculin-mAChE crystals. A,B: Fas1-mAChE and Fas2-mAChE crystals spontaneously grown in a 4-μL hanging drop from 1.35 M $(NH_4)_2SO_4$, pH 6.75. C: Half Fas2-mAChE crystals (0.6 mm × 0.3 mm × 0.25 mm) spontaneously grown in a 10-μL sitting drop from 1.35 M $(NH_4)_2SO_4$, pH 7.25. D: Fas2-mAChE crystal (1 mm × 0.5 mm × 0.5 mm) grown from 1.35 M $(NH_4)_2SO_4$, pH 7.0, by macroseeding of a 10-μL drop.

as parallel axes from the hexagons was sometimes observed, suggesting that the three forms crystallize in related, if not identical, space groups. Buffering the $(NH_4)_2SO_4$ solutions with 0.1 M NaAc, ImMal, or $NaKPO_4$, as well as adding 0.25% (w/v) β-octylglucoside, did not change the crystallization behavior significantly. Triangular crystals could not be dissociated to monocrystals, even when grown in the presence of 0.25% or 0.5% (w/v) β-octylglucoside or 0.1% (w/v) heptanediol or of the detergent screening kit solutions. Growing the hexagonal Fas2-AChE crystals in sitting drops occasionally led to half-crystals adhering tightly to the siliconized cover-slip, presumably arising from epitaxial nucleation (Fig. 5C).

Except for the hexagonal form, which grew almost specifically from the Fas2-mAChE complex (only three hexagonal Fas1-mAChE crystals were obtained in a unique drop after ~10 weeks of equilibration), the same crystal forms were obtained for the two complexes. They all could be enlarged by macroseeding. Larger hexagonal Fas2-mAChE crystals were so obtained (Fig. 5D). Cross-seeding of the Fas1-mAChE complex with seeds from a hexagonal Fas2-mAChE crystal led to both triangular and hexagonal Fas1-mAChE crystals, although the later grew more slowly than their Fas2 counterparts and displayed a slightly different geometry (not shown). The two fasciculins differ by single substitution Fas1-Tyr to Fas2-Asn at position 47. No difference, however, could be found in their affinity for mAChE (P. Marchot, unpubl. data). Differences in solubility of the two complexes should therefore account for their different crystallization behavior. The protein content of all crystal forms was checked by SDS-PAGE and native-gel electrophoresis after several successive rinses of the crystals in decreasing concentrations of the precipitating agent, then dissolution in distilled water (Fig. 4A,B). In all cases, the patterns were the same as observed initially upon analysis of the complexes in solution, indicating actual crystallization of the fasciculin–mAChE complexes rather than mAChE alone. Free mAChE, even when concentrated to 18–20 mg mL^{-1}, remained totally soluble in all conditions that yielded fasciculin–mAChE crystals.

Data collection

Preliminary X-ray studies were performed at beam line X12B of the National Synchrotron Light Source (NSLS) equipped with a standard MarResearch imaging plate detector. The highest diffracting patterns (2.8 Å) were obtained for the hexagonal Fas2-mAChE crystals as compared to triangles (3.5 Å) and PEG- or $(NH_4)_2SO_4$-grown needles (5 Å) from both complexes, but the diffraction limit dropped to about 4 Å after the first 15° rotation of data collection. With the aim of protecting the crystals from radiation damage, numerous cryoprotection and flash-cooling assays were performed, but all failed because of immediate cracking of the crystal or/and dramatic loss of resolution. Preliminary data were therefore collected at 4 °C. The crystals belong to space group $P6_122$ or $P6_522$ with cell dimensions $a = b = 75.5$ Å, $c = 556$ Å, giving a V_m value of 3.1 $Å^3$/Da or 60% of solvent, consistent with the presence of a single molecule of complex (72 kDa) in the asymmetric unit (Matthews, 1968). Efforts to collect data at beam line X12B, however, were hampered by the large dimension of the c axis and the resulting overlap of the diffraction spots. Diffraction data were therefore collected at beam line X12C of the NSLS, equipped with a MarResearch imaging plate detector mounted on an Enraf Nonius 4-circle goniometer. A distance of 540 mm (λ = 1.5 Å) and 860 mm (λ = 1.0 Å) with a tilt of 11° and 12°, respectively, was used with 2° oscillation steps. A total of ca. 62,200 observations was obtained at 3.2 Å from four Fas2-mAChE crystals, giving ca. 14,500 unique reflections (85% complete, R_{sym} = 8.9%). Further details on the crystallographic parameters of the Fas2-mAChE complex have been presented elsewhere (Bourne et al., 1995).

The same resolution limit was observed for the spontaneously grown hexagonal Fas1-mAChE crystals, which belong to the same space group with similar cell dimensions $a = b = 75.4$ Å, $c = 550$ Å. In spite of the apparently different conformations of their first disulfide loop, loop I (Le Du et al., 1992, 1995), Fas1 and Fas2 would therefore be expected to adopt the same conformation upon binding to mAChE. The crystals, however, were most probably heterogeneous because double diffraction patterns were obtained. Diffraction patterns from triangles and needles were also consistent with a particularly long c axis.

In summary, the expression of a recombinant cDNA-derived form of AChE, truncated by nine amino acids from native mouse AChE, has yielded a monomeric enzyme appropriate for structural studies. The solubility of mAChE decreased in the presence of fasciculin, and crystals of fasciculin–mAChE complexes suitable for X-ray analysis have been obtained (Bourne et al., 1995). This structure offers a new template for further structure–function studies of mammalian cholinesterases. The structures of the fasciculin–AChE complexes (Bourne et al., 1995; Harel et al., 1995) contribute to at least three lines of investigation. First, they help reveal how fasciculin inhibits AChE. Second, they represent the first structures of three-fingered snake toxins bound to their macromolecular receptors. Establishing the contact points between fasciculin and AChE provides a framework for understanding the bases of the high affinities and unusual specificities of the family of three-fingered peptidic toxins.

Materials and methods

Materials

HEK-293 cells were obtained from American Type Culture Collection. Ultraculture cell culture medium was purchased from Biowhittaker. Dialysis tubing (Spectra/Por 6) was from Spectrum Medical Industries. Centriprep, Centricon, and Microcon concentration units were from Amicon. Sterile 0.22-μm SpinX units were from Costar. The BCA kit for protein assays was from Pierce. Prepacked Superose-12 HR 10/30 column was from Pharmacia. Gel-filtration molecular weight markers (Mw-GF-70 Kit) were from Sigma. Precast Tris-glycine 4–20% gradient gels were from Novex. Prestained protein Mw standards for SDS-PAGE (14,300–200,000 Mw range) were from Gibco BRL. PNGaseF (S.A., 12,500,000 U mg^{-1}) was from BioLabs. DTNB, ATCh, decamethonium bromide, and PEG 200 were from Sigma. All other PEG (600, 2000, 4000, and 10000), as well as ammonium sulfate of biochemical grade, were from Fluka. The Detergent Screening Kit was from Hampton Research. All buffers used for crystallization were made with deionized water from a Millipore MilliRO/MilliQ system and filtered through 0.22-μm cellulose acetate membrane filtration units (Corning).

Proteins

Fas1 and Fas2 were from the same purification batches as those used previously for crystallization and structure determination (Le Du et al., 1989, 1992, 1995). The concentrations of stock solutions were determined from their UV spectra (ϵ_{276nm} = 6,300 M^{-1} cm^{-1} for Fas1 and 4,900 M^{-1} cm^{-1} for Fas2). mAChE was a soluble form derived from the cDNA encoding the glycophospholipid-linked form of mouse AChE (Li et al., 1993). The cDNA was truncated after Pro 548 by insertion of a stop codon (TGA) in place of the Cys 549 codon (Fig. 1). Sequence of the mutant cDNA was confirmed by direct sequencing of the insert. The cDNA was inserted behind a CMV promoter. Transfection into HEK cells was with $Ca_3(PO_4)_2$ co-precipitation (Vellom et al., 1993). Selection of clones depended on incorporation of the neomycin-resistance gene and selection of cells with G418 sulfate (800 $\mu g\ mL^{-1}$) (Radić et al., 1993; Vellom et al., 1993). HEK-293 cells in which the mutated mAChE cDNA was stably integrated were grown to confluency in Dulbecco's modified Eagle's medium supplemented with 10% fetal bovine serum, then switched into serum-free media (Ultraculture) for collection of secreted mAChE.

Assay of AChE activity

AChE activity measurements were conducted spectrophotometrically (Ellman et al., 1961) with 0.5 mM acetylthiocholine iodide and 0.33 mM DTNB in 100 mM NaH_2PO_4/Na_2HPO_4, pH 7.0, BSA 0.1 mg mL^{-1}, to a final volume of 1.5 mL (room temperature). Initial kinetics of duplicate samples were recorded at $\lambda = 412$ nm during 5 min with a Response™ spectrophotometer (Gilford). A specific activity of 30,000 $\Delta A\ min^{-1}\ mg^{-1}$ was used. Relative AChE activities were screened at room temperature by microtitration on a Vmax kinetic microplate reader (Molecular Devices Corp.) with $\lambda = 405$ nm. Gel-filtration fractions were diluted 20–50,000-fold for screening of free mAChE and 30-fold for screening of the residual activity of the fasciculin–AChE complexes. Free fasciculin in the chromatographic fractions was screened by recording the residual activity of an extra AChE sample (~8 pM) after incubation for 1 h at 37 °C with a 30–100-fold dilution of the fractions (Marchot et al., 1993).

Sedimentation velocity analysis

mAChE-containing culture medium was sedimented into linear 3–20% sucrose gradients containing 0.1 M NaCl, 0.04 M $MgCl_2$, 0.01 M Tris-HCl, pH 8.0, and 0.1% (v/v) Triton X-100, for 20 h at 200,000 × *g* (4 °C). The layered sample (100 μL) was supplemented with carbonic anhydrase (20 μg, 3.3 S), alkaline phosphatase (0.2 μg, 6.1 S), catalase (2 μg, 11.4 S), and β-galactosidase (0.4 μg, 16 S) as sedimentation standards (Camp et al., 1995). The sedimented 12-mL tubes were fractionated in 96-tube racks with the microtitration plate format allowing further screening of the respective enzyme activities.

Purification and characterization of mAChE

Soluble mAChE was purified by affinity chromatography using *m*-trimethylaminophenyl amine coupled to Sepharose through a successively coupled succinic acid and diaminodipropylamine arm (Taylor & Jacobs, 1974). The conjugated resin was stored as a 50% suspension in 100 mM NaCl, 40 mM $MgCl_2$, 10 mM $NaHCO_3$, pH 8.0, containing NaN_3 0.02% (w/v). Harvested Ultraculture medium containing the expressed mAChE was centrifuged (2,000 g, 15 min, 4 °C) to remove cell debris, and assayed for AChE activity. $MgCl_2$ (1 M) was added to a final concentration of 40 mM, then the resin suspension (1 mL for each 2 mg AChE), and the mixture was allowed to stir in a spinner flask overnight at 4 °C in the presence of NaN_3 0.02% (w/v). The mixture was assayed for residual AChE activity and, if required, supplemented with the exact amount of resin necessary to achieve total inhibition of the enzyme. It was poured into a Bio-Rad econo column, allowed to pack by sedimentation, then washed with the equilibrating buffer (50–100-fold the bed volume). The bound AChE was eluted with 100 mM decamethonium bromide (30 × K_i, Radić et al. 1993) in the same buffer, at a low flow rate (1–1.5 mL h^{-1}). Elution fractions were assayed for AChE activity with a 10^6-fold final dilution, which reduced the final decamethonium concentration to well below its K_i for the mouse enzyme. The purified enzyme was dialyzed *extensively* against the crystallization buffer with SpectraPor6 dialysis tubing, then rinsed again and concentrated to 10–20 mg mL^{-1} in a Centriprep3 or Centricon3 unit. Purified mAChE was quantified independently from catalytic activity, BCA protein assay, absorbance at $\lambda = 280$ nm, and titration by Fas2 (Marchot et al., 1993), which yielded a close correlation. It was stored on ice.

N-linked carbohydrate removal

Purified mAChE (20 μg in 100 μL) was boiled for 10 min in denaturing buffer (20 mM Tris-HCl, pH 8.0, 5 mM EDTA, 5 mM β-mercaptoethanol, 0.5% (w/v) SDS, cooled, added with 1% (v/v) Nonidet P-40, then incubated in the presence of PNGaseF (2,000 U) for 5 h at 37 °C. A further aliquot of 2,000 U was added after 2 h of incubation.

Complexation of mAChE with fasciculins and crystallization of the complexes

The respective complexes were formed in 50 mM NaCl, 1 mM Mes, pH 6.5, NaN_3 0.01% (w/v) (crystallization buffer) with a fasciculin-to-AChE molar ratio of 1.2:1 to preclude stoichiometric deficiency assuming a maximal 10% error in the quantification of protein and peptide. After equilibration overnight on ice, the complexes were assayed for residual AChE activity and free fasciculin, respectively. The enzyme was considered to be totally complexed to fasciculin when no decrease in its residual activity (usually 0.1–0.5% of the initial activity of the sample) was observed upon further addition of fasciculin and extended incubation, and when free fasciculin could be detected in the mixture through inhibition of a second AChE sample. Excess fasciculin was then dialyzed from the complexes with the crystallization buffer in a Centricon10 or Microcon10 concentrator, until no free fasciculin could be detected in both the filtrate and the sample. Total removal was confirmed by gel-filtration chromatography. The complexes were concentrated to 12–15 mg mL^{-1}, then filtered through a SpinX unit. They were stored on ice and were used within a week with no change in their crystallization behavior. Both Fas1- and Fas2-AChE complexes were crystal-

lized at 20 °C by the vapor diffusion method using hanging drops (4 μL) or sitting drops (10 μL) with a protein-to-well solution ratio of 1:1. Macroseeding of 10 μL sitting drops previously equilibrated overnight was performed according to Stura and Wilson (1992).

Electrophoresis

SDS-PAGE under reducing conditions and native gel electrophoreses of mAChE and Fas-AChE complexes were performed according to the discontinuous system of Laemmli (1970) with a vertical gel electrophoresis apparatus (JM Specialty Parts) or a Mighty Small Slab gel electrophoresis unit (Hoefer Scientific Instruments). Precast Tris-glycine 4–20% gradient gels, or 15% or 10% resolving/5% stacking gels, were used for SDS-PAGE. A 7.5% resolving/5% stacking gel made with no SDS was used for native gel electrophoresis. Samples loaded were typically 5 μL and contained 10% (v/v) glycerol. Silver nitrate staining was performed according to Morrisey (1981).

Gel-filtration chromatography

Analytical gel-filtration chromatography of mAChE and fasciculin–AChE complexes was conducted at 4 °C on a Superose-12 column using the FPLC system from Pharmacia. The column was equilibrated in, then eluted with, the crystallization buffer (flow rate, 0.5 mL min^{-1}). The loaded samples were 5 μL of the concentrated protein solutions used for complexation (mAChE) or crystallization (complexes), sandwiched into 25 μL of the crystallization buffer. Absorbance of column effluents was monitored at λ = 280 nm. Fractions (0.5 mL) were collected and assayed for AChE activity. The column was calibrated with a molecular weight standard kit.

Acknowledgments

We thank Dr. P.E. Bougis, in whose group at the Centre National de la Recherche Scientifique the fasciculins have been purified; Dr. John A. Tainer at The Scripps Research Institute and Dr. K.I. Varughese at UCSD, for the use of their crystallization facilities; and Dr. Robert M. Sweet, for access to the National Synchrotron Light Source beam line X12C. Expert assistance from Malcom Capel at the NSLS beam line X12B is much appreciated. This work was supported by USPHS GM18360 and DAMD 17C grants to P.T. and the Biology Department at the Brookhaven National Laboratory to J.L.S.

References

Adem A, Asblom A, Johansson G, Mbugua PM, Karlsson E. 1988. Toxins from the venom of the green mamba *Dendroaspis angusticeps* that inhibit the binding of quinuclidinylbenzylate to muscarinic acetylcholine receptors. *Biochim Biophys Acta 968*:340–345.

Bougis P, Rochat H, Piéroni G, Verger R. 1981. Penetration of phospholipid monolayers by cardiotoxins. *Biochemistry 20*:4915–4920.

Bourne Y, Taylor P, Marchot P. 1995. Acetylcholinesterase inhibition by fasciculin: Crystal structure of the complex. *Cell 83*:503–512.

Camp S, Bon S, Li Y, Getman DK, Engel AG, Massoulié J, Taylor P. 1995. Patients with congenital myasthenia associated with end-plate acetylcholinesterase deficiency show normal sequence, mRNA splicing, and assembly of catalytic subunits. *J Clin Invest 95*:333–340.

Cerveñansky C, Dajas F, Harvey AL, Karlsson E. 1991. Fasciculins, anticholinesterase toxins from mamba venoms: Biochemistry and pharmacology. In: Harvey AL, ed. *Snake toxins*. New York: Pergamon Press Inc. pp 303–321.

Changeux JP, Kasai M, Lee CY. 1970. The use of a snake venom toxin to characterize the cholinergic receptor protein. *Proc Natl Acad Sci USA 67*:1241–1247.

Dufton MJ, Hider RC. 1991. The structure and pharmacology of elapid cytotoxins. In: Harvey AL, ed. *Snake toxins*. New York: Pergamon Press Inc. pp 259–302.

Duval NE, Krejci E, Grassi J, Coussen F, Massoulié J, Bon S. 1992. Molecular architecture of acetylcholinesterase collagen-tailed forms; construction of a glycolipid-tailed tetramer. *EMBO J 11*:3255–3261.

Eastman J, Wilson EJ, Cerveñansky C, Rosenberry TL. 1995. Fasciculin 2 binds to the peripheral site on acetylcholinesterase and inhibits substrate hydrolysis by slowing a step involving proton transfer during enzyme acylation. *J Biol Chem 270*:19694–19701.

Ellman GL, Courtney KD, Andres V Jr, Featherstone RM. 1961. A new rapid combination method for acetylcholinesterase activity. *Biochem Pharmacol 7*:88–95.

Endo T, Tamiya N. 1991. Structure–function relationship of postsynaptic neurotoxins from snake venoms. In: Harvey AL, ed. *Snake toxins*. New York: Pergamon Press Inc. pp 165–222.

Harel M, Kleywegt GJ, Ravelli RBG, Silman I, Sussman JL. 1995. Crystal structure of an acetylcholinesterase–fasciculin complex: Interaction of a three-fingered toxin from snake venom with its target. *Structure 3*: 1355–1366.

Laemmli UK. 1970. Cleavage of structural proteins during the assembly of the head of bacteriophage T4. *Nature (Lond) 227*:680–685.

Le Du MH, Housset D, Marchot P, Bougis PE, Navaza J, Fontecilla-Camps JC. 1995. Crystal structure of fasciculin 2 from mamba snake venom: Evidence for unusual loop flexibility. *Acta Crystallogr* [illegible]

Le Du MH, Marchot P, Bougis PE, Fontecilla-Camps JC. 1989. Crystals of fasciculin 2 from green mamba snake venom: Preparation and preliminary X-ray analysis. *J Biol Chem 264*:21401–21402.

Le Du MH, Marchot P, Bougis PE, Fontecilla-Camps JC. 1992. 1.9 Å resolution structure of fasciculin 1, an anti-cholinesterase toxin from green mamba snake venom. *J Biol Chem 267*:22122–22130.

Li Y, Camp S, Rachinsky TL, Getman D, Taylor P. 1991. Gene structure of mammalian acetylcholinesterase. *J Biol Chem 266*:23083–23090.

Li Y, Camp S, Taylor P. 1993. Tissue-specific expression and alternative mRNA processing of the mammalian acetylcholinesterase gene. *J Biol Chem 268*:5790–5797.

Marchot P, Khélif A, Ji YH, Mansuelle P, Bougis PE. 1993. Binding of ^{125}I-fasciculin to rat brain acetylcholinesterase. The complex still binds diisopropyl fluorophosphate. *J Biol Chem 268*:12458–12467.

Massoulié J, Pezzementi L, Bon S, Krejci E, Vallette FM. 1993. Molecular and cellular biology of the cholinesterases. *Prog Neurobiol 41*:31–91.

Matthews BW. 1968. Solvent content of protein crystals. *J Mol Biol 33*: 491–497.

Morrisey J. 1981. Silver stain for proteins in polyacrylamide gels; a modified procedure with enhanced uniform sensitivity. *Anal Biochem 117*:307–310.

Rachinsky TL, Camp S, Li Y, Ekström J, Newton M, Taylor P. 1990. Molecular cloning of mouse acetylcholinesterase: Tissue distribution of alternatively spliced mRNA species. *Neuron 5*:317–327.

Radić Z, Duran R, Vellom DC, Li Y, Cerveñansky C, Taylor P. 1994. Site of fasciculin interaction with acetylcholinesterase. *J Biol Chem 269*: 11233–11239.

Radić Z, Pickering NA, Vellom DC, Camp S, Taylor P. 1993. Three distinct domains in the cholinesterase molecule confer selectivity for acetyl- and butyrylcholinesterase inhibitors. *Biochemistry 32*:12074–12084.

Radić Z, Quinn DM, Vellom DC, Camp S, Taylor P. 1995. Allosteric control of acetylcholinesterase catalysis by fasciculin. *J Biol Chem 270*:20391–20399.

Segalas I, Roumestand C, Zinn-Justin S, Gilquin B, Ménez R, Ménez A, Toma F. 1995. Solution structure of a green mamba toxin that activates muscarinic acetylcholine receptors, as studied by nuclear magnetic resonance and molecular modeling. *Biochemistry 34*:1248–1260.

Stura E, Wilson IA. 1992. Seeding techniques. In: Ducruix A, Giege R, eds. *Crystallization of nucleic acids and proteins, a practical approach*. Oxford: IRL Press, Oxford University Press. pp 99–126.

Sussman JL, Harel M, Frolow F, Oefner C, Goldman A, Toker L, Silman I. 1991. Atomic structure of acetylcholinesterase from *Torpedo californica*: A prototypic acetylcholine-binding protein. *Science 253*:872–879.

Sussman JL, Harel M, Frolow F, Varon L, Toker L, Futerman AH, Silman I. 1988. Purification and crystallization of a dimeric form of acetylcholinesterase from *Torpedo californica* subsequent to solubilization with phosphatidylinositol-specific phospholipase C. *J Mol Biol 203*:821–823.

Taylor P, Jacobs NM. 1974. Interaction between bisquaternary ammonium ligands and acetylcholinesterase: Complex formation studied by fluorescence quenching. *Mol Pharmacol 10*:93–107.

Taylor P, Radić Z. 1994. The cholinesterases: From genes to proteins. *Annu Rev Pharmacol Toxicol 34*:281–320.

van den Born HKL, Radić Z, Marchot P, Taylor P, Tsigelny I. 1995. Theoretical analysis of the structure of the peptide fasciculin and its docking to acetylcholinesterase. *Protein Sci 4*:703–715.

Velan B, Kronman C, Leitner M, Grosfeld H, Flashner Y, Marcus D, Lazar A, Kerem A, Bar-Nun S, Cohen S, Shafferman A. 1992. Molecular organization of recombinant human acetylcholinesterase. In: Shafferman A, Velan B, eds. *Multidisciplinary approches to cholinesterase functions*. New York: Plenum Press. pp 39–47.

Vellom DC, Radić Z, Li Y, Pickering NA, Camp S, Taylor P. 1993. Amino acid residues controlling acetylcholinesterase and butyrylcholinesterase specificity. *Biochemistry 32*:12–17.

Reprinted from Biochemistry, 1995, 34.

Specificity and Orientation of Trigonal Carboxyl Esters and Tetrahedral Alkylphosphonyl Esters in Cholinesterases†

Natilie A. Hosea,‡,§ Harvey A. Berman,|| and Palmer Taylor*,‡

Department of Pharmacology, University of California at San Diego, La Jolla, California 92093-0636, and Department of Biochemical Pharmacology, State University of New York at Buffalo, Buffalo, New York 14260

Received April 20, 1995; Revised Manuscript Received June 19, 1995®

ABSTRACT: We have examined the specificity of planar carboxyl and tetrahedral phosphonyl esters for mouse cholinesterases and have delineated the orientation of these ligands in the enzyme active center. The approach involved altering acyl pocket dimensions by site-specific mutagenesis of two phenylalanines and varying ligand size and enantiomer presentation. Substrate catalysis rates by wild type acetylcholinesterase (AChE) of acetyl-, butyryl-, and benzoylthiocholine diminished with increasing size of the acyl moiety. In contrast, substitution of the acyl pocket phenylalanines giving the mutants F295L and F297I of AChE yielded more efficient catalysis of the larger substrates and a specificity approaching that of butyrylcholinesterase. Extension from planar substrates to enantiomerically pure organophosphonates allowed for an analysis of enantiomeric selectivity. We found that AChE reactions are 200-fold faster with the S_p than the R_p enantiomer of cycloheptyl methylphosphonyl thiocholine. Upon the acyl pocket size being enlarged, the R_p enantiomer became more reactive while reaction with the S_p enantiomer was slightly reduced. In fact, the F297I mutant displayed inverted stereospecificity. A visual correlation with the kinetic data has been developed by docking the ligands in the active site. Upon placement of the phosphonyl oxygen in the oxyanion hole and the leaving group being directed out of the gorge, the R_p, but not the S_p, enantiomer engendered steric hindrance between the alkoxyl group and the acyl pocket. Replacing F297 with Ile accommodated the bulky alkoxyl group of the R_p isomer in the acyl pocket, allowing similar orientations of the phosphonyl oxygen and the leaving group to the S_p isomer. Thus, analysis of reaction rates and absolute stereochemistry enabled us to position the organophosphonates and ascertain loci of interaction of their functional groups in the active center gorge.

Acetylcholinesterases (AChEs)[1] catalyze ester hydrolysis of the neurotransmitter acetylcholine, resulting in termination of neurotransmission. As found in the serine hydrolase family of enzymes, mammalian AChE employs a catalytic triad of Glu 334, His 447, and Ser 203, where the serine residue is the proximal nucleophile in the hydrolysis mechanism (Gibney et al., 1990; Sussman et al., 1991). The butyrylcholinesterases (BuChEs), which share about 55% amino acid sequence identity (Cygler et al., 1993), also hydrolyze acetylcholine with high efficiency. However, AChE and BuChE differ in their capacity to catalyze the hydrolysis of substrates larger than acetylcholine, where BuChE can efficiently hydrolyze butyrylcholine and benzoylcholine and AChE shows diminished catalysis rates with substrates larger than propionylcholine (Augustinsson, 1948). The side chains of two phenylalanines, numbered as Phe (F) 295 and 297 in mouse, form a boundary to the site of binding of the substrate acyl moiety sterically restricting larger acyl containing substrates from optimal positioning for catalysis in the active site (Harel et al., 1992; Vellom et al., 1993; Radic′ et al., 1993; Ordentlich et al., 1993). Aliphatic residues of smaller dimensions are found at the corresponding positions in BuChE (Cygler et al., 1993), for example Leu (L) and Ile (I) in mouse, allowing larger substrates to fit into the active site in an orientation appropriate for efficient catalysis. Individual mutant cholinesterases containing F295L and F297I have enabled us to examine the basis of the divergence between AChE and BuChE inhibitor specificity and kinetics (Vellom et al., 1993).

Cholinesterases also catalyze the acylation of the enzyme by organophosphonates, ligands which react with the enzyme by rapidly phosphonylating the active site serine (Oosterbaan & Cohen, 1964; Aldridge & Reiner, 1972). However, unlike carboxyl ester substrates, the phosphonyl enzyme reacts slowly with water, and thus, these ligands behave as hemisubstrates (Froede & Wilson, 1971). Their selectivity for the cholinesterases has been a subject of continued study over the past fifty years [cf. Froede and Wilson (1971) and Aldridge and Reiner, (1972)]. Furthermore, AChE reaction with organophosphonates displays marked stereospecificity and dependence on substituent size with differences generally greater than 200-fold in reaction rates between enantiomers (Berman & Leonard, 1989). This specificity might arise from steric hindrance by the acyl pocket phenylalanines as found for carboxyl ester substrates.

† Supported by USPHS Grant GM 18360 and DAMD Grant 17-95-I 5027 to P.T. and by the U.S. Army Research Office (Research Triangle Park, NC) and NIH ES-03085 to H.A.B.

‡ University of California at San Diego.

§ Formerly Natilie A. Pickering.

|| State University of New York at Buffalo.

® Abstract published in *Advance ACS Abstracts,* August 15, 1995.

[1] Abbreviations: AChE, acetylcholinesterase; BuChE, butyrylcholinesterase; Phe or F, phenylalanine; Leu or L, leucine; Ile or I, isoleucine; Ala or A, alanine; Tyr or Y, tyrosine; ATC, acetylthiocholine; BuTC, butyrylthiocholine; BzTC, benzoylthiocholine; OP, organophosphonates; CHMP, cycloheptyl methylphosphonyl; iPrMP, isopropyl methylphosphonyl; DMBMP, 3,3-dimethylbutyl methylphosphonyl; k_i, bimolecular rate constant in min^{-1} M^{-1}.

0006-2960/95/0434-11528$09.00/0

Organophosphonates, by virtue of their tetrahedral configuration, afford an additional dimension in the study of structure−activity relationships and, therefore, complement and extend the analyses derived from the study of planar substrate molecules. Moreover, the availability of resolved enantiomerically pure methylphosphonates offers a unique means for analysis of configuration and spatial orientation in the active center with respect to the available three dimensional crystal coordinates of *Torpedo californica* AChE (Sussman et al., 1991). Herein, we examine the role of the acyl pocket of mouse cholinesterases in dictating stereospecificity for enzyme acylation by the organophosphonates and describe the positioning of tetrahedral and planar ligands in the active center of the enzymes. Structural models consistent with the reaction kinetics provide plausible orientations achieved by the phosphonates within the active site.

MATERIALS AND METHODS

Materials. Acetylthiocholine iodide (ATC), butyrylthiocholine iodide (BuTC), and 5,5′-dithiobis(2-nitrobenzoic acid) (DTNB) were products of Sigma Chemical Co, St. Louis, MO. Benzoylthiocholine iodide (BzTC) was a product from TCI-GR, Japan. (S_p)- and (R_p)-alkyl methylphosphonyl thioates were synthesized and isolated as resolved R_p and S_p enantiomers as described previously (Berman & Leonard, 1989). 7-[[(Methylethoxy)phosphinyl]-oxyl]-1-methylquinolinium (MEPQ) was a gift of Y. Ashani and B. P. Doctor (Walter Reed Army Research Center, Washington, DC; Levy & Ashani, 1986).

Production of Enzymes. Wild type AChE and BuChE and mutant AChE constructs were generated as described in Radic′ et al. (1993). Site-specific mutants not described previously were generated using the same procedures except pBluescriptKSII(-) vector and VCSM13 helper phage (Stratagene) were used to obtain a single stranded template. Mutations were conducted in cassettes flanked by BstXI sites (490 bp fragment) which were sequenced in their entirety by double stranded sequencing. The pRCCMV (Invitrogen) expression plasmids were purified by standard procedures involving poly(ethylene glycol) precipitation and centrifugation on CsCl gradients.

Human embryonic kidney (HEK-293) cells obtained from American Type Culture Collection (Atlanta, GA) were plated at 1.5×10^6 cells/10 cm of plate in 10% fetal bovine-serum supplemented Dulbecco's modified Eagle's (DME) medium 24 h prior to transfection. Cells were transfected with 15 μg of plasmid/plate of mutant or wild type cholinesterase−pRCCMV constructs using a standard HEPES-based calcium phosphate precipitation protocol (Ausubel et al., 1994). After 16−24 h, the transfected plates were washed with phosphate-buffered saline and maintained in serum free/DME for 48−72 h. The medium, containing a secreted form of cholinesterase, was collected, and the transfected cells were supplied fresh serum free DME. This process was continued for three to four harvests of enzyme. The medium was then concentrated using Centriprep30 Centicons (Amicon, Beverly, MA) to approximately 1−2% of original volume and stored at 4 °C.

To produce larger quantities of enzyme for detailed kinetic studies, stable transfectants were generated by selecting transiently transfected HEK cells with G418 for 2−3 weeks or until cell death subsided. Pools of selected cells were frozen in 10% serum and 5% DMSO-containing DME for future uses.

Enzyme Activity Measurements and Active Site Quantitation. AChE, BuChE, and mutant cholinesterase activities were measured in 0.1 M $NaPO_4$, pH 7.0, and 0.3 mM DTNB at 22 °C according to the procedure of Ellman et al. (1961) using ATC, BuTC, or BzTC as substrates. Maximum concentrations used were 100 mM for ATC and BuTC and 10 mM for BzTC due to spontaneous substrate hydrolysis and maximum solubility, respectively. Active sites were quantitated according to the procedures of Levy and Ashani (1986) and Radic′ et al. (1992) by titrating the enzyme samples with known concentrations of MEPQ.

Organophosphonate Inhibition. Enzyme samples (tens of picomoles) were incubated for various amounts of time with the inhibitor in the above assay mixture in the absence of substrate; typically, four inhibitor concentrations were used. The extent of inhibition was determined by measuring the residual activity with 5 mM ATC after a designated time of incubation. From the slopes of semilogarithmic plots of activity versus time, pseudo-first order rate constants (k_{obs}) were plotted against inhibitor concentration to obtain the bimolecular rate constants (k_i) (Radic′ et al., 1992).

Computer Modeling. Binding of butyrylcholine, benzoylcholine, and (S_p)- & (R_p)-cycloheptyl methylphosphonyl thiocholines to AChE as reversible ligands was modeled using InsightII (version 2.3.5), Discover (Biosym Technologies, San Diego, CA), and the X-ray crystal structure of *Torpedo californica* AChE (Sussman et al., 1991). The ligands were docked manually in the active site in a position that would minimize collisional interactions between molecules and in a position appropriate for an S_N2 type reaction involving Ser 203 in mouse (200)[2] in *Torpedo*. Mutant structures were generated by replacing Phe 295 (288) with Leu and Phe 297 (290) with Ile prior to docking and energy minimization. The choline and acyl moieties of BuTC and BzTC were directed toward Trp 86 (84) and towards residues Phe 295 and 297, respectively.

The OP inhibitors were docked initially for a nucleophilic attack of the plane defined as the methylalkoxylphosphonyl oxygen (CH_3-OR-P(O)) face, or the plane opposite the leaving group, by Ser 203. This places the leaving group approximately 180° from the side chain oxygen of Ser 203 and directed out of the gorge, facilitating concomitant apical displacement with apical attack. The bulky moieties of the R_p and S_p enantiomers were directed to different domains, R_p to the acyl pocket and S_p to the choline subsite, in order to satisfy the leaving group position and to place the phosphonyl oxygen with in hydrogen-bonding distance with the oxyanion hole defined by Gly 121 (118) and 122 (119) and Ala 204 (201) (Sussman et al., 1991; Harel et al., 1991; Barak et al., 1992; Cygler et al., 1994). For all the ligands, generic constraints between serine oxygen and the carbonyl carbon of the substrates or phosphorus of the organophosphonates were set at 3.5 Å and between the carbonyl or phosphonyl oxygen and the nitrogens of the amide backbone constituting the oxyanion hole at 3.0 Å, as the upper limit with no lower limit constraint. An upper force (upr–K) limit of 1000 was used to satisfy the distance constraints with the

[2] The numbers in parentheses denote residue positions in the *T. californica* AChE sequence from which the molecular models were built.

Scheme 1

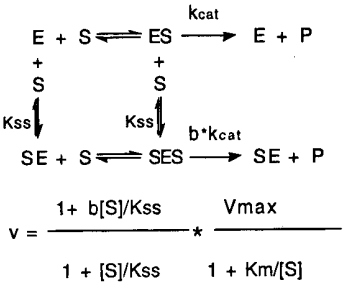

lower force (lwr–K) set at 0. Energy minimizations were completed on the restrained molecules with the side chains proximal to the bound ligand left free to move. They were run until convergence was achieved at a maximum derivative of 0.001.

RESULTS

Acyl Pocket Dimensions and Carboxyl Ester Substrate Size. Wild type and mutant cholinesterases have been examined kinetically with acylthiocholine esters of varying chain length in order to examine the relationship between the catalytic parameters and substrate dimensions. In particular, with a wider selection of mutant enzymes, we have measured substrate catalysis as a function of substrate concentration for ATC, BuTC, and BzTC and have fitted the corresponding data to Scheme 1[3] as described in Radic' et al. (1993).

As shown in Scheme 1, the enzyme associates reversibly with carboxyl substrates in two distinct fashions, resulting in ES and SE binary complexes. These two complexes differ in their affinities and in affecting substrate catalysis. The ES complex represents substrate bound to the active site and leads to hydrolysis. The SE complex, on the other hand, results from binding of substrate to a secondary site peripheral to the active site and does not lead to direct hydrolysis. Since binding to the two sites is not mutually exclusive, a ternary complex SES can also form. The SES complex could lead to substrate hydrolysis with varying degrees of efficiency, described as a fraction of ES turnover and represented by b. Three possible scenarios are possible: when $b < 1$, the SES complex is less productive than the ES complex which indicates that binding to the secondary site leads to substrate inhibition; when $b = 1$, SES is as productive as ES and is silent in substrate catalysis measurements; and finally, when $b > 1$, the SES complex is more productive than ES and results in substrate activation. When K_{ss} approaches the maximum substrate concentration employed experimentally (100 mM for ATC and BuTC and 10 mM for BzTC), uncertainties of both K_{ss} and b increase.

The three substrates, ATC, BuTC, and BzTC (Figure 1), were examined with wild type mouse AChE, wild type mouse BuChE, and acyl pocket mutants, where the Phes 295 and 297 were mutated to Leu and Ile, respectively, to Ala, or to Tyr. Table 1, which tabulates the K_m, K_{ss}, b, and k_{cat} values, shows that mutating 295 and 297 to the corresponding aliphatic groups found in mouse BuChE, Leu and Ile respectively, gives rise to a reduction in k_{cat} for ATC and an enhancement in k_{cat} for BuTC and BzTC, kinetic properties which approach BuChE's catalytic behavior. When examined in terms of efficiency of catalysis (k_{cat}/K_m, Table 1), F295L and F295A display the most dramatic increase in BuTC catalysis, and in fact, mutation at this position yields constants exceeding those of BuChE wild type. With the largest substrate BzTC, F295L and F297I show similar enhancements of catalysis; however, the constants are still diminished compared to those of BuChE. This indicates that while the acyl pocket dimensions may constrain catalytic rates of large substrates, they are not the sole determinant in the dependence of catalytic constants on substrate dimensions.

Mutating Phe 295 and Phe 297 to alanines and tyrosines gave unexpected results. F295A demonstrated kinetic parameters (k_{cat} and K_m) with all three substrates similar to those of the corresponding Leu mutation. However, F297A displayed greater catalytic turnover rates (k_{cat}) for ATC and lower rates for BzTC than seen with the corresponding Ile mutation, indicating that simply removing steric bulk does not ensure a greater capacity to hydrolyze choline substrates with large acyl groups. Examining the mutation to tyrosine further supports this contention, since enlarging the residues at 295 and 297 by the addition of a hydroxyl group to a phenyl ring does not further limit the rates of hydrolysis of the largest substrate BzTC. In fact, k_{cat}/K_m values for F295Y and F297Y with BzTC are approximately 10-fold greater than those found with AChE wild type. This phenomenon may be a consequence of altered structural integrity of the acyl pocket in the mutant enzymes. It should be noted that no native cholinesterases thus far sequenced contain Ala or Tyr at positions corresponding to 295 and 297 in mouse AChE (Cygler et al., 1993).

As initially reported by Radic' et al. (1993), and extended by the data in Table 1, AChE and BuChE show distinct behaviors when a second molecule of substrate binds to the enzyme, forming a ternary complex. The SES complex of BuChE with ATC is more active than ES, whereas this ternary complex in AChE is less active. The acyl pocket mutants F295L and F297I differ when ATC and BuTC bind at a peripheral site; while F295L resembles AChE in that this mutant species displays substrate inhibition ($b < 1$). F297I resembles BuChE in that the mutant species shows substrate activation ($b > 1$). Hydrolysis of the largest substrate BzTC by AChE wild type, F295L, and F297I occurs with substrate activation and therefore displays behavior that differs qualitatively from that of BuChE, which shows substrate inhibition with BzTC. Nonetheless, these observations signify that the residue at position 297 plays a role in linking occupation at a peripheral site with substrate hydrolysis at the base of the active center gorge. When the residue at 297 is a Phe, as in AChE wild type, the enzyme displays substrate inhibition; when the residue at 297 is Ile, as in BuChE wild type, substrate activation is evident [see also, Radic' et al., 1993)].

Influences of Acyl Pocket Dimensions on Reaction Rates with Enantiomeric Organophosphonates. Reaction of enantiomeric phosphonates with AChE is known to be dependent on the chemical nature of the leaving group and the size and stereochemical configuration of substituents about phosphorus (Berman & Leonard, 1989). The analysis of the organophosphonate (OP) reactions affords a clear kinetic

[3] Scheme 1 assumes that S has equivalent affinity for the active site of E and SE as does S for a peripheral site of E and ES. Should these affinities differ, a more complex equation would describe substrate catalysis and modulation of catalysis [cf. Webb, 1963].

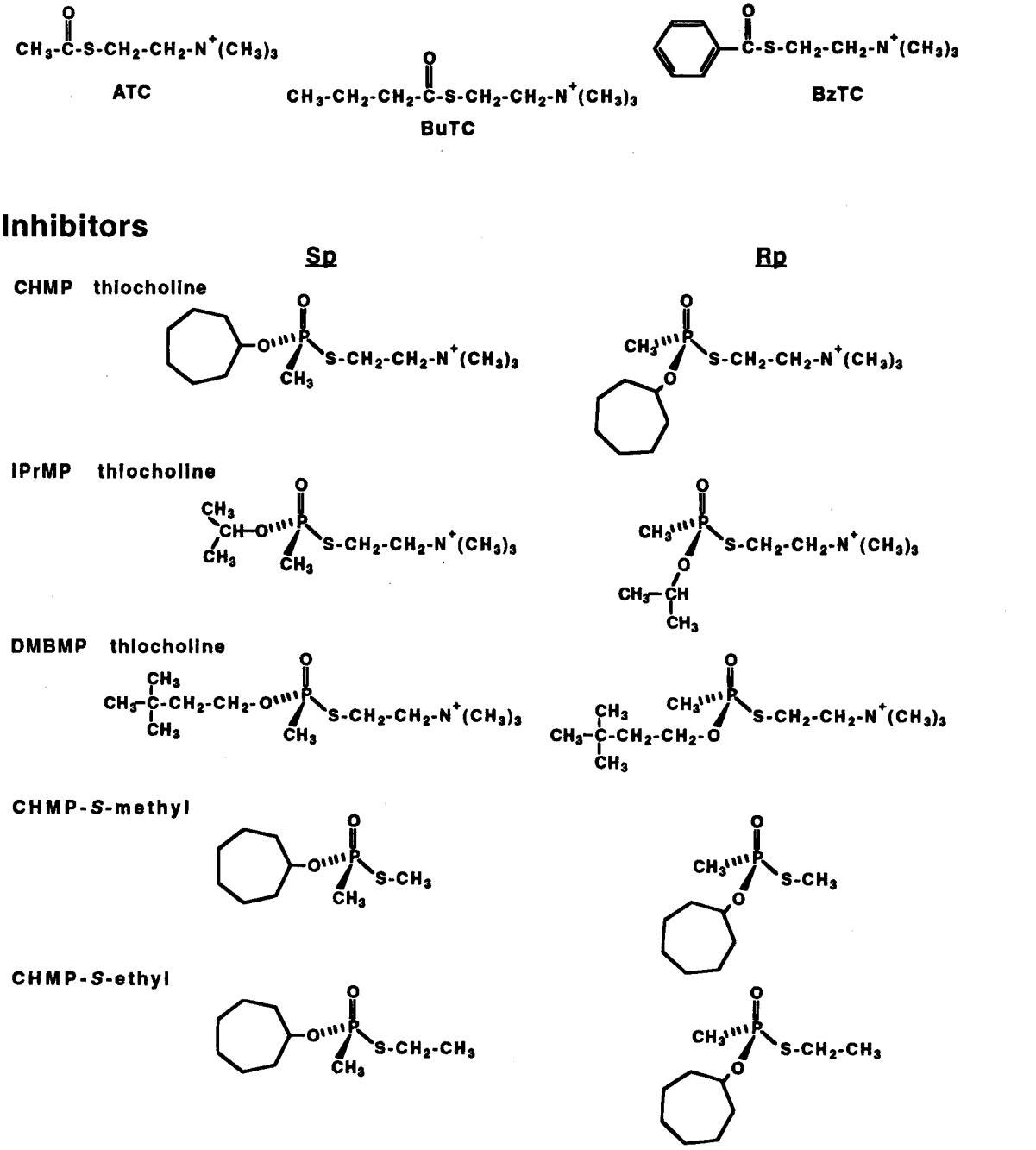

FIGURE 1: Structures of substrates and inhibitors employed. ATC, BuTC, and BzTC refer to acetyl-, butyryl-, and benzoylthiocholine substrates, respectively. CHMP, iPrMP, and DMBMP refer to cycloheptyl-, isopropyl-, and 3,3-dimethylbutyl methylphosphonyl, respectively. CHMP *S*-methyl and CHMP *S*-ethyl refer to cycloheptyl methyl *S*-methylphosphonyl thioate or cycloheptyl methyl *S*-methyl phosphonyl thioate.

separation of the acylation step (Froede & Wilson, 1971), and presents two additional features that complement analysis of planar carboxyl substrates. First, the tetrahedral configuration of organophosphonates provides a structural dimension outside the plane of the sp^2 trigonal geometry of substrate molecules. Second, the availability of enantiomerically pure phosphonates allows one to assess the spatial orientations of individual residues within the dissymmetric active center.

The series of compounds shown in Figure 1 have been analyzed with mouse AChE and mouse BuChE and the acyl pocket mutants, F295L, F295A, F297I, and F297A. Bimolecular rate constants (*ki*) for inhibition by enantiomers of cycloheptyl methylphosphonyl, isopropyl methylphosphonyl, and 3,3-dimethylbutyl methylphosphonyl thiocholine are shown in Table 2.

The S_p enantiomer is the most reactive for both CHMP and iPrMP thiocholine with a selectivity difference of more than 2 orders of magnitude for AChE; this ratio decreases significantly for BuChE. More specifically, the R_p enantiomers of CHMP and iPrMP thiocholine show a 10−20-fold increase in the reaction rate for BuChE over AChE, whereas the S_p enantiomers show little difference between the wild types. Hence, the (S_p)-OPs are binding and phosphonylating

Table 1: Kinetic Constants[a] Calculated for the Catalysis of Acetylthiocholine, Butyrylthiocholine, and Benzoylthiocholine by Recombinat DNA-Derived Cholinesterases

	acetylcholine					butyrylthiocholine					benzoylthiocholine				
enzyme	K_m (μM)	K_{ss} (mM)	b	k_{cat}[b] (10^3 min^{-1})	k_{cat}/K_m (10^8 min^{-1} M^{-1})	K_m (μM)	K_{ss} (mM)	b	k_{cat} (10^3 min^{-1})	k_{cat}/K_m (10^8 min^{-1} M^{-1})	K_m (μM)	K_{ss} (mM)	b	k_{cat} (10^3min^{-1})	k_{cat}/K_m (10^8min^{-1} M^{-1})
AChE	46	13	0.21	140	30	93	7.1	0.48	1.1	0.12	46	3.3	13	0.03	0.0063
BuChE	23	1.0	3.9	40	17	55	1.7	2.0	37	6.7	27	3.7	<0.2	3.8	1.4
F295A	64	75	<0.2[c]	73	11	3.6	>100	ID	8.0	22	16	4.2	<0.2	0.39	0.24
F295L	52	67	<0.2	44	8.5	10	23	0.40	12	12	10	1.0	2.4	0.24	0.24
F295Y	17[d]	27	<0.2	6.1	3.6	84	1.4	0.74	0.8	0.10	5.1	0.44	6.2	0.02	0.031
F297A	61	1.6	1.7	61	10	86	2.5	2.0	17	2.0	4.8	0.54	1.5	0.13	0.27
F297I	170	43	1.8	15	0.9	82	2.4	1.7	60	7.3	19	>4	ID	0.45	0.24
F297Y	58[d]	>100	ID[e]	39	6.7	45	0.96	2.7	1.8	0.40	13	1.1	3.1	0.08	0.062

[a] Values come from three measurements. Standard errors are typically within 20% of the mean, except where K_{ss} approached the maximal substrate concentrations employed (see text). Then K_{ss} and b incurred greater uncertainties. [b] k_{cat} was determined from titrations of the inhibition assay with MEPQ. Values for K_m, K_{ss}, and b were calculated using nonlinear computer fit according to $v = [V_{max}(1 + b[S]/K_{ss})]/[(1 + K_m/[S])(1 + [S]/K_{ss})]$ using Sigma Plot. [c] When substrate inhibition is evident, resulting b values less than 0.2 cannot be distinguished from zero. [d] Data of Radic' et al. (1933). [e] When K_{ss} was greater than the highest substrate concentration employed, the b values were indeterminable (ID).

Table 2: Bimolecular Rate Constants (min^{-1} M^{-1}) Determined for the Inhibition of Recombinant DNA-Derived Mouse Cholinesterases by Alkyl Methylphosphonyl Thiocholine Enantiomers[a]

	cycloheptyl methylphosphonyl thiocholine			isopropyl methylphosphonyl thiocholine			3,3-dimethylbutyl methylphosphyl thiocholine		
enzyme	$S_p \times 10^6$	$R_p \times 10^6$	S_p/R_p	$S_p \times 10^6$	$R_p \times 10^6$	S_p/R_p	$S_p \times 10^6$	$R_p \times 10^6$	S_p/R_p
AChE	190 ± 30	0.81 ± 0.09	230	16 ± 1	0.14 ± 0.03	110	360 ± 10	19 ± 9	19
BuChE	470 ± 90	6.7 ± 0.7	70	10 ± 1	3.3 ± 0.1	3	500 ± 150	32 ± 16	16
F295A	290 ± 50	7.1 ± 0.7	37	16 ± 1	1.2 ± 0.1	14	530 ± 40	15 ± 0	35
F295L	66 ± 9	8.7 ± 1.1	7.6	3.4 ± 0.1	1.2 ± 0.1	3	140 ± 10	10 ± 5	14
F297A	17 ± 4	2.4 ± 0.3	7.1	1.5 ± 0.3	0.098 ± 0.012	15	56 ± 1	1.8 ± 0.1	31
F297I	16 ± 3	62 ± 3	0.3	0.95 ± 0.46	1.2 ± 0.1	0.8	56 ± 4	12 ± 4	5

[a] Data shown as means ± standard deviations.

the two enzymes at similar rates, while the amino acid differences presumably in the acyl pocket with BuChE confer a selective increase in rate of reaction of the R_p enantiomers. Examination of the acyl pocket mutants supports this conclusion since replacing either F295 or F297 with smaller aliphatic residues results in a 10−100-fold increase in the k_i values for (R_p)-CHMP and (R_p)-iPrMP thiocholine. The F297 mutation also decreases the reaction rate for the S_p enantiomers, resulting in an inversion in chiral specificity for F297I where the reaction rate of the R_p enantiomer exceeds that of the S_p enantiomer.

The third asymmetric OP, DMBMP thiocholine, shows reaction rates similar to those of (S_p)-CHMP thiocholine but is distinctive in lacking the enantiomeric selectivity of the other two inhibitors. Moreover, little difference in reaction rate for AChE and BuChE is seen for the two DMBMP thiocholine enantiomers. Mutations to smaller residues in the acyl pocket region do not affect the bimolecular rate constants for (R_p)-DMBMP thiocholine, unlike the other two asymmetric OPs, although, as with the other inhibitors, some reduction in rate is seen with F297A.

Influence of Thioalkyl and Thiocholine Leaving Groups on Reaction Kinetics. The second set of compounds for kinetic analysis of enantiomers is made up of two neutral cycloheptyl methylphosphonyl organophosphonates, shown in Figure 1. Table 3 displays the inhibition kinetics for two CHMP thioate congeners with thiomethyl and thioethyl leaving groups. These CHMP compounds, with neutral leaving groups of diminished molecular dimensions, show stereospecificity of a magnitude comparable to that of the corresponding methylphosphonyl thiocholines, although the reaction rates are 2−3 orders of magnitude slower for the uncharged CHMP OPs.

Table 3: Bimolecular Rate Constants (k_i in min^{-1} M^{-1}) for the Inhibition of Recombinant DNA-Derived Cholinesterases by Neutral (S_p)- and (R_p)-Cycloheptyl Methylphosphonyl Thioates[a]

	leaving group					
	S-methyl			*S*-ethyl		
enzyme	$S_p \times 10^4$	$R_p \times 10^4$	S_p/R_p	$S_p \times 10^4$	$R_p \times 10^4$	S_p/R_p
AChE	31 ± 4	0.18 ± 0.07	170	7.6 ± 0.5	0.018 ± 0.002	420
BuChE	23 ± 6	0.25 ± 0.07	92	13 ± 1	0.17 ± 0.02	76
F295L	34 ± 2	0.29 ± 0.11	120	16 ± 2	0.100 ± 0.03	160
F297I	5.5 ± 0.1	2.2 ± 0.4	2.5	5.5 ± 1.3	2.6 ± 0.6	2.1

[a] Data shown as means ± standard deviations.

Also, as shown in Table 3, the R_p enantiomers react with F297I more rapidly than with AChE; the S_p enantiomer agents display a slight reduction in rate. Consequently, substitution for Phe at position 297 with the Ile found in BuChE virtually eliminates the enantiomeric preference. The similarity in S_p/R_p chiral specificity seen for the cationic and uncharged CHMP compounds suggests that the charge on the leaving group does not dictate enantiomeric preference.

DISCUSSION

Analysis of substrate specificity reveals that differences between AChE and BuChE substrate specificity are largely due to the phenylalanines at 295 and 297. Clearly, replacement of these residues by Leu and Ile results in an enhancement in catalysis of larger substrates that can be attributable to enlarging the acyl pocket region (Figure 2A,B). With their sp^2 planar geometry, the substrates dock for catalysis presumably by placing the carbonyl oxygen toward the oxyanion hole. With the choline moiety toward Trp 86, and the acyl moiety toward F295 and F297 (Sussman et al., 1991), only one of the two faces of the planar compound is

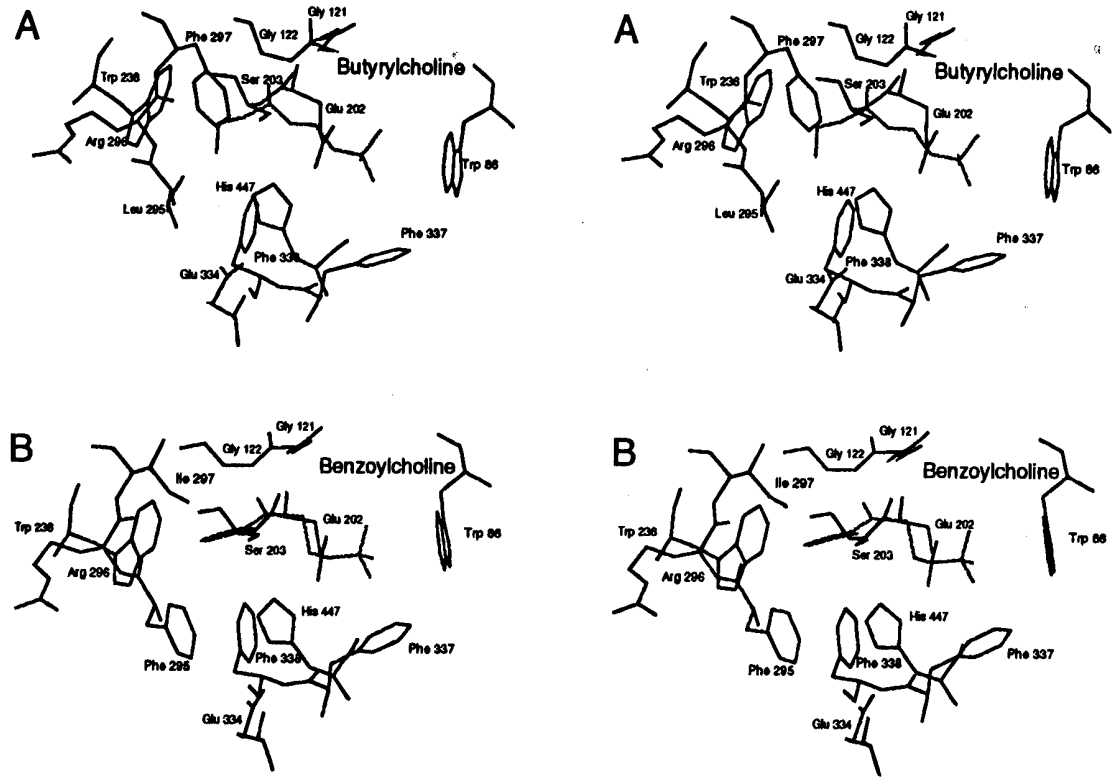

FIGURE 2: Energy-minimized stereoviews of carboxyl choline substrates in the active center of mutant acetylcholinesterase structures as described in the Materials and Methods: (A) F295L with butyrylcholine and (B) F297I with benzoylcholine. In parts A and B of this figure, the carbonyl oxygen resides within the oxyanion hole defined by the hydrogen bonds (<3 Å) with amide backbone hydrogens of Gly 121, Gly 122, and Ala 204. The residue numbers correspond to mouse sequence.

Table 4: Summary of $\Delta\Delta G$ Values[a] (Kilocalories per Mole) Obtained from Free Energy (ΔG) Calculations of k_{cat}/K_m for the Catalysis of Acetylcholine (ATC), Butyrylthiocholine (BuTC), and Benzoylthiocholine (BzTC) and from the Bimolecular Rate Constants (k_i) for (S_p)- and (R_p)-Cycloheptyl Methylphosphonyl, Isopropyl Methylphosphonyl, and 3,3-Dimethylbutyl Methylphosphonyl Thiocholines

	substrates			CHMPTCH		IMPTCH		DMBMPTCH	
enzyme	ATC	BuTC	BzTC	S_p	R_p	S_p	R_p	S_p	R_p
BuChE	−0.34	+2.4	+3.2	+0.54	+1.30	−0.28	+1.90	+0.19	+0.31
F295A	−0.59	+3.1	+2.2	+0.25	+1.30	0	+1.30	+0.23	−0.14
F295L	−0.75	+2.7	+2.2	−0.63	+1.40	−0.92	+1.30	−0.56	−0.38
F297A	−0.65	+1.7	+2.2	−1.40	+0.64	−1.40	−0.21	−1.10	−1.40
F297I	−2.1	+2.4	+2.2	−1.50	+2.60	−1.67	+1.30	−1.10	−0.27

[a] $\Delta\Delta G$ values obtained using values in Tables 1 and 2 and the equation $\Delta\Delta G = \Delta G_{AChE} - \Delta G_{BuChE/mutant} = RT \ln (k_i'/k_i)$, where k_i = the bimolecular rate constant for the organophosphonates and is equal to k_{cat}/K_m for carboxyl ester substrates (Fersht, 1988). The ′ refers to either BuChE or mutant AChE; $R = 1.99 \times 10^{-3}$ kcal/mol K, and $T = 298$ K.

available for nucleophilic attack by the active center serine. Upon such attack of the carbonyl carbon, the bond angles change with formation of a tetrahedral intermediate. The change in bond angles might move the thiocholine slightly in the direction of the gorge exit, a position well-suited for leaving the active site where no hindrance to exit would be encountered by other substituents on the substrate. Furthermore, with the planar configuration and the acyl moiety directed toward the residues F295 and F297, changes in the acyl chain length will be reflected only in the acyl pocket direction.

The OP compounds have an additional substituent due to their tetrahedral configuration with 109° bond angles, and thus, the substituent groups will project differently in the active site than for the planar (trigonal) substrates with 120°-bond angles. This becomes evident with AChE wild type which most efficiently catalyzes the hydrolysis of carboxyl choline substrates with small acyl group size while the same enzyme is acylated by organophosphonates with bulkier substituents (Tables 1−3). Table 4 tabulates the relative free energies of reaction for the various substrates, where a positive $\Delta\Delta G$ value indicates a more energetically favorable reaction relative to AChE wild type. The direction of the free energy changes between AChE and mutant cholinesterases with the S_p enantiomers reflects that of acetylthiocholine, while the R_p compounds parallel that of the larger acyl containing substrates.

The CHMP and iPrMP thiocholine compounds display a similar enantiomeric selectivity with AChE even though iPrMP thiocholine is approximately 10-fold less reactive. From the analysis of the individual enantiomers, the diminished inhibition rates of (R_p)-CHMP and iPrMP thiocholine with AChE also can be attributed to the phenylalanines at 295 and 297 since their replacement with smaller residues gives a substantial enhancement in the bimolecular rate constant, approaching or exceeding that with BuChE.

Therefore, the respective alkoxyl substituents of these two R_p compounds are restricted from optimal positioning in the active site of AChE due to occlusion by F295 and F297 in a manner similar to restricting large carboxyl ester substrates.

The third charged inhibitor, DMBMP thiocholine, shows diminished stereoselectivity for AChE which seems to be a consequence of an enhanced rate of inhibition by the R_p enantiomer, with little to no change by the S_p enantiomer when compared to (S_p)-CHMP thiocholine. Therefore, (R_p)-DMBMP thiocholine with a primary instead of secondary alkoxyl substituent probably orients slightly differently in AChE than do the other two congeners. In addition, the inhibitory efficiencies of reaction with (R_p)-DMBMP thiocholine for the acyl pocket mutants are similar to those of AChE wild type, indicating that the two phenylalanines play a diminished role in dictating the rate of reaction with (R_p)-DMBMP thiocholine and in sterically occluding the DMB substituent. Part of this may arise from steric restrictions of a secondary alkoxyl constituent, rather than solely being a consequence of molecular volumes.

The S_p enantiomers of all three thiocholine inhibitors show equivalent or slower rates of inhibition with the acyl pocket mutants where F297I and F297A show the largest reduction. Removing the aromatic group from the side chain reduces the potency of the S_p thiocholine inhibitors which may be attributed to increased degrees of freedom of the organophosphonate in the active site region. BuChE, lacking the large aromatic side chains at 295 and 297, reacts more efficiently with the S_p compounds, supplying evidence that the mutant AChEs do not precisely mimic BuChE and that other groups close to the substrate, such as Tyr 337 in mouse AChE (Phe in *T. californica*), might indirectly influence substrate positions. In addition, the reduced reaction rates with (S_p)-CHMP and iPrMP enantiomers along with the concomitant increased reaction rates with the R_p enantiomers give rise to the dramatic inversion in enantiomeric preference for the F297I mutant relative to AChE wild type.

Interestingly, the F297A mutation does not display the same kinetics as F297I with the (R_p)-alkyl methylphosphonyl thiocholine inhibitors, where the Ala mutant gives a 10-fold lower k_i for common inhibitors than for the Ile mutant. A similar lack of reactivity was noted for the carboxyl esters (k_{cat} values, Table 1). Replacement of the large Phe residue with Ala can be expected to yield a void area which should be filled with water or which may result in collapse of the α-carbon chain. For the F297I substitution, the volume reduction is smaller and would require a smaller structural perturbation than would the equivalent Ala mutant.

A final factor in determining the rate of reaction of organophosphonates with AChE is the chemical nature of the leaving group. The uncharged cycloheptyl methylphosphonyl thioates display a chiral selectivity similar to that of the cationic cycloheptyl methylphosphonyl thiocholines. Since the uncharged phosphonyl thioates react at rates that are 3 orders of magnitude slower than the corresponding charged compounds, the large difference in reaction rates depends on the nature of the leaving group. As analyzed by Kitz et al. (1967), the reaction rates reflect the interaction energy gained upon formation of the phosphonate−enzyme complex rather than p*K*a differences between the leaving groups. As discussed by Berman and Leonard (1989), the slower reaction rate typical of the uncharged methylphosphonyl thioates reflects diminished electrostatic attraction for the enzyme. Therefore, stabilization of the quaternary choline group enhances the reaction of the charged compounds but carries little influence in enantiomeric preference. These findings are consistent with the thiocholine or thioalkyl leaving group residing in a common position for the individual enantiomers.

Substrate and Organophosphonate Orientation. As a model for the orientation of substrates and organophosphonates begins to emerge, it is first instructive to compare the tetrahedral phosphonyl esters with the planar carboxyl esters. The phenylalanines in the acyl pocket of AChE hinder noncovalent association of reactive substrates and phosphonates containing large bulky substituents. The phenylalanine residues also serve to enhance association of reactive substrates and phosphonates containing small, less bulky substituents, as seen for ATC and (S_p)-methylphosphonates. In Figure 2, the large carboxyl substrates are modeled in the active site region of F295L and F297I and are positioned with their acyl moieties occupying the region of the acyl pocket where butyryl is directed toward 295 (Figure 2A) and where benzoyl is closer to the 297 side chain (Figure 2B). By comparison, the F297I mutant modeled with (R_p)-CHMP thiocholine (Figure 3B) shows that the mutation at 297 to the smaller residue, Ile, allows the bulky cycloheptyl group to be accommodated in a manner similar to BzTC. Therefore, steric occlusion by the phenylalanines within the acyl pocket of AChE, in particular Phe 297, represents a primary determinant of substrate selectivity and enantiomeric preference. Such steric constraints can be relieved by replacing the phenylalanines with dimensionally smaller aliphatic residues.

A comparison of AChE covalent reactivity with respect to large substrates, such as BuTC and BzTC, and large phosphonates, such as the most reactive (S_p)-CHMP and (S_p)-DMBMP thiocholines, indicates that reaction efficiency is governed in part by the spatial orientation achieved at the base of the active center gorge by the substrate molecules and the organophosphonates. This conclusion is supported by the observations that AChE reacts 10-fold more rapidly with large alkoxyl (S_p)-methylphosphonates than the large acylcholine substrates (k_i in Table 2 versus k_{cat}/K_m in Table 1; Table 4). Furthermore, mutations of the two Phes to smaller aliphatic residues give rise to enzymes with reduced efficiency in catalyzing the hydrolysis of small ligands such as ATC and the reactions with ligands, such as (S_p)-CHMP thiocholine, whose binding of the large alkoxyl moiety does not necessitate interaction with the acyl pocket. From the modeling of AChE with (S_p)-CHMP thiocholine (Figure 3A), it can be inferred that removal of aromatic groups at 295 and 297 permits increased degrees of freedom for binding, association of nonproductive complexes, and resulting slower reaction rates. Thus, a systematic study of a series of congeneric compounds with a graded diminution of side chain volume in the acyl pocket reveals an optimal volume or dimension, a feature unresolvable from substrate structure−activity relationships alone. This demonstrates that the Phes in wild type AChE, in addition to occluding substrates exceeding a critical dimension, may serve to stabilize and orient substrates of smaller dimensions for efficient catalysis. Opening the acyl pocket creating a larger dimension may lead to additional orientations of bound substrate, whose alignment may not be optimal for catalysis.

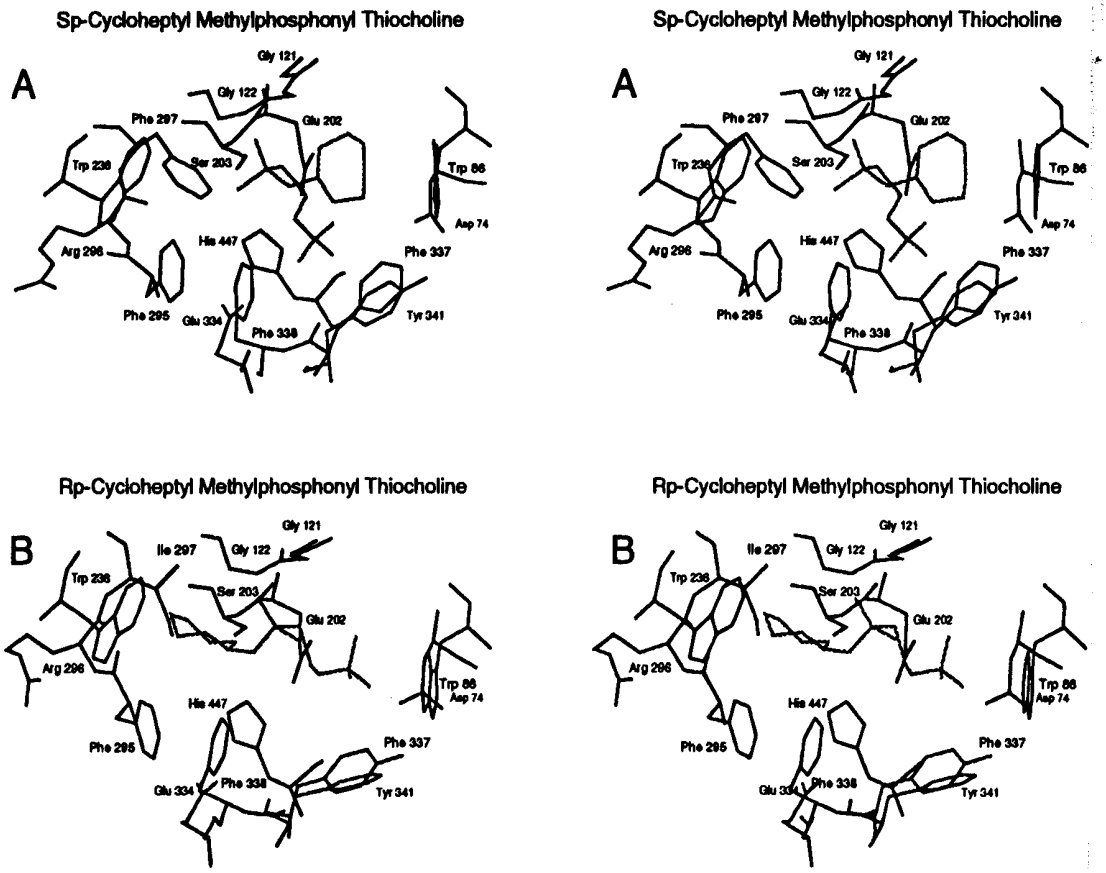

FIGURE 3: Energy-minimized stereoviews of the reversible complex in the active center of (A) acetylcholinesterase with (S_p)-cycloheptyl methylphosphonyl thiocholine and (B) F297I mutant acetylcholinesterase with (R_p)-cycloheptyl methylphosphonyl thiocholine as described in the Materials and Methods. In parts A and B of this figure, the phosphonyl oxygen resides within the oxyanion hole defined by the hydrogen bonds (<3 Å) with amide backbone hydrogens of Gly 121, Gly 122, and Ala 204. The residue numbers correspond to mouse sequence.

Enantiomeric Selectivity. The information to be gained from the analysis of enantiomeric selectivity requires the absolute stereochemical assignment of the R_p and S_p enantiomers along with the positioning of a primary functional group on the dissymmetric macromolecular surface. Formation of the alkylphosphonyl conjugate in addition to the obvious nucleophilic attack by the serine requires polarization of the phosphonyl bond through hydrogen bonding to the phosphonyl oxygen in the oxyanion hole. The region in AChE is likely created by hydrogen bond donors of the backbone amide hydrogens from Gly 121, Gly 122, and Ala 204 (Sussman et al., 1991). Evidence for the obligate phosphonyl oxygen−oxyanion hole interactions stems from the rapid rates of conjugation by the cholinesterases and the X-ray crystal structure of a phosphonyl enzyme conjugate in *Candida rugosa* lipase, a structure homologous to cholinesterase (Cygler et al., 1993, 1994).

With this initial substituent placement, orientation of the leaving group in the direction of the mouth of the active center gorge allows for preferential nucleophilic attack by the γ-oxygen of Ser 203 at the one face of the tetrahedron, comprising CH_3-OR-P(O), not containing the leaving group (Figure 3A). Such attack at this face opposite the leaving group results in formation of a trigonal bipyramidal intermediate in which both the attacking nucleophile and the potential leaving group assume apical positions. In this case, displacement of the leaving group can occur without a requirement for pseudorotation of the trigonal bipyramidal enzyme conjugate (Berman & Decker, 1989). In the case of docking (S_p)-CHMP thiocholine, these initial residue placements find the cycloheptyl group oriented toward the more space-accommodating choline subsite (Figure 3A).

By contrast, these requirements enforce an orientation of (R_p)-CHMP thiocholine in which the cycloheptyl moiety encounters obvious steric hindrance from the Phes 295 and 297, precluding either optimal positioning of the phosphonyl oxygen in the oxyanion hole or displacement of the leaving group from an optimal position for in-line attack by Ser 203. The former case would lead to loss of stabilization energy which would arise from polarization of the phosphonyl−oxygen bond; the latter would result in equatorial positioning of the leaving group and thus would require pseudorotation of the intermediate prior to apical displacement (Berman & Decker, 1989). Since both cases require an expenditure of additional energy (Berman & Decker, 1989; Cygler et al., 1994; Ashani et al., 1995), steric interference engendered upon docking (R_p)-enantiomers is expected to reduce the rates of reaction. Such steric constraints are relieved in the F297I mutation, as shown for association of (R_p)-CHMP thiocholine in Figure 3B, leading to the increased reaction rates observed for the R_p methylphosphonates.

This study clearly shows that substrate selectivity and enantiomeric preference of AChE as well as rates of covalent reaction are all governed in large part through steric limitations imposed with the acyl pocket. One component of the acyl pocket that plays a prominent role is identified

as F297. This postulate can be subjected to further analysis through modification of the gorge dimensions and charge distribution of the residues within the gorge.

ACKNOWLEDGMENT

We thank Dr. Zoran Radic′ for his advice and valuable discussions related to the study.

REFERENCES

Aldridge, W. N., & Reiner, E. (1972) in *Enzyme Inhibitors as Substrates* (Neuberger, A., & Tatum, E. L., Eds.) North-Holland Publishing Co., Amsterdam & American Elsevier Publishing Co., Inc., New York.

Ashani, Y., Radic′, Z., Tsigelny, I., Vellom, D. C., Pickering, N. A., Quinn, D. M., Doctor, B. P., & Taylor, P. (1995) *J. Biol. Chem. 270,* 6370−6380.

Augustinsson, K. B. (1948) *Acta Physiol. Scand., Suppl. 52,* 1−182.

Ausubel, F. M., Brent, R., Kingston, R. E., Moore, D. D., Seidman, J. G., Smith, J. A., & Struhl, K. (1994) in *Current Protocols in Molecular Biology,* pp 9.1.1 Green Publishing Associates, Inc., & John Wiley & Sons, Inc.

Barak, D., Ariel, N., Velan, B., & Shafferman, A. (1992) in *Multidisciplinary Approaches to Cholinesterase Functions* (Shafferman, A., & Velan, B., Eds.) pp 195−199, Plenum Press, New York.

Berman, H. A., & Decker, M. M. (1989) *J. Biol. Chem. 264,* 3951−3956.

Berman, H. A., & Leonard, K. (1989) *J. Biol. Chem. 264,* 3942−3950.

Cygler, M., Schrag, J. D., Sussman, J. L., Harel, M., Silman, I., Gentry, M. K., & Doctor, B. P. (1993) *Protein Sci. 2,* 366−382.

Cygler, M., Grochulski, P., Kazlauskas, R. J., Schrag, J. D., Bouthillier, F., Rubin, B., Serreqi, A. N., & Gupta, A. K. (1994) *J. Am. Chem. Soc. 116,* 3180−3186.

Ellman, G. C., Courtney, K. D., Andres, V., Jr., & Featherstone, R. M. (1961) *Biochem. Pharmacol. 7,* 88−95.

Fersht, A. R. (1988) *Biochemistry 27,* 1577−1580.

Froede, H. C., & Wilson, I. B. (1971) in *The Enzymes* (Boyer, P. D., Ed.) pp 87−114, Academic Press, New York.

Gibney, G., Camp, S., Dionne, M., MacPhee-Quigley, K., & Taylor, P. (1990) *Proc. Natl. Acad. Sci. U.S.A. 87,* 7546−7550.

Harel, M., Su, C.-T., Frolow, F., Ashani, Y., Silman, I., & Sussman, J. L. (1991) *J. Mol. Biol. 221,* 909−918.

Harel, M., Sussman, J. L., Krejci, E., Bon, S., Chanal, P., Massoulié, J., & Silman, I. (1992) *Proc. Natl. Acad. Sci. U.S.A. 89,* 10827−10831.

Kitz, R. J., Ginsburg, S., & Wilson, I. B. (1967) *Mol. Pharmacol. 3,* 225−232.

Levy, D., & Ashani, Y. (1986) *Biochem. Pharmacol. 35,* 1079−1085.

Oosterbaan, R. A., & Cohen, J. A. (1964) *Proc. 1st FEBS Meet.,* 87.

Ordentlich, A., Barak, D., Kronman, C., Flashner, Y., Leitner, M., Segall, Y., Ariel, N., Cohen, S., Velan, B., & Shafferman, A. (1993) *J. Biol. Chem. 268,* 17083−17095.

Radic′, Z., Gibney, G., Kawamoto, S., Mac-Phee-Quigley, K., Bongiorno, C., & Taylor, P. (1992) *Biochemistry 31,* 9760−9767.

Radic′, Z., Pickering, N. A., Vellom, D. C., Camp, S., & Taylor, P. (1993) *Biochemistry 32,* 12074−12084.

Sussman, J. L., Harel, M., Frolow, F., Oefner, C., Goldman, A., Toker, L., Silman, I. (1991) *Science 253,* 872−878.

Vellom, D. C., Radic′, Z., Li, Y., Pickering, N. A., Camp, S., & Taylor, P. (1993) *Biochemistry 32,* 12−17.

Webb, J. L. (1963) *Enzyme & Metabolic Inhibitors,* Vol. 1, pp 45−47, Academic Press, New York & London.

BI950882S

THE JOURNAL OF BIOLOGICAL CHEMISTRY

Vol. 270, No. 11, Issue of March 17, pp. 6370–6380, 1995
Printed in U.S.A.

Amino Acid Residues Controlling Reactivation of Organophosphonyl Conjugates of Acetylcholinesterase by Mono- and Bisquaternary Oximes*

(Received for publication, August 22, 1994, and in revised form, November 28, 1994)

Yacov Ashani‡§, Zoran Radić¶‖, Igor Tsigelny¶, Daniel C. Vellom¶, Natilie A. Pickering¶, Daniel M. Quinn¶, Bhupendra P. Doctor‡ ‡‡, and Palmer Taylor¶**

From the ‡Division of Biochemistry, Walter Reed Army Institute of Research, Washington, D. C. 20307-5100 and the ¶Department of Pharmacology, University of California, San Diego, La Jolla, California 92093-0636

Single and multiple site mutants of recombinant mouse acetylcholinesterase (rMoAChE) were inhibited with racemic 7-(methylethoxyphosphinyloxy)-1-methylquinolinium iodide (MEPQ) and the resulting mixture of two enantiomers, $CH_3P_{R,S}(O)(OC_2H_5)$-AChE($EMP_{R,S}$-AChE), were subjected to reactivation with 2-(hydroxyiminomethyl)-1-methylpyridinium methanesulfonate (P2S) and 1-(2′-hydroxyiminomethyl-1′-pyridinium)-3-(4″-carbamoyl-1″-pyridinium)-2-oxapropane dichloride (HI-6). Kinetic analysis of the reactivation profiles revealed biphasic behavior with an approximate 1:1 ratio of two presumed reactivatable enantiomeric components. Equilibrium dissociation and kinetic rate constants for reactivation of site-specific mutant enzymes were compared with those obtained for wild-type rMoAChE, tissue-derived *Torpedo* AChE and human plasma butyrylcholinesterase. Substitution of key amino acid residues at the entrance to the active-site gorge (Trp-286, Tyr-124, Tyr-72, and Asp-74) had a greater influence on the reactivation kinetics of the bisquaternary reactivator HI-6 compared with the monoquaternary reactivator P2S. Replacement of Phe-295 by Leu enhanced reactivation by HI-6 but not by P2S. Of residues forming the choline-binding subsite, the E202Q mutation had a dominant influence where reactivation by both oximes was decreased 16- to 33-fold. Residues Trp-86 and Tyr-337 in this subsite showed little involvement. These kinetic findings, together with energy minimization of the oxime complex with the phosphonylated enzyme, provide a model for differences in the reactivation potencies of P2S and HI-6. The two kinetic components of oxime reactivation of MEPQ-inhibited AChEs arise from the chirality of *O*-ethyl methylphosphonyl moieties conjugated with Ser-203 and may be attributable to the relative stability of the phosphonyl oxygen of the two enantiomers in the oxyanion hole.

Inhibition of acetylcholinesterase (AChE; EC 3.1.1.7)[1] and butyrylcholinesterase (BChE; EC 3.1.1.8) by organophosphorus (OP) esters is attributed to the formation of a covalent conjugate between the OP moiety and the active-site serine of the enzyme (1). OP-inhibited cholinesterases (ChEs)[2] can be reactivated by certain oxime nucleophiles, if the enzyme does not undergo a prior "aging" reaction (1, 2). Since the discovery of powerful reactivators of OP-inhibited ChEs, 2-(hydroxyiminomethyl)-1-methylpyridinium iodide (2-PAM; Fig. 1) (3), and the bispyridinium dioxime 1,1′-trimethylene bis(4-hydroxyiminomethylpyridinium)-dibromide (4), several reports have described the preparation, structure, and biochemical properties of mono- and bisquaternary oximes. The limited scope of antidotal activity of commonly used reactivators such as the methanesulfonate salt of 2-PAM (P2S; Fig. 1) or 1,1′-trimethylene bis(4-hydroxyiminomethylpyridinium)-dibromide against certain types of OP anti-ChE, prompted the evaluation of a new series of oxime reactivators (5). One such compound, 1-(2′-hydroxyiminomethyl-1′-pyridinium)-3-(4″-carbamoyl-1″-pyridinium)-2-oxapropane dichloride (HI-6; Fig. 1) is among the most potent reactivating agents that serve as antidotes against organophosphate toxicity (6, 7).

The effectiveness of oxime reactivators as antidotes is primarily attributed to the nucleophilic displacement rate of the OP moiety from the inhibited enzyme (Fig. 2) and varies with the structure of the bound OP, the source of the enzyme, and the oxime. In spite of three decades of progress in improving the reactivation properties of the lead compounds, structure-function relationships are not clearly understood.

The elucidation of the three-dimensional structure of *Torpedo* AChE (TcAChE) (8), together with kinetic and mechanistic studies of site-directed mutants (9), have added a new dimension to the study of organophosphate inhibition and reactivation. In this report we describe studies on P2S- and HI-6-induced reactivation of wild-type recombinant mouse AChE (rMoAChE) and its mutants inhibited with 7-(methylethoxyphosphinyloxy)-1-methylquinolinium iodide (MEPQ; Fig. 2) (10). Delineation of amino acid residues that are important for reactivation highlight several aspects of the mechanism by which oximes enhance displacement of an OP from

* This work was supported in part by U. S. Army Research and Material Command Grant DAMD17–91-C-1056 (to P. T.). The costs of publication of this article were defrayed in part by the payment of page charges. This article must therefore be hereby marked "*advertisement*" in accordance with 18 U.S.C. Section 1734 solely to indicate this fact.

§ Visiting scientist from the Israel Institute for Biological Research, Ness-Ziona, Israel.

‖ Visiting fellow from the Institute for Medical Research and Occupational Health, University of Zagreb, Croatia.

** Visiting scientist from the Department of Chemistry, University of Iowa, Iowa City, IA.

‡‡ To whom correspondence should be addressed. Tel.: 202-782-3001; Fax: 202-782-6304.

[1] The abbreviations used are: AChE, acetylcholinesterase; BChE, butyrylcholinesterase; OP, organophosphorus; ChE, cholinesterase; 2-PAM, 2-(hydroxyiminomethyl)-1-methylpyridinium iodide; P2S, 2-(hydroxyiminomethyl)-1-methylpyridinium methanesulfonate; HI-6, 1-(2′-hydroxyiminomethyl-1′-pyridinium)-3-(4″-carbamoyl-1″-pyridinium)-2-oxapropane dichloride; rMoAChE, recombinant mouse AChE; MEPQ, 7-(methylethoxyphosphinyloxy)-1-methylquinolinium iodide; EMP-ChE, *O*-ethyl methylphosphonyl-ChE; HuBChE, human BChE; TcAChE, *Torpedo californica* AChE; paraoxon, diethyl *p*-nitrophenyl phosphate; ATC, *S*-acetylthiocholine iodide; BTC, *S*-butyrylthiocholine iodide; 7-HQ, 7-hydroxy-1-methylquinolinium ion.

[2] The abbreviation ChE was used whenever AChE was not distinguished from BChE.

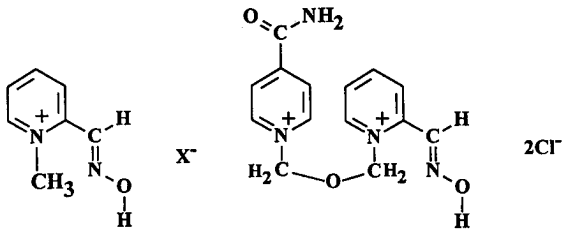

2-PAM, X=I **HI6**

P_2S, X=CH_3SO_3

FIG. 1. **Structures of 2-PAM, P2S, and HI-6.** The *syn* configurations shown are in accordance with the crystal structure of 2-PAM (19) and HI-6 (20).

EMP-ChEs and provide an explanation for differences between the reactivation potency of HI-6 and P2S. In addition, owing to chirality of the phosphorus in MEPQ and the potent anti-ChE activity of both of its enantiomers (10, 11), the inhibited enzyme consists of two enantiomeric components, EMP_R-ChE, and EMP_S-ChE, that are amenable to analysis of the stereospecificity of the reactivation process.

EXPERIMENTAL PROCEDURES

Materials—MEPQ was prepared as described elsewhere (10). *O,O'*-Diethyl *p*-nitrophenyl phosphate (paraoxon) was purchased from Sigma. P2S and HI-6 were obtained from the Division of Experimental Therapeutics, Walter Reed Army Institute of Research, Washington, D. C.

Wild-type and mutant rMoAChEs were prepared as described previously (12, 13). The cDNA insert encompassing exons 2, 3, 4, and 6 was placed behind the human cytomegalovirus promoter. Most of the expression plasmids exist as stable transfectants in human embryonic kidney (HEK-293) and Chinese hamster ovary (CHO-K1) cells. They secrete into the medium hydrophilic enzyme which was concentrated by ultrafiltration for the kinetic studies. *Torpedo californica* AChE, wild-type mouse AChE, and some of the mutant enzymes were purified by affinity chromatography as described previously (14). HuBChE was purified by procainamide-Sepharose® 4B gel affinity chromatography. One mg of pure enzyme contained approximately 11 and 14 nmol of active sites of BChE and AChE, respectively. Inhibition and reactivation experiments were carried out in enzyme solutions prepared in microfiltered 0.05% bovine serum albumin containing 25 mM phosphate buffer, pH 7.8, at 25 °C.

pK_a Determinations—pH-optical density profiles were recorded in 25 mM phosphate buffer (pH 6.4–8.3; 25 °C) at 336 and 354 nm for P2S and HI-6, respectively. Extinction maxima were measured in 0.1 M NaOH and 1% carbonate buffer at pH 10.2 for P2S and HI-6, respectively; pK_a values were calculated as described by Albert and Serjeant (15).

Hydrolysis of MEPQ—Rate constants of the hydrolysis of MEPQ were determined in 25 mM phosphate, pH 7.8 and 7.0, at 25 °C. Release of the leaving group 7-hydroxy-1-methylquinolinium ion (7-HQ, Fig. 2) was monitored at 406 nm (10).

Enzyme Assays—AChE and BChE activities were determined by the method of Ellman *et al.* (16), using 1.5 mM acetylthiocholine (ATC) and butyrylthiocholine (BTC) as substrates, respectively. Assays were carried out in 0.05% bovine serum albumin, 50 mM phosphate buffer, pH 8.0, at 25 °C. Due to the low catalytic efficiency of the W86A[3] mutant and the need to minimize nonspecific hydrolysis of ATC, its assay was carried out with 60 mM ATC in the above buffer adjusted to pH 6.3.

Determination of the Dissociation Constants of AChE·Oxime Complexes—The dissociation constants, K_{ox} and αK_{ox}, were determined by examining the dependence on the concentration of P2S or HI-6 for the K_m and V_{max} of the enzyme-catalyzed hydrolysis of ATC. ATC between 0.01 and 0.4 mM was added to the enzyme that had been incubated for 5 min with specified concentration of oxime and 5,5'-dithiobis(2-nitrobenzoic acid) at 25 °C. Activities were corrected for oxime catalyzed hydrolysis of ATC. Secondary plots of the slopes and the intercepts derived from Lineweaver-Burk plots against the concentration of the oxime were used to obtain K_{ox}, and αK_{ox}, respectively (17).

[3] MoAChE numbering system.

Titration of the AChE Active Center by MEPQ and Paraoxon—Increasing amounts of MEPQ, in 5–20-μl aliquots, were added to 0.3–1 unit of wild-type or mutant enzyme in 0.6–2 ml of 25 mM phosphate buffer, pH 7.8. Final concentrations of enzyme and MEPQ ranged between 1 and 10 nM with MEPQ in slight substoichiometric amounts to minimize the presence of appreciable ChE inhibitor in the reactivation media. Active-site titrations of W86A were carried out with 10–20 nM enzyme. Inhibition was allowed to proceed until no further changes in enzyme activity were observed. Titration curves were constructed by plotting residual enzyme activity against the number of equivalents of MEPQ. Wild-type rMoAChE and HuBChE were incubated for 20 h at room temperature with substoichiometric amounts of paraoxon. Approximately 90% of enzyme activity was inhibited.

Reactivation of MEPQ- and Paraoxon-inhibited ChEs—Reactivation was started by mixing 2–5 μl of 2–20 mM oxime stock solution in water with 0.1–0.2 ml of OP-ChE conjugate equilibrated for 5 min at 25 °C. Final concentration of oximes in the reactivation media ranged between 0.01 and 3 mM. At specified time intervals, 5–10 μl of reactivation mixture were diluted into 0.6–1 ml of assay mixture and enzyme activity (E_t) was monitored as described above. Control activity (E_c) was measured in the same volume ratio of oxime to nonphosphonylated enzyme. Both E_t and E_c were corrected for oxime-induced hydrolysis of ATC and BTC. Inhibited enzyme without oxime was monitored for spontaneous reactivation and/or the presence of residual anti-ChE activity. Fluoride-induced reactivation was conducted as described above except the final concentration of NaF was 0.005–0.01 M.

Calculations of Enzyme Activity—Prior to reactivation OP-ChEs contained 4–14% residual activity (E_0). The actual percentage of reactivatable enzyme at time t was calculated according to Equation 1:

$$\%(E_{react})_t = 100[E_t - E_0]/[E_{max} - E_0] \quad \text{(Eq. 1)}$$

where $E_{max} = 100\ E_{t=\infty}/E_c$.

Since reactivation profiles of EMP-ChEs displayed marked deviations from a first-order approach to reactivation of a single reactivatable species, Equation 2 was used to determine the best-fit values of the following parameters:

$$\%(E_{reac})_t = E_1(1 - e^{-k(1)t}) + E_2(1 - e^{-k(2)t}) \quad \text{(Eq. 2)}$$

where E_1 and E_2 are the percent-amplitudes of two reactivatable forms of MEPQ-inhibited ChE and the parameters $k(1)$ and $k(2)$ are the corresponding fast and slow pseudo first-order rate constants of the reactivation of E_1 and E_2, respectively. Ratios of E_1/E_2 ranged between 0.8 and 1.2. In those cases where nonlinear regression did not converge due to insufficient data points, curve fittings were processed assuming an E_1 to E_2 ratio of 1. To fit the data to a single exponential curve, E_2 in Equation 2 was set to zero. A statistical F test was used to compare single and biexponential nonlinear regression fits to the data. E_1, E_2, $k(1)$, and $k(2)$ were determined by computer iterations to give best-fit values for these parameters. Nonlinear regression and statistical F test analyses were performed by Graphpad Inplot Software, version 4.01, 1992 (GraphPad Software, Inc., San Diego, CA).

Molecular Modeling—Molecular modeling was done on Silicon Graphics Indigo Elan using Discover 2.9, a module of InsightII 2.2.0 program (Biosym, San Diego). Coordinates from the crystal structure of TcAChE (8) and coordinates from a model of HuBChE (18) were used in calculation of energy-minimized conformations of oximes in phosphonylated TcAChE and HuBChE. Coordinates of crystal structures of 2-PAM (19) and HI-6 (20) were used in docking the respective oximes in the models of EMP-ChEs.

Modelling was done *in vacuo*, with the dissociation state of ionizable groups set equivalent to pH 7.8. First, the *O*-ethyl methylphosphonyl group was covalently attached to the O^γ of the active-site serine and the conformation of the conjugate minimized. By the initial placement of the oxygen of P=O bond in the oxyanion hole, the phosphonyl moiety is susceptible to an "in-line" S_N2 displacement. Oxime groups were ionized and then partial charges of oximes calculated using the MOPAC module of InsightII. Then 2-PAM and HI-6 were minimized in the model of the phosphonylated enzymes leaving specified residues to rotate freely.

The assumed complex of the transition state for the reactivation of $EMP_{R,S}$-AChE by HI-6 (Fig. 2*b*) was analyzed by initially constraining the three putative hydrogen bonds between the phosphonyl oxygen and the oxyanion hole to distances <2.7 Å. Water molecules found in the gorge in the crystal structure were included. Amino acid side chain residues surrounding the EMP conjugate and EMP itself were allowed to rotate, whereas the peptide backbone and distal side chains were fixed. The pentacoordinate complex containing the covalently attached

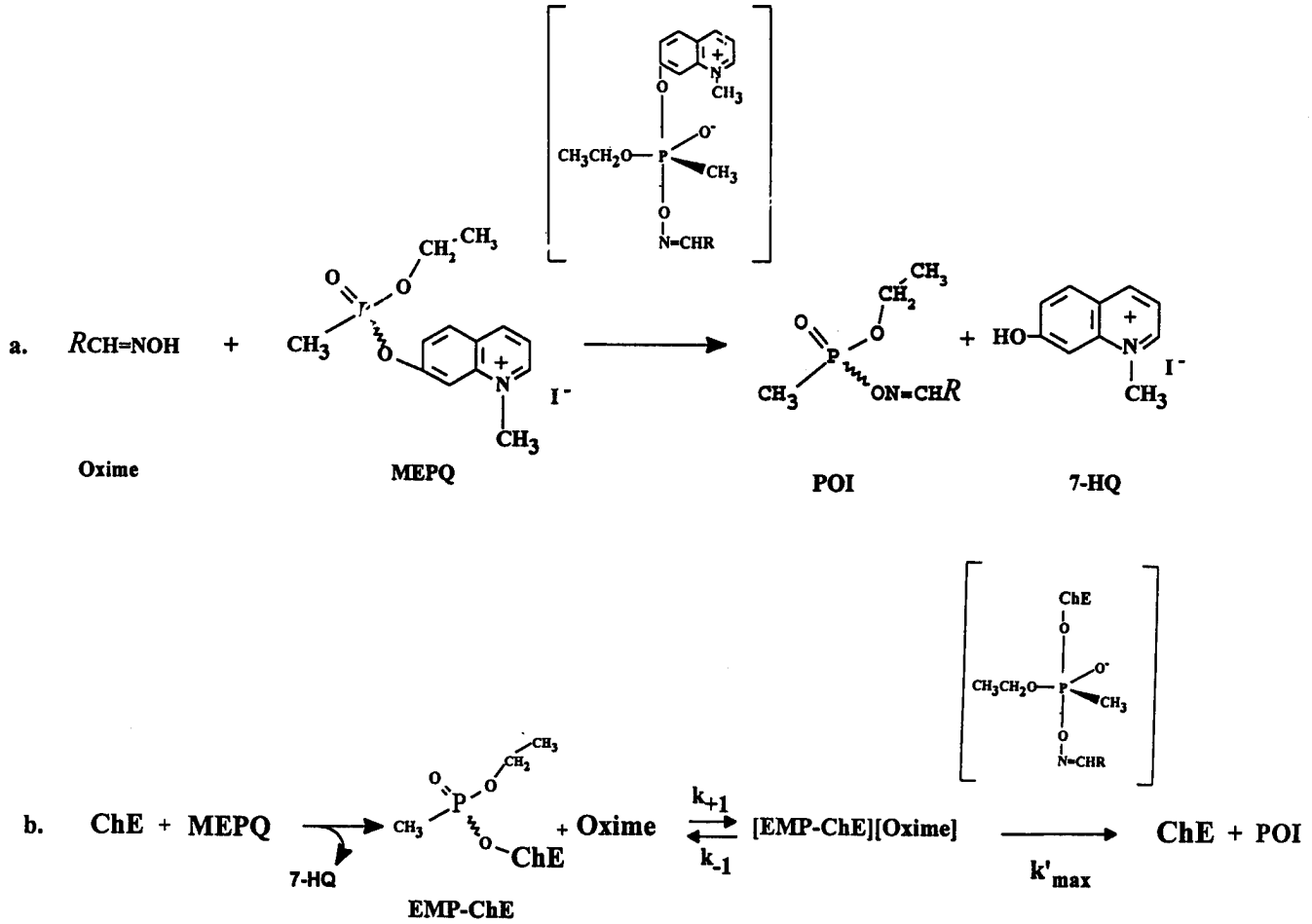

FIG. 2. **Chemical pathways and kinetic schemes of the reaction of oximes with MEPQ (*a*), and the inhibition and oxime-induced reactivation of ChEs (*b*).** The structure in *parentheses* depicts the assumed pentacoordinate transition state having a trigonal bipyramidal geometry. Both the nucleophile and the leaving group occupy apical positions when assuming an in-line S_N2 displacement reaction.

HI-6 to the phosphorus was initially minimized by 100 iterations, equilibrated by running dynamics at 300 K for 100 fs and then at 700 K by 50 subsequent runs of 50 fs. The seed number of the random number generator is changed after each 50-fs run. Data on possible structures were collected from the last 0.5 ps of each run. These structures were then slowly cooled using steps of 50° from 700 to 300 K. Then, the system was minimized with 1000 iterations using a conjugate gradient method. A dielectric constant of 4.0 was used. The above algorithm was created to avoid falling into local energy minima. This algorithm raises the temperature of the EMP-AChE conjugates to an equilibrium state where upon cooling they should approach global energy minima.

RESULTS[4]

Nucleophilicity of 2-PAM, HI-6, and Fluoride—To compare chemical reactivity with the reactivation rate constants, the relative nucleophilicities of reactivators were ranked by determining bimolecular rate constants of MEPQ hydrolysis (Fig. 2*a*). Semilogarithmic plots conforming to a pseudo first-order reaction resulted in straight lines (not shown), indicating that the two enantiomers of MEPQ react at similar rates. The following bimolecular rate constants (k_{nuc}, M^{-1} min^{-1}) were calculated for the nucleophiles: 2-PAM, 34.6 ± 1.4; HI-6, 34.2 ± 3.1; NaF, 27.7 ± 0.9. Lowering the pH from 7.8 to 7.0 decreased k_{nuc} of both oximes by 3.5-fold, consistent with the actual nucleophile being the oximate anion rather than its conjugate acid. The rate constant of spontaneous hydrolysis of MEPQ was 0.005 (± 0.001) min^{-1} at either pH, and the bimolecular rate constant of the reaction between MEPQ and water was estimated to be 9×10^{-5} M^{-1} min^{-1}.

To compare reactivity of the actual nucleophiles, bimolecular rate constants were corrected by dividing k_{nuc} by the fraction of the oximate anion at pH 7.8, $[1 + 10^{(pK_a-7.8)}]^{-1}$. Using pK_a values 8.07 ± 0.02 (2-PAM) and 7.47 ± 0.01 (HI-6), k_{nuc} increased to 98.9 and 49.9 M^{-1} min^{-1}, respectively. Fluoride anion is approximately 1.8 and 3.6-fold less potent as a nucleophile than the oximate forms of HI-6 and 2-PAM, respectively.

Dissociation Constants of 2-PAM and HI-6 for Nonphosphonylated rMoAChE—A comparison of K_{ox} and αK_{ox} (Scheme I) for wild-type and mutant rMoAChE may provide insight into the binding regions of mono- and bisquaternary oximes at the entrance or within the active center gorge of both the free and substrate-bound enzyme. In several cases an increase in oxime concentration appeared to enhance enzyme-catalyzed hydrolysis of either ATC or BTC. To calculate K_{ox} and αK_{ox}, the concentrations of both oximes were adjusted to a range that enabled the use of the secondary plots (17).

Plots of 1/*V* *versus* 1/S were linear, and, for most of the enzyme preparations, the intersections from Lineweaver-Burk plots occurred in the upper left quadrant (not shown). These observations suggest that both 2-PAM and HI-6 are likely to exhibit linear mixed-type inhibition in accordance with Scheme I (17). For the series of enzymes, dissociation constants of HuBChE·oxime and rMoAChE-W286R·HI-6 could not be defined due to significant deviations from simple equilibrium schemes for reversible association of inhibitor with an enzyme. The high concentrations of ATC required to saturate mutant

[4] Since 2-PAM and P2S generate the same 2-(hydroxyiminomethyl)-1-methylpyridinium cation, the abbreviation 2-PAM was used for both salts.

$$\begin{array}{ccccc} \text{AChE} + \text{ATC} \leftrightharpoons [\text{AChE·ATC}] & \rightarrow & \text{acetate} + \text{thiocholine} \\ + & & + \\ \text{Oxime} & & \text{Oxime} \\ K_{ox} \Updownarrow & & \alpha K_{ox} \Updownarrow \\ [\text{AChE·oxime}] + \text{ATC} \leftrightharpoons [\text{AChE·oxime·ATC}] & & \end{array}$$

SCHEME I. **Equilibria for reversible inhibition of AChE by oximes.** The [AChE·oxime·ATC] complex is assumed not to lead to hydrolysis.

W86A enzyme[5] precluded an accurate determination of K_{ox} and αK_{ox} for either oxime.

The dissociation constants of 2-PAM (Table I) for the mutants tested were only moderately perturbed relative to wild-type rMoAChE. The largest destabilization was observed with Y337A and W86F as reflected by an approximately 6–7-fold increase in the corresponding K_{ox} compared with that of wild-type enzyme. Replacement of Tyr-337 by phenylalanine produced a mutant with the same aromatic amino acid residues within the active-site gorge as TcAChE. K_{ox} values for Y337F and TcAChE were virtually equivalent. These findings are consistent with previous observations that established a role for aromatic residues at positions 337 (13, 21, 22) and 86 (21–23) in the stabilizing interactions of quaternary ammonium-containing ligands within the active-site gorge. However, the influence of aromatic side chains at these positions is relatively small. Similarly K_{ox} of F295L·2-PAM decreased less than 3-fold and single (W286R) and triple (W286A/Y72N/Y124Q) mutations at the entrance to the gorge increased the dissociation constants of 2-PAM 2.7- and 4.7-fold, respectively.

As summarized in Table II, K_{ox} of HI-6 for wild-type rMoAChE is 4-fold lower than that of 2-PAM, suggesting that the second pyridinium ring of HI-6 contributes less than 1 kcal/mol to the stabilization of the bisquaternary oxime-enzyme complex relative to the monoquaternary pyridinium oxime. Replacement of Tyr-337 by alanine increased HI-6 dissociation constant 8-fold compared to the wild-type enzyme, whereas K_{ox} of HI-6 with E202Q, F295L, and wild type rMoAChE were essentially equivalent. The three aromatic amino acid residues at the entrance to the gorge have been shown to constitute part of the peripheral anionic site for bisquaternary ligands (13, 24). Their replacement with the residues found in BChE increased K_{ox} of the association of HI-6 with mutant W286A/Y72N/Y124Q only 6.5-fold relative to wild-type rMoAChE.

In Scheme I, αK_{ox} is the dissociation constant for the AChE·oxime·ATC complex. If association of substrates decreases the affinity of the oxime relative to the free enzyme, then α should be >1. Whenever plots of V_{max}^{-1} *versus* [oxime] gave straight lines, αK_{ox} was calculated from the intercept on the x axis. Both 2-PAM and HI-6 displayed α values of 1.5 to 6 with the following rank order: for 2-PAM, TcAChE ≈ wild-type rMoAChE > W286R ≈ W86F > E202Q ≈ triple mutant; for HI-6, wild-type rMoAChE > triple mutant ≈ E202Q. Thus, binding of substrate to AChEs moderately increased the dissociation constant of either oxime. The relative destabilization of the ternary complex of substrate, oxime, and enzyme complex is in agreement with the dissociation constants determined for the corresponding EMP-AChE·oxime complexes (see below).

Inhibition and Stability of MEPQ-inhibited Enzymes—MEPQ-ChE conjugates are likely to be composed of a mixture of two enantiomers (10, 11), designated as EMP_R-ChE and EMP_S-ChE. The symbols R and S denote absolute configuration around the phosphorus atom of the inhibited enzyme.

[5] D. M. Quinn and Z. Radic, unpublished data.

Rates of spontaneous reactivation of $EMP_{R,S}$-ChE conjugates were slow; all were less than 0.5% h^{-1}, with the exception of $EMP_{R,S}$-W86A which was slightly increased to 0.8% h^{-1}. The extent of reactivation did not differ significantly for preparations that were allowed to incubate for 1–24 h at 25 °C before the addition of reactivator. The almost negligible spontaneous reactivation and aging reactions simplify evaluation of the kinetic profiles. The absence of competing processes, together with the high bimolecular rate constants for the inhibition of AChE (11, 25) and HuBChE (11) by MEPQ, resulted in rapid formation of an inhibited enzyme with defined species that could be transferred immediately to reactivation buffer. It should be pointed out that the concentration of the product 7-HQ in the reactivation medium is equal to the active site concentration of the inhibited enzyme (Fig. 2*b*). To ascertain whether 7-HQ interferred with reactivation, up to 5 times the initial concentration of MEPQ-inhibited enzyme in reactivation medium of 7-HQ was added to reactivation buffer. Increased 7-HQ did not significantly affect reactivation rate constants.

Is Reactivated Enzyme Subsequently Inhibited by the Phosphonyl-oxime?—A kinetic study of 2-PAM-induced reactivation of EMP-AChE, prepared from bovine erythrocyte AChE using R_p and S_p enantiomers of $CH_3P(O)(OC_2H_5)X$, demonstrated inhibition of reactivated AChE by a reaction product under certain conditions (26). This phenomenon was attributed to formation of a phosphonyl-oxime intermediate (Fig. 2*a*) (27). While preparation of EMP-AChE conjugates from MEPQ ensures that the phosphonyl-oxime will not be generated through direct reaction between either 2-PAM or HI-6 and MEPQ, it might be formed upon addition of oxime to $EMP_{R,S}$-ChE conjugates. To examine this, we measured rates of reactivation as a function of increasing the initial concentration of $EMP_{R,S}$-ChEs with a fixed concentration of oxime. Representative data are shown in Fig. 3 (*panels A* and *B*).

At concentrations of $EMP_{R,S}$-ChE_0, ranging between 2 and 20 nM of $EMP_{R,S}$-AChE and between 3.4 and 10 nM $EMP_{R,S}$-BChE the kinetics of oxime reactivation were virtually identical. Hence, inhibition by reactivation product in these concentration ranges is not likely to influence reactivation rates.

Kinetics of Reactivation of EMP-ChEs—Analysis of kinetic data by curve fitting clearly showed that oxime-induced reactivation of all EMP-ChEs progressed in a manner that indicates non-homogeneity in reactivatable enzyme (Fig. 3, *panels A* and *B*). A curve constructed in accordance with a two-component reactivation model provided a better fit than that obtained for a single exponential equation. The difference in component rate constants was even more pronounced for HuBChE. Semilogarithmic plots of the reactivation of MEPQ-rMoAChE by three different reactivators showed approximately equal distribution of fast and slow components irrespective of the nucleophile used (Fig. 4).

These findings are satisfactorily explained by the presence of two kinetically distinguishable EMP-ChE enantiomers. However, since it was observed for bovine erythrocyte AChE that the achiral inhibitor, paraoxon, also produces more than one class of reactivatable species (26), it was necessary to compare the reactivation profile of paraoxon- and MEPQ-ChE conjugates under the same experimental conditions. Results are depicted in Fig. 3 (*panels C* and *D*). Indeed, for both achiral paraoxon-inhibited rMoAChE and HuBChE, the biexponential equation improved the fit only slightly, but significantly, better than a single component model.

Although the deviations from kinetics of a homogenous class of inhibited enzyme species were substantially larger for the $EMP_{R,S}$-ChE conjugates compared to similar preparations using paraoxon, we could not ascertain the basis of an intrinsic,

TABLE I

Biochemical parameters for the binding of 2-PAM to ChE and the reactivation of $EMP_{R,S}$-ChEs by 2-PAM

In 25 mM phosphate, pH 7.8, 25 °C.

Enzyme	K_{ox}[a] (mM)	K'_{ox}[b] (mM)		k'_{max}[b] (min^{-1})		$k_r \times 10^{2}$[c] (M^{-1} min^{-1})		$k_{oximate} \times 10^{2}$[d] ($M^{-1}$ min^{-1})	
		Fast	Slow	Fast	Slow	Fast	Slow	Fast	Slow
MoAChE wt	0.049 (±0.007)	0.18 (±0.08)	0.57 (±0.38)	0.093 (±0.010)	0.028 (±0.006)	5.2	0.49	14.9	1.40
W86A	ND[e]	0.26 (±0.11)	0.62 (±0.20)	0.11 (±0.01)	0.013 (±0.002)	4.2	0.21	12.0	0.60
W86F	0.297	NR[f]	NR	NR	NR	3.8[g] (±0.6)	0.21[g] (±0.02)	10.9	0.60
Y337F	0.086	0.29 (±0.11)	0.58 (±0.38)	0.22 (±0.04)	0.039 (±0.017)	7.6	0.67	21.7	1.92
Y337A	0.357	0.60 (±0.27)	1.75 (±0.63)	0.36 (±0.05)	0.054 (±0.012)	6.0	0.31	17.2	0.88
E202Q	0.172 (±0.038)	0.82 (±0.23)	2.86 (±1.08)	0.013 (±0.001)	0.006 (±0.003)	0.16	0.021	0.45	0.06
F295L	0.141	0.27 (±0.04)	0.17 (±0.06)	0.038 (±0.002)	0.007 (±0.001)	1.4	0.41	4.0	1.17
W286R	0.132 ±0.018	0.077 (±0.049)	0.17 (±0.08)	0.036 (±0.004)	0.014 (±0.002)	4.7	0.82	13.4	2.35
W286A Y72N Y124Q	0.229 (±0.021)	0.73 (±0.37)	1.16 (±0.45)	0.23 (±0.04)	0.019 (±0.003)	3.2	0.16	9.2	0.46
TcAChE	0.089 (±0.008)	0.40 (±0.12)	0.96 (±0.64)	0.39 (±0.09)	0.029 (±0.007)	9.8	0.30	28.0	0.86
HuBChE	ND	1.59 (±0.28)	1.35 (±0.66)	0.58 (±0.04)	0.009 (±0.001)	3.6	0.07	10.3	0.20

[a] Mean ± S.E. (n = four determinations). Values without S.E. are average from two determinations (4–5 data points each) that differ <30%.
[b] Obtained from nonlinear regression analysis of the data points in accordance with Equation 3. Numbers in parentheses are S.E. (n = 5–12).
[c] Obtained by dividing k'_{max} by K'_{ox}.
[d] Normalized to oximate anion concentration at pH 7.8.
[e] Not determined (see "Results").
[f] Individual constants could not be resolved.
[g] Calculated from the slope of the line obtained by plot of k_{obs} against [2-PAM].

TABLE II

Parameters for the binding of HI-6 to ChE and the reactivation of $EMP_{R,S}$-ChEs by HI-6

In 25 mM phosphate, pH 7.8, 25 °C.

Enzyme	K_{ox}[a] (mM)	K'_{ox}[b] (mM)		k'_{max}[b] (min^{-1})		$k_r \times 10^{2}$[c] (M^{-1} min^{-1})		$k_{oximate} \times 10^{2}$[d] ($M^{-1}$ min^{-1})	
		Fast	Slow	Fast	Slow	Fast	Slow	Fast	Slow
MoAChE wt	0.013 (±0.002)	0.066 (±0.017)	0.071 (±0.045)	0.25 (±0.02)	0.0250 (±0.007)	37.9	3.5	55.7	5.2
W86A	ND[e]	0.45 (±0.11)	NR[f]	0.77 (±0.13)	NR	17.1	0.68 (±0.08)[g]	25.1	1.0
Y337A	0.108	0.095 (±0.032)	0.067 (±0.032)	0.53 (±0.12)	0.0175 (±0.006)	55.8	2.6	82.0	3.8
E202Q	0.0134 (±0.004)	0.045 (±0.029)	0.091 (±0.063)	0.011 (±0.002)	0.0024 (±0.0006)	2.4	0.26	3.5	0.4
F295L	0.0125	0.080 ±0.038)	0.051 (±0.018)	0.66 (±0.21)	0.091 (±0.019)	82.5	17.8	121.3	26.2
W286R	ND	NR	0.29 (±0.02)	NR	0.021 (±0.003)	0.94[-g] (±0.08)	0.72	1.4	1.1
W286A Y72N Y124Q	0.085 (±0.011)	0.57 (±0.15)	0.091 (±0.020)	0.031 (±0.003)	0.0055 (±0.0004)	0.54	0.60	0.79	0.9
HuBChE	ND	NR	NR	NR	NR	1.47[-g] (±0.04)	0.076[-g] (±0.011)	2.16	0.1

[a] Mean ± S.E. (n = four determinations). Values without S.E. are averages from two determinations (4–5 data points each) that differ <30%.
[b] Obtained from nonlinear regression analysis of the data in accordance with Equation 3. Figures in parentheses are S.E. (n = 5–12).
[c] Obtained by dividing k'_{max} by K'_{ox}.
[d] Normalized to oximate anion concentration at pH 7.8.
[e] Not defined (see "Results").
[f] Individual constants could not be resolved.
[g] Calculated from the slope of the line obtained by plot of k_{obs} against [HI-6].

but small, contribution to the deviation from monoexponential decay function for the achiral *O,O'*-diethylphosphoryl-AChE conjugate. Therefore, we categorize the two phases in Equation 2 as fast and slow components of oxime-induced reactivation, and $k(1)$ and $k(2)$ are the corresponding first-order rate constants of the fast and slow components, respectively, in the presence of large stoichiometric excesses of the reactivator.

The mathematical solution for the kinetic scheme of the reactivation depicted in Fig. 2*b* is:

$$k_{obs} = k'_{max}(1 + K'_{0x}/[\text{oxime}])^{-1} \quad \text{(Eq. 3)}$$

where k_{obs} is either $k(1)$ or $k(2)$, and $K'_{ox} = (k_{-1} + k'_{max})/k_{+1}$. Assuming $k_{-1} \gg k'_{max}$, K'_{ox} is approximated by k_{-1}/k_{+1} which is the corresponding dissociation constant of the complex EMP-ChE·oxime. The individual constants k'_{max} and K'_{ox} were determined by nonlinear regression analysis of the data shown in

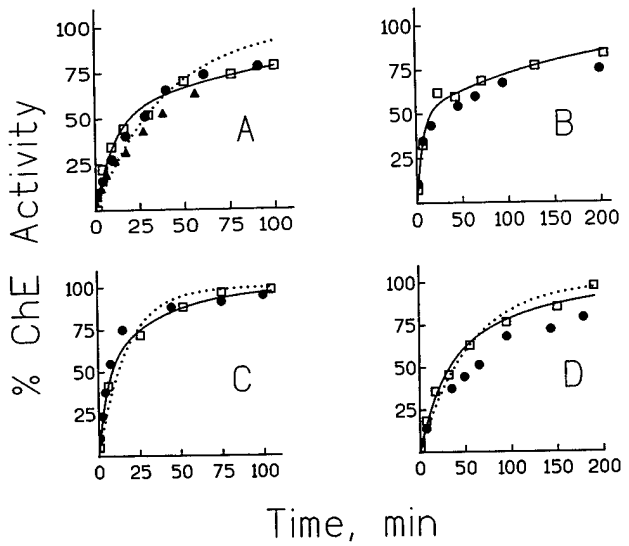

FIG. 3. **Time course of reactivation of MEPQ- and paraoxon-inhibited ChEs, by 1 mM 2-PAM (P2S).** *Broken* and *solid lines* were fitted to the *open squares* using mono- and biexponential equations, respectively. *A*, MEPQ-inhibited wild-type rMoAChE, □, 2 nM; ●, 5 nM; ▲, 20 nM. *B*, MEPQ-inhibited HuBChE, □, 3.4 nM; ●, 10 nM. *C*, paraoxon-inhibited wild-type rMoAChE, □, 2 nM; ●, 10 nM. *D*, paraoxon-inhibited HuBChE, □, 0.5 nM; ●, 34 nM. The *ordinates* show percent of maximal reactivation after 48 h.

Fig. 5, according to Equation 3. The bimolecular rate constant of reactivation (k_r) was obtained by dividing k'_{max} by K'_{ox}.

In several cases (Fig. 5, *panel E*) the plots of k_{obs} *versus* [oxime] were linear rather than asymptotically approaching a constant value. In this situation, the individual component constants could not be resolved. Assuming $K'_{ox} \gg$ [oxime], Equation 3 is approximated by the following expression:

$$k_{obs} = (k'_{max}/K'_{ox})[\text{oxime}] \qquad \text{(Eq. 4)}$$

Thus, $k_r = k'_{max}/K'_{ox}$ was obtained from the slopes of straight lines constructed by plots of k_{obs} *versus* [oxime].

Tables I and II summarize the kinetic constants of the reactivation of EMP-ChEs by 2-PAM and HI-6, respectively. The last column also gives the bimolecular rate constant for the reactivation by the oximate ions, RCH=N-O$^-$ ($k_{oximate}$). In general, dissociation constants of the reactivators for $EMP_{R,S}$-AChEs (K'_{ox}) are increased compared with nonphosphonylated enzyme (*i.e.* $K_{ox} < K'_{ox}$). The magnitude of destabilization of the inhibited enzyme-oxime complex was in the range obtained for the ratio $\alpha K_{ox}/K_{ox}$, an observation that is consistent with the interpretation of α. Thus, the presence of bound ATC or its reaction product and conjugated EMP decreased the affinity of the oximes to an equivalent extent.

Mutations at the Choline Binding Subsite—The side chains of Trp-86, Tyr-337, and Glu-202 appear to contribute to the stabilization of binding of both the choline moiety of ATC and the positive poles of quaternary reversible inhibitors of AChE (13, 21, 22, 25). Replacement of Glu-202 by glutamine ($EMP_{R,S}$-E202Q) remarkably decreased the bimolecular rate constant of reactivation by 2-PAM or HI-6. Both reactivatable components were affected similarly. In the case of HI-6, the decrease in $k_{oximate}$ (13–16-fold) compared with wild-type enzyme almost exclusively arises from a smaller unimolecular rate constant k'_{max}. By contrast, the reduction in $k_{oximate}$ of 2-PAM (23–33-fold) contains contributions from both the affinity of the oxime for the phosphonylated enzyme (K'_{ox}) and k'_{max}. These findings indicate that the stability of the initial complex $EMP_{R,S}$-AChE·HI-6 is largely controlled by residues located outside the choline-binding region. The 13–33-fold decrease in $k_{oximate}$ of both reactivators, compared with wild-type $EMP_{R,S}$-rMoAChE, is highlighted by the fact that $k_{oximate}$ values of mutants of other constituents of the choline binding site, namely, W86F, W86A, Y337F, and Y337A, are approximately within 2-fold of the wild-type enzyme, for the fast reactivatable component.

Replacement of the π-electron-rich indole side chain of Trp-86 by alanine decreased only slightly (1.2–2.3-fold) and moderately (2.2–5.1-fold) $k_{oximate}$ (slow) of 2-PAM and HI-6, respectively, compared with wild-type phosphonylated rMoAChE. Furthermore, $k_{oximate}$ (fast) of both 2-PAM and HI-6 were slightly enhanced with the EMP-Y337A conjugate relative to the corresponding reactions with wild-type rMoAChE. These findings suggest that Trp-86, and Tyr-337 play only a limited role in binding the oxime in a conformation suitable for reactivation of phosphonylated AChEs.

The reactivatability of the two components of $EMP_{R,S}$-TcAChE by 2-PAM was comparable to that of mutant Y337F. Replacement of tyrosine by phenylalanine in rMoAChE produces a mutant that contains aromatic side chain residues of the choline subsite identical to TcAChE (8, 13, 28).

Mutation at the Acyl Pocket—Of the two aromatic side chains that constitute the acyl pocket, Phe-295 and Phe-297, mutation of the former (F295L) produced the greater enhancement of butyrylthiocholine hydrolysis (k_{cat}/K_m) (12). Dimensions of the acyl pocket are likely to determine, in part, the stability of the two enantiomeric *O*-ethyl methylphosphonyl conjugates of AChE in a manner analogous to their influence on carboxyl ester specificity. Since F295L appears to place the essential constraint in limiting butyrylthiocholine hydrolysis by AChE, it is interesting to compare $k_{oximate}$ of R_p and S_p enantiomers of EMP-F295L with wild-type $EMP_{R,S}$-rMoAChE. MEPQ-inhibited F295L reactivated only up to 50–65% of the expected activity at t_∞. By contrast, the extent of reactivation of other MEPQ-inhibited mutants, as well as that of wild-type rMoAChE and tissue-derived TcAChE and HuBChE, ranged from 80 to 98%. The reactivation profiles of $EMP_{R,S}$-F295L constructed for either 2-PAM or HI-6 were fitted significantly better to a two-component model rather than to a single class of inhibited enzyme (not shown), but the difference in the ratio of k_r (fast) and k_r (slow) was markedly reduced from the ratio found for the wild-type enzyme.

One enantiomeric form of $EMP_{R,S}$-F295L reactivated profoundly faster than the other, which appeared resistant to reactivation. Since the extent of maximal reactivation was independent of the time of prior incubation of F295L with MEPQ, slow dealkylation (*i.e.* aging) cannot explain the relative resistance of the second component to oxime-induced reactivation. Similar observations were made previously with the *O*-cycloheptyl methylphosphonyl-TcAChE conjugate (29).

Interestingly, replacement of phenylalanine in position 295 by leucine had opposing effects on $k_{oximate}$ for 2-PAM (decreased 3.7-fold) and HI-6 (increased 2.2-fold). These findings are consistent with the relative changes observed in the affinity of the oximes (K_{ox} and K'_{ox}) for F295L (Table I). F295L alters the spatial constraints surrounding the O^γ Ser-203-bound phosphonyl moiety and thereby changes the stereochemical requirements of the reactivation process.

Mutations at the Entrance to the Gorge—The potency of 2-PAM in reactivating both the fast and slow components decreased only 1.6 to 3-fold with the triple mutant involving residues at the entrance to the gorge (W286A/Y72N/Y124Q) and with W286R, relative to the wild-type enzyme. By contrast, HI-6-induced reactivation of the triple mutant decreased 70- and 6-fold for the fast and slow components, respectively. Similarly, $k_{oximate}$ of HI-6 with EMP-W286R, a mutation to the residue found in mouse BChE, was 40- and 5-fold lower for the

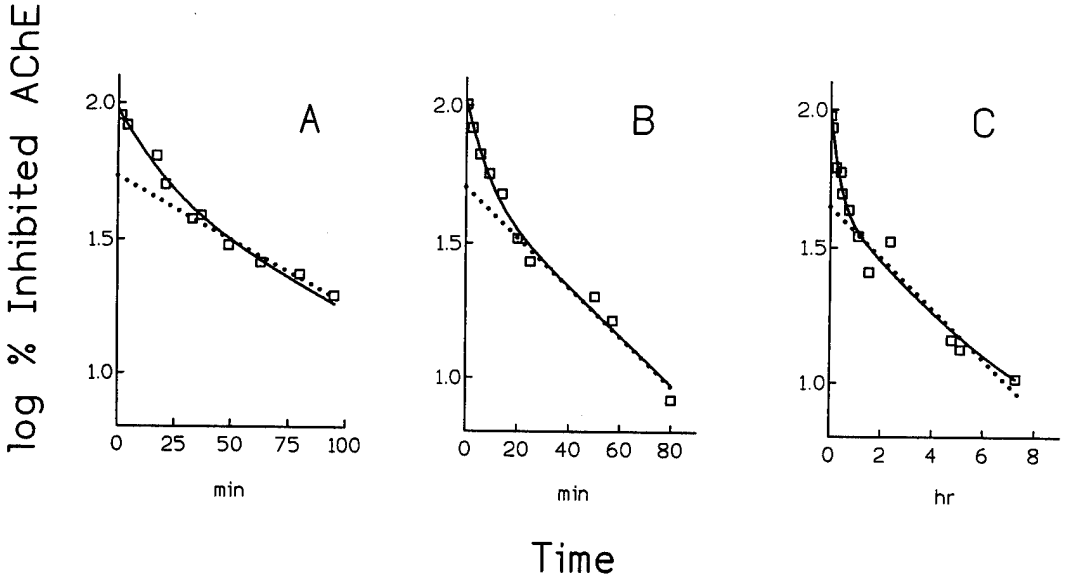

FIG. 4. **Semilogarithmic plots of % $EMP_{R,S}$-rMoAChE *versus* time of incubation with various nucleophiles.** *Solid lines* were fitted to the data assuming two distinguishable reactivatable components. The *broken lines* were fitted to data (n = 5–6 each) that represent the slow component, in accordance with a single species of reactivatable enzyme, and extrapolated to t = 0 to calculate the ratios of the two reactivatable components. *A*, 0.9 mM 2-PAM (P2S), [fast]/[slow] = 0.89; *B*, 0.12 mM HI-6, [fast]/[slow] = 0.96; *C*, 10 mM NaF, [fast]/[slow] = 1.2. The ratios of k(fast) to k(slow) were 5.5, 7.1, and 8.0 for 2-PAM, HI-6, and NaF, respectively.

fast and slow components, respectively, compared with those observed for wild-type rMoAChE.

Finally, $k_{oximate}$ values of $EMP_{R,S}$-HuBChE that contains aliphatic amino acid residues in positions homologous to 286, 124, and 72 of AChE, revealed that 2-PAM is superior to HI-6 in reactivating HuBChE, and the $k_{oximate}$ ratio of rMoAChE to HuBChE is >25 with HI-6, whereas it is <2 for 2-PAM. This further underscores the importance of the aromatic amino acids at the entrance to the gorge of AChEs in enhancing reactivation potency of HI-6 as compared with 2-PAM.

Molecular Modeling—A stereo view of energy minimized conformations of complexes between EMP_R-AChE, EMP_S-AChE, EMP_R-HuBChE, and EMP_S-HuBChE with 2-PAM is shown in Fig. 6. In addition, the EMP_R·AChE and EMP_R·HuBChE complexes with HI-6 are also shown. The overall geometries of the side chain residues that are lining the gorge of EMP-ChE·2-PAM complexes were similar to the starting models of $EMP_{R,S}$-ChE conjugates with one exception. The indole ring of Trp-86 that is aligned with the gorge axis of TcAChE (22) and HuBChE model (18) is slightly moved to face the gorge entrance, a rotation that appears to increase parallel contacts between the aromatic rings of 2-PAM and Trp-86.

Although the charge on the pyridinium nitrogen (N^+) is delocalized (30), it is interesting to measure distances between N^+ and some of the atoms surrounding 2-PAM. Trp-86 $C^{\delta 2}$ is 5.4 and 4.8 Å from N^+ of the R_p and S_p enantiomers, respectively. Both Tyr-337 C^{ζ}, and Phe-338 C^{ζ} of the enantiomeric EMP-AChE conjugates are >6.2 Å away from the pyridinium nitrogen. These distances are in fair agreement with experimental observations showing that $k_{oximate}$ is not significantly affected by single replacement of an aromatic side chain by aliphatic amino acids at positions 86 and 337.

Of the two carboxylate side chains that are projected into the gorge, the carboxylate oxygen of Asp-74 is 4.2 and 5.0 Å from the quaternary nitrogen of 2-PAM modeled in the R_p and S_p conjugates, respectively, whereas Glu-202 carboxylate is about 9.5 Å from nitrogen in both enantiomers. Despite the greater distance of Glu-202 carboxylate from the pyridinium nitrogen compared with Asp-74 carboxylate, perturbation of reactivation with 2-PAM was significantly greater with E202Q compared to D74N. We note that the distance of either Glu-202 carboxylate or His-447 $N^{\epsilon 2}$ from the oximate oxygen ranged from 5.8 to 8.8 Å in all $EMP_{R,S}$-AChE·oxime complexes.

The oxime-containing pyridinium ring of HI-6 is oriented essentially as described above for the 2-PAM complex. The carbamoyl, $C(O)NH_2$ moiety of the distal pyridinium ring is projected toward the peripheral binding site and forms close contacts with aromatic side chains of Trp-286, Tyr-72, and Tyr-124. Computer-simulated molecular dynamics of the ground state (not shown) and the pentacoordinate transition state (Fig. 7*a*) of $EMP_{R,S}$-AChE·HI-6 clearly point to the ability of the hydroxyl of Tyr-124 to hydrogen bond to the oxygen of the bismethylene ether moiety that connects the two pyridinium rings. These interactions appear to restrict movements of HI-6 within the gorge. Apparently, anchoring of the distal pyridinium moiety results in shortening of the distances between N^+ of the proximal pyridinium ring and Trp-86 $C^{\delta 2}$ (4.6 Å), Tyr-337 C^{ζ} (3.9 Å), and Phe-338 C^{ζ} (5.1 Å), compared to EMP_R-AChE·2-PAM. The model of EMP_R-AChE·HI-6 is consistent with the finding that mutations of residues Trp-286, Tyr-72, and Tyr-124 decreased dramatically $k_{oximate}$ of HI-6 but not of 2-PAM. Molecular dynamics carried out by equilibration of the $EMP_{R,S}$-AChE·HI-6 complexes at high temperature followed by cooling yields a dramatic difference for the EMP_R-AChE and EMP_S-AChE enantiomers. In the case of the *R* enantiomer the phosphonyl oxygen remains within the oxyanion hole (Fig. 7*b*) while the *S* enantiomer assumes multiple conformations. Binding in the oxyanion hole should enhance reactivity by lowering the energy of the transition state and this factor could account for the different rates of reaction of the *R* and *S* enantiomers.

DISCUSSION

The overall mechanism of displacement of the phosphonyl-bound moiety of $EMP_{R,S}$-AChE by oxime reactivators is assumed to parallel analogous reactions with low molecular weight organophosphate model compounds. Thus, reactivation is expected to proceed from a tetrahedral ground state of the phosphonyl moiety to a trigonal bipyramidal transition state (Fig. 2*a*) (31). For both oximes the carboxylate side chain of Glu-202 appears to be important for stabilizing intermediates along the chemical pathway by an inductive electronic influence on the phosphorus which facilitates the nucleophilic at-

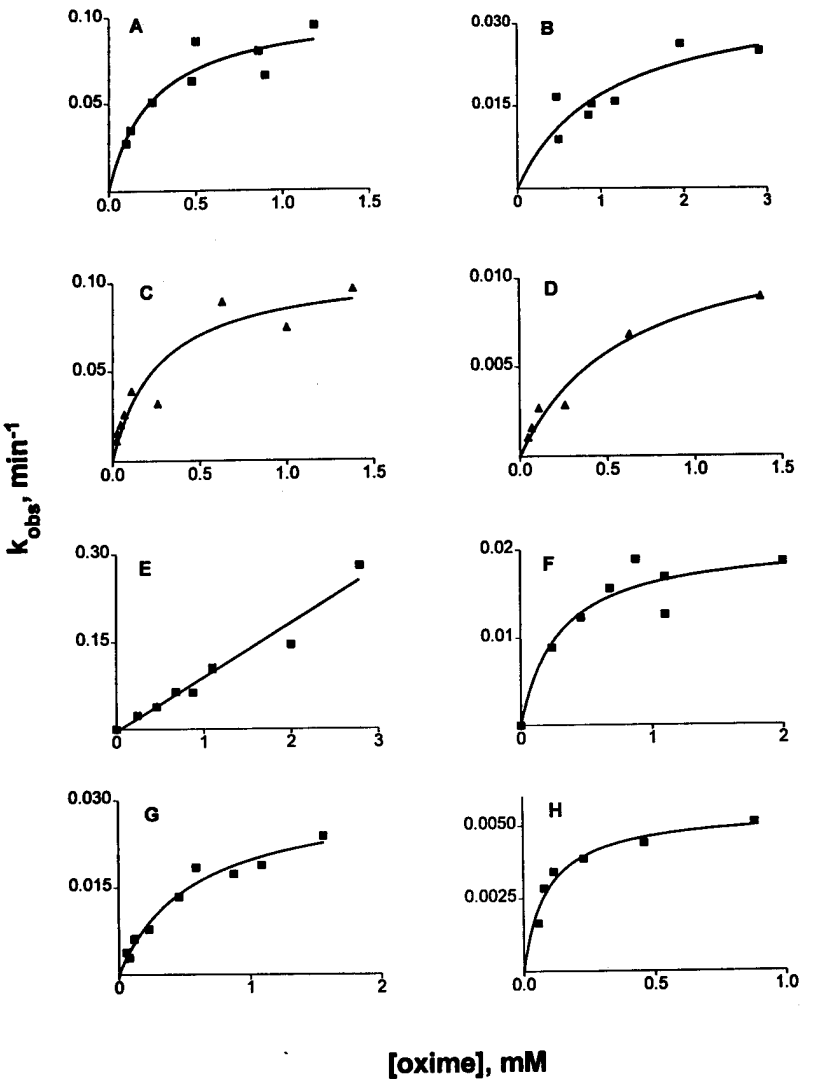

FIG. 5. **Representative plots of k_{obs} *versus* [oxime] for reactivation of $EMP_{R,S}$-AChE.** *Lines* were fitted to the data in accordance with Equation 3 except for *panel E* that was fitted to Equation 4. The *left-* and *right-hand* side panels of each pair show the fast and the slow rate constants, respectively. *A* and *B*, P2S with wild-type rMoAChE; *C* and *D*, 2-PAM (P2S) with W86A; *E* and *F*, HI-6 with W286R; *G* and *H*, HI-6 with W286A/Y72N/124Q.

tack. This was suggested previously to account for the diminished rates of phosphorylation of the E202Q mutant (25). The acquisition of a negative charge of the transition state is likely to be stabilized by both the amide hydrogens in the oxyanion hole and the positive charge of the pyridinium ring. The contribution of the latter interaction to the overall stabilization of the transition state is evident from the high ratios of $k_{oximate}$ for 2-PAM (>125) and for HI-6 (>500) compared with the estimated bimolecular rate constant of the reactivation by NaF ($<10\ M^{-1}\ min^{-1}$), even though the nucleophilicity of fluoride is only 3.6- and 1.8-fold smaller than that of 2-PAM and HI-6, respectively.

The unimolecular rate constants of the reactivation of wild-type phosphonylated AChE by both oximes (k'_{max}, 0.25–0.58 min^{-1}) are 2500-fold higher than the estimated rate constants for spontaneous restoration of enzyme activity. Such an enhancement suggests a decrease of more than 4.5 kcal/mol in energy barrier, in going from initial state of oxime-bound complex to the activated state, compared with a general base or H_2O-catalyzed reactivation. This consideration together with results shown here reveals a specific molecular recognition of quaternary oximes in the active-site gorge.

Comparative Reactivating Potencies of HI-6 and 2-PAM—The nucleophilicity of the oximate anion of 2-PAM is 2-fold greater than that of HI-6, as would be expected from the stronger basicity of 2-PAM (32). Nevertheless, variations of $k_{oximate}$ ratio for HI-6 to 2-PAM with wild-type $EMP_{R,S}$-rMoAChE is approximately 4 yielding an overall enhancement of 8-fold for $k_{oximate}$ of HI-6 over 2-PAM. A similar trend was reported for human erythrocyte EMP-AChE that was obtained using *O*-ethyl *p*-nitrophenyl methylphosphonate (33). The superiority of HI-6 over 2-PAM is well established with respect to other *O*-alkyl methylphosphonyl conjugates of rat, bovine, and human AChEs (34–37).

Considerations of energy barriers suggest that reactivation will be favored by an in-line displacement where the nucleophile and the enzyme occupy apical positions in the trigonal bipyramidal transition state (31). Molecular modelling showed that the oximate oxygen of various $EMP_{R,S}$-AChE·oxime complexes is positioned 4.4 to 4.9 Å from the P atom, suggesting that a change in conformation is required in order for the hydroxamate oxygen atom to form a covalent bond with the phosphonyl moiety. This view is supported by the observation that the ratio of dissociation constants of the HI-6 complexes with nonphosphonylated (K_{ox}) and EMP conjugate (K'_{ox}) of the triple mutant is 6 to 9 as opposed to a ratio of 70 for wild-type rMoAChE. Of all the models examined, the bond angle RCH=NO—P—O^{γ} Ser-203 that approaches an optimal 180° for in-line displacement was found to be 169° for EMP_R-AChE·HI-6. The most likely explanation for the overall 8-fold increase in $k_{oximate}$ of HI-6 over 2-PAM stems from a better orientation of the oximate oxygen of the former oxime toward an apical approach to the phosphorus atom from the face formed by three atoms and perpendicular to P-O^{γ} Ser-203 bond.

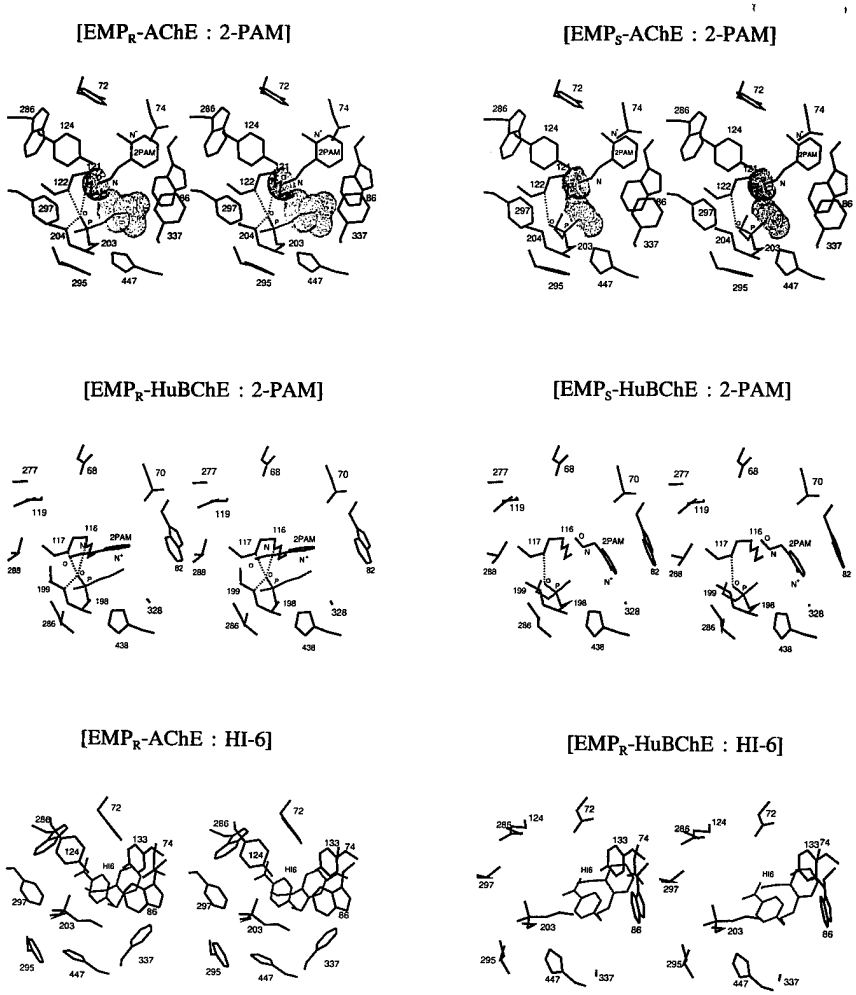

FIG. 6. **Stereo views of the final conformations of energy minimized 2-PAM and HI-6 in models of EMP$_R$-AChE, EMP$_S$-AChE, EMP$_R$-HuBChE, and EMP$_S$-HuBChE.** Energy minimizations were carried out using the atomic coordinates obtained from the crystal structure of TcAChE (8), and HuBChE model based on the TcAChE structure (18). Amino acid residues are labeled in accordance with the numbering system of rMoAChE (EMP$_R$-AChE) and HuBChE (EMP$_R$-HuBChE). Hydrogen bonds between the phosphonyl oxygen and the amide hydrogens in the oxyanion hole are shown by *dotted lines*. The hydrogen bond formed between the hydroxyl of Tyr-124 and the etheral oxygen of HI-6 is not shown. Selected final geometries of energy minimized 2-PAM within the corresponding conjugates were included to illustrate differences in steric hindrance around the P-atom. *Dotted spheres* are van der Waals surfaces of $\mathbf{CH_3}$-P, $\mathbf{CH_3CH_2}$O-P, and RC=N-$\mathbf{O^-}$ of 2-PAM modeled and energy minimized within the corresponding EMP-AChE conjugates. The final conformation of 2-PAM shown is one of several closely related overlapping structures with similar energy content.

Eventually, this might lead to greater stabilization of the transition state.

Using similar arguments, the smaller molecular volume of 2-PAM may confer to this reactivator sufficient flexibility to accommodate itself at various overlapping orientations within the gorge of wild-type phosphonylated AChE as well as within a gorge of diminished aromaticity seen with BChE. This view is supported by energy minimization yielding different final conformations with similar energy depending on the starting positions of the oxime within EMP$_{R,S}$-ChEs (not shown). This flexibility may diminish the dependence of $k_{oximate}$ on structural changes with the active-site gorge and give rise to unproductive binding conformations.

Sequence alignments of AChE and BChE reveal that aromatic amino acids at positions Trp-286, Tyr-124, and Tyr-72 in mammalian AChE are replaced by aliphatic residues in BChE (13, 28). For EMP$_{R,S}$-HuBChE the reduced $k_{oximate}$ for HI-6 to values less than $k_{oximate}$ of 2-PAM further substantiates the contribution of the aromatic cluster at the gorge entrance to the enhanced potency of HI-6. Interestingly, the ratio $k_{oximate}$(fast)/$k_{oximate}$(slow) for the reactivation of EMP$_{R,S}$-HuBChE by HI-6 was similar to wild-type rMoAChE, whereas the ratio approached one for the mutant enzymes W286A/Y72N/Y124Q and W286R. The diminished differences in the susceptibility of the two enantiomeric mutant EMP conjugates to undergo reactivation with HI-6 show that productive binding of the fast reactivatable component by peripheral residues is significantly greater than for the slow enantiomer of wild-type rMoAChE. Initial experiments show that replacement of aspartic acid by asparagine at position 74 produced approximately 24- and 3-fold decreases in $k_{oximate}$(fast) for HI-6 and 2-PAM, respectively. These observations suggest that the role of the conserved carboxylate side chain of Asp-74 in stabilizing a productive conformation of AChE·HI-6 is manifest mainly in combination with the aromatic residues of the peripheral site.

An interesting feature of the energy minimized EMP$_R$-AChE·HI-6 complex is hydrogen bonding of the hydroxyl of Tyr-124 to the etheral oxygen of HI-6. The proposed stabilization of HI-6 is consistent with a reported decrease in reactivation potency of a congener of HI-6 in which a three carbon methylene chain (CHS-6) was substituted for the bisoxymethylene bridge (HS-6) (34).

Finally, it is of interest to point out that $k_{oximate}$ of 2-PAM was reported to be significantly larger than $k_{oximate}$ of HI-6 for the reactivation of homologous EMP conjugate of electric eel AChE (33). The anomalously low potency of HI-6 as reactivator of phosphonylated eel AChE allows one to speculate that one or more amino acids that control the enhanced reactivity of HI-6 toward EMP-AChE from mammals are not conserved in eel AChE.

Stereospecificity of Oxime-induced Reactivation—Molecular modeling of R_p and S_p enantiomers of *O*-isopropyl methylphosphonyl-AChE conjugates predicted distinct enantiomeric selectivity for nucleophilic displacement of the organophosphonyl moiety (38). However, *O*-isopropyl- and *O*-3,3-dimethylbutyl methylphosphonyl-TcAChE conjugates were found to undergo reactivation by 1 mM HI-6 and 1,1′-trimethylene bis(4-hydroxyiminomethylpyridinium)-dibromide at rates that were largely independent of configuration around the P atom of the inhibitor or the structure of the alkyl group (29). The concentration of the oximes could be well above K'_{ox} and therefore the observed rate constant might actually reflect k'_{max}. Our data show that

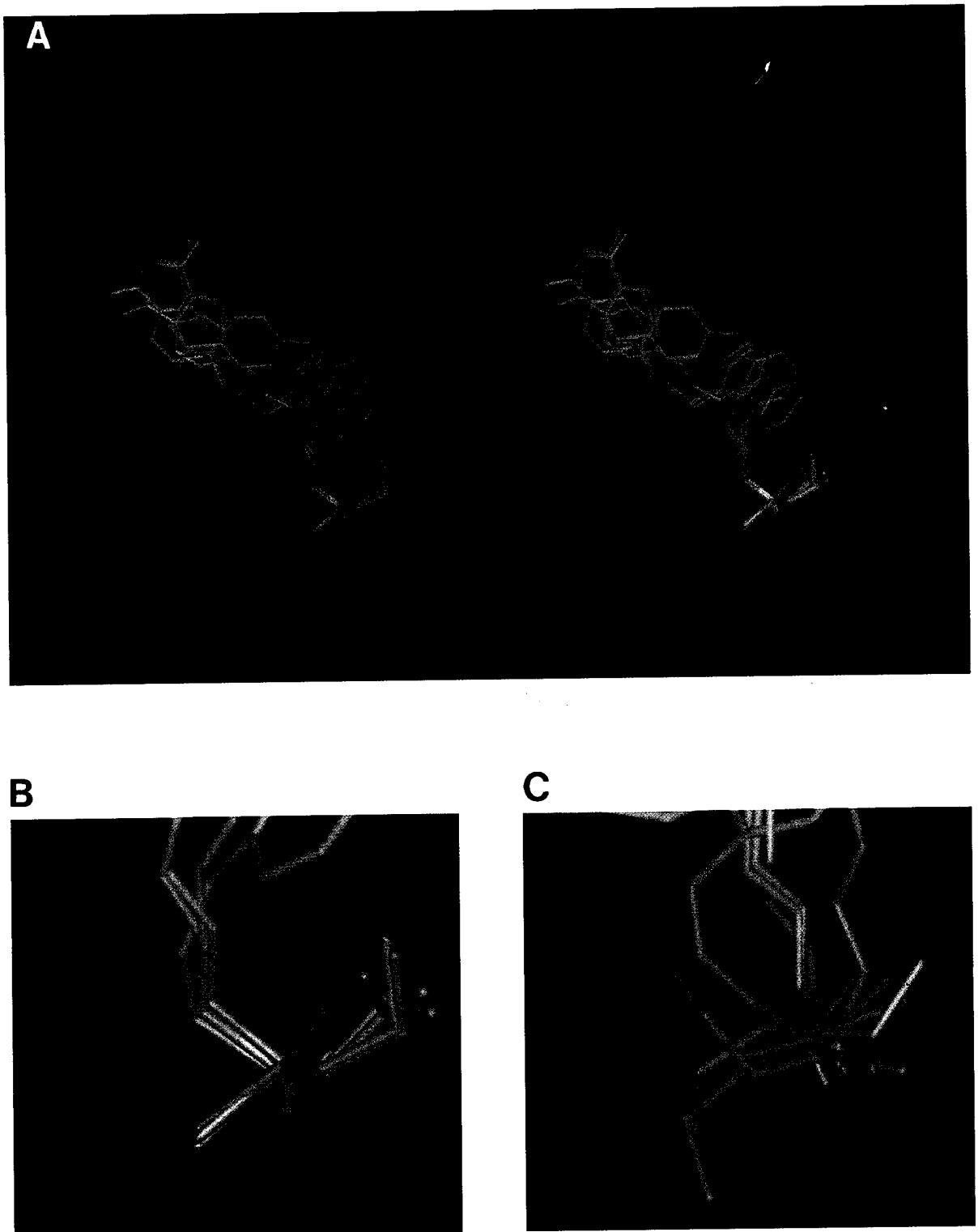

FIG. 7. **Molecular dynamics of the pentacoordinate transition state between $EMP_{R,S}$-AChE and HI-6.** A stereoview of EMP_R-AChE·HI6. Geometry around phosphorus was pentacoordinate with the oxime and Ser-203 oxygen assuming apical positions. Shown are the results of five simulations with heating and equilibrating at 700 K with subsequent cooling to 300 K. Simulations were constructed for *R* and *S* enantiomers of EMP. *B* shows an enlarged view in the region of the pentacovalent phosphorus for the EMP_R-AChE·HI-6 transition state. Note the fixed position of the phosphonyl oxygen. *C* shows an identical simulation for EMP_S-AChE·HI-6 where a large variation of position of the residues around the phosphorus are noted.

the rank orders of k'_{max} do not correlate closely with the bimolecular rate constants of reactivation and therefore comparative analysis should include K'_{ox}. Below we rationalize the two kinetically distinguished components in terms of stereospecific reactivation of the enantiomeric conjugates.

Energy minimization of the putative covalent enantiomeric conjugates revealed that the bond angles P=O- - -H—N(C=O) of either EMP_R-AChE (residues 121, 122, and 204) or EMP_R-HuBChE (corresponding residues 116, 117, and 199), as well as the relevant interatomic distances, should produce three hydrogen bonds between the phosphonyl oxygen and the backbone nitrogen atoms of the oxyanion hole region (Fig. 6, *broken*

lines). By contrast, the bond lengths increase and only a single hydrogen bond appears to stabilize the S_p enantiomers of *O*-ethyl methylphosphonyl conjugates of AChE and HuBChE. Furthermore, molecular dynamic simulations (Fig. 7) indicate that stabilization of the putative P-O^- of the transition state (Fig. 2*b*), by hydrogen bonding to the oxyanion hole, is likely to be greater for EMP_R-ChE than for the EMP_S-ChE conjugates. In the latter conjugate the P-O^- moiety of several of the lowest energy conformers are shifted out of the oxyanion hole. These considerations predict that the R_p enantiomer is the fast reactivatable component. The importance of the oxyanion hole in stabilizing the phosphonyl oxygen is underscored in the recently reported crystal structures of phosphonate complexes with lipases that are homologous to the ChE's (39).

The van der Waals surfaces of the methyl group $\mathbf{CH_3}$-P of EMP_S-AChE, as well as of EMP_S-HuBChE, that are aligned in both cases toward the oxime moiety, reveal that the oximate oxygen should experience greater steric hindrance for its approach toward the P atom, compared with the homologous EMP_R-ChE conjugates (Fig. 6). In the latter conjugate, $\mathbf{CH_3}$-P is projected toward the acyl pocket (Phe-295, Phe-297), the methylene of the ethyl moiety that faces the oximate oxygen is removed from the phosphorus by an oxygen ester linkage (P-$\mathbf{OCH_2CH_3}$), and thereby a larger space is opened to the oxime from the side envisaged for the nucleophilic attack. These observations are also consistent with EMP_R-ChE being the enantiomer of MEPQ-inhibited ChEs exhibiting rapid reactivation.

Acknowledgments—We acknowledge the expert technical assistance of Ann M. Gallaher and Anthony Schmidt in carrying out this investigation.

REFERENCES

1. Aldridge, W. N., and Reiner, E. (1972) *Enzyme Inhibitors as Substrates*, North Holland Publishing Co., Amsterdam
2. Segall, Y., Waysbort, D., Barak, D., Ariel, N., Doctor, B. P., Grunwald, J., and Ashani, Y. (1993) *Biochemistry* **32,** 13441–13450
3. Wilson, I. B., and Ginsburg, S. (1955) *Biochim. Biophys. Acta* **18,** 168–170
4. Poziomek, E. J., Hackley, B. E., Jr., Steinberg, G. M. (1958) *J. Org. Chem.* **23,** 714–717
5. Erdman, W. D. (1969) *Naunyn-Schmiedebergs Arch. für Pharmakol. Exper. Therap.* **263,** 61–72
6. Oldiges, H., and Schoene, K. (1970) *Arch. Toxicol.* **26,** 293–305
7. Lundy, P. M., Hansen, A. S., Hand, T. H., and Boulet, C. A. (1992) *Toxicology* **72,** 99–105
8. Sussman, J. L., Harel, M., Frolov, F., Oefner, C., Goldman, A., Toker, L., and Silman, I. (1991) *Science* **253,** 872–879
9. Taylor, P., and Radić, Z. (1994) *Annu. Rev. Pharmacol. Toxicol.* **34,** 281–320
10. Levy, D., and Ashani, Y. (1986) *Biochem. Pharmacol.* **35,** 1079–1085
11. Raveh, L., Grunwald, J., Marcus, D., Papier, Y., Cohen, E., and Ashani, Y. (1993) *Biochem. Pharmacol.* **45,** 2465–2474
12. Vellom, D. C., Radić, Z., Li, Y., Pickering, N. A., Camp, S., and Taylor, P. (1993) *Biochemistry* **32,** 12–17
13. Radić, Z., Pickering, N. A., Vellom, D. C., Camp, S., and Taylor, P. (1993) *Biochemistry* **32,** 12074–12084
14. Lee, S. L., Camp, S., and Taylor, P. (1982) *J. Biol. Chem.* **257,** 12302–12309
15. Albert, A., and Serjeant, E. P. (1962) *Ionization Constants of Acids and Bases*, Methuen and Co. Ltd., London
16. Ellman, G. L., Courtney, K. D., Andres, V., Jr., and Featherstone, R. M. (1961) *Biochem. Pharmacol.* **1,** 88–95
17. Segel, I. H. (1976) *Biochemical Calculations*, John Wiley & Sons, New York
18. Harel, M., Sussman, J. L., Krejci, E., Bon, S., Chanal, P., Massoulié, J., and Silman, I. (1992) *Proc. Natl. Acad. Sci. U. S. A.* **89,** 10827–10831
19. Carlstrom, D. (1966) *Acta Chem. Scand.* **20,** 1240–1246
20. Kamenar, B., Vicković, I., and Bruvo, M. (1986) *Acta Crystallogr. Sect. C Cryst. Struct.* **42,** 1818–1821
21. Ordentlich, A., Barak, D., Kronman, C., Flashner, Y., Leitner, M., Segall, Y., Ariel, N., Cohen, S., Velan, B., and Shafferman, A. (1993) *J. Biol. Chem.* **268,** 17083–17095
22. Harel, M., Schalk, I., Ehret-Sabatier, L., Bout, F., Goeldner, M., Hirth, C., Axelson, P. H., Silman, I., and Sussman, J. L. (1993) *Proc. Natl. Acad. Sci. U. S. A.* **90,** 9031–9035
23. Nair, H. K., Seravalli, J., Arbuckle, T., and Quinn, D. M. (1994) *Biochemistry* **33,** 8566–8576
24. Barak, D., Kronman, C., Ordentlich, A., Ariel, N., Bromberg, A., Marcus, D., Lazar, A., Velan, B., and Shafferman, A. (1994) *J. Biol. Chem.* **269,** 6296–6305
25. Radić, Z., Gibney, G., Kawamoto, S., MacPhee-Quigley, K., Bongiorno, C., and Taylor, P. (1992) *Biochemistry* **31,** 9760–9767
26. Harvey, B., Scott, R. P., Sellers, D. J., and Watts, P. (1986) *Biochem. Pharmacol.* **35,** 745–751
27. Hackley, B. E., Jr., Steinberg, G. M., and Lamb, J. C. (1959) *Arch. Biochem. Biophys.* **80,** 211–214
28. Cygler, M., Schrag, J. D., Sussman, J. L., Harel, M., Silman, I. Gentry, M. K., and Doctor, B. P. (1993) *Protein Sci.* **2,** 366–382
29. Berman, H. A., and Decker, M. M. (1989) *J. Biol. Chem.* **264,** 3951–3956
30. van Havere, W., Lenstra, A. T. H., and Geise, H. J. (1982) *Acta Crystallogr. Sect. B Struct. Sci.* **38,** 2516–2518
31. Hall, C. R., and Inch, T. D., (1980) *Tetrahedron* **36,** 2059–2095
32. Ashani, Y., and Cohen, S. (1970) *J. Med. Chem.* **13,** 471–474
33. Bedford, C. D., Howd, R. A., Daily, O. D., Miller, A., Nolen, H. W., III, Kenley, R. A., Kern, J. R., and Winterle, J. S. (1986) *J. Med. Chem.* **29,** 2174–2183
34. de Jong, L. P. A., and Kossen, S. P. (1985) *Biochim. Biophys. Acta* **830,** 345–348
35. de Jong, L. P. A., and Wolring, G. Z. (1984) *Biochem. Pharmacol.* **33,** 1119–1125
36. Hanke, D. W., and Overton, M. A. (1991) *J. Toxicol. Environ. Health* **34,** 141–156
37. Bismuth, C., Inns, R. H., and Marrs, T. C. (1992) in *Clinical and Experimental Toxicology of Organophosphates and Carbamates* (Ballantyne, B., and Marrs, T. C., eds) pp. 555–577, Butterworth-Heinemann Ltd., Oxford, United Kingdom
38. Barak, D., Ariel, N., Velan, B., and Shafferman, A. (1992) in *Multidisciplinary Approaches to Cholinesterase Functions* (Shafferman, A., and Velan, B., eds) pp. 195–199, Plenum Press, New York
39. Cygler, M., Grochulski, P., Kazlauskas, R. J., Schrag, J. D., Bouthillier, F., Rubin, B., Serreqi, A. N., and Gupta, A. K. (1994) *J. Am. Chem. Soc.* **116,** 3180–3186

Acetylcholinesterase Inhibition by Fasciculin: Crystal Structure of the Complex

Yves Bourne, Palmer Taylor, & Pascale Marchot

Cell, Vol. 83, 503-512, Nov. 3, 1995

Please read:

The unusual shape of loop II, comprised of two vicinal Pro residues at its tip with **Pro-31** in the *cis* conformation, fits perfectly... (p. 506, right, lines 18-20).

Of the five ion pairs involved in the interaction of the gorge rim of TcAChE and the symmetry-related molecule, three residues (Glu-73 **-Thr-75 in mAChE-**, Asp-276 **-Asp-283 in mAChE-**, and Asp-285 **-Glu-292 in mAChE-**) contribute to the Fas2-mAChE interaction and... (p. 509, right, lines 1-5)

Cell, Vol. 83, 503–512, November 3, 1995, Copyright © 1995 by Cell Press

Acetylcholinesterase Inhibition by Fasciculin: Crystal Structure of the Complex

Yves Bourne,*† Palmer Taylor,* and Pascale Marchot*
*Department of Pharmacology
University of California, San Diego
La Jolla, California 92093-0636
†Department of Molecular Biology
The Scripps Research Institute
La Jolla, California 92037

Summary

The crystal structure of the snake toxin fasciculin, bound to mouse acetylcholinesterase (mAChE), at 3.2 Å resolution reveals a synergistic three-point anchorage consistent with the picomolar dissociation constant of the complex. Loop II of fasciculin contains a cluster of hydrophobic residues that interact with the peripheral anionic site of the enzyme and sterically occlude substrate access to the catalytic site. Loop I fits in a crevice near the lip of the gorge to maximize the surface area of contact of loop II at the gorge entry. The fasciculin core surrounds a protruding loop on the enzyme surface and stabilizes the whole assembly. Upon binding of fasciculin, subtle structural rearrangements of AChE occur that could explain the observed residual catalytic activity of the fasciculin-enzyme complex.

Introduction

Acetylcholinesterase (AChE), which terminates the action of the neurotransmitter acetylcholine (ACh) at cholinergic synapses in the central and peripheral nervous systems, is a target site for a variety of pharmacologic agents, insecticides in widespread use, and nerve gases (Massoulié et al., 1993; Taylor and Radić, 1994). The Torpedo californica AChE (TcAChE) molecule, with its α/β hydrolase fold (Sussman et al., 1991), has defined the structures of a large family of enzymes that includes other esterases and several lipases, as well as proteins without hydrolase activity (Cygler et al., 1993). The active center triad, consisting of the catalytic Ser-200, Glu-327, and His-440 in TcAChE, is found nearly centrosymmetric to the subunit at the bottom of a narrow gorge. The narrow gorge width, coupled with its depth of 18–20 Å, has raised questions regarding the compatibility of these dimensions with a near diffusion-limited rate of substrate entry and catalysis (Tan et al., 1993). The charge distribution on the enzyme creates a dipole that not only directs ligands to the gorge entry, but may also facilitate diffusion to the active center. This, in turn, has led to the suggestion of a "back door," a portal of substrate access distinct from the gorge entrance, to accommodate the rapid product removal or solvent contact (Ripoll et al., 1993; Gilson et al., 1994). However, mutations of AChE in areas where solvent exposure to the gorge might be increased have not yielded evidence for a second site of access (Shafferman et al., 1994). Inhibitors, in addition to binding at the active center, may associate with a peripheral anionic site, remote from the active center, to influence catalysis allosterically. Labeling and site-specific mutagenesis studies indicate that this site resides near the lip of the active center gorge (for review see Taylor and Radić, 1994).

Fasciculins are 61 amino acid peptides isolated from mamba (Dendroaspis) venoms. They belong to the family of three-fingered snake toxins that includes the α-neurotoxins, selective nicotinic receptor blockers (Changeux et al., 1970; Endo and Tamiya, 1991), and the subtype-specific muscarinic receptor agonists (Adem et al., 1988; Segalas et al., 1995). The fasciculins are the only known peptidic AChE inhibitors and are highly selective; they inhibit mammalian and electric eel AChE with K_i values in the picomolar range, but have only micro- to millimolar K_is for avian and insect AChEs and for butyrylcholinesterases (BuChE) (for review see Cerveñansky et al., 1991). Chemical labeling (Duran et al., 1994), ligand competition (Karlsson et al., 1984; Marchot et al., 1993; Radić et al., 1995; Eastman et al., 1995), and site-directed mutagenesis studies (Radić et al., 1994, 1995), indicate that fasciculin does not completely occlude ligand access to the active center Ser, but rather binds to the peripheral site to inhibit catalysis, perhaps allosterically. Although the X-ray structures of the fasciculins Fas1 and Fas2 have been solved (Le Du et al., 1992; 1995), they have not revealed the nature of the binding interface.

To delineate the structural determinants of the fasciculin specificity for AChE and how the fasciculins inhibit AChE, we have determined the crystal structure of the complex formed between Fas2 and a recombinant monomeric AChE from mouse (mAChE) and refined it to 3.2 Å resolution. The current model (model A) contains one molecule of mAChE (residues 4–257 and 265–543; Rachinsky et al., 1990), one molecule of Fas2 (residues 1–61), and one N-acetylglucosamine (GlcNAc) moiety linked to mAChE at Asn-350. The structure, which has an excellent stereochemistry with a R factor of 18.4% for data between 10 and 3.2 Å, reveals the nature of AChE inhibition by Fas2 with implications for the binding of structurally related α-neurotoxins and muscarinic agonists to their respective ACh receptors.

Results and Discussion

Overall Structure of the Complex

The excellent quality of the 3.2 Å electron density map unambiguously reveals the positions of the side chains in Fas2 and mAChE, as well as those located at the interface of the complex (Figure 1). The mAChE molecule has the α/β hydrolase fold and consists of the same 12-stranded central-mixed β sheet surrounded by 14 α helices as the TcAChE molecule (Sussman et al., 1991). Secondary structure motifs are specified according to Cygler et al. (1993): the strands of the small amino-terminal β sheet

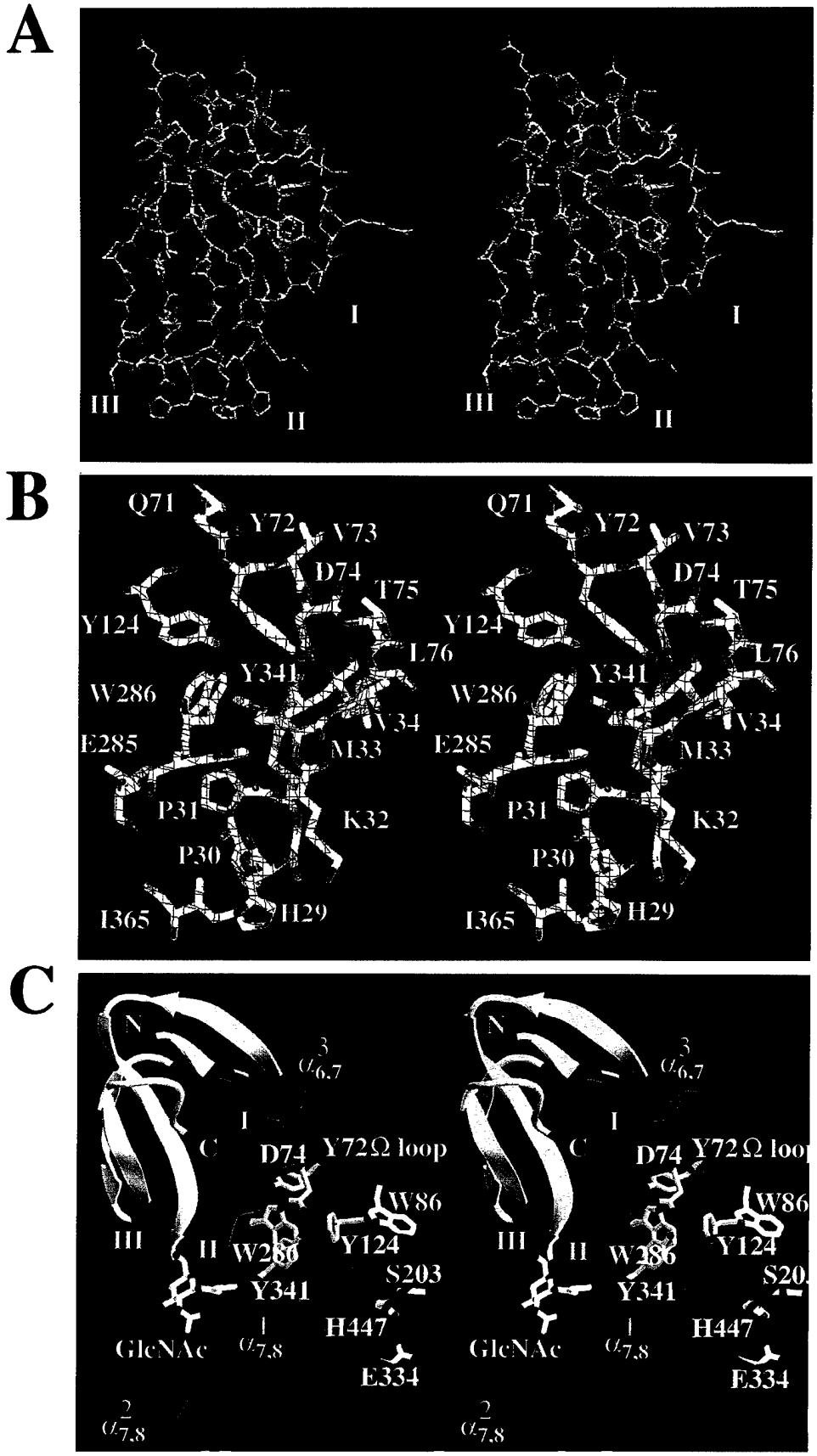

Figure 1. Quality of the Structure and Overall View of the Complex

(A) Stereoview of the final σ_A weighting $2F_o - F_c$ electron density map (contoured at 1 σ) of the entire Fas2 molecule at 3.2 Å resolution. Labels I, II, and III refer to Fas2 loop I (residues 4–16), loop II (residues 23–38), and loop III (residues 42–51). The Fas2 molecule is particularly well ordered in the complex. The Arg-11 side chain extends on the right of the molecule.

(B) Stereoview of the 3.2 Å resolution omit $F_o - F_c$ electron density map of the tip of Fas2 loop II and the surrounding mAChE residues (5% of the total number of atoms, contoured at 2.5 σ). The coordinates of this region were omitted and the protein coordinates refined by simulated annealing before the phase calculation for the map. Residues are labeled in white for mAChE and in yellow for Fas2.

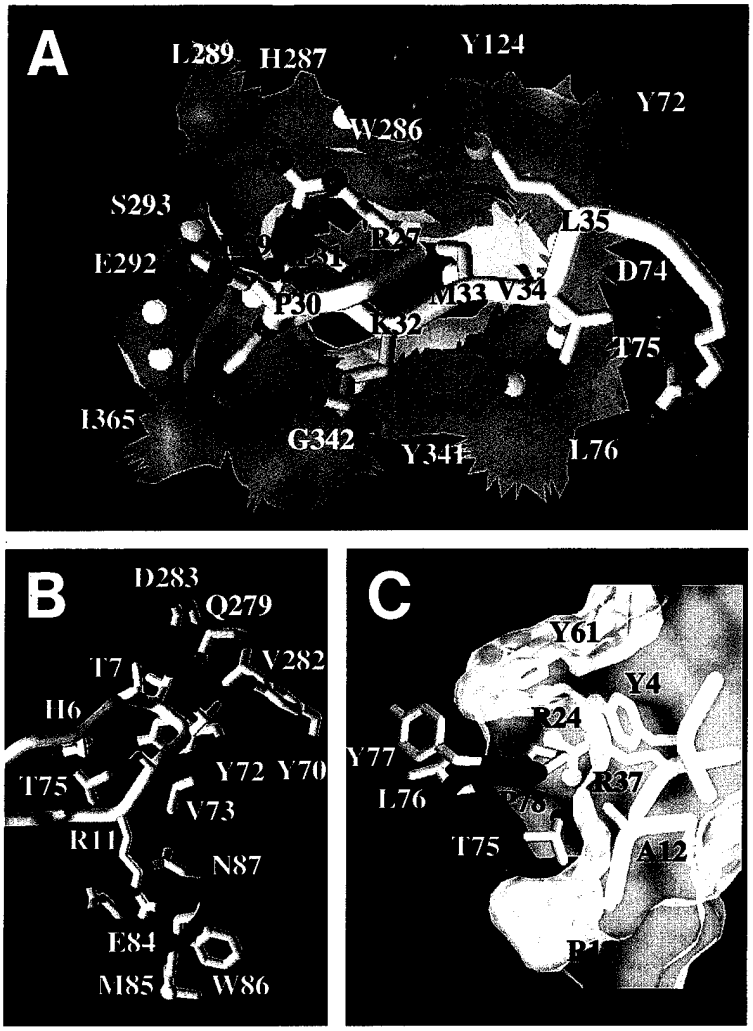

Figure 2. Three-Point Interface of the Fas2–mAChE Complex

(A) Side chain to side chain interactions between mAChE (blue Cα tubes with green side chains and colored spheres) and the tip of Fas2 loop II (yellow Cα tubes with light yellow side chains and colored sphere). A part of the molecular surface of mAChE buried in the complex is displayed in transparency and shows the cavities around the gorge entrance for Fas2 Pro-30, Pro-31, and Met-33. The tip of Fas2 loop II interacts with mAChE peripheral anionic site residues Tyr-72(70), Tyr-124(121), Trp-286(279), Tyr-341(334), and Gly-342(335). Extensive polar and van der Waals interactions between Fas2 loop II and mAChE residues surrounding the gorge entrance stabilize this interface of the complex.

(B) Side chain to side chain interactions between mAChE (blue Cα tubes with light blue side chains and colored spheres) and the tip of Fas2 loop I (yellow Cα tubes with light yellow side chains and colored spheres). The side chain of Fas2 Arg-11 comes in close apposition with mAChE Glu-84(82) and Asn-87(85) and surrounds mAChE Trp-86(84), a proposed second portal for entry of substrate and exit of product (Gilson et al., 1994). mAChE Asp-283(276) and Gln-279(272), suspended from helix $\alpha^3_{6,7}$, are hydrogen bonded to Fas2 Thr-8 and Thr-9. For clarity, Fas2 residues Thr-8, Thr-9, and Ser-10 at the tip of loop I are not labeled, but their side chains are clearly visible. The capacity for hydrogen bonding of the hydroxyl groups of Thr-8 and Thr-9 is evident.

(C) Side chain to side chain interactions between mAChE (blue Cα tubes with light blue side chains and colored spheres) and the core region of Fas2 (yellow Cα tubes with orange side chains and colored spheres). The cavity formed at the molecular surface of Fas2 by the side chains of Arg-11 (protruding at the front), Ala-12, Tyr-4, and Tyr-61 is filled by mAChE Pro-78(76). Fas2 Arg-24, a structurally important residue, is hydrogen bonded to the carbonyl atom of Tyr-61 and stabilizes the carboxy-terminal region of Fas2. Fas2 Arg-37, a residue conserved in the three-fingered peptide toxin family, is in stacking interaction with Fas2 Arg-24 and is hydrogen bonded to mAChE Thr-75(73).

are identified as β_i; the strands of the large central β sheet are identified as β_j; the α helices are identified as $\alpha^k_{i,j}$, where subscripts refer to the loop-connecting strands i and j of the β sheet in which the helix is embedded, and superscripts refer to the sequential number of this helix within the loop (no superscript is used when there is a single helix in the connecting loop). The number in parentheses that follows the mAChE residue number denotes the corresponding position in the TcAChE sequence.

The Fas2 molecule consists of two antiparallel β sheets with a three-stranded β sheet formed by residues 22–27, 34–39, and 48–53 and a short two-stranded β sheet formed by residues 3–4 and 14–15 (Le Du et al., 1992). Fas2, with its three loops emerging from a dense core containing the disulfide bridges, forms a slightly concave flat disk that fits into an elongated cavity at the surface of mAChE (Figure 1C). This cavity, located between helix $\alpha^3_{6,7}$ and the Ω loop Cys-69(67) to Cys-96(94), which corresponds to the lid region in lipases (Grochulski et al., 1994), forms the entrance of the mAChE active site gorge. The inner side of Fas2 β strand 4 is oriented roughly 45° away from the direction of the gorge entrance. Three distinct, separated anchorage points of Fas2 on mAChE result in a particularly well-ordered molecule of bound Fas2 (Figures 1 and 2) consistent with its picomolar dissociation constant for mAChE. All three regions of Fas2 responsible for com-

(C) Stereoview ribbon diagram of Fas2 (yellow and green) bound to mAChE (blue and magenta). The tip of loop II and the inner side of β strand 4 of Fas2 are tightly associated with the peripheral anionic site of mAChE, whereas loop I binds on the other side of the lid region (Ω loop) of mAChE. The residues of Fas2 and the secondary structure elements of mAChE involved in the complex are highlighted in green and in magenta, respectively. Residues within the mAChE catalytic site, Ser-203(200), Glu-334(327), His-447(440), and Trp-86(84), are displayed as white bonds with colored spheres. Residues belonging to the mAChE peripheral anionic site, Tyr-72(70), Asp-74(72), Trp-286(279), and Tyr-341(334), are displayed as green bonds with colored spheres. The GlcNAc moiety linked to Asn-350(343) is displayed in white with colored spheres. Secondary structure elements of mAChE are labeled according to Cygler et al. (1993).

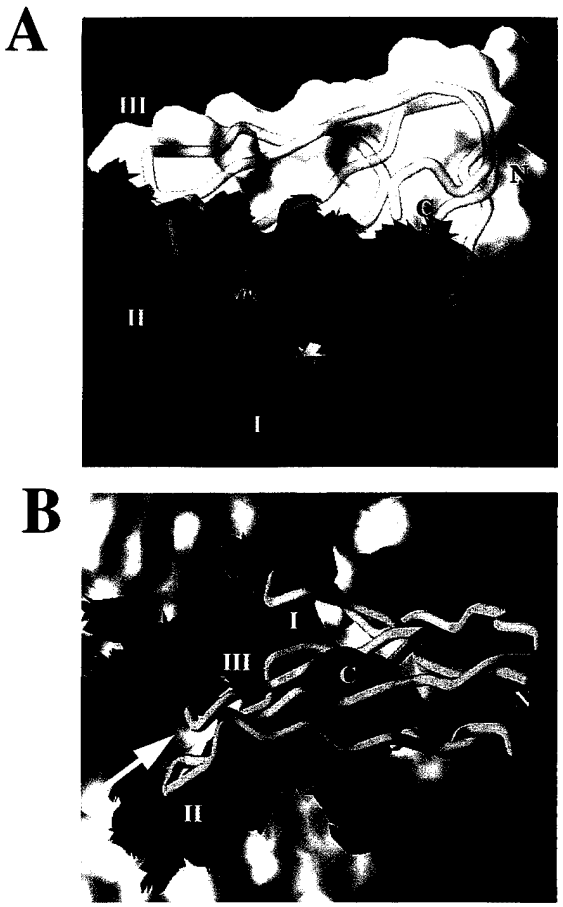

Figure 3. Molecular Surfaces of Fas2 and mAChE at the Complex Interface

(A) Fas2 molecular surface, colored in blue for the residues buried to a 1.6 Å probe radius and shown in white for the nonburied residues. A Cα trace (yellow) is shown through the surface. The buried residues are found at the tip of loop I (bottom center), where Arg-11 is clearly visible (bottom) and at the tip of loop II (middle left) and extend to the concave face of β strand 4 (center). Only two residues are buried at the tip of loop III (back left). This interfacial area represents 27% of the total accessible surface area of Fas2 and comprises 21 residues of Fas2, of which only four are positively charged. The cavity formed by the side chains of Tyr-4, Arg-37, and Tyr-61 is visible at the center of the molecule.

(B) mAChE molecular surface, viewed looking down into the gorge. The color code is the same as in (A). Buried residues cluster in and largely around the gorge of the enzyme and on the other side of the lid region (top). This interface area represents 5% of the total accessible surface area of the molecule and comprises 25 residues of mAChE. Fas2 (yellow Cα trace) is superimposed on the molecular surface and is oriented ~90° away from that in (A). Labels I, II, and III refer to the loops of Fas2. The arrow indicates the active site gorge entrance.

plex formation are located in the concave face of the molecule (Figures 1C and 3A).

Detailed Structure of the Complex

Loop II of Fas2, formed by residues Tyr-23 to Arg-38, is central to the interface (Figure 1C). The tip of loop II, which contains the Pro–Pro–Lys–Met sequence motif characteristic of the fasciculin family, is tightly bound to the peripheral anionic site along with numerous residues surrounding the gorge entrance in mAChE (including residues from the lid and from helices $\alpha^3_{6,7}$, $\alpha^1_{7,8}$, and $\alpha^2_{7,8}$) and sterically occludes substrate access to the gorge (Figures 1C, 2A, and 3B). Loop II residue Met-33 establishes several key van der Waals contacts with mAChE Tyr-72(70), Tyr-124(121), and Tyr-341(334) and packs against mAChE Trp-286(279) (Figure 2A). Predominant hydrophobic interactions are found between Fas2 Pro-30 and Pro-31 and mAChE Ile-365(358) and Leu-289(282), which form a tight cluster of buried residues at the binding interface. The side chains of Fas2 His-29 and Pro-30 also participate in van der Waals interactions with the side chain of mAChE Glu-292 (Asp-285 in TcAChE), one of the few acidic residues present at the top of the gorge and contributing to its negative charge (Sussman et al., 1991). In addition, Fas2 Val-34 and Leu-35 in β strand 4 establish van der Waals contacts with mAChE Leu-76(74), Tyr-72(70), and His-287(280). The unusual shape of loop II, comprised of two vicinal Pro residues at its tip with Pro-30 in the *cis* conformation, fits perfectly the mAChE peripheral anionic site without requiring a dramatic conformational change in the two partners of the complex (Figures 1C, 2A, 3B, and 4A). In addition, Fas2 Arg-27 is hydrogen bonded to Fas2 His-29, Pro-30, and Pro-31 and to mAChE Trp-286(279) carbonyl oxygen atoms and thus stabilizes the conformation of the entire loop in bound Fas2 (Figure 2A). Polar interactions are established between the nitrogen atom of Fas2 Pro-31 and the carbonyl oxygen atom of mAChE Ser-293(286), between the amide backbone nitrogen of Fas2 Lys-32 and the carbonyl oxygen atom of mAChE Tyr-341(334), and between the side chains of Fas2 Arg-37 and mAChE Thr-75(73). A critical role is played by mAChE Gly-342(335), which is in van der Waals contact with the side chain of Fas2 Lys-32 and, thus, cannot be substituted by a larger side chain without perturbing the complex.

The precise orientation of loop II allows loop I, formed by residues Tyr-4 to Asn-16, to abut on top of the lid region of mAChE and be the second interaction point (Figure 1C). The tip of loop I, which contains the motif Thr–Thr–Thr–Ser–Arg–Ala that is also characteristic of fasciculins, inserts within a small crevice at the surface of mAChE and interacts with residues from loop b_3–$\alpha_{b3,2}$ and helices $\alpha_{b3,2}$ and $\alpha^3_{6,7}$, located 25 Å away from the gorge entrance (Figure 1C). Numerous polar interactions are found between the Fas2 Thr-8 side chain and the nitrogen backbone atoms of mAChE Val-73(71), Gln-279(272), and the Asp-283(276) side chains, between the Fas2 Thr-9 side chain and the mAChE Gln-279(272) side chain, and between the Fas2 Arg-11 side chain and the side chains of mAChE Glu-84(82) and Asn-87(85), conserved in all cholinesterase sequences (Figure 2B). Van der Waals contacts are observed between Fas2 His-6 and mAChE Thr-75(73), between Fas2 Thr-8 and mAChE Tyr-72(70), and between Fas2 Thr-9 and mAChE Tyr-70(68), Leu-92(90), and Val-282(275). The most critical residue in this interaction is Fas2 Ala-12, whose close packing with mAChE Pro-78(76), an amino acid protruding at the top of the gorge entrance, precludes substitution of a bulkier residue (Figure 2C).

The third interaction point between Fas2 and mAChE involves the side chains of residues Tyr-4 and Tyr-61, respectively located near and at the amino and carboxyl termini of Fas2, which establish van der Waals interactions with mAChE Tyr-77(75) and completely surround mAChE Pro-78(76) (Figure 2C). The close proximity of Fas2 Arg-37 also contributes to exclusion of Pro-78(76) from the solvent. These interactions substantially extend the area of the complex interface to a total of 1100 Å^2 buried to a 1.6 Å radius probe on each protein and encompasses 27% of the total surface area of Fas2 (Figure 3), two values in the highest range of general patterns for high affinity peptide–protein complexes (Janin and Chothia, 1990). Fas2 loop III, formed by residues Pro-42 to Lys-51, contributes weakly to the complex interface, as only residues Asn-47 and Leu-48, located at its tip, are in van der Waals interaction with mAChE through the His-287(280) side chain (Figure 3A); the other residues and the outside of β strand 5 are facing the solvent and are stabilized within the crystal by a symmetry-related mAChE molecule.

The Peripheral Anionic Site of mAChE

The key role played by the side chains of mAChE Tyr-72(70), Tyr-124(121), Trp-286(279), and Tyr-341(334), located at the rim of the gorge (Figure 2), in the binding of Fas2 closely matches previous site-directed mutagenesis data that defined these residues as belonging to the peripheral anionic site of the enzyme (Barak et al., 1994; Harel et al., 1992; Ordentlich et al., 1993; Radić et al., 1993; Shafferman et al., 1992) and, specifically, the binding site for Fas2 (Radić et al., 1994, 1995). This constellation of residues is unique to those AChEs that have high affinity for fasciculins. In contrast, the location of the conserved residue Asp-74(72) in the gorge entrance, relative to the other residues of the peripheral anionic site, is consistent with the limited influence of mutation of this residue on mAChE inhibition by Fas2 (Radić et al., 1994). Pro-78(76) and Gly-342(335) on mAChE also contribute to the fasciculin-binding site. Whether they should also be considered as part of the peripheral anionic site is, however, not certain. mAChE Pro-78(76) is conserved in all cholinesterase sequences and is positioned at the top of the lid rather than in the depression of the gorge entrance. The residual low affinity of fasciculins for insect and avian AChE as well as for BuChE could therefore arise from the interaction of Pro-78(76) with Fas2 residues Tyr-4, Ala-12, Arg-37, and Tyr-61, even in the absence of a contribution for loop II. Residue mAChE Gly-342(335), in close contact with Fas2 Lys-32, is highly conserved among the various cholinesterases, with the exception of insect AChE, where Asp is found. That substitution may partly explain the resistance of Drosophila AChE toward fasciculin inhibition.

Functional Residues of the Fasciculin Molecule

The predominance of basic amino acids on fasciculin, together with evidence for its interaction with an anionic site on AChE shared with cationic inhibitors of the enzyme, initially suggested a primary role for the positively charged side chains of fasciculin in its interaction with AChE. Recent studies, probing the functional role of the amino and guanidino groups of Fas2 through chemical modification, suggested that five positive residues, Arg-11, Lys-25, Arg-27, Lys-32, and Lys-51, comprise interacting sites of Fas2 (Cerveñansky et al., 1994, 1995). Initial site-directed mutagenesis data indicate that three to four positive residues, Arg-11, Arg-27, Lys-32, and perhaps Arg-24, contribute to the interaction sites of Fas2, whereas three others, Lys-25, Arg-28, and Lys-51, do not (P. M., unpublished data). These mutagenesis data correlate well with the Fas2–mAChE structure, including the role played by Arg-24 in stabilizing the side chain of Tyr-61 (the Fas2 Tyr-61 to mAChE Pro-78 interaction would weaken in the absence of Arg-24) (Figure 2C). Changes in the Fas2 structure may have occurred upon chemical modification of residues Lys-25 and Lys-51. In contrast, the reported absence of reactivity of Arg-24 to 1,2-cyclohexanedione is consistent with internal bonding within Fas2 rather than direct contact with mAChE.

Actually, only four out of the nine positively charged residues of Fas2 directly interact with mAChE: Arg-11, Arg-27, Lys-32, and Arg-37. The picomolar K_i values of the fasciculin–AChE complexes (Karlsson et al., 1984; Lin et al., 1987; Marchot et al., 1993; Radić et al., 1994; Eastman et al., 1995) arise in large part from the interactions of the hydrophobic residues located at the tips of loops I and II of Fas2. Nevertheless, six of the nine positively charged residues of fasciculin are located along loop II and, together with the isolated charge at the tip of loop I, play a major role in the approach and initial docking of the fasciculin to AChE (van den Born et al., 1995), consistent with the strong directional electrostatic field existing along the active center gorge axis (Ripoll et al., 1993).

Structural Adaptability and Specificity of the Fasciculin Molecule

Superimposition of the structure of Fas2 bound to mAChE with that of free Fas2 (Le Du et al., 1995) reveals that the tips of loops I and II are shifted by 2–2.5 Å within their respective mAChE-binding sites, resulting in a root mean square (rms) deviation of 0.77 Å for 61 Cα atoms (Figure 4A). Comparison of the crystal structures of Fas1 and Fas2, which differ by single mutation Tyr/Asn at position 47, revealed a large difference in the conformation of loop I, perhaps influenced by the detergent employed for crystallizing Fas2 (Le Du et al., 1992, 1995). It is noteworthy that mAChE Pro-78(76) plays exactly the same role as the side chain of Thr-9 in the structure of Fas1 in mimicking the detergent molecule that fills the hydrophobic pocket formed by Tyr-4, Arg-37, and Tyr-61 in the structure of Fas2 and allows free Fas2 to crystallize in a conformation resembling the bound state. In contrast, superimposition of free Fas1 with bound Fas2 reveals steric occlusion between loop I of Fas1 and the lid region of mAChE (Figure 4A), indicating that Fas1 binds to mAChE with a conformation of loop I different from that in the Fas1 crystal. The observations that crystallization yielded hexagonal Fas1–mAChE crystals belonging to the same space group and having the same cell dimensions as the Fas2–mAChE crystals (Marchot et al., submitted) and that Fas1 forms Fas2-type crystals in the presence of the detergent (Le

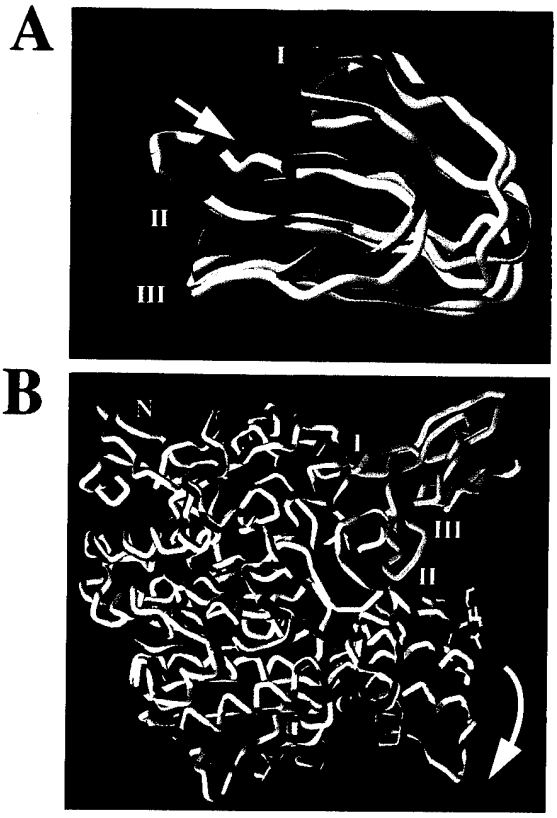

Figure 4. Comparison of Fas2 and mAChE with Their Respective Homologs

(A) Molecular surface of mAChE (blue) buried in the Fas2–mAChE complex, with the Cα traces of bound Fas2 (yellow), free Fas2 (green), free Fas1 (magenta), and toxin α (white). The toxin molecules are superimposed according to their Cα atoms. Steric occlusions of toxin α loops I and II and of Fas1 loop I with the mAChE interface are demonstrated by the surface transparency. The disulfide core and loop III conformations are conserved in all three-fingered toxins of known structure. The arrow indicates the mAChE active site gorge entrance.

(B) Superimposition of the mAChE monomer (blue) with a TcAChE monomer (white) according to their Cα atoms. The Fas2 molecule bound to mAChE is in yellow. The rigid body motion of residues Tyr-341(334) to Ser-399(392), at the bottom of the gorge entrance, is indicated by the curved arrow. The amino and carboxyl termini of the monomer are indicated by N and C, respectively. The GlcNAc moiety linked to Asn-350(343) is displayed in white with colored spheres.

Du et al., 1995) strongly support this hypothesis. These findings demonstrate the adaptability of the fasciculin molecule to its binding site on AChE, consistent with the general flexibility of the three-fingered toxins found by nuclear magnetic resonance (NMR) spectrometry (Brown and Wüthrich, 1992, and references therein).

Detailed structural information is available for the members of the three-fingered toxin family: α-neurotoxins, cardiotoxins, and muscarinic toxins (Endo and Tamiya, 1991; Rees and Bilwes, 1993; Segalas et al., 1995), and comparisons with fasciculins have already been made (Le Du et al., 1992, 1995: van den Born et al., 1995; Segalas et al., 1995). A cluster of Thr/Ser residues (loop I) exists in several short α-neurotoxins but is shifted by four to six residues and lacks an equivalent to Arg-11. Ala-12 exists only in fasciculins and in four of the short α-neurotoxins, all from Dendroaspis venoms. A unique short α-neurotoxin, toxin α from black mamba venom, possesses several of the fasciculin determinants for binding to AChE with Ser-8 (in place of Thr-8), Thr-9, Arg-11, and Ala-12 at the tip of its loop I, together with Tyr-4 in its disulfide core and, notably, a carboxy-terminal Tyr-61; it is, however, a fully potent α-neurotoxin (Strydom, 1972). Loop II of toxin α has none of the fasciculin determinants, except for the widely conserved Arg-37 and two Ile residues in place of Val-34 and Leu-35, and adopts the α-neurotoxin-typical conformation and orientation (Brown and Wüthrich, 1992). The presence of a Glu residue in toxin α in place of Gly-36 in Fas2 β strand 4 appears to be critical for dictating the backbone direction and, consequently, the bond angles of loop II (Figure 4A). Bond angles in loop II, governed by the above substitution and side chain compositions, distinguish the fasciculins from the α-neurotoxins and the muscarinic toxins (Le Du et al., 1992; Segalas et al., 1995). The specific shape of loop II allows perfect positioning of the key residue located at its tip: Met-33 in fasciculins, the conserved Arg residue in α-neurotoxins, and Lys-34 in the muscarinic agonist. In contrast, the conformation of loop III is highly conserved in all structures of three-fingered toxins. In fasciculins, loop III essentially appears to maintain a specific conformation of loop II through an extensive set of stabilizing interactions.

Comparison of mAChE and TcAChE Structures

Overall, a close structural similarity is observed between mAChE and TcAChE (Figure 4B). An rms deviation value of 0.84 Å for 509 Cα atoms is obtained when the two structures are superimposed. The largest difference is in the conformation of loop Glu-319(312) to Leu-324(317), resulting from the formation of a salt bridge between Asp-323(316) and Arg-223(216). Such a salt bridge cannot form in TcAChE, where Lys-316 is found. Within the active site, the shorter side chain of mAChE Pro-446, relative to Ile-439 in TcAChE, induces several rearrangements of the neighboring side chains: the Trp-439(432) side chain moves by 1.5 Å to maintain van der Waals contacts with the Pro-446 side chain, and the Phe-80(78) side chain slips in concert to keep interacting with Trp-439. The Tyr-337(330) side chain, which is hydrogen bonded to Tyr-441(334), adopts the conformation of the Phe-330 side chain in the edrophonium–TcAChE complex (Harel et al., 1993). Incidentally, this result confirms that no decamethonium was retained in the mAChE active site during purification (Marchot et al., submitted).

Some other substitutions are located at the binding interface that do not alter the backbone conformation but could modulate Fas2 interaction with the respective enzymes: mAChE Tyr-70 (Gln-68 in TcAChE), Thr-75 (Glu-73), Leu-76 (Gln-74), Tyr-77 (Phe-75), Leu-92 (Met-90), His-287 (Asn-280), and Glu-292 (Asp-285). The most critical of these appear to be the Leu-76→Gln substitution that brings to TcAChE a larger side chain that might interact differently with Arg-24, Val-34, and Arg-37 of Fas2 loop II, and the Thr-75→Glu and His-287→Asn substitutions

that cause charge differences that might change the interaction of loops II and III of Fas2. These substitutions could contribute to the ~100-fold lower affinity of Fas2 toward TcAChE compared to mAChE, mainly owing to a difference in the dissociation rate constants of the respective complexes (Z. Radić and G. Amitai, personal communication). Analysis of the Fas2–mAChE structure also revealed a GlcNAc moiety linked to mAChE at Asn-350 (Ser-343 in TcAChE), located ~14 Å away from the Fas2 Pro-30 anchoring point at the gorge entrance (Figures 2, 4, and 5).

Conformational Rearrangements in mAChE upon Binding of Fas2

The binding of Fas2 to mAChE does not induce a dramatic conformational change in the structure of complexed mAChE, when compared with TcAChE (Sussman et al., 1991). Several differences, however, are observed that might be related to conformational rearrangements of mAChE upon binding of Fas2. The first one is a rigid body motion of residues Tyr-341(334) to Ser-399(392), located at the bottom of the gorge entrance, with the largest deviation (up to 2.5 Å for residue Tyr-341) located closer to the top of the entrance (Figure 4B). However, the Asp-74(72) side chain moves in concert, and the hydrogen-bonding distance between the side chains of these two residues is conserved. The second difference between the two structures is a 1–1.5 Å deviation of the Asp-74(72) to Glu-84(82) region of mAChE, relative to its position in TcAChE. This displacement likely results from the tight fit of this region with the Pro-78(76)-binding area on Fas2. Finally, the surface cavity located near Glu-84(82) (and solvent molecule 27 in TcAChE) is enlarged owing to the translational movements of Tyr-341(334) and Asp-74(72), while the dimensions of the active site cavity near Trp-86(84) slightly increases owing to the internal movement of the Trp-439(432) side chain. In the Fas2–mAChE complex, the side chain of mAChE Thr-83(81) constitutes the unique barrier between the two cavities. A small gap between Fas2 loop I and mAChE keeps the surface cavity accessible to the solvent.

The tight packing of loop II of Fas2 at the gorge entrance seems to preclude the entrance of other molecules, even as small as water (Figure 2A). The structure of the Fas2–mAChE complex would suggest that the fasciculin mode of action is occlusion of substrate entry. Such a model, however, is not consistent with kinetic evidence showing that bound Fas2 and Fas3 fail to block completely subsequent organophosphate acylation and trifluoromethylacetophenone conjugation of the active center Ser (Marchot et al., 1993; Radić et al., 1995) and demonstrating the existence of detectable levels (0.1%–5%) of residual catalytic activity toward acetylthiocholine for the fasciculin–AChE complexes (Marchot et al., 1993; Marchot et al., submitted; Radić et al., 1994; 1995; Eastman et al., 1995). Fractional inhibition by fasciculin is even less for larger substrates of lower turnover rates such as p-nitrophenylacetate (Radić et al., 1995).

A similar enigma is encountered for the entry of active-site ligands in crystalline TcAChE, the gorge entrance of which is occluded by a symmetry-related molecule (Harel et al., 1993; Axelsen et al., 1994). Of the five ion pairs involved in the interaction of the gorge rim of TcAChE and the symmetry-related molecule, three residues (Glu-73 to Thr-75 in mAChE, Asp-276 to Asp-283 in mAChE, and Asp-285 to Glu-292 in mAChE) contribute to the Fas2–mAChE interaction and constitute ~20% of the buried interface area of the Fas2–mAChE complex. In addition, loop I of Fas2 resides on the lid of mAChE with Arg-11, extending to interact with mAChE Glu-84(82) and Asn-87(85), residues also conserved in TcAChE (Figure 2B). Both residues belong to the proposed back door region (Ripoll et al., 1993; Axelsen et al., 1994) and are immediate neighbors of Trp-86(84) that stabilizes the quaternary group of the substrate (Gilson et al., 1994). Thus, compatibility between the kinetic data and these new structural results requires either a second portal for both entry of substrates and exit of products in the complex or a conformational change in mAChE, not obvious in the crystal structure, opening a gap between the gorge wall and the bound fasciculin. A discrete shutter-like movement of the

Figure 5. Dimeric Assembly of Monomeric mAChE

Ribbon diagram of the mAChE dimer (blue) with bound Fas2 (yellow) viewed down the crystallographic two-fold axis. The enzyme is devoid of an intersubunit disulfide-linking Cys and is monomeric in solution, but a dimer forms within the crystal. A four-helix bundle is formed by the tight packing of helices $\alpha^3_{7,8}$ and α_{10} (magenta) from each monomer. The amino and carboxyl termini of each monomer are indicated by N and C, respectively. The two gorge entrances are at opposite faces. The GlcNAc moiety linked to Asn-350 (Ser-343 in TcAChE) is displayed in white with colored spheres.

side chain of Thr-83(81), located midway in the channel that we observe between Glu-84(82) and the mAChE active site, could occur simultaneously to the opening of a back door at Trp-86(84).

Dimeric Assembly of Monomeric mAChE

Recombinant mAChE was created by truncation of the carboxyl terminus through an early stop codon at position 549 (541 in TcAChE) and elimination of the intersubunit disulfide-linking Cys of recombinant form mAChE-H. The resulting product is monomeric and devoid of a carboxy-terminal hydrophobic segment (Marchot et al., submitted). Analysis of the Fas2–mAChE complex structure revealed that a homodimer assembles between two symmetry-related molecules in the crystal, arising from the tight packing of helices $\alpha^3_{7,8}$ and α_{10} from each mAChE monomer, which thus form the same four-helix bundle as previously observed for the disulfide-linked dimeric TcAChE (Sussman et al., 1991) (Figure 5). Since in dilute solution dimers were not detected by hydrodynamic and chromatographic analyses, oligomeric assembly of mAChE monomers through hydrophobic interactions outside of the Cys-containing carboxy-terminal segment may be facilitated by the high protein concentration or the high salt concentration in use for crystallization of the Fas2–mAChE complex (or both). However, hydrophobic interactions account for 77% of the 870 Å^2 interface area buried on each of the two mAChE monomers. Similarity of these values with general patterns observed in oligomeric proteins (Janin et al., 1988) suggests that the linking disulfide bridge is not the major determinant for dimer formation.

Significance and Implications

The crystal structure of the Fas2–mAChE complex offers a model for a three-fingered snake toxin in a complex with its specific receptor and reveals several features that are likely to be characteristic of the fasciculins, the α-neurotoxins, and the peptidic muscarinic agonists. First, the tips and exposed side surfaces of the loops govern the specificity of the toxin molecule. Additional segmental flexibility is accorded to these domains, and the φ and ψ bonds between the loop tip and base may serve essentially as joints to effect finger orientation. Second, an interdependence of the loop positions is also critical. In the case of fasciculin, loop I fits in a crevice near the lip of the gorge to maximize the surface area of contact of loop II at the gorge entry, therein serving to buttress the loop position.

Models of the muscarinic receptor, based on the bacteriorhodopsin structure (Henderson and Schertler, 1990), reveal that the seven transmembrane-spanning regions form the outer perimeter of a 20 Å cleft in which agonists and antagonists bind (Nordvall and Hacksell, 1993). Loop II of the muscarinic agonist toxin MTX2 contains the protruding Lys-34 at its tip (Segalas et al., 1995). Its position in the receptor cleft would enable it to interact with Asp-105, a residue found in transmembrane helix 3 and believed to contribute to the interaction sites for the quaternary moiety in ACh (Spalding et al., 1994). Insertion of the longer loop II into the muscarinic cleft could well arise from the appropriate apposition of loop I at a site near the cleft entrance (Segalas et al., 1995). Such a synergy between loops is also likely when the binding site encompasses an interface between two subunits, as for the α-neurotoxin-binding sites on the nicotinic receptor (Blount and Merlie, 1989; Bertrand and Changeux, 1995). Loop III in fasciculin may largely contribute to stabilizing the position in loop II, whereas in the α-neurotoxins it may interact more directly with the nicotinic receptor.

The structure of the fasciculin–AChE complex should enable the systematic design of mutations to ascertain the energetic contributions of the loops to the complex. Moreover, since loop II of fasciculin appears to occlude the entrance of the gorge of the enzyme, coupling of kinetic analyses, mutagenesis of individual residues comprising the interaction surface, and structural studies should prove informative for ascertaining the portal(s) of substrate entry into the complex.

Experimental Procedures

Crystallization and Data Collection

Details on expression and purification of recombinant mAChE and on preparation and crystallization of the Fas2–mAChE complex will be reported elsewhere (Marchot et al., submitted). The Fas2–mAChE complex generated two indistinguishable hexagonal crystal forms, A and B, obtained from identical crystallization conditions, both diffracting up to 2.8 Å. This resolution limit, however, could not be achieved because the crystals could not be flash cooled and were very sensitive to X-ray radiation. All data were therefore collected at 4°C. Form A crystals belong to space group $P6_522$ with cell dimensions a = b = 75.5 Å, c = 556.2 Å, giving a Vm value of 3.1 Å^3/Da (60% solvent; Matthews, 1968) for a single Fas2–mAChE complex in the asymmetric unit. A 3.2 Å resolution data set, which consisted of 62,214 observations for 14,488 unique reflections (85% complete; R_{sym} = 8.9%), was collected from four crystals with a crystal-to-detector distance of 862 mm (λ = 1 Å) and a 10.6° tilt or with a distance of 538 mm (λ = 1.5 Å) and a 12.4° tilt. In the 3.3–3.2 Å resolution range, the data set was 67% complete with an R_{sym} of 21%. Form B crystals also belong to space group $P6_522$ with cell dimensions a = b = 128.4 Å, c = 556.6 Å, giving the same Vm value as form A crystals for three Fas2–mAChE complexes in the asymmetric unit. A 3.5 Å resolution data set, which consisted of 92,846 observations for 33,798 unique reflections (87% complete; R_{sym} = 9.4%), was collected from four crystals with a distance of 757 mm (λ = 1.15 Å) and a 10° tilt. Data were collected at beam line X12C of the National Synchrotron Light Source with a MarResearch imaging plate detector and were processed with DENZO and SCALEPACK (Otwinowski, 1993).

Structure Solution and Refinement

Initial phases for the form A crystal data set were obtained by the molecular replacement method using the TcAChE model (PDB code, 1ACE) as a search model with the AMoRe program package (Navaza, 1994). The positioned mAChE (correlation = 51%; R factor = 41% in the 15 Å to 4 Å resolution range) was refined with X-PLOR (Brünger et al., 1987), which gave an R factor of 26% and a free R factor of 39% (5% of the reflections) in the 10 Å to 3.2 Å resolution range. The mAChE model was manually fitted, and a poly-Ala model corresponding to Fas2 was built into σ_A weighting electron density maps (Read, 1986) with the graphics program XFIT (McRee, 1992) and a modified version of TURBO-FRODO (Roussel and Cambillau, 1989; A. G. Inisan, A. Roussel, and C. Cambillau, personal communication). Subsequent refinements were performed alternating with model building until a 40 residue poly-Ala model, consisting of five segments, was obtained. Superimposition of Fas2 (PDB code, 1FSC) with the model revealed an orientation based on the position of the four disulfide bridges and the side chains of Tyr-27 and Tyr-61, together with the directions of loops I and II. This overlapped model was refined by rigid body motion in the 10 Å to 3.2 Å resolution range after removal of loops I and II, suspected of high flexibility, from Fas2. Successive

rounds of rebuilding and simulated annealing refinement allowed complete interpretation of both the Fas2 and mAChE structures. X-PLOR omit maps were used from the final model to check systematically every part of Fas2 and of the mAChE regions bound to Fas2: five and ten residues of the structures of Fas2 and mAChE, respectively, were deleted in each calculation, and simulated annealing was used to reduce model bias in the omit maps. The final model (model A, described herein) has a R factor of 18.4% for 13,823 reflections (all data) between 10 Å and 3.2 Å resolution and a free R factor of 29.4%. High temperature factors and weak electron density include mAChE residues Pro-492(485) to Pro-498. Fas2 residue Lys-51 and mAChE residues Arg-13(11), Arg-45(43), Arg-253(250), Arg-364(357), Arg-470(463), and Arg-493(486) are truncated to Cβ. The overall deviations from ideal geometry are 0.007 Å for bond distances and 1.5° for bond angles. The stereochemistry of the model was analyzed with PROCHECK (Laskowski et al., 1993), and 80% of the polypeptide backbone dihedral angles were found to lie in the most favored regions of the Ramachandran diagram. The coordinates of model A will be deposited with the Brookhaven Protein Data Bank.

The structure of form B was determined by molecular replacement with the AMoRe program using the refined model A. For three Fas2–mAChE complexes in the asymmetric unit, the correlation and R factors were 70% and 39%, respectively, in the 15 Å to 4 Å resolution range. Successive rounds of refitting were followed by refinement cycles. The final model (model B) has an R factor of 20.8% for 29,167 reflections (all data) in the 10 Å to 3.5 Å resolution range and a free R factor of 32.2%. The overall deviations from ideal geometry are 0.01 Å for bond distances and 1.7° for bond angles. Model B is essentially identical with model A and is not described herein.

Acknowledgments

Y. B. is a visiting scientist from the Laboratoire de Cristallisation et Cristallographie des Macromolécules Biologiques, Centre National de la Recherche Scientifique (CNRS), Institut Fédératif de Recherche Concertée, Marseille, France, and P. M. is a visiting scientist from the Laboratoire de Biochimie, CNRS, Univèrsité d'Aix-Marseille 2, Marseille, France. We are particularly indebted to Dr. Joel L. Sussman for encouragement and enthusiastic support of data collection at the National Synchrotron Light Source (NSLS), to Dr. Robert M. Sweet for access to the NSLS beam line X12C, and to Dr. John A. Tainer for liberal use of the facilities in his laboratory and for critical reading of the manuscript. We thank Dr. Zoran Radić for helpful discussions and details on unpublished kinetic data and Drs. Anne Gaël Inisan, Alain Roussel, and Christian Cambillau for the modified version of program TURBO-FRODO. This work was supported by United States Public Health Service GM18360 and Department of Army Medical Defense 17C grants to P. T. Drs. Michal Harel, Israel Silman, and Joel Sussman have independently developed a solution of the Fas2–TcAChE crystalline complex. A joint comparison of the coordinates of the two complexes should yield important information on the residue contributions to complex formation and conformation.

Received October 3, 1995; revised October 17, 1995.

References

Adem, A., Asblom, A., Johansson, G., Mbugua, P.M., and Karlsson, E. (1988). Toxins from the venom of the green mamba *Dendroaspis angusticeps* that inhibit the binding of quinuclidinylbenzylate to muscarinic acetylcholine receptors. Biochem. Biophys. Acta *968*, 340–345.

Axelsen, P.H., Harel, M., Silman, I., and Sussman, J.L. (1994). Structure and dynamics of the active site gorge of acetylcholinesterase: synergistic use of molecular dynamic simulation and X-ray crystallography. Protein Sci. *3*, 188–197.

Barak, D., Kronman, C., Ordentlich, A., Ariel, N., Bromberg, A., Marcus, D., Lazar, A., Velan, B., and Shafferman, A. (1994). Acetylcholinesterase peripheral anionic site degeneracy conferred by amino acid arrays sharing a common core. J. Biol. Chem. *264*, 6296–6305.

Bertrand, D., and Changeux, J.P. (1995). Nicotinic receptor: an allosteric protein specialized for intercellular communication. Neurosciences *7*, 75–90.

Blount, P., and Merlie, J. (1989). Molecular basis of the two nonequivalent ligand-binding sites of the muscle nicotinic acetylcholine receptor. Neuron *3*, 349–357.

Brown, L.R., and Wüthrich, K. (1992). Nuclear magnetic resonance solution structure of the α-neurotoxin from the black mamba (*Dendroaspis polylepis polylepis*). J. Mol. Biol. *227*, 1118–1135.

Brünger, A.T., Kuriyan, J., and Karplus, M. (1987). Crystallographic R-factor refinement by molecular dynamics. Science *235*, 458–460.

Cerveñansky, C., Dajas, F., Harvey, A.L., and Karlsson, E. (1991). Fasciculins, anticholinesterase toxins from mamba venoms: biochemistry and pharmacology. In Snake Toxins, A.L. Harvey, ed. (New York: Pergamon Press), pp. 303–321.

Cerveñansky, C., Engström, A., and Karlsson, E. (1994). Study of structure–activity relationship of fasciculin by acetylation of amino groups. Biochem. Biophys. Acta *1199*, 1–5.

Cerveñansky, C., Engström, A., and Karlsson, E. (1995). Role of arginine residues for the activity of fasciculin. Eur. J. Biochem. *229*, 270–275.

Changeux, J.P., Kasai, M., and Lee, C.Y. (1970). The use of a snake venom toxin to characterize the cholinergic receptor protein. Proc. Natl. Acad. Sci. USA *67*, 1241–1247.

Cygler, M., Schrag, J., Sussman, J.L., Harel, M., Silman, I., Gentry, M.K., and Doctor, B.P. (1993). Relationship between sequence conservation and three-dimensional structure in a large family of esterases, lipases, and related proteins. Protein Sci. *2*, 366–382.

Duran, R., Cerveñansky, C., Dajas, F., and Tipton, K.F. (1994). Fasciculin inhibition of acetylcholinesterase is prevented by chemical modification of the enzyme at a peripheral site. Biochem. Biophys. Acta *1201*, 381–388.

Eastman, J., Wilson, E.J., Cerveñansky, C., and Rosenberry, T.L. (1995). Fasciculin 2 binds to the peripheral site on acetylcholinesterase and inhibits substrate hydrolysis by slowing a step involving proton transfer during enzyme acylation. J. Biol. Chem. *270*, 19694–19701.

Endo, T., and Tamiya, N. (1991). Structure–function relationship of postsynaptic neurotoxins from snake venoms. In Snake Toxins, A.L. Harvey, ed. (New York: Pergamon Press), pp. 165–222.

Gilson, M.K., Straatsma, T.P., McCammon, J.A., Ripoll, D.R., Faerman, C.H., Axelsen, P.H., Silman, I., and Sussman, J.L. (1994). Open "back door" in a molecular dynamics simulation of acetylcholinesterase. Science *263*, 1276–1278.

Grochulski, P., Li, Y., Schrag, J.D., and Cygler, M. (1994). Two conformation states of *Candida rugosa* lipase. Protein Sci. *3*, 82–91.

Harel, M., Sussman, J.L., Krejci, E., Bon, S., Chanal, P., Massoulié, J., and Silman, I. (1992). Conversion of acetylcholinesterase to butyrylcholinesterase: modeling and mutagenesis. Proc. Natl. Acad. Sci. USA *89*, 10827–10831.

Harel, M., Schalk, I., Ehret-Sabatier, L., Bouet, F., Goeldner, M., Hirth, C., Axelsen, P.H., Silman, I., and Sussman, J.L. (1993). Quaternary ligand binding to aromatic residues in the active-site gorge of acetylcholinesterase. Proc. Natl. Acad. Sci. USA *90*, 9031–9035.

Henderson, R., and Schertler, G.F.X. (1990). The structure of bacteriorhodopsin and its relevance to the visual opsins and other seven-helix G-protein coupled receptors. Phil. Trans. R. Soc. (Lond.) B *326*, 379–389.

Janin, J., and Chothia, C. (1990). The structure of protein–protein recognition sites. J. Biol. Chem. *265*, 16027–16030.

Janin, J., Miller, S., and Chothia, C.H. (1988). Surface, subunit interfaces and interior of oligomeric proteins. J. Mol. Biol. *204*, 155–164.

Karlsson, E., Mbugua, P.M., and Rodriguez-Ithurralde, D. (1984). Fasciculins, anticholinesterase toxins from the venom of the green mamba *Dendroaspis angusticeps*. J. Physiol. *79*, 232–240.

Laskowski, R.A., MacArthur, M.W., Moss, D.S., and Thornton, J.M. (1993). PROCHEK: a program to check the stereochemical quality of protein structures. J. Appl. Cryst. *26*, 283–291.

Le Du, M.H., Marchot, P., Bougis, P.E., and Fontecilla-Camps, J.C. (1992). 1.9 Å resolution structure of fasciculin 1, an anti-cholinesterase toxin from green mamba snake venom. J. Biol. Chem. *267*, 22122–22130.

Le Du, M.H., Housset, D., Marchot, P., Bougis, P.E., Navaza, J., and Fontecilla-Camps, J.C. (1995). Crystal structure of fasciculin 2 from mamba snake venom: evidence for unusual loop flexibility. Acta Crystallogr., in press.

Lin, W.W., Lee, C.Y., Carlsson, F.H.H., and Joubert, F.J. (1987). Anticholinesterase activity of angusticeps-type toxins and protease inhibitor homologues from mamba venoms. Asia Pac. J. Pharmacol. *2*, 79–85.

Marchot, P., Khélif, A., Ji, Y.H., Mansuelle, P., and Bougis, P.E. (1993). Binding of ^{125}I-fasciculin to rat brain acetylcholinesterase: the complex still binds diisopropyl fluorophosphate. J. Biol. Chem. *268*, 12458–12467.

Massoulié, J., Pezzementi, L., Bon, S., Krejci, E., and Vallette, F.M. (1993). Molecular and cellular biology of the cholinesterases. Prog. Neurobiol. *41*, 31–91.

Matthews, B.W. (1968). Solvent content of protein crystals. J. Mol. Biol. *33*, 491–497.

McRee, D.E. (1992). A visual protein crystallographic software system for X11/Xview. J. Mol. Graph. *10*, 44–47.

Navaza, J. (1994). AMoRe: an automated package for molecular replacement. Acta Crystallogr. *A50*, 157–163.

Nordvall, G., and Hacksell, U. (1993). Binding-site modeling of the muscarinic m1 receptor: a combination of homology-based and direct approaches. J. Med. Chem. *36*, 967–976.

Ordentlich, A., Barak, D., Kronman, C., Flashner, Y., Leitner, M., Segall, Y., Ariel, N., Cohen, S., Velan, B., and Shafferman, A. (1993). Dissection of the human acetylcholinesterase active center determinants of substrate specificity. J. Biol. Chem. *268*, 17083–17095.

Otwinowski, Z. (1993). Oscillation data reduction program. In Proceedings of the CCP4 Study Weekend, L. Sawyer, N. Isaacs, and S. Burley, eds. (Warrington, England: Science and Engineering Research Council/Daresbury Laboratory), pp. 56–62.

Rachinsky, T.L., Camp, S., Li, Y., Ekström, J., Newton, M., and Taylor, P. (1990). Molecular cloning of mouse acetylcholinesterase: tissue distribution of alternatively spliced mRNA species. Neuron *5*, 317–327.

Radić, Z., Pickering, N.A., Vellom, D.C., Camp, S., and Taylor, P. (1993). Three distinct domains in the cholinesterase molecule confer selectivity for acetyl- and butyrylcholinesterase inhibitors. Biochemistry *32*, 12074–12084.

Radić, Z., Duran, R., Vellom, D.C., Li, Y., Cerveñansky, C., and Taylor, P. (1994). Site of fasciculin interaction with acetylcholinesterase. J. Biol. Chem. *269*, 11233–11239.

Radić, Z., Quinn, D.M., Vellom, D.C., Camp, S., and Taylor, P. (1995). Allosteric control of acetylcholinesterase catalysis by fasciculin. J. Biol. Chem. *270*, 20391–20399.

Read, R.J. (1986). Improved Fourier coefficients for maps using phase from partial structure with errors. Acta Crystallogr. *A42*, 140–149.

Rees, B., and Bilwes, A. (1993). Three-dimensional structure of neurotoxins and cardiotoxins. Chem. Res. Toxicol. *6*, 385–406.

Ripoll, D.R., Faerman, C.H., Axelsen, P.H., Silman, I., and Sussman, J.L. (1993). An electrostatic mechanism for substrate guidance down the aromatic gorge of acetylcholinesterase. Proc. Natl. Acad. Sci. USA *90*, 5128–5132.

Roussel, A., and Cambillau, C. (1989). TURBO-FRODO. In Silicon Graphics Geometry Partners Directory, Silicon Graphics Committee, eds. (Mountain View, California: Silicon Graphics), pp 77–78.

Segalas, I., Roumestand, C., Zinn-Justin, S., Gilquin, B., Ménez, R., Ménez, A., and Toma, F. (1995). Solution structure of a green mamba toxin that activates muscarinic acetylcholine receptors, as studied by nuclear magnetic resonance and molecular modeling. Biochemistry *34*, 1248–1260.

Shafferman, A., Velan, B., Ordentlich, A., Kronman, C., Grosfeld, H., Leitner, M., Flashner, Y., Cohen, S., Barak, D., and Ariel, N. (1992). Substrate inhibition of acetylcholinesterase: residues affecting signal transduction from the surface to the catalytic center. EMBO J. *11*, 3561–3568.

Shafferman, A., Ordentlich, A., Barak, D., Kronman, C., Ber, R., Bino, T., Ariel, N., Osman, R., and Velan, B. (1994). Electrostatic attraction by surface charge does not contribute to the catalytic efficiency of acetylcholinesterase. EMBO J. *13*, 3448–3455.

Spalding, T.A., Birdsall, N.J.M., Curtis, C.A.M., and Hulme, E.C. (1994). Acetylcholine mustard labels the binding site aspartate in muscarinic acetylcholine receptors. J. Biol. Chem. *269*, 4092–4097.

Strydom, D.J. (1972). Snake venom toxins: the amino acid sequences of two toxins from *Dendroaspis polylepis polylepis* (black mamba) venom. J. Biol. Chem. *247*, 4029–4042.

Sussman, J.L., Harel, M., Frolow, F., Oefner, C., Goldman, A., Toker, L., and Silman, I. (1991). Atomic structure of acetylcholinesterase from *Torpedo californica*: a prototypic acetylcholine-binding protein. Science *253*, 872–879.

Tan, R.C., Truong, T.N., McCammon, J.A., and Sussman, J.L. (1993). Acetylcholinesterase: electrostatic steering increases the rate of ligand binding. Biochemistry *32*, 401–403.

Taylor, P., and Radić, Z. (1994). The cholinesterases: from genes to proteins. Annu. Rev. Pharmacol. Toxicol. *34*, 281–320.

van den Born, H.K.L., Radić, Z., Marchot, P., Taylor, P., and Tsigelny, I. (1995). Theoretical analysis of the structure of the peptide fasciculin and its docking to acetylcholinesterase. Protein Sci. *4*, 703–715.

Protein Science (1995), *4*:703–715. Cambridge University Press. Printed in the USA.

Theoretical analysis of the structure of the peptide fasciculin and its docking to acetylcholinesterase

HARALD K.L. VAN DEN BORN,[1,3] ZORAN RADIĆ,[1,5] PASCALE MARCHOT,[1,4] PALMER TAYLOR,[1] AND IGOR TSIGELNY[1,2]

[1] Department of Pharmacology, University of California at San Diego, La Jolla, California 92093-0636
[2] Department of Chemistry and Biochemistry, University of California at San Diego, La Jolla, California 92093-0636

(RECEIVED December 5, 1994; ACCEPTED January 20, 1995)

Abstract

The fasciculins are a family of closely related peptides that are isolated from the venom of mambas and exert their toxic action by inhibiting acetylcholinesterase (AChE). Fasciculins belong to the structural family of three-fingered toxins from Elapidae snake venoms, which include the α-neurotoxins that block the nicotinic acetylcholine receptor and the cardiotoxins that interact with cell membranes. The features unique to the known primary and tertiary structures of the fasciculin molecule were analyzed. Loop I contains an arginine at position 11, which is found only in the fasciculins and could form a pivotal anchoring point to AChE. Loop II contains five cationic residues near its tip, which are partly charge-compensated by anionic side chains in loop III. By contrast, the other three-fingered toxins show full charge compensation within loop II. The interaction of fasciculin with the recognition site on acetylcholinesterase was investigated by estimating a precollision orientation followed by determination of the buried surface area of the most probable complexes formed, the electrostatic field contours, and the detailed topography of the interaction surface. This approach has led to testable models for the orientation and site of bound fasciculin.

Keywords: acetylcholinesterase; elapid peptides; electrostatic fields; fasciculin; snake toxins

The fasciculins are 6,800-Da peptides found in the venom of snakes from the mamba family. The isolated peptides have been shown to be potent inhibitors of acetylcholinesterase (AChE) (Karlsson et al., 1984). Four fasciculins have been described to date: fasciculin 1 (Fas1) and fasciculin 2 (Fas2) from *Dendroaspis angusticeps* (eastern green mamba), toxin C from *Dendroaspis polylepis* (black mamba), and fasciculin 3 (Fas3) from *Dendroaspis viridis*. Their primary structures are known (Karlsson et al., 1985). Fas3 and toxin C were found to have identical primary structures (Marchot et al., 1993). All three fasciculin structures contain 61 amino acids and differ only by one to three residues. So far only the crystal structure of Fas1 has been solved (Kinemage 1; le Du et al., 1992). These peptides fall into a larger family of small three-fingered peptide toxins from Elapidae snake venoms; other members of this family are the cardiotoxins, which interact with cell membranes, and the α-neurotoxins, such as erabutoxin (Ebt) and α-bungarotoxin (Bgt), which are antagonists at the acetylcholine receptor (Karlsson et al., 1984; Endo & Tamiya, 1991).

The fasciculins inhibit AChE of mammals and fish with dissociation constants between 0.4 and 100 pM; the fasciculin–AChE complex, as measured with Fas1 and Fas3, has an extremely slow rate of dissociation, with half times of several hours. Fasciculins are also selective in their action because avian, insect, and snake AChEs are relatively resistant to them and micromolar concentrations are required to inhibit butyrylcholinesterases (BuChEs) from mammals (Karlsson et al., 1984; Cervenansky et al., 1991; Radić et al., 1994). Fas1 and Fas2 have nearly equivalent dissociation constants, whereas Fas3 has a 10-fold lower dissociation constant for rat brain AChE (Marchot et al., 1993).

Recent studies show that Fas3 binds to diisopropylfluorophosphate (DFP)-inhibited enzyme, and that DFP can still enter the active center gorge of the Fas3–AChE complex (Marchot et al., 1993). Moreover, peripheral site inhibitors such as propidium (Taylor & Lappi, 1975), and not active center inhibitors, are competitive with the binding of fasciculins (Karlsson et al., 1984; Marchot et al., 1993). Thus, fasciculin appears to influence AChE catalysis in an allosteric fashion. Indeed, modification of residues residing at the rim of the active center gorge and not residues at the substrate binding site markedly influences fas-

Reprint requests to: Igor Tsigelny, Department of Chemistry and Biochemistry, 0654, University of California at San Diego, 9500 Gilman Drive, La Jolla, California 92093-0654; e-mail: itsigeln@ucsd.edu.

[3] Visiting Scholar, Utrecht University, Faculty of Pharmacy, Utrecht, The Netherlands.

[4] Visiting Scholar, CNRS Unité de Recherche Associée 1455, Université d'Aix-Marseille II, Faculté de Médecine Secteur Nord, Marseille, France.

[5] Visiting Scholar, Institute for Medical Research and Occupational Health, University of Zagreb, Croatia.

ciculin binding (Radić et al., 1994). Hence, fasciculin inhibition could arise both from a gating influence, therein restricting substrate entry into active center gorge and from exerting allosteric control over the commitment to catalysis of the bound substrate.

The availability of the three-dimensional structure of AChE from *Torpedo californica* (Sussman et al., 1991) provides the first structure of the target site for the family of three-fingered Elapidae toxins and has prompted renewed interest in studying the highly selective interactions between this family of toxins and their binding sites. In this study we detail the structure of the fasciculins in relation to related toxins in order to delineate features responsible for their specificity for the AChEs. Secondly, we analyze fasciculin interaction with the peripheral site on AChE by procedures that initially establish a precollision orientation and subsequently analyze probable complexes on the bases of electrostatic forces, surface area of contact, and surface topography of the respective molecules.

Results

Electrostatic properties of the toxins deduced from their three-dimensional structures

Internal structure stabilization

The complete structural maps of Fas1 (le Du et al., 1992) and Ebt-b (Smith et al., 1988) obtained from their crystal coordinates are presented in Figure 1A and B. Figure 1C and D shows only the regions of Fas2 and Fas3 that differ from Fas1. The overall folding of fasciculins as shared with other toxins mainly consists of three loops forming a large and flat triple-stranded antiparallel β-sheet (Kinemage 1; le Du et al., 1992; Pillet et al., 1993). In Fas1 the β-sheet is formed by residues Cys 22–Arg 27, Val 34–Cys 39, and Leu 48–Cys 53. Formally Cys 3–Cys 4 and Leu 14–Thr 15 also form a β-strand. Loop I consists of residues 5–15, loop II of residues 24–38 and loop III of residues 43–50 (le Du et al., 1992).

Fasciculin 1. The vast majority of residues of Fas1 are solvent accessible. Only two, the disulfide-linked Cys 3 and Cys 22, show no solvent accessibility. Several residues (Tyr 4, Leu 14, Tyr 23, Arg 37, Leu 48) are only partly solvent accessible. Several of these residues located in homologous positions on other toxins are less accessible. Virtually all potentially charged residues in this family of toxins are fully accessible to solvent; only Arg 37 is partly accessible.

Initial observations of the three-dimensional structure of Fas1 reveal the following distribution of charged residues (Kinemage 1). The electrostatic fields produced by the cationic side chains of Arg 11, Lys 25, Arg 27, and the anionic side chains of Asp 45 and Asp 46 are located on a common surface area of the molecule. This confers a small overall positive charge to this side. The cationic side chains of Arg 24, Arg 37, Lys 51, Lys 58, the obliquely oriented side chains of Arg 28 and Lys 32, and the negatively charged side chains of Asp 57, Glu 49, and carboxyl-terminus of Tyr 61 are located on the opposite surface of the molecule. Cationic residues Arg 27, Arg 28, and Lys 32 are located at the tip of loop II, whereas anionic Glu 19 and positive amino-terminus of Thr 1 reside on the opposite end of the molecule.

There are three significant clusters of hydrophobic residues in this molecule: (1) a cluster that contains Pro 42, Pro 43, and Val 50 of loop III and Tyr 23 of loop II; (2) a cluster that contains Leu 48 and Tyr 47 of loop III, the hydrophobic portion of the side chains of Arg 27, and Leu 35 of loop II; (3) a cluster formed by Tyr 4 and Leu 14 of loop I, and the hydrophobic parts of the side chains of Lys 58 and Tyr 61 located in the area of the disulfide core of the molecule. This system of hydrophobic clusters likely stabilizes the overall structure of the fasciculin molecule, as found for other toxins (Fig. 1B).

Salt bridges formed between positively charged residues of loop II and negatively charged residues of loop III constrain these loops significantly in Fas1; such strong electrostatic constraints do not occur in the α-neurotoxins, Ebt, Bgt, α-cobratoxin (Cbt), and in cardiotoxin V_4^{II} (Cdt). Those bridges impart additional rigidity to the fasciculin molecule loops when compared with the homologous α-neurotoxins.

Fasciculin 2. Fas1 and Fas2 differ by single substitution Tyr 47 Asn. This difference does not affect the rigidity of the fasciculin molecule because all of the strong electrostatic constraints between loop II and loop III are maintained in the presence of the Asn residue (Fig. 1C).

Fasciculin 3. In Fas3 two additional charges appear in loop I: Lys 15 and Asp 16 (Fig. 1D). These are significant modifications because Arg 11 is the lone positive charge in this area for Fas1 and Fas2. In the minimized structure of Fas3 Lys 15 is not linked by any salt bridge to other residues. This imparts an additional density of positive charges in the loop I area. The negative charge on Asp 16 is mostly compensated by the amino-terminus strengthening rigidity of loop I together with an additional (Ile 2–Leu 14) hydrophobic interaction. Because Fas3 has an order of magnitude higher affinity than Fas1 for rat brain AChE (Marchot et al., 1993), this positively charged area of loop I is presumed to contribute substantially to the stabilization energy for Fas3 binding to AChE.

Structural bases of functional properties

To determine the structural features in the fasciculin molecule that contribute to its mode of action, we compared the three-dimensional structures of the fasciculins to those of α-neurotoxins, which are antagonists at the nicotinic receptor: Cbt, Bgt, Ebt (Fig. 1B), and to that of Cdt. Fas1 shows substantive differences at the following positions.

Loop I. Conservation of Arg 11 is a feature unique to the fasciculins. Only four α-neurotoxins out of a family of 104 have a positively charged residue in this position, but two of them have a neighboring negative residue yielding charge compensation (Endo & Tamiya, 1987). Several α-neurotoxins (19 out of 104) have a negatively charged residue in this position. The maps of toxins shown in Figure 1 reveal the uniqueness of Arg 11, contributing to the exposed positive charge of its loop I to the electrostatic profile of fasciculin. Similar positive residues are not found in Bgt and Ebt (Fig. 1B). The uncompensated positively charged residue Lys 15 of Bgt and Ebt is located much closer to the base of loop I and to the amino-terminal positive residue Thr 1. Accordingly, it does not change significantly the electrostatic profile in the area of the amino-terminal residues. Lys is the most common residue for α-neurotoxins in position 15. A far smaller number of α-neurotoxins (12 of 104) have a positively

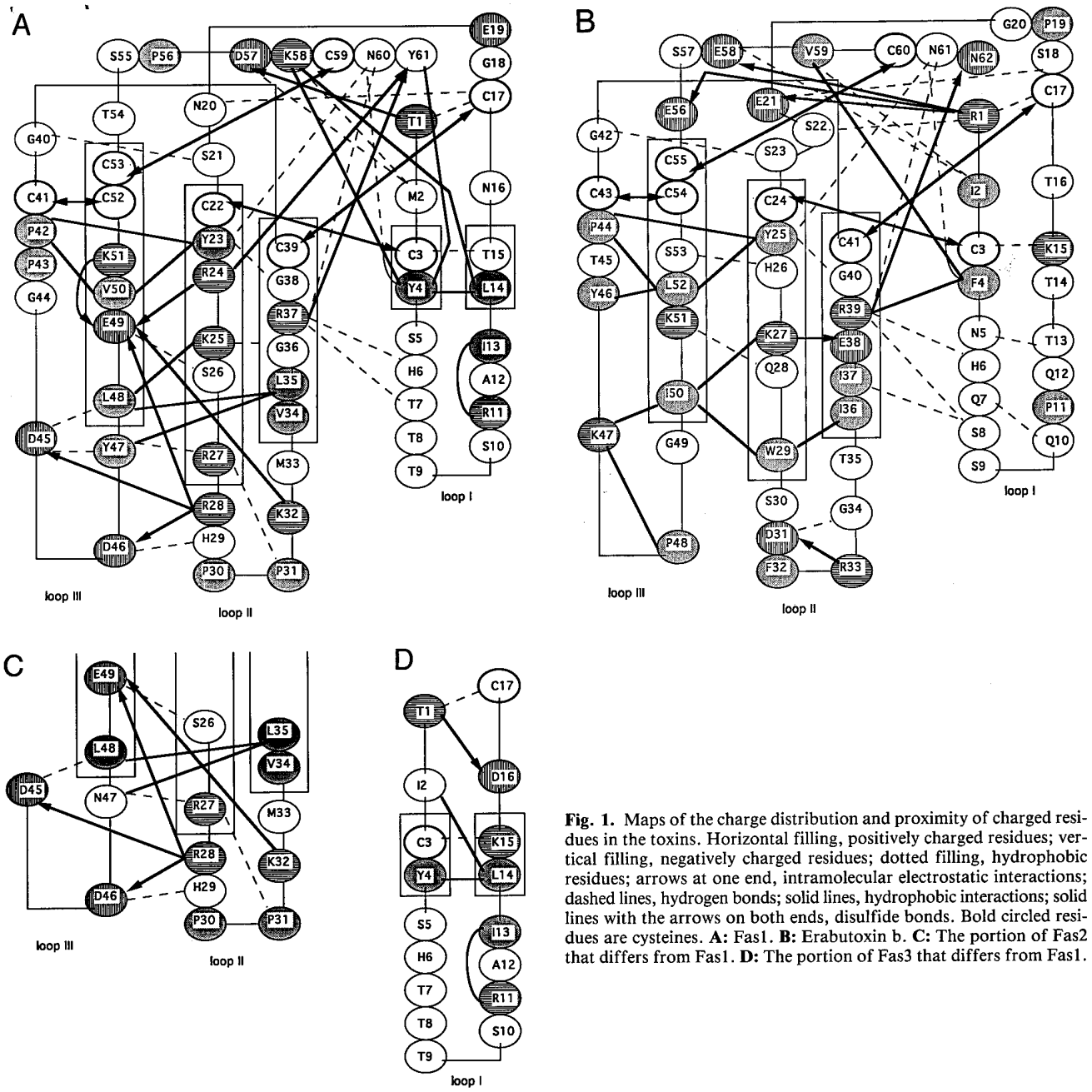

Fig. 1. Maps of the charge distribution and proximity of charged residues in the toxins. Horizontal filling, positively charged residues; vertical filling, negatively charged residues; dotted filling, hydrophobic residues; arrows at one end, intramolecular electrostatic interactions; dashed lines, hydrogen bonds; solid lines, hydrophobic interactions; solid lines with the arrows on both ends, disulfide bonds. Bold circled residues are cysteines. **A:** Fas1. **B:** Erabutoxin b. **C:** The portion of Fas2 that differs from Fas1. **D:** The portion of Fas3 that differs from Fas1.

charged residue in position 13. In Cbt, the positively charged Lys 12 is compensated by negative Asp 13, and the electrostatic field only influences the very amino-terminal residues Ile 1 and Arg 2. These differences cause significant changes in electrostatic field distribution between the fasciculins and the α-neurotoxins (Fig. 2). The specific positioning of positive residues Lys 12 and Lys 5 in Cdt differs from Cbt, Ebt, and Bgt, and confers to loop I an electrostatic profile closer to that of fasciculin.

Loop II. The noteworthy feature of loop II in the fasciculin molecule is the presence of six positively charged residues: Arg 24, Lys 25, Arg 27, Arg 28, Lys 32, and Arg 37. Two of them, Lys 25 and Arg 27, are weakly compensated. Nevertheless, these residues are positioned to have the nearest opposite charge neighbor at the distance about 8 Å. The closest negatively charged residue to Arg 11 is more than 21 Å away. In this arrangement the charge on Arg 11 is more likely to interact with a distant charge on AChE than would the charges on Lys 25 and Arg 27. The difference between energies of interaction with AChE of the uncompensated charge and dipole are significant at the distance of 20 Å. These considerations point to an uncompensated charge of Arg 11 from loop I playing the more significant role in fasciculin docking to the surface of AChE. Other toxins have much smaller differences in charges between loops. In Ebt (Figs. 1B, 2B) the charges of polar residues are compensated, creating pairs of opposite charged residues within the

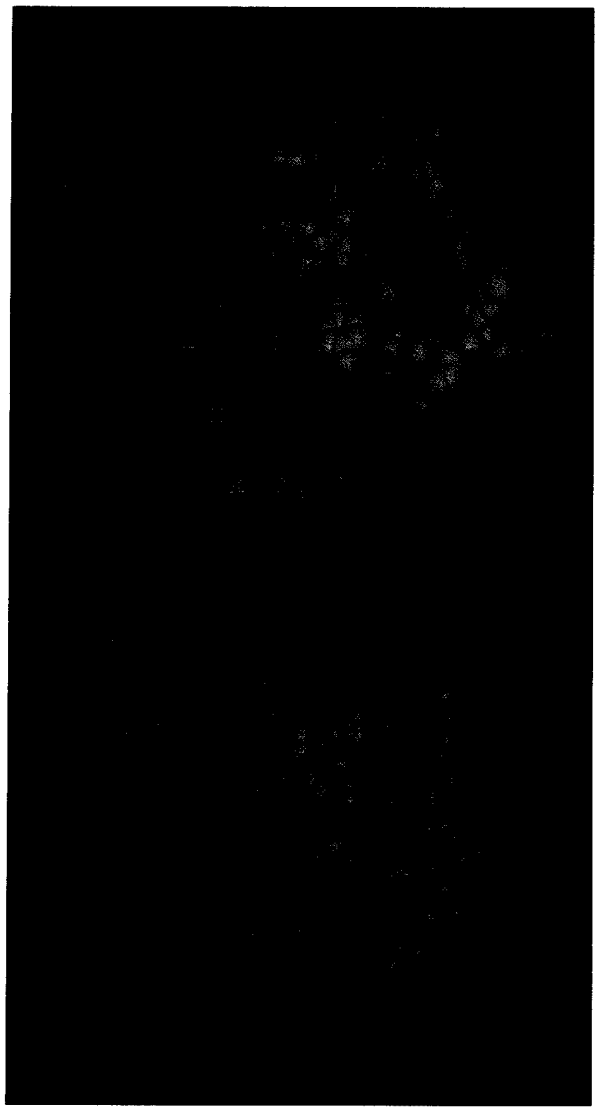

Fig. 2. Electrostatic isopotential surfaces superimposed with the CPK model (gray spheres) of toxins. The red surface corresponds to the isopotential contour -1 kT/e, and the blue surface corresponds to the isopotential contour $+1$ kT/e, where k is the Boltzmann constant, T is temperature, and e is the electronic charge. In the upper right quadrant is shown the α-carbon structure oriented with the CPK model. **A:** Fasciculin 1. **B:** Erabutoxin b.

loop: Asp 31–Arg 33, Lys 27–Glu 38. The residue Arg 39 is partly compensated by the carboxyl-terminal charge, and as a result, the overall charge of this loop in Ebt is smaller. A similar situation exists in Bgt where compensating pairs are created: Asp 30–Arg 36 and Arg 25–Glu 56, whereas Glu 41 and Lys 26 are not close enough for charge compensation. The overall positive charge of loop II is mainly due to uncompensated Lys 38. In Cbt, loop II contains four cationic residues and two anionic residues, which makes its overall charge positive. Cdt has a distribution of positive charges close to fasciculin, but the position of uncompensated cationic residues, Lys 29 and Lys 30, at the tip of loop II makes it possible for this loop to play a significant role in the binding of this toxin.

Some of the positive charges in loop II are not specific to fasciculin: Arg 24 (represented by Arg 25 in α-Bgt and by Lys 23 in Cdt) and Lys 25 (represented by Lys 26 in α-Bgt and by Lys 27 in Ebt). The short neurotoxins of 60–62 amino acids (Karlsson, 1984; Endo & Tamiya, 1987) often have both of these positive charges on positions 24 and 25. For Ebt, Lys 27 was proposed to be at the receptor binding site (Faure et al., 1983; Martin et al., 1983; Pillet et al., 1993). Arg 37 is common to many toxins represented as Arg 39 in Ebt and Arg 36 in Cdt (Rees et al., 1990). However, the following residues are unique to the fasciculins:

Arg 27: The majority of short α-neurotoxins, Ebt (residue 29), Cbt (residue 25), and long neurotoxin α-Bgt (residue 28) have a Trp residue at this position. Trp is conserved as a part of a β-strand and is also thought to be involved in the binding of the these toxins to the nicotinic receptor (Faure et al., 1983; Pillet et al., 1993).

Arg 28: Although present in 23 of 104 three-fingered toxins (Endo & Tamiya, 1987), this positive charge in all fasciculins is immediately compensated by the highly conserved neighboring residue, Asp 46 from loop III.

Phe 31 in fasciculins is substituted in many α-neurotoxins for a positively charged residue (Arg 33 in Ebt, Arg 33 in Cbt, Lys 30 in Cdt). A possible role for this residue in α-neurotoxins is to create a specific electrostatic profile selective for the nicotinic acetylcholine receptor (nAChR) binding site.

Lys 32 is present only in fasciculins. Although no other toxin has a positive charge in this position, many contain a positive residue at position 33 or 34.

Loop III. This loop in the fasciculins has unique characteristics due to two negatively charged neighbors Asp 45 and Asp 46. Instead of Asp 45 most α-neurotoxins have a positive charge in the corresponding position (Lys 49 in Cbt, Lys 47 in Ebt, Lys 52 in Bgt). Only 9 of 106 members of the three-fingered toxin group have a negatively charged residue in this area. Only the fasciculins have a negative charge at position 46. Also, no short α-neurotoxin has a negative charge in position 49 (Glu 49 in Fas), although about 30% of long α-neurotoxins have negatively charged residues close to this position (Asp 53 in Cbt, Glu 56 in α-Bgt).

Lys 51 appears less important to specificity. About 5 three-fingered toxins have the negatively charged group in the closest position (equivalent to 51 in Fas), whereas 30 of 104 toxins have a positively charged residue in this position (Endo & Tamiya, 1987).

Precollision orientations of Fas1 and AChE

The most favorable electrostatic energies of intermolecular interaction for almost all rotational orientations of Fas1 (lowest in the free energy profile) are found in the sectors of orbits (Fig. 3): circles 1, 2, and 5 from $-45°$ to $45°$; circles 3 and 4 from $0°$ to $90°$. This first step of selection gave a significant reduction in the number of possible bound conformations of Fas1.

Rotational conformers that minimize electrostatic energy were selected more precisely in the next step. The highest energy levels occur when charges of the same sign come in close apposition to each other, and the lowest occur when these charges are distant and the opposite charges are proximal. Table 1 shows the most favorable rotational positions of Fas1 in a precollision

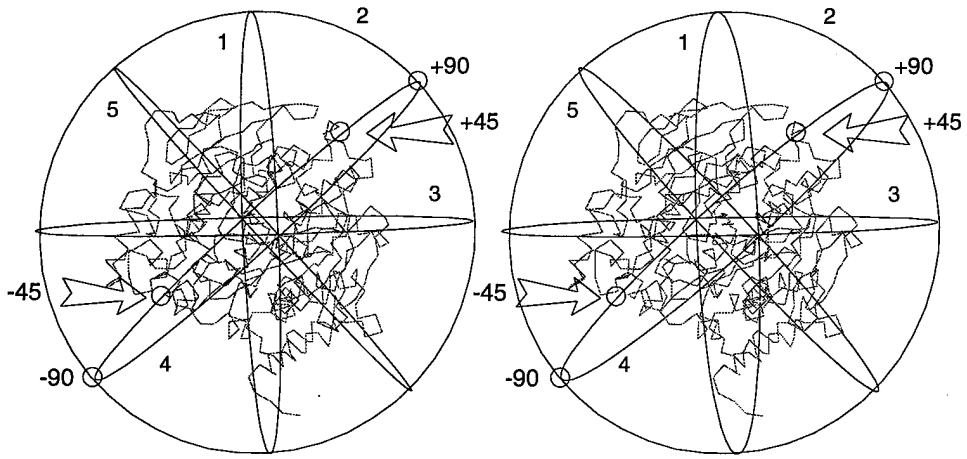

Fig. 3. Stereo view of five circular tracks along which the Fas1 molecule was moved across the acetylcholinesterase surface for evaluating intermolecular electrostatic energy. Shown is the AChE orientation with a central axis perpendicular to the plane of the paper, entering the active center gorge.

orientation to AChE. The main low-energy positions are *X*, *Z* and *Y*, *X*, which occur in all circles. We also included other low energy positions for further investigation: *Y*, $-Z$; *Y*, $-X$; *Z*, $-Y$; $-Y$, *Z*. The chosen positions (Table 1) were further investigated with the addition of five rotational Fas positions to increase the overall number of investigated positions to 15. To avoid overlooking of possible positions generally due to the digital increments of angles, only the very high energy positions were eliminated. The selected positions were investigated with 6° increments of orbital rotation.

In each orbital position, three orientations with the lowest energy were chosen. These energy values are shown in Figure 4. Regions where the electrostatic energy values are the most favorable were selected at each orbital circle. The selected positions are: circle 1: angles from −30° to 6° and angles from 12° to 36°, orientations *X*, $-Y$ and *X*, *Z*; circle 3: angles from −48° to −30°, orientations *X*, $-Y$ and $-Y$, *X*; angles from 36° to 54°, orientation *X*, $-Y$; *X*, $-Z$ and *X*, *Z*; circle 4: angles from −24° to 6°, orientations *X*, $-Y$ and *X*, $-Z$; angles from 24° to 42°, orientations *Y*, *X* and *X*, *Z*; circle 5: angles from −42° to −18°, orientations *X*, *Z* and *X*, *Z*.

The area of the most favorable AChE–Fas1 interactions is shown on Figure 5A. This specific area surrounds the gorge entrance of AChE. By investigating the precollision orientation of Fas1, the results were refined. The preferred orientation of Fas is found to vary with its translational position. At the central point (Fig. 5A) position *X*, *Z* is favored, as the loops of Fas1 are directed toward the entrance of the gorge. Around the central point (0°), the *X*, *Z* orientations are preferred to $-X$, *Z* for all circles. In the *X*, *Z* orientation the electrostatic field direction of Fas1 roughly points toward the enzyme. The large negative electrostatic potential existing in this region of AChE (Ripoll et al., 1993; Tan et al., 1993) is the basis for the favorable interactions with the positively charged loops I and II of the fasciculin molecule.

Loop I is more likely to be oriented toward the enzyme than loop III because on one hand *Y*, *X*; *X*, $-Z$, and *X*, $-Y$ rotations have very low energies and on the other hand $-X$, $-Z$ and *Y*, $-X$ rotations have very high values. It appears that loop I is attracted toward the right side of AChE defined by an angle of 90° in circle 3 (Figs. 3, 5A). When the Fas1 molecule is moved on circle 1 from −30° to 30°, the most preferred orientation is changed from *X*, $-Y$ to *X*, *Z*, again turning loop I toward the right side of the AChE molecule (Fig. 3).

Orientation *X*, $-Y$ with the loop tips toward the right side of the gorge (Fig. 3) is more favorable than $-Z$, $-X$. Movement toward this side is nearly parallel with the general direction of the electric field in the AChE molecule.

Analyses of the preferred orientations of all circles over a 10-Å intermolecular distance reveal that the electric fields of AChE

Table 1. *Favorable orientations of Fas1 as found at the various circles (according to Fig. 3)*

Circle	−45°	0°	+45°	90°
1	*Y*, *X*	*X*, *Z*; *Y*, *X*	*X*, *Z*; *Y*, *X*; *Z*, $-Y$	
2	*Y*, $-Z$	*X*, *Z*; *Y*, *X*; *Z*, $-Y$	*X*, *Z*	
3		*X*, *Z*	*X*, *Z*; *Z*, $-Y$	*X*, *Z*; *Y*, *X*
4		*X*, *Z*; *Y*, *X*	*X*, *Z*; *Y*, *X*; *Z*, $-Y$	*X*, *Z*; *Y*, *X*
5	*Y*, *X*; *Y*, $-X$; *Z*, $-Y$	*X*, *Z*; $-Y$, *Z*	*X*, *Z*	

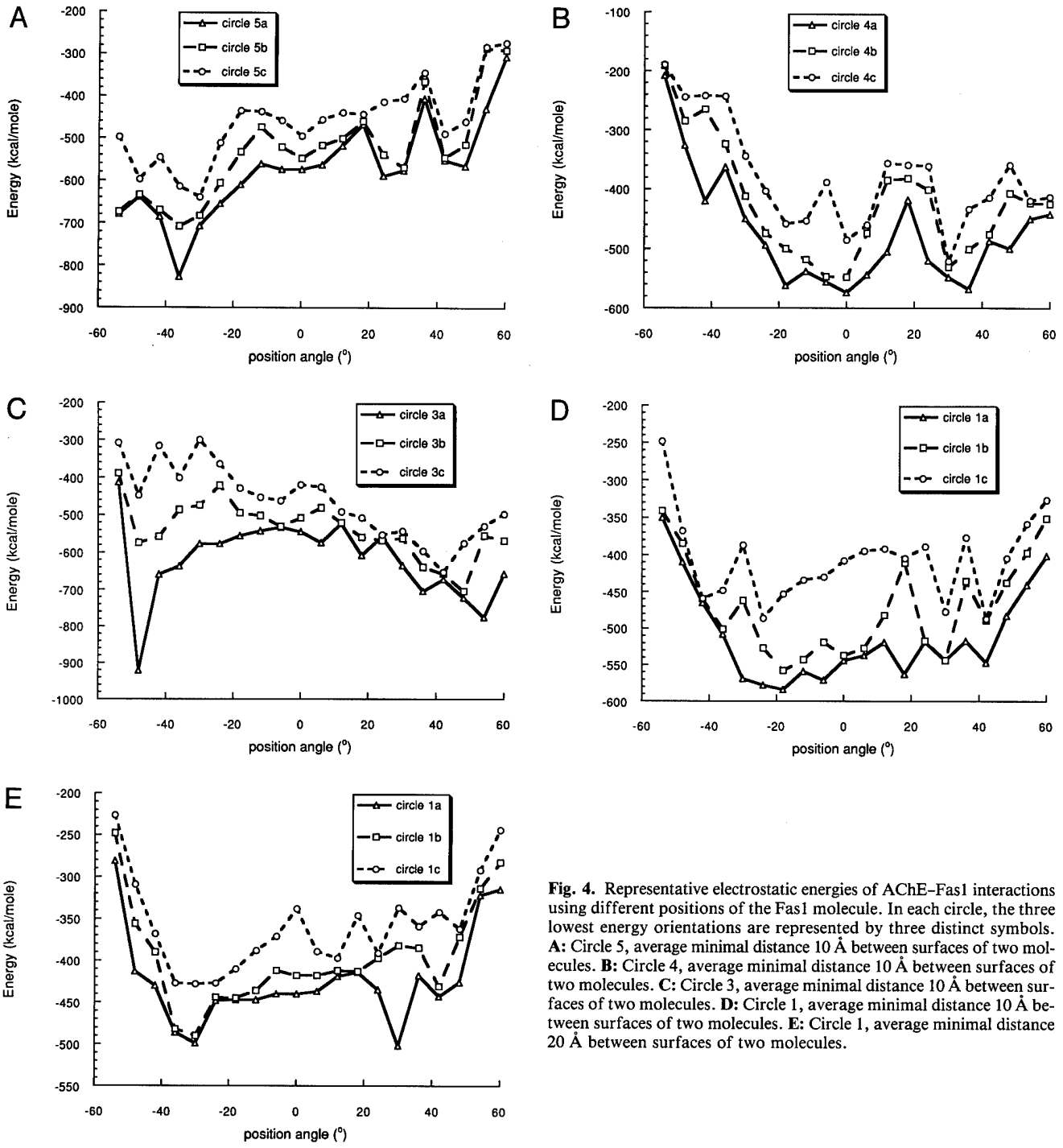

Fig. 4. Representative electrostatic energies of AChE–Fas1 interactions using different positions of the Fas1 molecule. In each circle, the three lowest energy orientations are represented by three distinct symbols. **A:** Circle 5, average minimal distance 10 Å between surfaces of two molecules. **B:** Circle 4, average minimal distance 10 Å between surfaces of two molecules. **C:** Circle 3, average minimal distance 10 Å between surfaces of two molecules. **D:** Circle 1, average minimal distance 10 Å between surfaces of two molecules. **E:** Circle 1, average minimal distance 20 Å between surfaces of two molecules.

and Fas1 are closely aligned. This suggests an approach with either Arg 11 of loop I or the tip of loop II facing toward the gorge of AChE. At intermolecular distances greater than 15 Å, the differences between various orientations of Fas1 begin to vanish.

Hence, a focused electrostatic guidance of Fas1 alone leads to a precollision position at the surface of the AChE molecule, near the gorge entry. This position results mainly from the orientation of the electrostatic fields of AChE and Fas1. The next step is the determination of possible AChE–Fas1 complexes.

Complexation of AChE and Fas1

The orientations of Fas1 with loop I and the tip of loop II approaching the region of the aromatic triad cluster (Tyr 70, Tyr 121, Trp 279) at the peripheral site of AChE were considered for further analysis. These three residues residing at the rim of the AChE gorge account for the selectivity of the fasciculins for AChE over BuChE (K_I = 2 pM versus 200 μM for mouse enzymes) (Radić et al., 1994). The distance between Arg 11 of

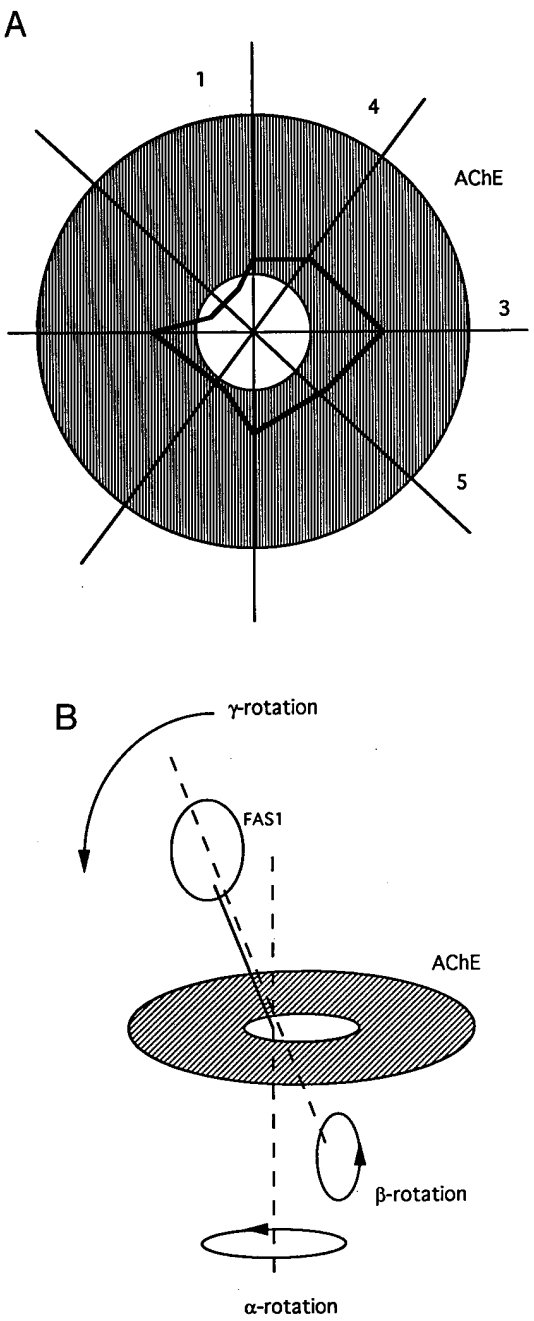

Fig. 5. Interaction of Fas1 with recognition site on AChE. **A:** Area of possible binding of Fas1 on the surface of AChE calculated from the precollision orientations (lighter area is the simplified region of the gorge). Position of the AChE peptide chain is shown in Figure 3. **B:** Movement of the Fas1 molecule during the complexation procedure.

Fas1 and each amino acid of the AChE peripheral aromatic triad cluster was constrained to 4–6 Å. Putative complexes were formed in two steps. Firstly the Fas1 molecule was rotated along its y-axes (Fig. 5B) for a complete circle of 360° in 30° increments (α-rotation). At each 30° position, Fas1 was rotated along its β-axis in 30° increments again in a complete circle. The β-axis starts at the center of the peripheral aromatic triad cluster and leads to the center of Fas1. Then, after each Fas1 β-rotation, an AChE–Fas1 complex was created by moving the Fas1 molecule (γ-rotation) toward AChE surface to maximize intermolecular contacts within the distance where van der Waals forces could be considered. The three rotations are depicted in Figure 5B. In this way, 144 putative complexes were generated.

The orientations of AChE and Fas1 side chains in selected complexes were then minimized to make the complex less dependent on the fixed orientations of the respective crystal structures. Sixty complexes of lowest interaction energy were selected. After minimization the final energy values showed a significant drop and were nearly equivalent. About 90% of this energy arises from the electrostatic component and the remainder from van der Waals' forces. A similar general pattern of local minimal energies was seen for both cutoff distances of 12 Å and 100 Å. We eliminated the largest electrostatic energy complexes. Forty-one complexes remained after this selection. The following selection was based on the electrostatic energy and buried surface calculations. For the selected complexes the range of electrostatic energies at a 100-Å cutoff distance were from −663 to −1,014 kcal/mol; at a 12-Å cutoff distance, they were from −439 to −807 kcal/mol and the buried surface areas ranged from 832 to 2,378 Å^2. The absolute values of energies do not have a specific reference point, and we considered only the differences between these energies for various complexes. The electrostatic energy values with the 12-Å cutoff mainly reflect the short-range interactions of fasciculin with AChE and 100-Å cutoff values also encompass the long-range electrostatic interactions. Taking into account the numerous approximations of theoretical calculations of this kind, we used both energy values for the selection of complexes. For six selected complexes, the values of these parameters are the following: complex 25: electrostatic energy (100 Å) −1,015 kcal/mol, electrostatic energy (12 Å) −767 kcal/mol, buried surface 1,688 Å^2; complex 36: −927 kcal/mol, −734 kcal/mol, 1,431 Å^2; complex 39: −860 kcal/mol, −808 kcal/mol, 1,508 Å^2; complex 45: −823 kcal/mol, −698 kcal/mol, 1,411 Å^2; complex 58: −862 kcal/mol, −699 kcal/mol, 1,216 Å^2; complex 60: −880 kcal/mol, −697 kcal/mol, 1,300 Å^2. Other complexes with larger buried surface areas have the higher electrostatic energy values and were eliminated. Complex 25 appears most favorable among the list, where it is found to have the global minimum of electrostatic energy (100 Å) and close to the global minimum in 12-Å cutoff calculations. It also has a substantial buried surface area.

We then calculated the favorable interactions between side chains of fasciculin and AChE of these complexes to make a final selection. We find that complex 36 has the same intermolecular interactions as complex 25 and very similar energy values. It falls into the same family as complex 25 and was eliminated because of slightly higher energy than complex 25. Similarly, two complexes, 45 and 39, happen to be in one family, and complex 39 was chosen. Complexes 58 and 60 were also nearly identical, but complex 58 has the larger number of favorable intermolecular contacts (Table 2), so it was selected.

Three complexes emerged based on optimizing the parameters used in this strategy: 25, 39, and 58. Table 2 shows the residues of AChE in contact with Fas1 in the selected complexes. Table 3 shows their intermolecular interactions, and the coordinates of the complexes are contained in the Electronic Appendix. A comparison of possible contacts of AChE and BuChE in the final complexes leads to the following considerations.

Table 2. *Calculated contact regions of the AChE-Fas1 complexes*

Complex	Contact residues of *Torpedo* AChE
25	70–76, 121, 279–280, 285–287, 332–342, 348–358, 362–372
39	68–78, 120–121, 250–256, 265–285, 333–336
58	39–42, 63–93, 121, 268–285, 333–336

Complex 25 (Fig. 6A; Kinemage 2)

In this complex, Arg 24, Arg 27, and Arg 28 in Fas1 are likely to be stabilized by negative charges in AChE, of which Glu 350 is a primary candidate. Because this residue exists as Lys in BuChE, the change in binding energy associated with the mutation would be one means for assessing this complex.

Complex 39 (Fig. 6B; Kinemage 3)

Near the contact positions in this complex, several residue differences exist between AChE and BuChE: Glu 73 Gln, Glu 268 Asn, Lys 270 Asp, Asp 276 Leu, and Asp 285 Gly. Some of these substitutions might be expected to diminish the contributions of Arg 11 and Arg 37 in Fas1 for stabilization of this complex. Substitution of Glu 268 Asn in the AChE molecule should result in the loss of the Arg 27–Glu 268 interaction. Substitution of Lys 270 Asp should result in the loss of the Asp 45–Lys 270 interaction and create repulsion between two negatively charged side chains. Substitution of Asp 276 Leu should result in loss of interaction with Arg 24, Lys 25, and Arg 37. Substitution of Asp 285 Gly should diminish the attraction of Arg 11 toward the gorge.

Complex 58 (Fig. 6C; Kinemage 4)

The area of intermolecular interactions in this complex is nearly identical for AChE and BuChE and points to the aromatic triad cluster (Tyr 70, Tyr 121, Trp 279) at the peripheral site as primarily accounting for the selectivity differences between AChE and BuChE.

Discussion

Taking into consideration the high electrostatic potential of AChE and its unique surface charge distribution oriented toward the gorge, one may assume that these factors can play a decisive role in guidance of the molecules found to associate with AChE. Recent theoretical calculations revealed the importance of this concept for association of cationic substrates with AChE (Ripoll et al., 1993; Tan et al., 1993). The question of specificity of peptide toxin binding to AChE is critical because among the family of more than 100 three-fingered toxins, only the fasciculins bind with high affinity to AChE.

Elimination of surface charges peripheral to the gorge through mutagenesis appeared to have little influence on substrate catalysis (Shafferman et al., 1994). However, several changes within the gorge itself were not included in the permutations of mutations. Glu 199 and Glu 443 within the gorge are critical for both inhibitor binding and catalysis (Radić et al., 1992, and unpubl. data). Other anionic residues also exist within or near the gorge, which give rise to mutant enzymes with sufficiently low

Table 3. *Contact residues of Fas1 (shown in italics) and Torpedo AChE in the selected complexes*

	Electrostatic interactions		Hydrophobic contacts		
Complex	<6 Å	6–9 Å	<4 Å	4–5 Å	Possible hydrogen bonds
25	*R24*-E350	*R11*-D72	*P31*-L368	*R27*-L368	*T7*-D285
	R24-D351	*R11*-D276	*L35*-K357	*P31*-V356	*T9*-P337
	R27-D365	*K32*-E350	*R37*-P337	*Y61*-P337	*T9*-G338
	R27-D369	*R37*-D285			*S10*-L332
	R37-D351	*R37*-E350			*R11*-Y70
	K51-E350				*R11*-W279
					R24-E350
					R27-V365
					K32-M353
					Y61-D351
39	*R11*-D72	*R24*-E273	*P31*-K269	*I13*-P76	*S5*-E73
	R27-E268	*R24*-D276	*L35*-K270		*H6*-Y70
	R27-E273	*K25*-D276	*Y47*-K270		*R11*-Y70
	D45-K270	*R37*-D276	*L48*-K270		*R11*-Y334
		D46-K270			*Y47*-E268
58	*R11*-D72	*D45*-R88	*P31*-P271	*P31*-K270	*H6*-Q74
	R27-E89	*K25*-E73			*H6*-Y70
	R37-D276	*K25*-E82			*T7*-V71
		R24-D276			*S10*-D276
		R27-E89			*R11*-Y70
		R27-E92			*R37*-E73
		R27-D93			*Y47*-E89
		R37-E73			

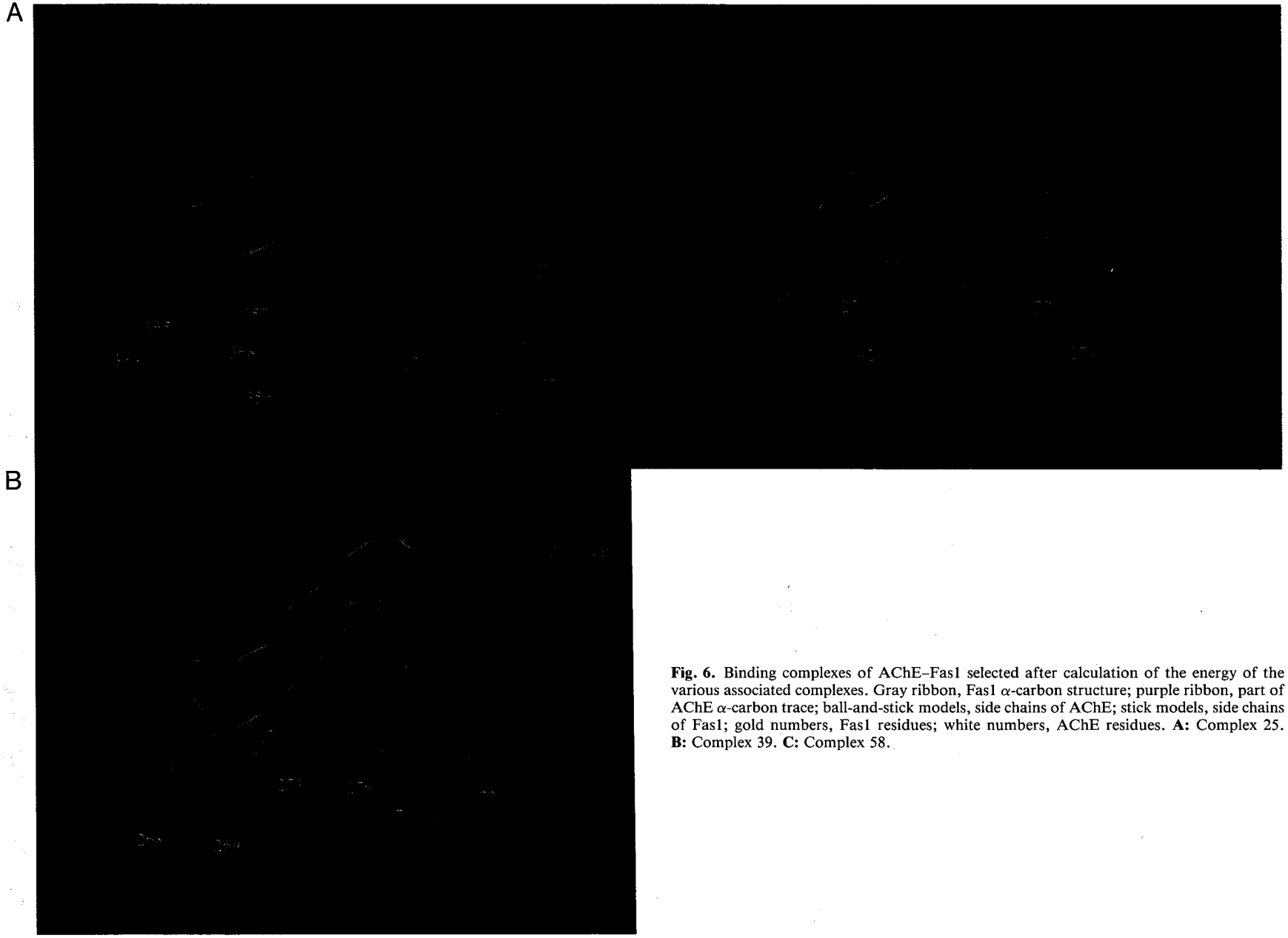

Fig. 6. Binding complexes of AChE–Fas1 selected after calculation of the energy of the various associated complexes. Gray ribbon, Fas1 α-carbon structure; purple ribbon, part of AChE α-carbon trace; ball-and-stick models, side chains of AChE; stick models, side chains of Fas1; gold numbers, Fas1 residues; white numbers, AChE residues. **A:** Complex 25. **B:** Complex 39. **C:** Complex 58.

activity to preclude study. This may point to a cluster of charges focused toward the gorge as being responsible for the associations of small ligands and the orientation of associating fasciculin.

The potential intramolecular interactions stabilizing loop III in Fas1 relative to Fas2 can be compared to the increase in number of interactions in loop I of Fas3 relative to Fas1 and Fas2. Only Fas3 has an appreciably higher affinity among the fasciculins (Marchot et al., 1993), which suggests that loop I could play the more important role in association of Fas and AChE. The six positively charged residues in loop II of fasciculin with their distinctive charge compensation are likely to be critical for its orientation toward the enzyme. These differences create an electrostatic potential for Fas unique among the three-fingered toxins. Our calculations of precollision orientation of Fas1, which took into account only the charge distribution on AChE and Fas1 and no other preconditions, resulted in positioning of the fasciculin molecule in the region of AChE close to the gorge entrance and near the three aromatic residues that have been shown by mutagenesis to be involved in the AChE–fasciculin interaction (Radić et al., 1994). Electrostatic guidance calculations can therefore lead to a reasonable positioning of fasciculin in apposition to a specific region of AChE. The drastic change of electrostatic field of AChE after the binding of Fas (Fig. 7) can definitely affect the electrostatic guidance mechanism of the AChE–fasciculin complex toward subsequent entry of charged substrates. Recent kinetic experiments where fasciculin can serve as an allosteric activator and/or inhibitor of AChE depending on the nature of the substrate and mutated residues (Z. Radić

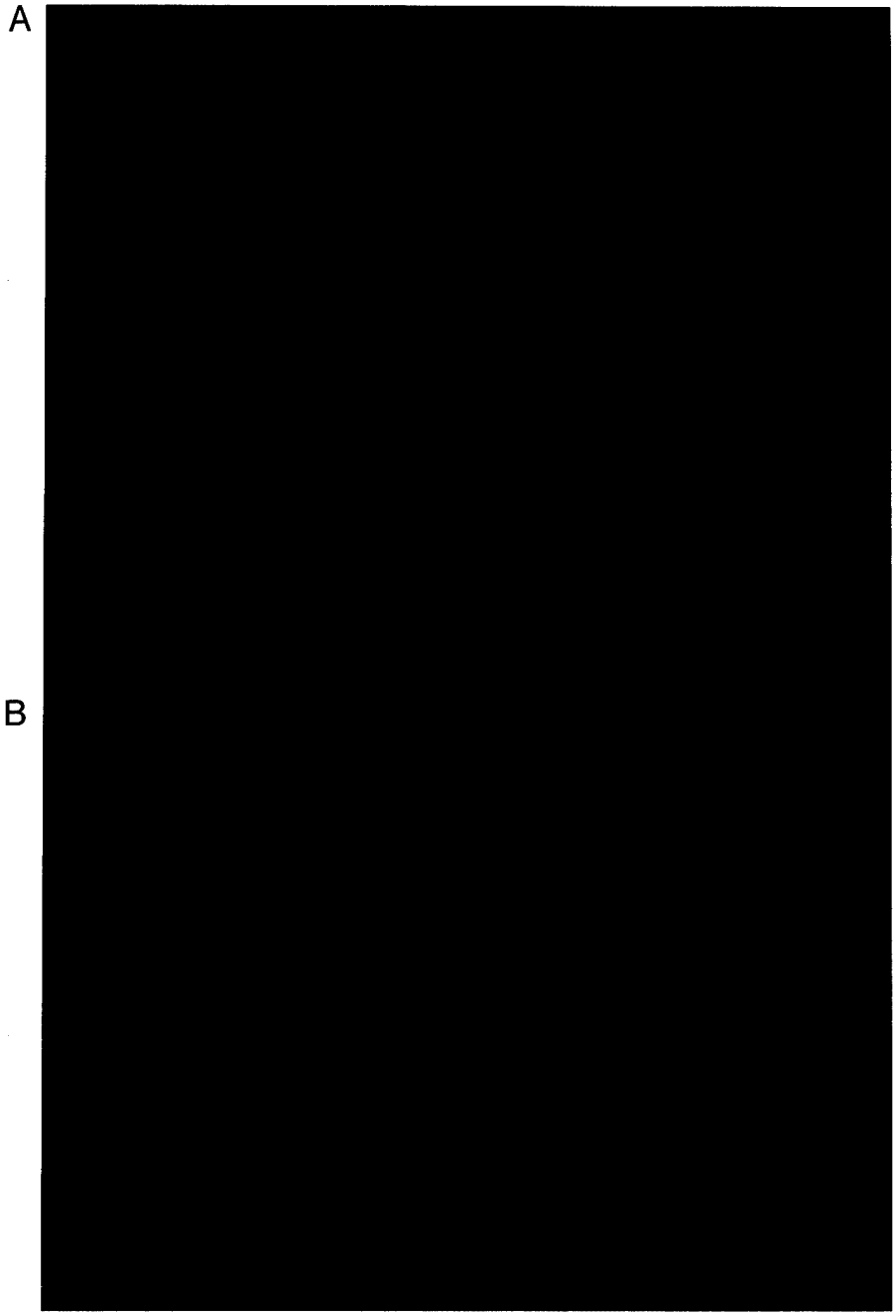

Fig. 7. Electrostatic isopotential surfaces of Fas1 and AChE. Orientation of the proteins is the same in A and B. Red surface corresponds to the isopotential contour $-1\ kT/e$; blue surface corresponds to the isopotential contour $+1\ kT/e$. **A:** Free state. **B:** Bound state of the complex.

D. Quinn, D. Vellom, S. Camp, & P. Taylor, submitted for publication) are in accord with this notion. Calculations of the buried surface of the complex delimited the possible orientations of the complex to a number realistic for designing mutagenesis studies on fasciculin and AChE.

Of the three complexes (Fig. 6A,B,C), for complexes 58 and 39, Fas is located on the surface of AChE, actually capping a disulfide loop between residues Cys 60 and Cys 97. This loop serves as a flap that opens the binding site for substrates in *Candida rugosa* and *Rhizomucor miehei* lipases (Brzozowski et al., 1991; Grochulski et al., 1994). These enzymes show homology in sequence and overall α-β-hydrolase fold characteristics of AChE (Ollis et al., 1992). Hence, it is possible that the diminished catalytic capacity of the fasciculin–AChE complex may also arise from constraints imposed on this region that restrict the conformational flexibility of AChE.

The known three-dimensional structures of Fas1 (le Du et al., 1992) and AChE (Sussman et al., 1991) allow for multiple and complementary approaches to study the complex. Initial studies showing competition between propidium and fasciculin pointed to fasciculin interactions not occurring at the active center of the enzyme (Karlsson et al., 1984). Subsequent studies showing that fasciculin will bind to the DFP-conjugated enzyme and that the active center of AChE can be phosphorylated by DFP when fasciculin is bound (Marchot et al., 1993) provide important documentation of accessibility to the active center gorge in the complex. Site-specific mutagenesis has revealed that residues that form the acyl pocket and the choline binding site have minimal influence on fasciculin binding, whereas modification of three residues Trp 279, Tyr 121, Tyr 70 at the rim of the gorge have the major influence and can actually account for the free energy difference of fasciculin binding to AChE versus BuChE (Radić et al., 1994). Moreover, the importance of cation–π-electron interactions that could arise between positively charged residues of fasciculin and this aromatic cluster have been well documented in quantum chemical calculations (Kim et al., 1994). Hence, the surface for binding can, at least in part, be defined by this aromatic cluster at the top of the gorge.

At present, there is only fragmentary chemical modification data and no mutagenesis evidence with the fasciculin molecule to aid in assignment of interacting residues. Cervenansky and colleagues (1994) have shown that acetylation of residues Lys 25, Lys 32, and Lys 51 of Fas2 partly reduces its interactions with AChE. These three residues appear involved in the intermolecular stabilization of loop II in fasciculin and their modification may lead to destabilization of its rigid structure, a finding not revealed upon examination of the CD spectra of the modified molecule. Also, in our calculations Lys 51 and Lys 32 are shown to play a role in electrostatic interactions with AChE in complex 25. Lys 25 is involved in electrostatic interaction with AChE in complexes 39 and 58 (Table 3). The theoretical considerations presented here define the unique features of the fasciculin structure and should enable us to distinguish the more probable binding orientations of the complex.

Methods

Initial protein structures

The crystallographic coordinates of *Torpedo* AChE, code 1ACE (Sussman et al., 1991), Fas1, code 1FAS (le Du et al., 1992), α-bungarotoxin, code 2ABX (Bgt) (Love & Stroud, 1986), cardiotoxin V_4^{II}, code 1CDT (Cdt) (Rees et al., 1990), erabutoxin b, code 3EBX (Ebt) (Smith et al., 1988), and α-cobratoxin, code 1CTX (Cbt) (Walkinshaw et al., 1980), were retrieved from Brookhaven Protein Data Bank (WWW: http://www.pdb.bnl). All structures were reexamined to add unresolved atoms with Insight 2.3.0 and Homology programs (Biosym Technologies, Inc., 1994, San Diego, California). Charges were assigned according to average pK_a's of the ionizable side chains at pH 7.5. We performed the short steepest decend minimization cycle to relieve strain in the side chains and also energy minimized the regions that deviated from the crystal structure with the Discover program (Biosym Technologies, Inc., 1994). Raman and NMR spectroscopy show general agreement between the solution and crystal structures of some members of the three-fingered toxin family (Love & Stroud, 1986; Endo & Tamiya, 1987). The molecular models of Fas2 and Fas3, whose crystal structures are not known, were constructed using the residue replacement with the Insight 2.3.0. program. Side chains were then minimized using the Discover program to avoid artificial constraints.

Calculations and display of electrostatic fields

Electrostatic potential fields of the toxins and AChE were determined using the linearized Poisson–Boltzmann equation solved numerically by the DelPhi 2.5 program (Biosym Technologies Inc., 1994). The dielectric constant of water was set to 80, and that of the protein interior to 2. An ionic strength of 0.145 was used. The grid had a spacing of 0.9 Å and overall size of 57.8 Å.

Precollision orientation procedure

The precollision orientation of the fasciculin molecule relative to AChE was calculated using a strategy that considered only electrostatic interactions. Coulombic energies of electrostatic interaction between AChE and Fas1 were calculated by summing the contributions of partial charges of all atoms of these two molecules using the Docking program of Insight 2.3.0 and CFF91 force field. Interactions were measured within short (12 Å) and long (100 Å) range cutoff distances.

The following strategy was used. Five full circles were defined around the center of mass for AChE (Fig. 3). The distance between the mass centers of the two molecules was kept constant at 56 Å, a value consistent with a 20-Å distance as an average shortest distance between AChE and Fas1 molecular surfaces. In local regions where the position was refined, we also used a distance of 10 Å. Each full circle was rotated in 45° incremental positions of Fas1, and the electrostatic interaction energies were calculated (Fig. 8). A zero angle refers to the position directly above an axis aligned down the center of the AChE gorge.

At each of the positions, orientations of Fas1 differing by 90° rotational angles around the respective *x*-, *y*-, and *z*-axes, presuming the tip of the molecule fixed at the zero point (Fig. 8A), were evaluated. The *x* orientation is perpendicular to the average surface of the AChE molecule (Fig. 8B). The overall number of possible orientations of the Fas molecule was 24. These orientations were named by the directions of the orientation of loops II and I (Fig. 8A), presuming the orientation of the loop II always is directly congruent with one of axes. The direction of the orientation of loop I is designated after the direction of

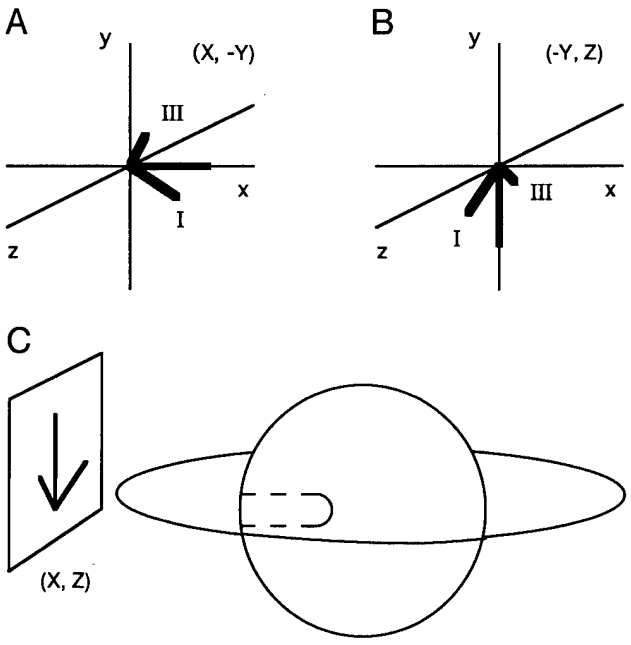

Fig. 8. Precollision orientation of Fas1. **A, B:** Representative examples of orientations of the Fas1 molecule used for evaluation of precollision orientations (positions X, Y and $-Y$, Z). Symbols I and III denote structural loops. **C:** Starting position of Fas1 (position X, Z) and AChE used in circle 3. Dashed line, position of the gorge.

the vector component associated with this loop that is perpendicular to the direction of the vector of loop II and lies in the same plane as loops I, II, and III. So, for example, orientation X, $-Y$ is the orientation where loop II is directed toward the surface of AChE along the x-axis (Fig. 8A) and loop I is oriented toward the $-Y$ direction. The structure of the Fas1 molecule is rigid and rather flat, so the direction of loop III always corresponds to the orientations of loops II and I. Some of orientations were skipped initially due to strong unfavorable electrostatic interaction between AChE and Fas1. We eliminated, for example, positions where the tip of Fas and/or loop III were directed to the surface of AChE (orientations Y, $-X$; $-Y$, $-X$; Z, $-X$). The positions with so-called "flat" orientation, where the largest surface of Fas1 is oriented perpendicular to AChE ($-Y$, Z; $-Z$, Y; Z, Y; $-Z$, $-Y$), also had relatively large electrostatic energies and were eliminated. The same situation holds for other orientations. In selected positions of Fas1 the energies then were measured at every 6° increment. All of these calculations were made using our own semi-autonomous programs in Insight II. The program kept the AChE molecule stationary while translating the Fas1 molecule to each position around AChE and rotating it to the chosen orientation. During the rotation of the Fas1 molecule, the axes connecting the mass centers of both molecules were kept at a constant length, and the point of internal rotation of the Fas1 molecule was fixed close to its center of mass. With this procedure, the shortest separation distance between the surfaces of molecules varied.

Areas of molecular surfaces that become inaccessible to solvent upon formation of AChE–Fas complexes were calculated using the Solvation 2.5 program (Biosym Technologies, Inc., 1994). In order to define these buried surface areas in the complex, we calculated the solvent-accessible surfaces of the individual molecules and of the complexes. A molecular surface algorithm (Connolly, 1983) with a 1.6-Å radius of probe was used to determine the solvent accessibility of each molecule.

Selection of fasciculin–AChE complexes

In the first selection procedure the area of the buried surface of interaction and its shape complementarity were weighed against the complementarity of electrostatic field vectors of both molecules. For example, complexes with relatively small contact areas were still selected if they had significant complementarity of electric fields, whereas structures with small contact areas and strongly opposing electric field orientations were eliminated.

The topography of residues at the interface was closely evaluated. Complementary groups were aligned to maximize salt bridges and hydrophobic clusters. Complexes with relatively small interfacial areas but significant complementarity of interfacial residues, by virtue of formation of a significant number of salt bridges and hydrophobic clusters, were selected for further investigation.

Each potential complex selected for further investigation was minimized using the Discover 3.1 program (Biosym Technologies, Inc., 1994) in CVFF force field. This afforded an opportunity to adjust the fit of the intermolecular complexes avoiding the problem of "rigid bodies." Using this approach, we avoided rejection of remaining favorable complexes because of artificial van der Waals energy barriers between nonenergy-minimized side chains of both molecules. A cutoff distance of 25 Å was used in these calculations. The peptide backbones of both molecules were constrained during the minimization.

Acknowledgments

We thank Drs. Stanislaw Wlodek, Jan Antosiewicz, at the University of Houston, and Dr. Anatoly Schmidt at Biosym Technologies, Inc. for helpful comments. We also thank Dr. Lynn Ten Eyck at the San Diego Supercomputer Center for his assistance and valuable advice during the course of this study. This work was supported by USPHS grant GM18360 and DAMD 17-91C-1056 to P.T.

References

Brzozowski AM, Derewenda U, Derewenda ZS, Dodson GG, Lawson DM, Turkenburg JP, Bjorkling F, Huge-Jensen B, Patkar SA, Thim L. 1991. A model for interfacial activation in lipases from the structure of a fungal lipase-inhibitor complex. *Nature 351*:491–494.

Cervenansky C, Dajas F, Harvey AL, Karlsson E. 1991. Fasciculins, anticholinesterase toxins from mamba venoms: Biochemistry and pharmacology. In: Harvey AL, ed. *Snake toxins*. New York: Pergamon Press, Inc. pp 303–321.

Cervenansky C, Engstrom A, Karlsson E. 1994. Study of structure–activity relationship of fasciculin by acetylation of amino groups. *Biochim Biophys Acta 1199*:1–5.

Connolly M. 1983. Solvent-accessible surfaces of proteins and nucleic acids. *Science 221*:709–713.

Endo T, Tamiya N. 1987. Current view on the structure–function relationship of postsynaptic neurotoxins from snake venoms. *Pharmacol Ther 34*:403–451.

Endo T, Tamiya N. 1991. Structure–function relationship of postsynaptic neurotoxins from snake venoms. In: Harvey AL, ed. *Snake toxins*. New York: Pergamon Press, Inc. pp 165–222.

Faure G, Boulain JC, Bouet F, Montenay-Garestier T, Fromageot P, Menez A. 1983. Role of indole and amino groups in the structure and function of *Naja nigricolis* toxin alpha. *Biochemistry 22*:2068–2076.

Grochulski P, Li Y, Schrag JD, Cygler M. 1994. Two conformation states of *Candida rugosa* lipase. *Protein Sci 3*:82–91.

Karlsson E, Mbugua PM, Rodriguez-Itthurralde D. 1984. Fasciculins, anticholinesterase toxins from the venom of the green mamba *Dendroaspis angusticeps*. *J Physiol (Paris) 79*:232–240.

Karlsson E, Mbugua PM, Rodriguez-Itthurralde D. 1985. Anticholinesterase toxins. *Pharmacol Ther 30*:259–276.

Kim KS, Lee JY, Lee SJ, Ha TK, Kim DH. 1994. On binding forces between aromatic ring and quaternary ammonium compounds. *J Am Chem Soc 116*:7399–3400.

le Du MH, Marchot P, Bougis PE, Fontecilla-Camps JC. 1992. 1.9-Å resolution structure of fasciculin 1, an anti-cholinesterase toxin from green mamba snake venom. *J Biol Chem 267*:22122–22130.

Love R, Stroud R. 1986. The crystal structure of α-bungarotoxin at 2.5 Å resolution: Relation to solution structure and binding to acetylcholine receptor. *Protein Eng 1*:37–46.

Marchot P, Khelif A, Ji YH, Mansuelle P, Bougis PE. 1993. Binding of ^{125}I-fasciculin to rat brain acetylcholinesterase. The complex still binds diisopropyl fluorophosphate. *J Biol Chem 268*:12458–12467.

Martin BM, Chibber BA, Maelicke A. 1983. The sites of neurotoxicity in α-cobratoxin. *J Biol Chem 258*:8714–8722.

Ollis DL, Cheah E, Cygler M, Dijkstia B, Frolow F, Franken SM, Harel M, Remington SJ, Silman I, Schrag JD, Sussman JL, Vercheuren KHG, Goldman A. 1992. The α,β hydrolase fold. *Protein Eng 5*:197–211.

Pillet L, Tremeau O, Ducancel F, Drevet P, Zinn-Justin S, Pinkasfeld S, Boulain JC, Menez A. 1993. Genetic engineering of snake toxins. *J Biol Chem 268*:909–916.

Radić Z, Duran R, Vellom D, Li Y, Cervenansky C, Taylor P. 1994. Site of fasciculin interaction with acetylcholinesterase. *J Biol Chem 269*:11233–11239.

Radić Z, Gibney G, Kawamoto S, MacPhee-Quigley K, Bongiorno C, Taylor P. 1992. Expression of recombinant acetylcholinesterase in a baculovirus system: Kinetic properties of glutamate 199 mutants. *Biochemistry 31*: 9760–9767.

Rees B, Bilwes A, Samana J, Moras D. 1990. Cardiotoxin V_4^{II} from *Naja mossambica*, the refined crystal structure. *J Mol Biol 214*:281–297.

Ripoll D, Faerman C, Axelsen P, Silman I, Sussman J. 1993. An electrostatic mechanism for substrate guidance down the aromatic gorge of acetylcholinesterase. *Proc Natl Acad Sci USA 90*:5128–5132.

Shafferman A, Ordentlich A, Barak D, Kriman C, Ber R, Bino T, Ariel N, Osman R, Velan B. 1994. Electrostatic attraction by surface charge does not contribute to the catalytic efficiency of acetylcholinesterase. *EMBO J 13*:34448–34455.

Smith JL, Corfield PWR, Hendrickson WA, Low BW. 1988. Refinement at 1.4 Å resolution of a model of erabutoxin *b*. Treatment of ordered solvent and discrete disorder. *Acta Crystallogr A 44*:357–368.

Sussman JL, Harel M, Frolow F, Oefner C, Goldman A, Toker L, Silman I. 1991. Atomic structure of acetylcholinesterase from *Torpedo californica*: A prototypic acetylcholine-binding protein. *Science 253*:872–879.

Tan R, Truong T, McCammon J, Sussman J. 1993. Acetylcholinesterase: Electrostatic steering increases the rate of ligand binding. *Biochemistry 32*:401–403.

Taylor P, Lappi S. 1975. Interaction of fluorescence probes with acetylcholinesterase. The site and specificity of propidium binding. *Biochemistry 14*:1989–1997.

Walkinshaw MD, Saenger W, Maelicke A. 1980. Three-dimensional structure of the "long" neurotoxin from cobra venom. *Proc Natl Acad Sci USA 77*:2400–2404.

ELSEVIER

Toxicology Letters 82/83 (1995) 453–458

Toxicology Letters

Structural bases for the specificity of cholinesterase catalysis and inhibition

Palmer Taylor[a,*], Zoran Radic[a,1], Natilie A. Hosea[a], Shelley Camp[a], Pascale Marchot[a,2], Harvey A. Berman[b]

[a]*Department of Pharmacology, University of California, San Diego, La Jolla, CA 92093-0636, USA*
[b]*Department of Biochemical Pharmacology, State University of New York at Buffalo, Buffalo, NY 14260-0001, USA*

Abstract

The availability of a crystal structure and comparative sequences of the cholinesterases has provided templates suitable for analyzing the molecular bases of specificity of reversible inhibitors, carbamoylating agents and organophosphates. Site-specific mutagenesis enables one to modify the structures of both the binding site and peptide ligand as well as create chimeras reflecting one type of esterase substituted in the template of another. Herein we define the bases for substrate specificity of carboxylesters, the stereospecificity of enantiomeric alkylphosphonates and the selectivity of tricyclic aromatic compounds in the active center of cholinesterase. We also describe the binding loci of the peripheral site and changes in catalytic parameters induced by peripheral site ligands, using the peptide fasciculin.

Keywords: Acetylcholinesterase; Cholinesterase; Serine hydrolase; Organophosphates; Fasciculin; Enantiomeric inhibitors

1. Introduction

Sequencing of the cholinesterases and the cloning of their genes a decade ago revealed that these enzymes defined a family of serine hydrolases distinct from the well characterized pancreatic protease and subtilisin families of enzymes [1]. The diversity in this hydrolase family is not only reflected in enzymes which hydrolyze complex ester structures such as juvenile hormone and lysophospholipids, but the family also includes enzymes with distinct differences in mechanism, the epoxide hydrolases and dehydrohalogenases [2,3]. Even more remarkable is the observation that several proteins without hydrolase function such as thyroglobulin, the tactins and the neuroligins show sequence identity with the hydrolases in this family [3,4]. Solutions of the crystal structures of acetylcholinesterase (AChE) and the fungal lipases revealed a structural motif, termed the α/β hydrolase fold [2,5]. Surprisingly, this motif is also shared by several enzymes that possess no discernible sequence

* Corresponding author.
[1] Visiting Scientist, Institute for Medical Research and Occupational Health, University of Zagreb, Zagreb, Croatia.
[2] Visiting Scientist, CNRS Unité de Recherche Associée 1455, Université d-Aix-Marseille II, Marseille, France.

SSDI 0378-4274(95)03575-6

identity with the cholinesterases [2,3]. Hence, this family continues to enlarge, and the α/β hydrolase fold emerges as a common structural motif associated with a wide variety of catalytic and surface contact functions.

The catalytic steps in ester hydrolysis involve an initial transacylation step in which the acyl group is transferred from substrate to the serine on the enzyme with the departure of the alcohol moiety of the substrate [3,6,7]. This is followed by water addition with the concomitant deacylation of the enzyme. Of importance is that both acylation and deacylation proceed through tetrahedral transition states which are facilitated by hydrogen bonding from amide backbone hydrogens to the carbonyl oxygen in the oxyanion hole.

The solution of the crystal structure of the enzyme [5] has revealed that the catalytic serine and the accompanying histidine and glutamate in the catalytic triad lie centrosymmetric to each subunit in the molecule at the base of a deep gorge. The crystal structure, sequence comparisons and site-specific mutagenesis now enable one to define distinct residues and discrete domains which contribute to overall specificity for substrates and inhibitors. Since AChE and butyrylcholinesterase (BuChE) show well defined differences in specificity, substitutions can be developed from either template. Table 1 outlines a series of selective and non-selective inhibitors of the cholinesterases and the residues in the enzyme which dictate specificity.

2. Specificity governed by acyl pocket dimensions

The acyl pocket in AChE is outlined by the side chains of two phenylalanines, F_{295} and F_{297}, in the mammalian enzyme; in BuChE the residues at corresponding positions are leucine (L) and isoleucine (I), therein occupying much smaller volumes. Substitution of L for F at the 295 position provides a sufficient reduction in side chain volume to allow butyrylcholine to become an efficient substrate, while substitution of I or V for F at the 297 position changes the kinetic profile of the enzyme from one that shows substrate inhibition to one of substrate activation (Fig. 1, Table 1). Substrate inhibition is characteristic of AChE, whereas substrate activation is characteristic of BuChE [8–10]. Hence, the two phenylalanines outlining the acyl pocket play distinct roles in governing the catalytic profile of the cholinesterases. The carboxylesters possess trigonal, planar acyl groups, and by extending these observations to tetrahedral substrates such

Table 1
Cholinesterase domains affecting ligand specificity

	Substrate	Selective inhibitors	AChE/BuChE preference	AChE residues[a]
1. Acyl pocket (active center)	Critical to acyl group dimensions; influences substrate inhibition	IsoOMPA	BuChE	Phenylalanine-$F_{295(288)}$ Phenylalanine-$F_{297(290)}$
2. Choline subsite (active center)	Specificity neutral versus cationic esters	Ethopropazine Huperzine	BuChE AChE	Tyrosine-$Y_{337(330)}$ Tryptophan-$W_{86(84)}$[b] Phenylalanine-$F_{449(442)}$[b] Glutamate-$E_{202(199)}$[b]
3. Rim of the gorge (peripheral site)	Little direct influence; only allosteric	Fasciculin Propidium	AChE AChE	Tyrosine-$Y_{72(70)}$ Tyrosine-$Y_{124(121)}$ Tryptophan-$W_{286(279)}$[b]
4. Rim of the gorge and choline subsite	Similar to 2 and 3	BW284c51	AChE	Aspartate-$D_{74(72)}$ Residues in domains 2 and 3

[a] The first subscript corresponds to the numbering system for mammalian AChE; the number in parentheses is the Torpedo numbering system.
[b] Conserved residues in AChE and BuChE.

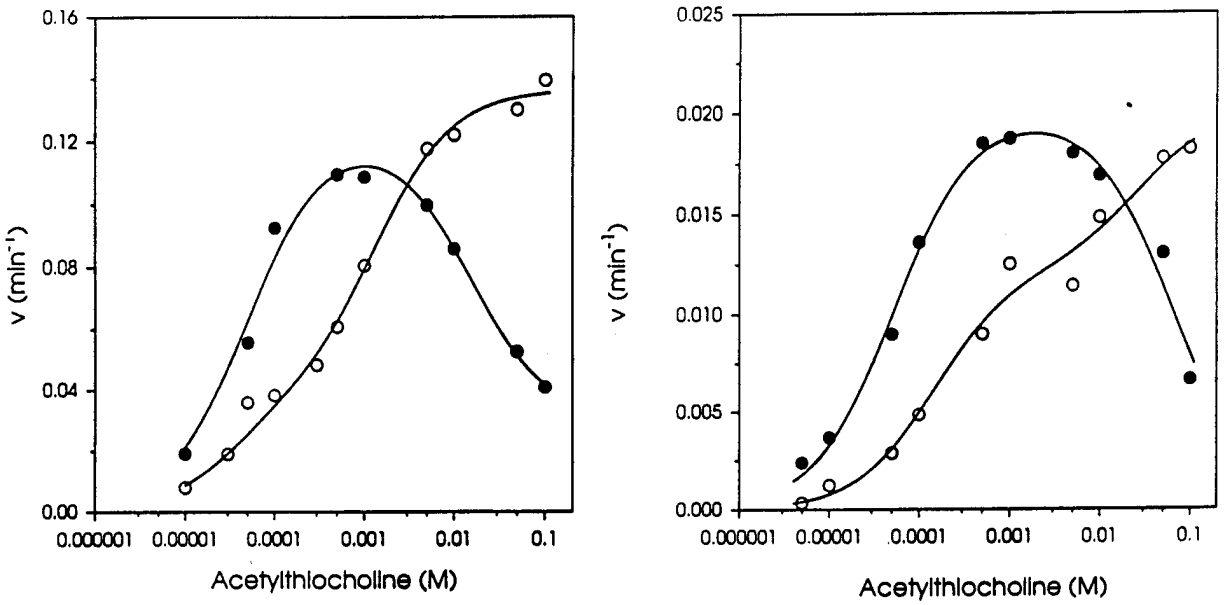

Fig. 1. Rates of acetylthiocholine hydrolysis as a function of substrate concentration. Left hand panel: Wild-type Mouse AChE (●); Wild-type Mouse BuChE (○). Right hand panel: Mutant $F_{295}L$ AChE (●); Mutant $F_{297}I$ AChE (○). The catalytic constants obtained from triplicate kinetic analyses and enzyme titrations are detailed in Table 1. Data are from Refs. [9,10].

as the alkylphosphonates, we can gain additional information on the specificity of enzyme acylation. Deacylation of the phosphonyl enzyme conjugates occurs slowly and may be studied as a separate step.

Berman and colleagues have found that a series of alkoxyl methyl phosphonylthiocholines show a 200- to 300-fold preference with the S_p-isomer over the R_p-isomer for *Torpedo* AChE [11,12]. A similar preference is seen with the mammalian enzyme and, through site-specific mutagenesis, we are able to define the structural determinants for enantiomeric specificity. It appears that the phosphonyl oxygen must be placed in the oxyanion hole and the leaving group directed out of the gorge to maximize acylation rates. A knowledge of the absolute stereochemistry of the phosphonates then reveals that the S_p-enantiomer positions its bulky alkoxyl group toward the choline binding site, while the small methyl group occupies the more space restrictive acyl pocket. On the other hand, the same constraints on the positioning of the phosphonyl oxygen and the leaving group require the bulky alkoxy group of the R_p-enantiomer to be oriented towards the acyl pocket where steric limitations do not allow an optimal fit. This orientation is consistent with the kinetic differences in S_p- and R_p-acylation, for as we enlarge the acyl pocket, we find that the R_p-isomer becomes a more efficient acylating agent [10] (Table 2). Other studies which compare cationic thiocholine and neutral thioalkyl leaving groups of these phosphonates are also consistent with this interpretation for orientation (N.A. Hosea, unpublished observations). Fig. 2 shows the orientations of S_p- and R_p-cycloheptyl methylphosphonylthiocholine when reversibly bound to AChE and $F_{297}I$ AChE, respectively.

3. The choline binding site in the active center

Tricyclic phenothiazine and acridine analogues are effective inhibitors and appear to associate with the choline subsite, located within the active center of the cholinesterases [5,9]. This region is also bounded by several aromatic side chains. While most tricyclic compounds do not exhibit a preference for AChE over BuChE, ethopropazine is a specific BuChE inhibitor with a 1800-fold preference over AChE (Table 3) [9].

Table 2
Influence of acyl pocket dimensions on substrate specificity

	Acetylthiocholine				Butyrylthiocholine				Cycloheptyl methyl phosphonothiocholine	
	K_m	k_{cat}	K_{ss}	b	K_m	k_{cat}	K_{ss}	b	k_a-S_p	k_a-R_p
AChE	46	140×10^3	13	0.21	93	1.1×10^3	7.1	0.48	1.8×10^8	0.008×10^8
BuChE	23	40×10^3	1.0	3.9	55	37×10^3	1.7	2.0	4.7×10^8	0.067×10^8
$F_{295}L$	52	44×10^3	67	<0.2	10	12×10^3	23	0.40	0.66×10^8	0.087×10^8
$F_{297}I$	170	15×10^3	43	1.8	82	60×10^3	2.4	1.7	0.16×10^8	0.62×10^8

K_m (μM), k_{cat} (min^{-1}), K_{ss} (mM), k_a (M^{-1} min^{-1}) and b (dimensionless) were determined as described in Refs. [10,14].

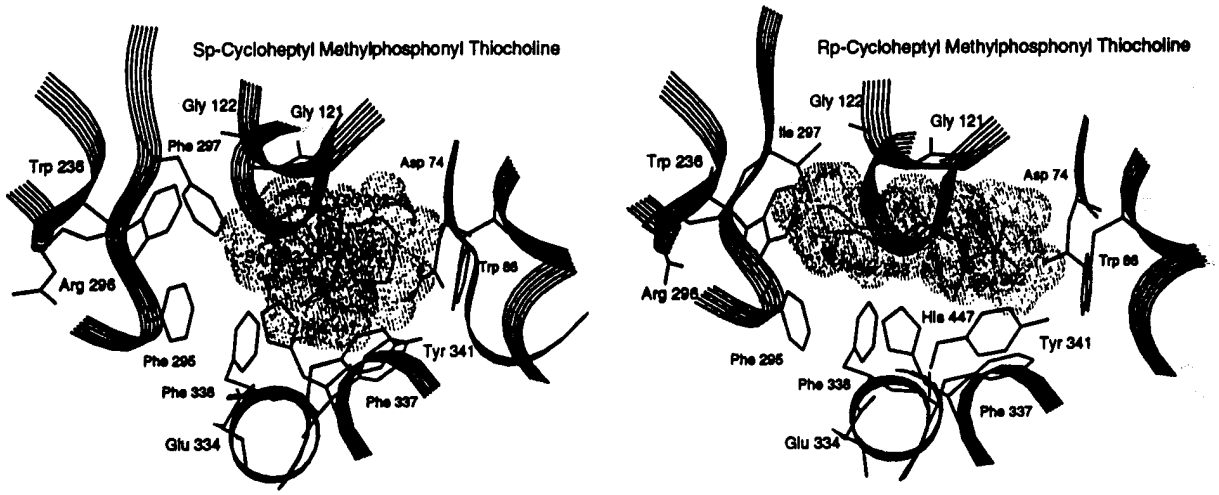

Fig. 2. Proposed orientations of R_p- and S_p-cycloheptylmethyl-phosphonylthiocholine in the active center of mammalian AChE. The model was developed from the coordinates of *Torpedo californa* AChE [5]. Shown are the side chains of several of the catalytically (S_{203}, H_{447} and E_{334}) and structurally (F_{295}, F_{297}, W_{86}, F_{337}, G_{121}, G_{122}, E_{202}, D_{74}) important residues in the active center. In both enantiomers the phosphonyl oxygen is directed back towards the plane of the paper forming hydrogen bonds with the amide backbone hydrogens of G_{121}, G_{122} and A_{204}. The thiocholine leaving group is directed out of the gorge toward the reader. The S_p-enantiomer is docked with the wild-type sequence and the R_p-enantiomer docked with the $F_{297}I$ mutant.

Since BuChE and AChE differ by having alanine versus tyrosine or phenylalanine at the 337 position, the basis for this specificity might arise from steric occlusion between the tyrosine or phenylalanine side chain at position 337 on AChE and the exocylic amine containing side chain on ethopropazine. Substitution of alanine for tyrosine at this position in AChE confers high affinity for ethopropazine binding to AChE substituted at a single position. In fact, the change in energy ($\Delta\Delta G$) is remarkably similar to the AChE-BuChE difference (Table 3). Docking of

Table 3
Specificity at the choline binding site[a]

Ethopropazine	K_d (nM)	$K_{d.M}/K_{d.WT}$	$\Delta\Delta G$ (kcal)
Mouse BuChE Wild Type	61	1.0	0
Mouse AChE Wild Type	110 000	1800	4.5
$Y_{337}A$ AChE Mutant	41	2700	4.7

[a] Mammalian AChE has tyrosine (Y) at the 337 position, while BuChE has alanine. $\Delta\Delta G$ was calculated from the ratio of dissociation constants.

the ethopropazine molecule in a BuChE template and energy minimization show that the diethylaminoisopropyl moiety occupies the same region as would the phenyl ring at position 337 in AChE [9]. Hence, the specificity difference for this widely used inhibitor results from steric hindrance by a single aromatic side chain.

4. Fasciculin and the peripheral site on AChE

A peripheral site of inhibitor binding to AChE was defined many years ago on the basis of steady-state kinetics [13,14] and by direct titration with propidium [14]. This site is also believed to be the locus through which substrate inhibition is allosterically transmitted to the active center [15]. A family of peptides of 6750 Da found in the venom of mambas, termed the fasciculins, also appear to bind to the peripheral site on AChE with high affinity, but they are ineffective inhibitors of BuChE. Modification of residues comprising the peripheral site at the rim of the gorge and the active center deep within the gorge shows that only those residues at the rim of the gorge appreciably affect fasciculin binding [16]. In fact, substitutions of R for W_{286}, N for Y_{72} and Q for Y_{124} result in a large reduction of fasciculin affinity ($K_d = 2.3$ pM vs. 220 μM). These substitutions reflect BuChE-AChE sequence differences. This increase in K_d is equivalent to 11 kcal of free energy and is exactly the same as the energy difference seen between AChE and BuChE (Table 4).

By contrast, modification of a tryptophan at the base of the gorge, W_{86}, results in unusual and intriguing kinetic behavior for the fasciculin complex [17]. In the uncomplexed enzyme, the substitutions of tyrosine, phenylalanine and alanine for the tryptophan result in progressive reductions in catalytic efficiency, k_{cat}/K_m. However, the fractional inhibition of ACh catalysis by fasciculin is proportionally decreased in the respective fasciculin mutant-AChE complexes. Hence, in no case does saturating fasciculin result in 100% inhibition of catalysis, but fractional inhibition is greatest with the more active mutants. In fact, the fasciculin complexes of the various enzymes mutated at position 86 have relatively similar catalytic efficiencies.

Table 4
Dissociation constants for fasciculin with wild-type and mutant acetylcholinesterases and butyrylcholinesterase

Enzyme	K_i (pM)
AChE (wild type)	2.3 ± 0.7
$F_{295}L$	16 ± 8
$F_{297}I^a$	57 ± 15
$F_{297}Y$	7.9 ± 1.7
$F_{338}G$	7.9 ± 1.7
$Y_{337}A$	4.2 ± 1.7
$D_{74}N$	43 ± 7
$Y_{124}Q$	248 ± 57
$Y_{72}N$	7800 ± 900
$W_{286}R$	2 100 000 ± 600 000
$Y_{72}N,Y_{124}Q$	72 000 ± 19 000
$Y_{124}Q,W_{286}R$	8 500 000 ± 3 100 000
$Y_{72}N,W_{286}R$	170 000 000 ± 66 000 000
$Y_{72}N,Y_{124}Q,W_{286}R$	235 000 000 ± 60 000 000
BuChE (wild type)	210 000 000 ± 98 000 000

If a neutral and less efficiently catalyzed substrate such as *p*-nitrophenylacetate is used instead of acetylthiocholine, fractional inhibition by fasciculin is diminished. Moreover, fasciculin is a less effective inhibitor of *p*-nitrophenylacetate hydrolysis by the mutant enzymes, and for the fasciculin-W_{86}A AChE complex is a more efficient catalyst than is W_{86}A AChE alone. Hence, for this mutant enzyme of diminished catalytic efficiency, fasciculin behaves as an activator rather than an inhibitor [17].

These data not only reveal the surface of fasciculin binding on the enzyme, but also confirm previous results with diisopropylfluorophosphate labeling in which the gorge remains open, or partially open, in the fasciculin complex [18]. A more detailed kinetic analysis shows that fasciculin may gate entry to the gorge for those substrates whose catalysis is limited or near-limited by diffusion. In the case of poorer substrates, such as *p*-nitrophenylacetate, whose catalysis is limited by substrate orientation or a similar unimolecular isomerization step [6], substrate entry is not rate limiting nor does it become rate limiting in the presence of fasciculin. Hence, the primary influence of fasciculin for these substrates is to induce a conformational change which affects chemical reactivity and orientation of the bound substrate. In most cases this diminishes catalytic efficiency, except for the W_{86}A

mutation where catalysis of *p*-nitrophenylacetate is enhanced slightly.

The binding of propidium at a peripheral site has also been shown to affect the conformation of the active center and catalytic efficiency of AChE [3]. Some of the residues involved in allosteric control by propidium have also been defined [19].

A knowledge of the structures of fasciculin and the cholinesterases enables one through mutagenesis to analyze which side chains in peptide and protein are energetically coupled in the formation of the complex. This approach should distinguish which residues in fasciculin contribute to formation of the surface of interaction, to alterations in kinetics through steric constraints or charge repulsion, and to inducing conformational changes in AChE. Hence, the wealth of natural and synthetic inhibitors of the cholinesterases will continue to yield important molecular details on the function of this family of enzymes.

Acknowledgements

Supported by grants USPHS-GM-18360 and DAMD17-95-1-5027.

References

[1] Schumacher, M., Camp, S., Maulet, Y., Newton, M., MacPhee-Quigley, K., Taylor, S.S., Friedmann, T. and Taylor, P. (1986) Primary structure of *Torpedo californica* acetylcholinesterase deduced from cDNA sequences. Nature 319, 407–409.

[2] Cygler, M., Schrag, J., Sussman, J.L., Harel, M., Silman, I., Gentry, M.K. and Doctor, B.P. (1993) Relationship between sequence conservation and three-dimensional structure in a large family of esterases, lipases, and related proteins. Protein Sci. 2, 366–382.

[3] Taylor, P. and Radic, Z. (1994) The cholinesterases: from genes to proteins. Annu. Rev. Pharmacol. Toxicol. 34, 281–320.

[4] Ichtchenko, K., Hata, Y., Nguyen, T., Ullrich, B., Missler, M., Moomaw, C. and Südoff, T.C. (1995) Neuroligin 1: A splice site-specific ligand for β-neurexins. Cell 81, 435–443.

[5] Sussman, J.L., Harel, M., Frolow, F., Oefner, C., Goldman, A. and Silman, I. (1991) Atomic structure of acetylcholinesterase from *Torpedo californica*: a prototypic acetylcholine-binding protein. Science 253, 872–879.

[6] Rosenberry, T.L. (1975) Acetylcholinesterase. Adv. Enzymol. Relat. Areas Mol. Biol. 43, 103–218.

[7] Quinn, D.M. (1987) Acetylcholinesterase: enzyme structure, reaction dynamics, and virtual transition states. Chem. Rev. 87, 955–979.

[8] Augustinsson, K.B., Bartfai, T. and Mannervik, B. (1974) A steady state model for butyrylcholinesterase from horse plasma. Biochem. J. 141, 825–834.

[9] Radic, Z., Pickering, N., Vellom, D.C., Camp, S. and Taylor, P. (1993) Three distinct domains in the cholinesterase molecule confer selectivity for acetylcholinesterase and butyrylcholinesterase inhibitors. Biochemistry 32, 12074–12084.

[10] Hosea, N.A., Berman, H.A. and Taylor, P. (1995) Specificity and orientation of trigonal carboxylesters and tetrahedral phosphonylesters in cholinesterases. Biochemistry, 34, 11528–11536.

[11] Berman, H.A. and Leonard, K. (1989) Chiral reactions of acetylcholinesterase probed with enantiomeric methylphosphonothioates: noncovalent determinants of enzyme chirality. J. Biol. Chem. 264, 3942–3950.

[12] Berman, H.A. and Decker, M.M. (1989) Chiral nature of covalent methylphosphonyl conjugates of acetylcholinesterase. J. Biol. Chem. 264, 3951–3956.

[13] Changeux, J.-P. (1966) Responses of acetylcholinesterase from *Torpedo marmorata* to salts and curarizing drugs. Mol. Pharmacol. 2, 369–392.

[14] Taylor, P. and Lappi, S. (1975) Interaction of fluorescence probes with acetylcholinesterase. The site and specificity of propidium binding. Biochemistry 14, 1989–1997.

[15] Radic, Z., Reiner, E. and Taylor, P. (1991) Role of the peripheral anionic site on acetylcholinesterase: inhibition by substrates and coumarin derivatives. Mol. Pharmacol. 39, 98–104.

[16] Radic, Z., Quinn, D.M., Vellom, D.C., Camp, S. and Taylor, P. (1995) Allosteric control of acetylcholinesterase catalysis by fasciculin. J. Biol. Chem., 270, 20391–20399.

[17] Radic, Z., Duran, R., Vellom, D.C., Li, Y., Cervenansky, C. and Taylor, P. (1994) Site of fasciculin interaction with acetylcholinesterase. J. Biol. Chem. 269, 11233–11239.

[18] Marchot, P., Khelif, A., Ji, Y.H., Mansuelle, P. and Bougis, P.E. (1993) Binding of ^{125}I-fasciculin to rat brain acetylcholinesterase. The complex still binds diisopropylfluorophosphate. J. Biol. Chem. 268, 12458–12467.

[19] Barak, D., Kronman, C., Ordentlich, A., Ariel, N., Bromberg, A., Marcus, D., Lazar, A., Velan, B. and Shafferman, A. (1994) Acetylcholinesterase peripheral anionic site degeneracy conferred by amino acid arrays sharing a common core. J. Biol. Chem. 269, 6296–6305.

[20] Bourne, Y., Taylor, P. and Marchot, P. (1995) Acetylcholinesterase inhibition by fasciculin: Crystal structure of the complex. Cell 83, 503–512.

30 Heider, H., Litynski, P., Stieger, S. and Brodbeck, U. (1991) Cell. Mol. Neurobiol. **11**, 105–118
31 Gisiger, V. and Stephens, H. R. (1988) J. Neurosci. Res. **19**, 62–68
32 Jasmin, B. J. and Gisiger, V. (1990) J. Neurosci. **10**, 1444–1454
33 Gisiger, V., Sherker, S. and Gardiner, P. F. (1991) FEBS Lett. **278**, 271–273
34 Gisiger, V. and Stephens, H. (1984) J. Neurochem. **43**, 174–183
35 Oliver, L., Chatel, J. M., Massoulié, J., Vigny, M. and Vallette, F. M. (1992) Neuromusc. Disord. **2**, 87–97
36 MacPhee-Quigley, K., Vedvick, T. S., Taylor, P. and Taylor, S. (1986) J. Biol. Chem. **261**, 13565–13570
37 Roberts, W. L., Doctor, B. P., Foster, J. D. and Rosenberry, T. L. (1991) J. Biol. Chem. **266**, 7481–7487
38 Anselmet, A., Fauquet, M., Chatel, J.-M., Maulet, Y., Massoulié, J. and Vallette, F.-M. (1994) J. Neurochem. **62**, 2158–2165

Received 24 March 1994

Expression and ligand specificity of acetylcholinesterase and the nicotinic receptor: a tale of two cholinergic sites

Palmer Taylor,* Zoran Radić, Hans-Jurgen Kreienkamp, Robert Maeda, Zhigang Luo, Maria Elena Fuentes, Daniel Vellom and Natilie Pickering

Department of Pharmacology, 0636, University of California, San Diego, La Jolla, CA 92093, U.S.A.

Introduction

Acetylcholinesterase (AChE) and the nicotinic acetylcholine receptor (nAChR) are the major functional proteins controlling postsynaptic events at the neuromuscular junction and in certain other central and peripheral nervous system synapses. In addition to AChE's and nAChR's common recognition capacity for acetylcholine and certain inhibitors, both proteins show proximal localization in synapses, function within a millisecond time frame and exhibit common features of expression during differentiation in muscle or following denervation [1,2]. The fidelity of neuromuscular transmission in the organism and the duration of miniature endplate potentials in individual synapses require that the active states of these proteins be functioning within close stoichiometric confines [3]. In autoimmune myasthenia gravis, functional receptor is diminished and the disease can be managed by prolonging the presence of acetylcholine in the synapse with AChE inhibitors [4]. AChE inhibition by insecticides and a congenital myasthenic state with diminished endplate AChE also lead to compromised synaptic neurotransmission [3,5].

Comparative sequences [6] and an X-ray crystal structure [7] have enabled examination of the structure of AChE and its inhibitor complexes at an atomic level of resolution, whereas the nAChR's disposition within integral membranes makes its crystallization a formidable endeavour. Nevertheless, electron microscopy image analysis [8] has provided structural details of the receptor approaching 10 Å resolution; this work, along with studies of sequence in relation to function, has contributed to the understanding of details of ligand specificity for the receptor at a molecular level of resolution.

Herein we present an overview of the factors governing ligand specificity and gene expression for these two proteins. Some general structural features prevail for stabilization of the quaternary ammonium moiety of bound ligands. However, the most noteworthy comparative aspects for these proteins do not result from evolutionary divergence of related structures, but rather emerge from parallel, independent evolutionary pathways aimed at achieving specificity and coordinated gene expression.

Gene expression of the nicotinic receptor and AChE

Cholinergic receptors are the products of two large gene families. The five known subtypes of muscarinic receptors are members of the seven membrane-spanning G-protein-linked receptors. Members of the nicotinic receptor family of receptors exist as ligand-gated ion channels assembled as pentamers of homologous subunits. Since as many as four different subunits can be found in the pentamers and at least 16 different nicotinic receptor subunits have been identified [2,8,9], the possibility for receptor diversity is enormous. Fortunately, not all permutations of subunits associate into functional receptors, and virtually all subunits which primarily contribute to the binding site (α subunits) require association

Abbreviations used: AChE, acetylcholinesterase; BuChE, butyrylcholine esterase; nAChR, nicotinic acetylcholine receptor.

*To whom correspondence should be addressed.

with non-α subunits to achieve function. Since each gene encoding these subunits has a distinct promoter region, transcription might be expected to be a dominant, differential regulatory mechanism of gene expression.

By contrast, AChE is encoded by a single gene and its structural variations arise from alternative mRNA splicing, yielding three distinct C-termini (Figure 1). The portion of the gene encoding the essential catalytic residues is invariant, giving rise to identical catalytic properties for all of the molecular species. The distinct C-termini allow the enzyme to be expressed as: (a) hydrophilic monomers, (b) homomeric dimers and tetramers which vary hydrophobicity through attachment of a fatty acid or exposure of an amphiphatic helix, (c) a glycophospholipid-linked species, and (d) heteromeric oligomers which link via a disulphide to a filamentous, triple-helical collagen unit or a lipid-linked subunit. RNA splicing governs the structural diversity of AChE, but multiplicity of species is further enhanced by post-translational events [10,11].

A second difference between AChE and the nAChR lies in the control of gene expression. Upon differentiation from myoblasts to myotubules, the enhanced expression of the *nAChR* gene is a consequence of increased transcription [12,13]. By contrast, we find that enhanced *AChE* gene expression in the same differentiation scheme arises from stabilization of otherwise rapidly turning over mRNA [14]. Decreased degradation of AChE mRNA with a concomitant increase in mRNA levels appears to be controlled, at least in part, by the release of cellular Ca^{2+} (Z. Luo, M.-E. Fuentes and P. Taylor, unpublished work). Ca^{2+} has little influence on the increased expression of the nAChR during muscle differentiation. Only AChE expression shows superinduction after initiation of differentiation of the myoblast and subsequent treatment with cycloheximide [14]. The distinction of transcriptional activation versus mRNA stabilization is shown by comparing (a) transcription rates in myoblasts and myotubes by run-on transcription, (b) transcription rates of reporter genes placed behind the nAChR and AChE promoters, and (c) differential rates of gene expression in cell lines containing or lacking the muscle differentiation genes.

In short, AChE and the nAChR show parallel increases in expression with differentiation and the capacity to express distinct molecular species in different tissues. Surprisingly, this co-ordinated expression employs very different mechanisms to increase the level of mRNA species available for translation.

Ligand specificity at cholinergic binding sites

The most notable difference between AChE and the nAChR, as two oligomeric proteins, is that the agonist sites in the receptor reside at subunit interfaces (Figure 2), whereas AChE's active centre is close to the geographic centre of each subunit at the base of a 18–20 Å gorge (Figure 3). A site at the interface between subunits for ligand binding to the nAChR accords with the co-operativity seen for ligand-gated channel opening and for ligand binding. By contrast, each AChE subunit appears to behave in an independent, non-cooperative fashion.

The crystal structure [7,15], sequence comparisons and mutagenesis studies [16–18] of AChE allow one to define three distinct domains respon-

Figure 1

Structure of the mammalian AChE gene

Splicing to alternative exons or acceptors is shown by the dashed lines. Transcriptional start sites (Cap), translational start sites (ATG), translational stop sites (TAA) and polyadenylation signals (pA) are also marked (cf. [10]).

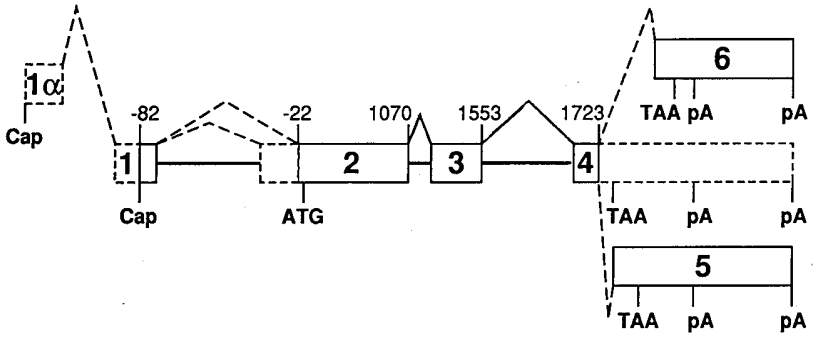

Figure 2

Stereoview of the structure of active-centre gorge of AChE

Shown are the critical residues governing the dimensions of the acyl pocket (F^{295} and F^{297}) choline subsite (E^{202}, Y^{341}, Y^{337} and W^{86}) and the peripheral site (D^{74}, W^{286}, Y^{72} and Y^{124}). The catalytic triad (E^{334}, H^{447} and S^{203}) is shown with hydrogen bonds between side chains. Residue numbering is for the mammalian enzyme.

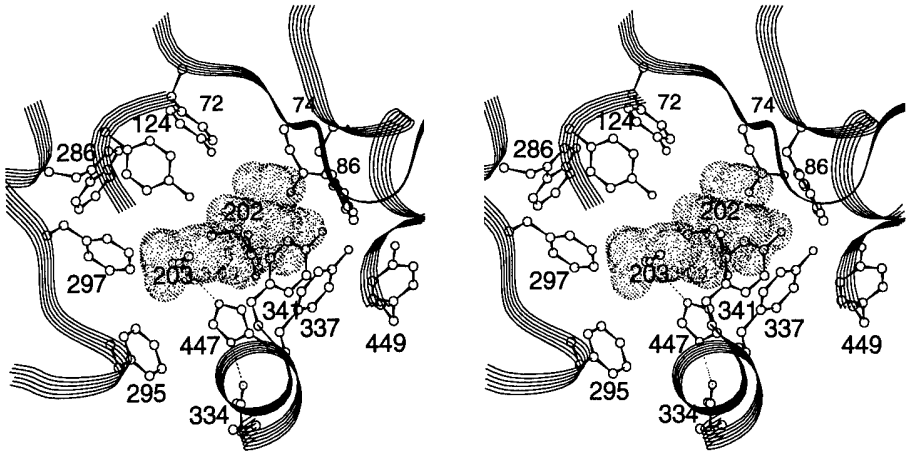

Figure 3

Subunit arrangement of the extracellular region of the nAChR

Shown are the arrangement of subunits and the location of the two ligand-binding sites at the $\alpha-\gamma$ and $\alpha-\delta$ interfaces. The wedge-shaped structures represent bound ligand. Receptor assembly forms stable $\alpha\gamma$ and $\alpha\delta$ dimers which bind α-toxin and various low-molecular-mass agonists and antagonists. Addition of the β subunit allows for the expression of stable pentamers on the cell surface. The subunits are homologous and should have the same stereosymmetric orientation. Accordingly, the anti-clockwise face of α and the clockwise faces of γ and δ form the ligand-binding sites. Mutagenesis of α residues and substitutions of γ/δ domains enable one to define residues that contribute to the binding sites and are responsible for subunit assembly.

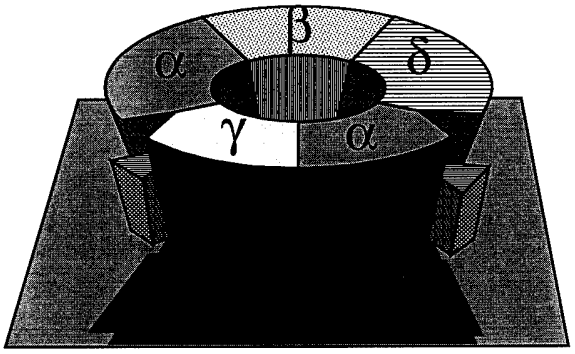

sible for ligand specificity. Two lie within the active centre. The first constitutes the acyl pocket which is formed by two phenylalanine (F^{295} and F^{297}) side chains that point towards the gorge. They permit substrates with small acyl groups (i.e. acetylcholine and small alkylphosphates) but not substrates containing large acyl groups (i.e. butyrylcholine, benzoylcholine and isoOMPA) to interact with AChE. F^{295} and F^{297} in mouse AChE are replaced with leucine and isoleucine respectively in butyrylcholine esterase (BuChE). The $F^{295}L$ substitution is the primary means of introducing BuChE substrate specificity into an AChE template. Accordingly, we can expect the butyryl moiety in butyrylcholine to be directed to the side chain of residue 295. AChE and BuChE also differ in showing substrate inhibition and activation respectively in the presence of excess substrate. Position 297 appears to be the primary determinant of substrate inhibition and activation behaviour. $F^{297}I$ substitution in an AChE template is sufficient by itself to convert the substrate inhibition seen in AChE to substrate activation.

The other active-centre locus is in the choline-binding subsite, which is formed by W^{86}, Y^{341}, Y^{449}, F/Y^{337} and E^{202}. Except for the substitution $Y^{337}A$, these residues are identical in BuChE. The crystal structure of edrophonium and acridine complexes of AChE [15] and energy minimization with docking of acetylcholine show that the aromatic residues surround the choline and contribute to the stabilization energy. However, an anionic side chain from E^{202} comes within 1–2 Å of the van der Waals radius of bound quaternary (trimethylammonio) groups. Both the Coulombic and hydrophobic interactions (dispersion forces) have been touted as primary

contributors to the stablization energy, but an analysis of free energy difference ($\Delta\Delta G$) associated with the mutations shows that both forces contribute to stabilization [16,18].

Certain tricyclic amines containing a bulky exocyclic group such as ethopropazine are highly selective for BuChE. This selectivity appears to be entirely a result of steric hindrance. The position of the diethylaminoisopropyl side chain of ethopropazine overlaps with that of Y^{337}. The $Y^{337}A$ substitution in an AChE template yields a mutant which virtually replicates the binding affinity of ethopropazine for BuChE [16]. Other participating side chains in the active centre, the catalytic triad (E^{334}, H^{447} and S^{203}), in which the active-centre serine (S^{203}) attacks the carbonyl carbon, and the oxyanion hole (G^{120}, G^{121} and A^{204}) are invariant among the cholinesterases.

The third domain responsible for ligand specificity lies outside the active centre and resides at the lip of the gorge. This region contributes to the peripheral anionic site. Certain ligands, the prototype of which is propidium, bind to the peripheral site, regulating catalysis in an allosteric fashion [10]. Fasciculin, a peptide toxin of molecular mass 6500 Da which is homologous to the three-loop, short α-toxins, also bind to this site. Bisquaternary ligands in which the quaternary groups are separated by at least 1.4 nm span between the peripheral site and the active centre. Site-specific mutagenesis show that at least four residues, W^{286}, Y^{72}, Y^{124} and D^{74}, encompass the peripheral site. H^{285} and Y^{130} may also be involved. W^{286}, Y^{72} and Y^{124} are replaced with R(A), Q and N respectively in BuChE. Remarkably, substitution at only these three positions to the residues found in BuChE confers BuChE characteristics to this site where fasciculin, propidium and certain bisquaternary ligands bind with markedly lower affinities [16,19]. Some bisquaternary ligands and propidium probably bind to BuChE with an orientation different to that with which they bind AChE.

Perhaps the most interesting peripheral site ligand is fasciculin, which binds to AChE with a K_D of 2 pM and to BuChE with a K_D of 230 μM. Partitioning of the free energy shows that $W^{286}R$, $Y^{124}Q$ and $Y^{72}N$ can account for the entire specificity difference [20]. Hence this relatively large peptide residing at the lip of the gorge could restrict substrate access and/or allosterically affect the alignment of residues in the active-centre gorge. Although mouse BuChE contains six more glycosylation sites than AChE, glycosylation is not a factor influencing fasciculin binding.

Ligand specificity at the nAChR

The absence of a high-resolution structure of the nAChR necessitates a different approach to the analysis of structure. Site-directed labelling with chemically reactive reagents [20], photoreactive reagents [21] and natural conjugating toxins [22] have defined candidate residues involved in agonist and antagonist binding to the receptor. Reactive residues in the α subunit include C^{192}, C^{193}, Y^{93}, Y^{190}, Y^{198} and W^{49}. Additional insights into the structural basis for conferring specificity and into how these residues affect the functional states of the receptor, i.e. the fractions in the open channel, activatible and desensitized states, come from mutagenesis.

Inserting mutations at residues where sequence differences between species might be responsible for functional differences offers a second approach. This approach, for example, enabled us to define residues responsible for conferring resistance to snake α-toxins for the snake and mongoose nAChR [23]. By selecting sequence differences [24], we have determined that glycosylation signals at N^{189} in snake and N^{187} in mongoose confer resistance to the α-toxin. This interference from presumed steric hindrance is seen with the 6800 Da α-toxins but not for the 1500 Da α-conotoxin or the 500 Da lophotoxin. The observation that only glycosylation affects α-toxin binding differs from data acquired with isolated peptides and fusion proteins [25] and probably reflects the necessity of a proper apposition of amino acid residues at the subunit interface to achieve ligand specificity.

The third approach relies on distinct sequences in the domains of the γ and δ subunits associating with the same interface of α. As shown in Figure 3, the counterclockwise face of α will associate with the clockwise face of γ and δ. These two interfaces form the two binding sites for agonists. When the dissociation constants at these sites differ, it becomes possible through substitutions in γ and δ to define residues contributing to the interfacial binding sites [26]. This approach has been used to define the residues that contribute to a 100-fold preference of $\alpha\gamma$ over $\alpha\delta$ in *d*-tubocurarine binding [27]. An even more dramatic example is the 10^4-fold preference in α-conotoxin binding found for the $\alpha\delta$ over that of the $\alpha\gamma$ interfaces [24].

A two-subunit transfection of $\alpha\gamma$ or $\alpha\delta$ yields dimeric receptor with appropriate ligand-binding properties. For example, the difference in specificity seen for the $\alpha\gamma$ in an intact pentameric receptor can be replicated in assembled dimers. However, the assembled dimers do not reach the cell surface.

Three subunit transfections of $\alpha\beta\gamma$, or $\alpha\beta\delta$ yields pentameric $\alpha_2\beta\gamma_2$ and $\alpha_2\beta\delta_2$ which are expressed on the cell surface as is the native $\alpha_2\beta\gamma\delta$. Only the four subunit transfection $\alpha\beta\gamma\delta$ gives the requisite cooperativity seen in the intact receptor [28].

In the case of the receptor, we chose to study the binding, at the primary site of acetylcholine recognition between subunits, of α-toxin (i.e. α-bungarotoxin, cobra α-toxin and erabutoxin). Binding of these three-fingered α-toxins is prevented competitively by agonists and the presumed site lies within the subsite interface. Reactions are slow (four orders of magnitude slower than diffusion) and glycosylation presumably diminishes α-toxin access.

The fasciculins are three-fingered peptide toxins, homologous to the α-toxins, that bind to AChE. By contrast, fasciculin binding is not competitive with substrate or active-site ligand; the differences in AChE and BuChE specificity are attributable to particular aromatic side chains at the lip of the gorge outside the active site. Glycosylation plays no role in the specificity difference. Hence, only in the case of α-toxin association with the receptor is the site of inhibition the primary acetylcholine recognition site.

Receptor subunit assembly

Studies of the influence of particular residues on the properties at a subunit interface possess the potential advantage that mutations can be matched in paired subunits to ascertain whether complementarity is required for either ligand binding or subunit assembly. In the case of the receptor, the assembling subunits can be examined as dimers after transfection of $\alpha\gamma$ or $\alpha\delta$ into cells not expressing receptor [26]. The α subunit alone binds α-toxin but with an affinity that is far lower than the intact receptor. Moreover, agonists ineffectively compete with α-toxin binding to the monomeric receptor. With the dimers, α-toxin and agonist affinities are increased. The pentameric receptor gives a better representation, but only the four-subunit pentamer $\alpha_2\beta\gamma\delta$ shows co-operativity. Just as in the case for ligand binding, the N-terminal 200 residues dictate subunit assembly, and this approach has enabled us to define residues and domains present on the clockwise and counterclockwise face of each subunit.

Summary

The functional design of the nAChR and AChE rather than their recognition capacities requires divergence in structure of the two binding sites. The receptor requires co-operativity to link ligand occupation to the response, rapid conformational transitions of activation, and slower transitions of desensitization. Hence, its binding sites have evolved at subunit interfaces. By contrast, AChE functions with a large k_{cat} and a comparatively large K_m. To do so, it must force acetylcholine through a low-energy transition site that features tetrahedral rather than the ground-state, trigonal conformation around the carbonyl carbon. This requires a high affinity ($K_D \sim 10^{-17}$ M) for the enzyme complex of the transient transition state. Interestingly, the three-finger peptide toxins (α-bungarotoxin and fasciculin), though closely homologous, use different interaction sites on the receptor (the agonist recognition site) and AChE (a peripheral site). Finally, although the two proteins show co-ordinated expression during muscle differentiation, the receptor relies primarily on transcriptional control while AChE expression is post-transcriptional, being controlled by mRNA stability.

Supported by USPHS grants GM18360 and GM24437 to P.T.

1 Hall, Z. W. and Sanes, J. R. (1993) Cell **72** Suppl., 22–121

2 Taylor, P. and Brown, J. H. (1994) in Basic Neurochemistry: Molecular, Cellular and Medical Aspects (Siegel, G. J., Agranoff, B. W., Albers, R. W. and Molinoff, P. B., eds.), pp. 231–260, Raven Press, New York

3 Taylor, P. (1990) in Goodman & Gilman's The Pharmacological Basis of Therapeutics (Gilman, A. G., Goodman, L. S., Rall, T. W., Murad, F., Nies, A. S. and Taylor, P., eds.), pp. 131–149, Pergamon Press, New York

4 Penn, A. S., Richman, D. P., Ruff, R. L. and Lennon, V. A. (eds.) (1993) Ann. N.Y. Acad. Sci. **681**, 1–622

5 Hutchinson, D. O., Walls, T. J., Nakano, S., Camp, S., Taylor, P., Harper, C. M., Groover, R. V., Peterson, H. A., Jamieson, D. G. and Engel, A. G. (1993) Brain **116**, 633–653

6 Cygler, M., Schrag, J., Sussman, J. L., Harel, M., Silman, I., Gentry, M. K. and Doctor, B. P. (1993) Protein Sci. **2**, 366–382

7 Sussman, J. L., Harel, M., Frolow, F., Oefner, C., Goldman, A., Toker, L. and Silman, I. (1991) Science **253**, 872–897

8 Unwin, N. (1993) Cell **72** Suppl., 31–41

9 Sargent, P. B. (1993) Annu. Rev. Neurosci. **16**, 403–443

10 Taylor, P. and Radić, Z. (1994) Annu. Rev. Pharmacol. **34**, 281–320

11 Massoulié, J., Pezzementi, L., Bon, S., Krejci, E. and Vallette, F. M. (1993) Prog. Neurobiol. **41**, 31–91

12 Buonanno, A. and Merlie, J. P. (1986) J. Biol. Chem. **261**, 11452–11455
13 Evans, S., Goldman, D., Heinemann, S. and Patrick, J. (1987) J. Biol. Chem. **262**, 4911–4916
14 Fuentes, M.-E. and Taylor, P. (1993) Neuron **10**, 679–687
15 Harel, M., Schalk, I., Ehret-Sabatier, L., Bouet, F., Goeldner, M., Hirth, C., Silman, I. and Sussman, J. L. (1993) Proc. Natl. Acad. Sci. U.S.A. **90**, 9031–9035
16 Radić, Z., Pickering, N., Vellom, D. C., Camp, S. and Taylor, P. (1993) Biochemistry **32**, 12074–12084
17 Radić, Z., Gibney, G., Kawamoto, S., MacPhee-Quigley, K., Bongiorno, C. and Taylor, P. (1992) Biochemistry **31**, 9760–9767
18 Ordentlich, A., Barak, D., Kronman, C., Flashner, Y., Leitner, M., Segall, Y., Ariel, N., Cohen, S., Velan, B. and Shafferman, A. (1993) J. Biol. Chem. **268**, 17083–17095
19 Radić, Z. Duran, R., Vellom, D. C., Li, Y., Cervanansky, C. and Taylor, P. (1994) J. Biol. Chem. **269**, 11233–11239
20 Karlin, A. (1993) Curr. Opin. Neurobiol. **3**, 299–309
21 Changeux, J.-P., Galzi, J.-L., Devillers-Thiéry, A. and Bertrand, D. (1992) Q. Rev. Biophys. **25**, 295–432
22 Abramson, S. N., Li, Y., Culver, P. and Taylor, P. (1989) J. Biol. Chem. **264**, 12666–12672
23 Barchan, D., Kachalsky, S., Neumann, D., Vogel, Z., Ovadia, M., Kochva, E. and Fuchs, S. (1992) Proc. Natl. Acad. Sci. U.S.A. **89**, 7717–7721
24 Kreienkamp, H. J., Maeda, R., Sine, S. and Taylor, P. (1994) J. Biol. Chem., in the press
25 Chaturvedi, V., Donnelly-Roberts, D. L. and Lentz, T. L. (1993) Biochemistry **32**, 9570–9576
26 Blount, P. and Merlie, J. P. (1989) Neuron **3**, 349–357
27 Sine, S. M. (1993) Proc. Natl. Acad. Sci. U.S.A. **90**, 9436–9440
28 Sine, S. M. and Claudio, T. (1991) J. Biol. Chem. **266**, 19369–19377

Received 28 March 1994

Three-dimensional structures of acetylcholinesterase and of its complexes with anticholinesterase agents

Israel Silman*§, Michal Harel†, Paul Axelsen†‡, Mia Raves† and Joel L. Sussman†

*Department of Neurobiology and †Department of Structural Biology, The Weizmann Institute of Science, Rehovot 76100, Israel and ‡Department of Pharmacology, University of Pennsylvania, Philadelphia, PA 19104, U.S.A.

Introduction

The principal biological role of acetylcholinesterase (AChE) is the termination of impulse transmission at cholinergic synapses by rapid hydrolysis of the neurotransmitter, acetylcholine (ACh) [1]. In keeping with this requirement, AChE possesses a catalytic activity that is unusually high, especially for a serine hydrolase [2], functioning at a rate approaching that of a diffusion-controlled reaction [3]. The powerful acute toxicity of organophosphorus and carbamate poisons is due primarily to their serving as potent cholinesterase inhibitors [4], by forming a covalent bond with the active-site serine of the enzyme [2]. Anticholinesterase agents are used in the treatment of various disorders, such as myasthenia gravis and glaucoma [5], and have been proposed as possible therapeutic agents in the management of Alzheimer's disease [6].

The active site of AChE comprises an esteratic subsite, containing the catalytic machinery, and an 'anionic' subsite, which binds the quaternary ammonium group of ACh [2]. A second, 'peripheral' anionic site exists, so named because it appears to be distant from the active site [7,8]. Bis-quaternary inhibitors of AChE are believed to derive their enhanced potency, relative to homologous monoquaternary ligands [9], from their ability to span the two anionic sites, which lie 14 Å apart [10,11]. The three-dimensional structure of *Torpedo* AChE reveals that, like other serine hydrolases, it contains a catalytic triad [12]. This triad is located at the bottom of a deep and narrow cavity, named the 'aromatic gorge' since a substantial part of its lining is composed of the rings of 14 conserved aromatic amino acids [12,13]. Docking studies suggest that the primary interaction of the quaternary group of ACh within the active site is with the indole of a conserved tryptophan, Trp-84 [12]. This is in agreement with earlier spectroscopic and labelling

Abbreviations used: ACh, acetylcholine; AChE, acetylcholinesterase; [^{3}H]DDF, *p*-(*N,N*-[methyl-^{3}H]dimethylamino)-benzenediazonium; DECA, decamethonium; EDR, edrophonium; THA, tacrine.

§To whom correspondence should be addressed.

studies [14,15], as well as with a recent affinity labelling study [16]. X-ray crystallography of complexes of AChE with ligands of pharmacological interest can provide direct information concerning the structures of the drug–AChE complexes and, thereby, reveal which residues in the active site of the enzyme are important for ligand binding. Such information is, of course, crucial for structure-based drug design.

In the following article, we present structural data for complexes of AChE with three drugs of biological interest, namely endrophonium, tacrine and decamethonium. Complexes of all three drugs were obtained by soaking the appropriate ligand into crystals of the native enzyme.

Decamethonium–AChE complex

Decamethonium (DECA), a bisquaternary ligand, is both a depolarizing neuromuscular blocker and an anticholinesterase [17]. Crystals of the complex obtained by soaking DECA into the native crystals display an elongated electron density within the gorge which is consistent with that expected for a DECA molecule (Figure 1). Only small differences can be detected, however, between the electron-density map for these crystals, and that obtained for 'native' crystals previously regarded as representing an unliganded form of the enzyme [12,13]. This suggests that DECA, which had been used to elute AChE from the affinity column used for its purification [18], had remained bound in the active-site gorge of the native enzyme, perhaps at lower occupancy, despite prolonged dialysis. In the complex, DECA assumes a curved shape along the gorge, with a mixture of *trans* and *gauche* rotamers along its length. Apart from space adequate to accommodate five or six water molecules, DECA defines and fills the volume of the gorge. Nevertheless, the possibility that the shape and dimensions of the gorge are determined in part by the presence of the DECA molecule can be excluded, because the structure of the gorge is essentially identical in crystals obtained using an AChE preparation which had been obtained by eluting the bound enzyme from the affinity column with the monoquaternary ligand tetramethylammonium, rather than with DECA. In the DECA–AChE complex, both quaternary groups of DECA are in van der Waals contact with tryptophan indole rings; one is apposed to that of Trp-84, at the base of the gorge, and the distal quaternary group is apposed similarly to the indole of Trp-279, ~12 Å distant, near the top of the gorge.

Figure 1

Electron-density map, at 0.28 nm resolution, of the DECA–AChE complex

The final refined co-ordinates of the complex are superimposed on the difference electron-density map. Broken lines indicate hydrogen bonds.

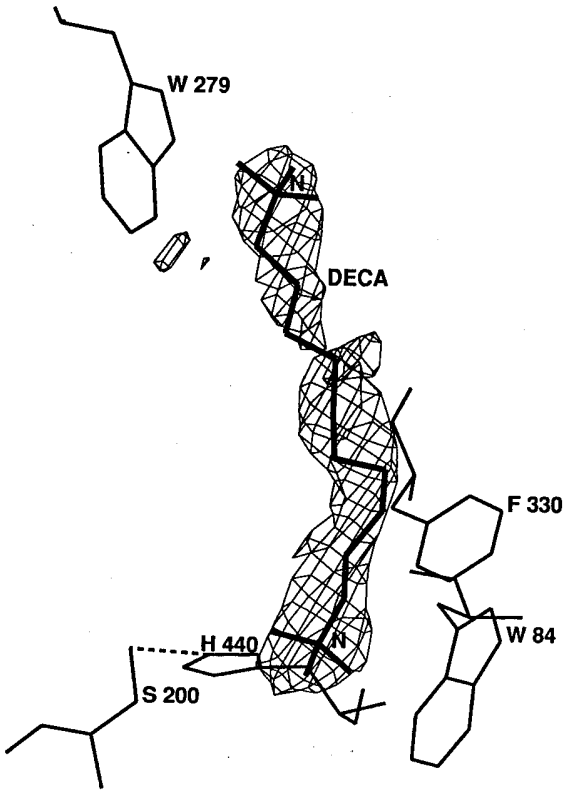

Edrophonium–AChE complex

Endrophonium (EDR, ethyl[3-hydroxyphenyl]dimethylammonium) is a powerful competitive inhibitor of AChE [19], which is used clinically to diagnose myasthenia gravis [1]. Since EDR is a quaternary nitrogen compound, it does not penetrate cell membranes or the blood–brain barrier, and acts peripherally [5]. In the EDR–AChE complex, the quaternary group of the ligand nestles adjacent to the indole of Trp-84, in a position virtually equivalent to that assumed by the proximal quaternary group of DECA and to that assigned to the quaternary group of ACh in the docking procedure [12]. Trp-84 is covalently labelled by the aziridinium ion [16], which is similar in structure to EDR, and EDR protects against labelling by aziridinium. Our data thus demonstrate good correspondence between the crystal structure and that in solution. The *m*-hydroxyl group is positioned between His-440 $N^{\varepsilon 2}$ and Ser-200 O^{γ}, thus making